# Novel Mechanisms that Antagonize Hedgehog Signaling at the Cell Surface During Vertebrate Embryogenesis

**by**

**Alexander Holtz**

**A dissertation submitted in partial fulfillment**
**of the requirements for the degree of**
**Doctor of Philosophy**
**(Cellular and Molecular Biology)**
**in the University of Michigan**
**2015**

**Doctoral Committee:**

**Assistant Professor Benjamin L. Allen, Chair**
**Associate Professor Scott E. Barolo**
**Professor Andrzej A. Dlugosz**
**Professor Deborah L. Gumucio**
**Professor Stephen J. Weiss**

## ACKNOWLEDGEMENTS

The work presented in this dissertation would not have been possible without the help of many talented and dedicated individuals in both my personal and professional life.

I would first like to acknowledge my mentor Ben Allen. I can't thank you enough for teaching me how to do science of the highest quality and integrity. You provided me with unwavering support and unconditional encouragement during my dissertation work. You were also extremely generous with both your time and resources; there were never any questions as to whether I could pursue a particular line of experimentation or attend an international conference (thank you for sending me to Montreal, Italy, and Spain!). I also can't thank you enough for being patient with me and for always making time to talk, without question. You embody all of the qualities of a true mentor and I will strive to live up to the example that you set.

I am also indebted to members of my thesis committee, Deb Gumucio, Scott Barolo, Anj Dlugosz, and Steve Weiss, for their valuable feedback and advice throughout the course of my graduate studies. Similarly I would like to extent my gratitude to the members of the Developmental Biology Group Meeting (including members of the Engel, Gumucio, Wellik, Barolo, Allen, Spence, Lucas, Mishina, and Maillard labs). These meetings were extremely useful to hone my presentation skills and receive critical feedback on my work. I would also like to thank several individuals who provided essential reagents and experimental expertise. I thank Doug Engel and Kim-Chew Lim for enlightening discussions and generously providing several key reagents and equipment. I would also like to acknowledge Jason Spence and Briana Dye for

teaching me everything that I know about working with the lung as a model system and for providing a number of antibodies without condition. Finally, I would like to thank Deb Gumucio and Deneen Wellik for giving me the opportunity to teach Organogenesis of Complex Tissues, which gave me invaluable teaching experience.

I would also like to express my gratitude to Ron Koenig for giving me the opportunity to pursue the MD/PhD degrees. You have gone above and beyond for me during my time at Michigan. You have also provided me with several exciting opportunities, including serving on the MSTP Operating Committee, for which I am extremely grateful. I would also like to extend my sincere gratitude to Ellen Elkin, Laurie Koivupalo, and Hilkka Ketola of the MSTP; Bob Fuller, Jessica Schwartz, Cathy Mitchell, Margarita Bekiares, and Jim Musgrave of CMB; and Melissa Karby and Kristen Hug and the rest of the CDB administrative staff for providing exceptional support throughout my graduate studies.

I would also like to acknowledge several people who were critical to my development as a scientist prior to coming to the University of Michigan. I thank Dave Lin for giving me the opportunity to work as an undergraduate in his lab at Cornell University. This experience sparked my interest in pursuing a career as a scientist. I also owe a debt of gratitude to Ashok Gopinath for teaching me everything I know about molecular biology. You provided me the strong foundation to hit the ground running in graduate school. Finally, I'd like to thank Heiner Westphal for giving me the opportunity to work at the NIH and Ginat Narkis for her mentorship during my time in Bethesda.

I would also like to thank past and present members of the Allen lab for their insightful discussions and for making work in the lab a truly enjoyable experience: Jane, Irene, Brandon, Justine, Martha, Katarina, Diane, Will, and Sam. I'm also grateful to Yevgenia, Katie, Travis,

and Jing-Ping for being the best lab neighbors and all around fun people! I am also truly lucky to have made some amazing friends over the past few years. I would not have made it through graduate school with my sanity in tact if it weren't for my close friends Gianna and Cicely; I am privileged to have met you both. To Meg, Steve, Brittany, Cher, Sharan, and Heather, thank you for helping me to raise my blood mercury content to dangerously high levels through our weekly sushi night. You are all a part of my most memorable and fun experiences of graduate school and I am a better person for having known you. I'd also like to thank the Cornell crew, Dan, Dan, Christine, Ben, Elliot, Jon, and Carlos for being amazing friends; you've all gone on to pursue incredible endeavors and I'm honored to be your friend. I'm also grateful for my life-long friends and partners in crime, Kaitlyn, Joe, Mike, Trista, and Alainah; you are like family to me. I'd also like to thank my mother, father, and brother for their continued love and support and for helping me become the person that I am today. Last, but not least, I'm extremely grateful for my life partner, Nick. You've been there for me through the highs and the lows and I'm so excited for our future together.

I would also like to acknowledge specific data contributions to this dissertation. In Chapter 2: Kevin A. Petersen and Yuichi Nishi performed the bioinformatic and transgenic analysis of the *Ptch2* enhancer; Steves Morin and Frédéric Charron performed the co-immunoprecipitation analysis of PTCH2 with GAS1, CDON, and BOC; and Jane Y. Song assisted with the chicken electroporation experiments. In Chapter 3: Samantha J. Davis performed the NIH/3T3 cell signaling assays with the HHIP1::CD4 constructs. Moreover, Samuel C. Griffiths, Benjamin Bishop, and Christian Siebold performed the molecular modeling of the HHIP1 CRD; the SPR studies between HHIP1 and HS/Heparin; and provided purified HHIP1 protein to generate a novel HHIP1 antibody.

# TABLE OF CONTENTS

## LIST OF FIGURES

FIGURE

# ABSTRACT

Hedgehog (HH) signaling is a conserved mode of cell-cell communication that is indispensible for embryogenesis. HH proteins are secreted ligands that travel over long distances within a developing tissue to induce distinct cellular responses in a concentration- and time-dependent manner. These properties necessitate precise spatial and temporal control of HH ligand production, distribution, and reception at the cell surface. Failure to properly regulate HH ligands during development produces debilitating congenital disorders. Moreover, deregulated HH pathway activity in adult tissues causes several human diseases. In particular, overactive HH signaling underlies many devastating pediatric and adult cancers. Therefore, understanding the mechanisms that restrain HH signaling will provide key insights into human development and disease pathogenesis.

A highly conserved negative feedback loop involving the canonical HH receptor Patched (Ptc in *Drosophila*; PTCH1 in vertebrates) limits the magnitude and range of HH signaling by binding and sequestering HH ligands. While Ptc up-regulation is essential during *Drosophila* embryogenesis, PTCH1-feedback inhibition plays only a limited role in mammals. In this dissertation, I have resolved this discrepancy by demonstrating redundant roles between PTCH1 and two additional vertebrate-specific HH-binding antagonists that are induced by HH signaling, PTCH2 and HHIP1. Importantly, I define PTCH1, PTCH2, and HHIP1 as a core network of HH pathway antagonists that play overlapping and essential roles to restrict HH signaling during mammalian embryogenesis. While any single antagonist is largely dispensable for normal

development, the combined loss of all three inhibitors yields unrestrained HH pathway activity in the mouse embryo. Moreover, I find that these vital HH antagonists function through distinct molecular mechanisms. In particular, I present evidence to define HHIP1 as a secreted inhibitor of vertebrate HH signaling. Surprisingly, secreted HHIP1 protein is enriched in epithelial basement membranes due to a direct, high affinity interaction with heparan sulfate. Intriguingly, HHIP1 also controls the tissue distribution of endogenous HH ligands within the basement membrane during development. Overall, these data provide novel insights into the mechanisms that restrain vertebrate HH signaling and establish a foundation for further investigation into the role of HH inhibitors during development, tissue homeostasis, and disease processes.

# CHAPTER I:

## Introduction

## Restricting the Hedgehog response in development and disease: mechanisms that antagonize Hedgehog signaling at the cell surface

### 1.1 Abstract

Hedgehog (HH) signaling plays essential and diverse roles during invertebrate and vertebrate embryogenesis. HH ligands are dually lipidated signaling molecules that are distributed over long distances in developing tissues to impact cellular behavior. In several contexts, HH proteins act as morphogens, where a gradient of HH ligands produce distinct functional consequences in a concentration- and time-dependent manner. These properties necessitate precise spatial and temporal control of HH ligand production, distribution, and reception at the cell surface. This is largely accomplished by a diverse array of molecules at the cell surface and in the extracellular matrix that directly bind to HH ligands to regulate HH signaling in a developing tissue. Of particular interest is a class of ligand-binding HH pathway antagonists that are critical for restricting HH signaling during embryogenesis; however, little is known concerning the molecular and cellular mechanisms employed by these structurally diverse proteins to antagonize HH pathway activity. Beyond the role for HH signaling during development, dysregulation of the HH pathway post-natally underlies many devastating pediatric and adult cancers. In several contexts, HH ligands produced by tumor cells mediate critical

interactions with the surrounding cancer microenvironment to support disease progression. Thus, elucidating the mechanisms that regulate HH ligand activity is not only crucial to understand the molecular basis of tissue development, but will also unveil novel strategies to therapeutically manipulate HH signaling for a growing number of HH-dependent diseases. In this chapter, I review the basic mechanisms that regulate HH signaling at the cell surface with an emphasis on molecules that function to antagonize HH pathway activity during vertebrate embryogenesis.

## 1.2 Hedgehog signaling: from *Drosophila* development to human pathophysiology

### 1.2.1 Discovery of Core Hedgehog Pathway Components in *Drosophila*

The HH ligand derives its name from a Nobel prize-winning genetic screen to identify mutations that affect embryonic patterning in *Drosphila melanogaster* embryos (Nüsslein-Volhard and Wieschaus, 1980). The *Hedgehog* mutation produced embryos with a lawn of spiny denticle bands, reminiscent of hedgehog spines (Nüsslein-Volhard and Wieschaus, 1980). Cloning of the *Hh* gene a decade later revealed HH to be a secreted signaling molecule that acted to pattern the developing embryo (Mohler and Vani, 1992; Lee et al., 1992; Tabata et al., 1992; Taylor et al., 1993). HH ligands were subsequently identified in mouse, chicken, and zebrafish, demonstrating conservation of the HH pathway from flies to vertebrates (Krauss et al., 1993; Chang et al., 1994; Roelink et al., 1994; Riddle et al., 1993; Echelard et al., 1993). In fact, three HH ligands were identified in mice: Sonic Hedgehog (SHH), Indian Hedgehog (IHH), and Desert Hedgehog (DHH), demonstrating an expansion of the HH family in vertebrates (Echelard et al., 1993).

The receptor for the HH pathway remained controversial due to the identification of two putative cell surface receptors, Patched (Ptc) and Smoothened (Smo). Smo is a 7-pass

transmembrane protein with homology to G-protein coupled receptors (GPCRs) (Alcedo et al., 1996). Smo was an attractive candidate due to its structural homology to other cell surface receptors and because *Smo* mutants resembled a loss of HH pathway function (Alcedo et al., 1996). *Ptc* encodes for a 12-pass transmembrane protein that is found at the plasma membrane (Capdevila et al., 1994a; Hooper and Scott, 1989; Nakano et al., 1989). In contrast to *Smo* mutants, loss of Ptc leads to ectopic activation of HH target genes downstream of HH ligand while Ptc overexpression inhibits HH pathway activity (Martizez Arias et al., 1988; Hidalgo and Ingham, 1990; Capdevila et al., 1994b; Johnson et al., 1995; Schuske et al., 1994; Ingham et al., 1991); thus, Ptc is a negative regulator of the HH pathway. The controversy was resolved when three groups independently verified that Ptc was indeed the HH receptor through genetic and biochemical studies demonstrating direct binding of HH ligands to Ptc, but not to Smo (Stone et al., 1996; Marigo et al., 1996; Chen and Struhl, 1996). Although not the definitive HH receptor, Smo is an essential transducer of the HH signal that acts downstream of Ptc to indirectly regulate the activity of Cubitus Interruptus (Ci), the transcriptional effector of HH signaling in flies (Alexandre et al., 1996; Chen and Struhl, 1996). Three GLI transcription factors are the vertebrate homologues of Ci [reviewed in (Hui and Angers, 2011; Aberger and Ruiz i Altaba, 2014; Falkenstein and Vokes, 2014)].

Overall, these initial studies in *Drosphila* demonstrated that HH signaling is a profoundly unique and unusual mode of cell-cell communication where the receptor, Ptc, acts as an antagonist of the pathway. In the absence of HH ligand, Ptc represses HH signaling through constitutive inhibition of Smo activity (Fig. 1-1, left panel). Ligand-binding to Ptc relieves this inhibition enabling Smo to transduce the HH signal (Fig. 1-1, right panel). Importantly, these relationships are conserved in vertebrates.

### 1.2.2 Processing, Release, and Distribution of HH Ligands

To understand the molecular strategies that regulate HH ligand activity, it is important to discuss the mechanisms that govern the biogenesis, packaging, release, and distribution of HH proteins in a developing tissue. HH ligands are synthesized as 45 kDa precursors that undergo an autocatalytic cleavage reaction generating the bioactive N-terminal 19 kDa ligands (Bumcrot et al., 1995; Lee et al., 1994; Porter et al., 1995; Martí et al., 1995). Two lipophilic moieties are covalently added to produce the active HH ligand. A C-terminal cholesterol is attached as a byproduct of the autocatalytic cleavage reaction and an N-terminal palmitate residue is added by the acyltransferase, Skinny Hedgehog (Ski) (Pepinsky et al., 1998; Chamoun et al., 2001; Porter et al., 1996a; b; Micchelli et al., 2002; Amanai and Jiang, 2001; Lee and Treisman, 2001). In *Drosophila*, HH ligand lacking the cholesterol modification exhibits an extended range of HH target gene activation in the developing embryo and wing imaginal disc, suggesting that the cholesterol moiety restricts the distribution of HH ligands within a target field (Porter et al., 1996b; Burke et al., 1999). While the evidence in vertebrates is mixed, the role of cholesterol in restricting HH ligand distribution is likely conserved (Lewis et al., 2001; Li et al., 2006). In contrast, the palmitic acid residue is required for the full signaling potency of HH ligands both *in vitro* and *in vivo*, based on phenotypic analysis of *Ski* mutants in both *Drosophila* and mice and through analysis of mutant forms of HH ligands that are not receptive to palmitoylation (Chamoun et al., 2001; Chen et al., 2004; Kohtz et al., 2001; Lee and Treisman, 2001; Lee et al., 2001c).

In general, these lipid modifications impart significant hydrophobic character to HH ligands, promoting a strong association with cell membranes (Porter et al., 1995; Bumcrot et al.,

1995; Porter et al., 1996b). This presents two key challenges: (1) a significant energetic barrier exists in the release of HH ligands from producing cells and (2) the solubility of HH proteins must be maintained as they distribute within a target field. The first challenge is overcome in part by Dispatched (DISP), a 12-pass transmembrane protein that is structurally similar to Patched, which is required for the release of HH ligands from producing cells (Burke et al., 1999; Caspary et al., 2002; Ma et al., 2002; Kawakami et al., 2002). Initial studies in flies demonstrated that DISP is required for the release of cholesterol-modified HH ligands from producing cells while HH ligand lacking the cholesterol modification is secreted independent of DISP (Burke et al., 1999). Vertebrates possess two DISP homologues, DISP1 and DISP2, with DISP1 being the predominant actor as *Disp1*$^{-/-}$ mice demonstrate a near complete loss of HH activity similar to *Smo*$^{-/-}$ embryos (Caspary et al., 2002; Ma et al., 2002; Kawakami et al., 2002; Tian et al., 2005; Zhang et al., 2001). Recent biochemical evidence demonstrates that DISP directly binds to the cholesterol moiety of HH ligands, which then catalyzes the release of HH proteins from the plasma membrane (Tukachinsky et al., 2012; Creanga et al., 2012). In vertebrates, DISP activity is not sufficient to liberate HH ligands from the cell surface; release also depends on the activity of the Signal sequence, CUB domain, EGF-related (SCUBE) family of proteins (Kawakami et al., 2005; Woods and Talbot, 2005; Hollway et al., 2006; Tukachinsky et al., 2012; Creanga et al., 2012). These secreted molecules directly bind to the cholesterol moiety of HH proteins in a manner distinct from that of DISP to shield this hydrophobic adduct and maintain the solubility of HH ligands in the extracellular space (Tukachinsky et al., 2012; Creanga et al., 2012). Importantly, combined loss of all three SCUBE family members leads to a complete loss of HH signaling in zebrafish (Johnson et al., 2012); however no SCUBE homologue has been identified in *Drosophila*.

Another key strategy to maintain the solubility and signaling capacity of HH proteins is the assembly of higher order, multivalent HH ligand complexes. One key observation is that HH proteins are often visualized by immunofluorescence within large punctate structures (LPS) (Gallet et al., 2003; 2006). The assembly of HH ligand into these LPS requires cholesterol modification in addition to interactions with Heparan Sulfate Proteoglycans (HSPGs, see below for in-depth discussion of HSPGs in HH signal transduction) and is thought to be important for the magnitude and range of HH signaling (Gallet et al., 2006; 2003; Vyas et al., 2008). Moreover, biochemical studies of purified, soluble HH proteins demonstrate the presence of HH ligands in both high molecular weight complexes in addition to monomeric species, with the multimeric HH ligands possessing significantly greater signaling potency (Zeng et al., 2001; Chen et al., 2004; Feng et al., 2004). The assembly of HH ligands into these multimeric complexes depends on both the cholesterol and palmitate moieties (Chen et al., 2004). The exact nature of these higher-order HH particles is controversial and may involve packaging into exosomes, lipoprotein complexes, or soluble HH multimers [reviewed in (Therond, 2012)]. More recently, data in *Drosophila* and vertebrates suggest that HH ligands may be transported along the membranes of specialized filopodia extended from producing cells, bypassing the need for long-range diffusion of HH proteins (Rojas-Ríos et al., 2012; Sanders et al., 2013; Bischoff et al., 2013; Kornberg and Roy, 2014); however, these various mechanisms of HH ligand dispersal are not mutually exclusive and organisms may employ several means to distribute HH proteins within a target field.

### 1.2.3 The Vertebrate Central Nervous System as a Model for Hedgehog Ligand Function

HH ligands play diverse roles in nearly every tissue during mammalian embryogenesis [reviewed in (McMahon et al., 2003)]; however, the neural tube represents one of the best-studied systems for the role of HH signaling during vertebrate development. In the embryonic spinal cord, HH signaling is directly required to induce five unique ventral neuronal progenitor populations (Wijgerde et al., 2002; Zhang et al., 2001). Towards this end, Sonic Hedgehog (SHH) ligand functions as a morphogen, acting over long distances to specify distinct cell fates in a concentration- and time-dependent manner [reviewed in (Ribes and Briscoe, 2009; Dessaud et al., 2007)]. *Shh* is initially expressed in the notochord, a mesodermal structure underlying the neural tube, which induces a secondary source of SHH production in the ventral midline of the neural tube known as the floor plate (Fig. 1-2 A) (Echelard et al., 1993; Roelink et al., 1994; Riddle et al., 1993). This establishes a ventral-to-dorsal gradient of SHH ligand that acts on neural progenitors by inducing (Class II genes: *Nkx6.1, Nkx2.2, Olig2, FoxA2, etc*.) and repressing (Class I genes: *Pax3, Pax7, etc.*) a series of transcriptional determinants depending on the concentration and duration of exposure to HH signaling (Fig. 1-2 A) (Briscoe et al., 2000; 1999; Ericson et al., 1997).

Combinatorial expression of these transcription factors along the dorsal-ventral (D-V) axis defines five distinct ventral neuronal progenitor domains; each of these domains give rise to unique mature neuronal cell populations (Briscoe et al., 2000). For example, ventral progenitors closest to the source of SHH production that are exposed to the highest levels of HH signaling are specified as v3 interneuron progenitors through expression of *Nkx2.2* (Briscoe et al., 1999). Progenitors situated further away from the source of HH production that are exposed to slightly lower SHH concentrations adopt an OLIG2+ motor neuron progenitor identity (Novitch et al., 2001; Briscoe et al., 2000). The induction of these distinct cell fates at different concentration

thresholds of SHH ligand is supported by early studies demonstrating that naïve neural plate explants isolated from chicken embryos exposed to varying concentrations of SHH ligand adopt unique cell identities (Roelink et al., 1995; Martí et al., 1995; Briscoe et al., 2000; Ericson et al., 1997). Importantly, the amount of HH ligand that is required to specify these distinct neuronal identities correlates to their dorsal-ventral position within the neural tube, with increasing concentrations of ligand inducing progressively more ventral cell types (Roelink et al., 1995; Martí et al., 1995; Briscoe et al., 2000; Ericson et al., 1997). Strikingly, as little as a two-fold change in HH ligand concentration is sufficient to specify unique cell fates (Briscoe et al., 2000; Ericson et al., 1997).

Moreover, increasing the duration of HH signaling also induces a ventral shift in progenitor cell identity, underscoring the importance of timing in HH-dependent ventral neural patterning (Dessaud et al., 2007; Stamataki et al., 2005). This is supported *in vivo* as ventral cells initially express the low level HH target *Olig2* at the onset of SHH exposure whereas induction of the higher threshold HH targets requires a longer duration of active HH signaling (Fig. 1-2 B) (Jeong and McMahon, 2005; Dessaud et al., 2007). Critically, a temporal adaptation mechanism de-sensitizes cells to ongoing HH pathway activity; thus, greater concentrations of HH ligand are required to maintain active HH signaling to induce a progressive shift form dorsal to ventral cell fates (Dessaud et al., 2007). The boundaries between these progenitor domains are subsequently refined through cross-repressive interactions between transcription factors expressed in neighboring populations (Fig. 1-2 B) (Briscoe et al., 2000; 1999; Ericson et al., 1997; Balaskas et al., 2012).

This graded nature of the HH response suggests that neural progenitors must possess exquisitely sensitive mechanisms to precisely interpret the extracellular concentration of HH

ligands and to integrate these signals over time to ensure proper positional specification of ventral cell domains. Moreover, the extracellular distribution of HH ligands must be carefully controlled in order to establish the morphogenetic gradient. Several lines of evidence suggest that this is accomplished, in part, through feedback regulation of a diverse array of HH ligand-binding proteins that have both positive and negative influences over HH pathway activity (Tenzen et al., 2006; Allen et al., 2007; 2011; Jeong and McMahon, 2005; Holtz et al., 2013; Chen and Struhl, 1996). In particular, negative feedback at the level of HH ligand is essential to limit HH signaling to the ventral aspect of the neural tube to preserve the requisite diversity of neuronal cell types (Milenkovic et al., 1999; Jeong and McMahon, 2005; Holtz et al., 2013). A diverse set of HH-binding molecules function to restrict the activity of HH ligands during embryogenesis (discussed below); however, the precise molecular mechanisms that antagonize HH signaling during ventral neural patterning remain poorly understood.

### 1.2.4 Hedgehog Signaling in Human Cancers: From Bench to Bedside

In addition to its role in development, HH signaling has been implicated in a diverse range of human diseases. Consistent with data in mice, mutations in HH pathway components in humans produce a broad spectrum of clinical developmental abnormalities in the limbs, face, brain, and skeleton, demonstrating an essential role for HH signaling in human embryogenesis (Gao et al., 2001; McCready et al., 2002; Bosse et al., 2000; Radhakrishna et al., 1997; Belloni et al., 1996; Roessler et al., 1996; 2003; Nanni et al., 1999; Bae et al., 2011). Importantly, overactive HH signaling post-natally is a driving force behind several devastating pediatric and adult cancers [reviewed in (Teglund and Toftgård, 2010)]. Broadly speaking, there are two distinct mechanisms that lead to pathologic HH pathway activation in the context of cancer.

Classically, mutations in HH pathway components can lead to high levels of ligand-independent pathway activation that cell autonomously drives HH signaling to promote cancer growth (Scales and de Sauvage, 2009). However, there is an emerging class of cancers where tumor cells aberrantly re-express HH ligands that signal to the surrounding tumor microenvironment to foster tumor development (Scales and de Sauvage, 2009).

*Ligand-independent HH pathway activation drives Basal Cell Carcinoma, Medulloblastoma, and Rhabdomyosarcoma*

Simultaneous with the identification of Ptc as the canonical HH receptor, mutations in the human *Ptch1* locus were identified as the driving mutation in hereditary basal cell nevus syndrome, or Gorlin's syndrome (Johnson et al., 1996; Hahn et al., 1996; Chidambaram et al., 1996; Wicking et al., 1997). Gorlin's syndrome is a dominantly inherited condition characterized by a severe predisposition to basal cell carcinomas (BCCs), a largely benign skin tumor (Gorlin and Goltz, 1960). Affected individuals can possess dozens to thousands of BCCs in addition to other abnormalities including palmar pitting in the hands and feet, odontogenic keratocysts, central nervous system calcifications, polydactyly, enlarged body size (similar to acromegaly) and a variety of skeletal defects (bifid ribs, enlarged skull, vertebral anomalies) (Gorlin and Goltz, 1960; Evans et al., 1993; Athar et al., 2014). In addition, Gorlin's syndrome patients are predisposed to a variety of other cancers, including medulloblastoma, meningiomas, ovarian tumors, and rhabdomyosarcomas (Evans et al., 1991; 1993; Athar et al., 2014). These observations suggested that PTCH1 functions as a tumor suppressor in several contexts. Consistent with this idea, inactivating mutations in PTCH1 have been isolated in sporadic BCCs, medulloblastomas, and rhabdomyosarcomas, demonstrating that PTCH1 is a key tumor

suppressor for a variety of human cancers (Hettmer et al., 2013; Johnson et al., 1996; Gailani et al., 1996; Hahn et al., 1996; Vorechovsky et al., 1997; Tostar et al., 2006). Since PTCH1 is required to antagonize HH pathway activity in the absence of ligand, these data suggest that ligand-independent HH signaling is a potent driver of tumorigenesis in several contexts.

Similar to Gorlin's syndrome patients, *Ptch1*$^{+/-}$ mice are predisposed to developing several forms of cancers. While *Ptch1* heterozygotes do not spontaneously develop BCCs, these tumors arise in response to ionizing radiation (Aszterbaum et al., 1998). *Ptch1*$^{+/-}$ mice do, however, develop medulloblastoma and rhabdomyosarcoma at varying frequencies depending on the genetic background, which is greatly enhanced after exposure to ionizing radiation (Goodrich et al., 1997; Svärd et al., 2006; Wetmore et al., 2000). BCCs and medulloblastomas can also be induced by conditional inactivation of *Ptch1* in the skin and cerebellum, respectively (Yang et al., 2008; Adolphe et al., 2006; 2014). Moreover, overexpression of a constitutively active form of SMO can drive BCC-like tumors, medulloblastomas, and rhabdomyosarcomas while BCCs have also been produced through overexpression of GLI2 in the skin (Grachtchouk et al., 2003; Xie et al., 1998; Mao et al., 2006; Wong et al., 2009; Schüller et al., 2008; Grachtchouk et al., 2000; Hutchin et al., 2005). Collectively, these data from mouse models confirm that ligand-independent HH pathway activation underlies tumor development.

*Ligand-dependent HH signaling controls pancreatic tumorigenesis*

While HH-dependent tumors classically arise through ligand-independent HH pathway activation, an emerging role for HH ligands has been described in several diseases, including pancreatic, intestinal, colorectal, and ovarian cancers (Yauch et al., 2008; Berman et al., 2003; Thayer et al., 2003; Theunissen and de Sauvage, 2009). In this context, cancer cells produce HH

ligands to signal to their surrounding microenvironment to promote tumor growth (Scales and de Sauvage, 2009). Pancreatic cancer represents the best example of this mode of HH signaling. Pancreatic ductal adenocarcinoma (PDA) is a terrible illness with an extremely poor prognosis. PDA tumors are surrounded by a dense desmoplastic stroma and are often metastasized at the time of diagnosis (Erkan et al., 2012). While pancreatic ducts do not normally express HH ligands, both pancreatic intraepithelial neoplasias (PanINs), the precursor lesions to pancreatic cancer, and PDAs aberrantly express SHH ligand, which activates HH target genes in the surrounding pancreatic mesenchyme (Berman et al., 2003; Thayer et al., 2003).

In this context, HH pathway activity is limited to the stromal environment while the tumor epithelial cells are largely refractory to HH ligands (Thayer et al., 2003; Tian et al., 2009; Yauch et al., 2008). In xenograft models where PDA cell growth is supported by co-injection of stromal fibroblast cells, deletion of SMO in the stromal compartment significantly impaired tumor growth, suggesting that this tumor-stromal cross-talk is critical for PDA development (Yauch et al., 2008). Moreover, pharmacologic inhibition of HH signaling in a mouse model of PDA sensitized tumors to gemcitabine treatment, likely through disruption of the desmoplastic environment to facilitate drug delivery (Olive et al., 2009). These data suggested that HH signaling is a promising drug target for PDA; however, clinical trials with HH pathway inhibitors in pancreatic cancer patients have not been successful (Amakye et al., 2013).

This failure in the clinic is consistent with recent reports suggesting that reducing HH pathway activity can actually accelerate pancreatic tumor growth (Mathew et al., 2014; Rhim et al., 2014; Lee et al., 2014). In PDA mouse models, both pharmacologic inhibition of HH signaling and conditional deletion of *Shh* in pancreatic epithelial cells lead to increased tumor growth and decreased overall survival. This was correlated with a reduction in the stromal

compartment, suggesting that the desmoplastic response might actually act to restrain PDA growth (Rhim et al., 2014; Özdemir et al., 2014; Lee et al., 2014). In these models, however, only a partial reduction in HH signaling is likely achieved, leading to accelerated disease. Consistently, using a PDA cell/fibroblast xenograft model, it was demonstrated that while partial loss of HH signaling in the stromal compartment enhanced tumor growth, complete inactivation of HH signaling lead to reduced tumor size (Mathew et al., 2014). These data underscore the critical need for novel strategies to manipulate ligand-dependent HH pathway activity to better treat a growing number of HH-dependent diseases.

*HH pathway inhibitors in the clinic*

The first small molecule inhibitor of HH signaling was isolated as the active component of the corn lily *Veratrum californicum* (BINNS et al., 1963; Cooper et al., 1998). This compound was named cyclopamine since pregnant sheep who ingested this plant produced offspring with severe holoprosencephaly, similar to mouse embryos lacking *Shh* (BINNS et al., 1963; Chiang et al., 1996). Cyclopamine is a cholesterol-like molecule that directly binds to SMO to antagonize HH signaling and can be used to reverse tumor growth in cancers driven by loss of *Ptch1* or by oncogenic SMO mutations (Chen et al., 2002b; Cooper et al., 1998; Taipale et al., 2000). These data suggested that pharmacologic inhibition of SMO may be a useful therapeutic to combat HH-dependent cancers. Additional SMO-binding HH pathway antagonists were identified in a small molecule screen, one of which was optimized for potency and pharmacokinetic properties in humans, leading to the development of GDC-0449 (Chen et al., 2002a; Robarge et al., 2009).

Initial phase I clinical trials with GDC-0449 yielded promising results. In patients with locally advanced or metastatic BCC, more than half of patients demonstrated a significant

clinical response (Hoff et al., 2009). Moreover, GDC-0449 induced dramatic tumor regression in a 26 year old man with metastatic medulloblastoma; however, drug-resistant tumors appeared within 3 months of therapy due to a point mutation in SMO that disrupted drug binding (Yauch et al., 2009; Rudin et al., 2009). Phase II trials in patients with Gorlin's syndrome or with advanced basal cell carcinomas also showed promising results leading to the FDA approval of GDC-0449, or vismodegib, for treatment of BCCs (Tang et al., 2012; Sekulic et al., 2012). While clinical trials are currently ongoing, GDC-0449 has not proven effective in treating other solid tumors (LoRusso et al., 2011; 2013; Italiano et al., 2013; Amakye et al., 2013).

These observations in the clinic demonstrate the challenges of treating patients with HH pathway inhibitors. Current approaches rely almost solely on targeting and inactivating SMO activity. Unfortunately, acquired resistance to these drugs rapidly develops in several clinical models (Rudin et al., 2009; Yauch et al., 2008; Chang and Oro, 2012); thus, novel approaches to antagonize HH pathway activity are desperately needed to combat the growing list of cancers driven by overactive HH signaling. In particular, there is a critical need to therapeutically target HH ligand-dependent signaling in several contexts, such as pancreatic cancer. Encoded within the vertebrate genome are highly effective HH inhibitors that function to restrict HH ligand activity during embryogenesis. Unfortunately, the molecular mechanisms underlying HH pathway inhibition by these endogenous antagonists remain largely undefined. One of the long-term goals of this dissertation research is to identify novel mechanisms that function to antagonize HH signaling during vertebrate embryogenesis to reveal additional strategies for therapeutic HH pathway inhibition. Since these endogenous HH antagonists reside at the cell surface, they may provide attractive drug targets in certain disease contexts, especially in pancreatic cancer where recent evidence suggests that activation of HH signaling could provide

therapeutic benefit (Lee et al., 2014). This could be achieved through pharmacologic inhibition of these endogenous HH antagonists.

## 1.3 Diverse Molecular Mechanisms Restrict HH Ligand Activity at the Cell Surface

Complex mechanisms exist to restrict the activity of HH ligands during embryogenesis and to maintain normal tissue homeostasis in adulthood. This involves a set of diverse molecules that reside at the cell surface and in the extracellular matrix that directly bind to HH ligands to regulate their HH protein distribution and activity within a developing tissue. These structurally divergent proteins act through distinct molecular mechanisms to antagonize HH signaling during embryogenesis. The following section will delineate the key molecules that act to inhibit HH ligand activity during embryogenesis.

### 1.3.1 Two Distinct Forms of Patched-Mediated Inhibition of HH Signaling

Seminal studies in *Drosophila* defined two distinct forms of Ptc-mediated inhibition of HH signaling (Chen and Struhl, 1996). In the absence of HH ligand, Ptc represses HH target genes through constitutive inhibition of SMO (Ingham et al., 1991; Tabata and Kornberg, 1994; Chen and Struhl, 1996). This basal inhibition of SMO activity is termed ligand-independent antagonism (LIA, Fig. 1-3, top panel). Ligand-binding to Ptc relieves this inhibition, culminating in modulation of HH target genes, including Ptc-itself (Alexandre et al., 1996; Forbes et al., 1993). Accumulation of Ptc at the cell surface in response to HH signaling unveils a second role for Ptc– to bind and sequester HH ligands, restricting their distribution away from the source of HH production (Chen and Struhl, 1996). HH ligand sequestration by Ptc is termed ligand-

dependent antagonism (LDA, Fig. 1-3, bottom panel). These distinct activities of Ptc are functionally separable and mediated by unique molecular mechanisms.

*Ligand Independent Antagonism of SMO Activity and Localization Involves the Transporter Function of Patched*

The mechanism underlying PTCH1-mediated inhibition of SMO (LIA) remains largely undefined. This activity is essential for embryogenesis as *Ptch1*$^{-/-}$ mouse embryos die at E9.5 and exhibit constitute activation of HH signaling throughout the embryo (Goodrich et al., 1997). Initial models postulated that PTCH1 and SMO could form a complex that sequesters and inactivates SMO activity (Stone et al., 1996). Ligand-binding to PTCH1 would cause dissociation and release of SMO from this inhibitory complex to activate downstream signaling (Stone et al., 1996). This model was called into question by a careful examination of the stoichiometric relationship between PTCH1 and SMO in relation to HH pathway activation (Taipale et al., 2002). The heteromeric PTCH1/SMO complex model relies upon a direct relationship between PTCH1 and SMO levels where roughly equal amounts of PTCH1 are required to suppress SMO activity. However, it was determined that PTCH1 sub-stoichiometrically inhibits SMO activity with one molecule of PTCH1 capable of inhibiting up to 40 molecules of SMO (Taipale et al., 2002). These data support a catalytic model wherein PTCH1 possesses enzymatic activity that restricts SMO function.

Clues as to the underlying catalytic nature of LIA come from structural homology of PTCH1 to the Resistance Nodular Division (RND) family of molecular transporters (Taipale et al., 2002). RND permeases are 12-pass transmembrane proteins that function as trimeric, protein-dependent antiporters that transport small molecules across lipid bilayers (Tseng et al., 1999).

The transport activity of RND efflux pumps rely on a conserved GxxxD motif present in the 4th transmembrane domain that is thought to form the proton-binding domain of the pore complex (Tseng et al., 1999). Similar to RND permeases, PTCH1 is a 12-pass transmembrane protein that possesses this conserved GxxxD motif (Hooper and Scott, 1989; Nakano et al., 1989; Johnson et al., 1996; Hahn et al., 1996; Taipale et al., 2002). Moreover, PTCH1 forms a stable trimeric complex, consistent with other RND permeases (Lu et al., 2006; Tseng et al., 1999). Missense mutations in the conserved glycine and aspartic acid residues within the GxxxD domain severely compromise PTCH1-mediated inhibition of SMO and have been identified as the causative mutation in several families with Gorlin's syndrome (Taipale et al., 2002; Chidambaram et al., 1996; Wicking et al., 1997; Aszterbaum et al., 1998). These data support the idea that the catalytic basis for LIA involves the RND transporter activity of PTCH1.

The substrate transported by PTCH1 remains elusive, yet likely involves transport and depletion of a molecule that is required for SMO activity. Pharmacologic and genetic evidence demonstrate that cholesterol is required for SMO activation (Cooper et al., 2003; Stottmann et al., 2011). Additionally, several oxysterols directly bind to SMO leading to potent activation of HH signaling (Nachtergaele et al., 2012; Corcoran and Scott, 2006; Nachtergaele et al., 2013; Myers et al., 2013; Nedelcu et al., 2013). These observations invoke a model where PTCH1 transports and depletes a sterol-like molecule that is required for SMO activation. Ligand-binding to PTCH1 would de-activate this transport activity, enabling accumulation of the SMO activator to stimulate HH pathway activity. Whether PTCH1 directly transports sterols remains unknown. PTCH1 possesses a conserved sterol sensing domain (SSD) that binds sterols in several proteins that regulate cholesterol synthesis and trafficking, including HMGCoA reductase, SREBP cleavage-activating protein (SCAP), and Niemann-Pick C1 (NPC1) (Carstea

et al., 1997; Loftus et al., 1997). While some mutations within the SSD of *Drosophila* Ptc lead to a loss of SMO inhibition, these do not affect the LIA activity of vertebrate PTCH1 (Strutt et al., 2001; Martín et al., 2001; Johnson et al., 2002). Interestingly, overexpression of Ptc in *Drosophila* wing imaginal disc cells increases sterol mobilization from endosomal compartments, which was not observed upon expression of a Ptc SSD mutant (Khaliullina et al., 2009). Moreover, overexpression of vertebrate PTCH1 in fibroblasts and yeast cells enhances cellular efflux of BODIPY-labeled cholesterol (Bidet et al., 2011); however, no direct evidence exists demonstrating direct cholesterol transport by Ptc/PTCH1. Importantly, evidence in *Drosophila* has also implicated lipoprotein-derived lipids and phosphatidylinositol-4 phosphate as candidate molecules involved in Ptc-mediated regulation of SMO (Callejo et al., 2008; Yavari et al., 2010; Khaliullina et al., 2009), suggesting that Ptc may possess several substrates, consistent with the broad specificity of other RND permeases (Tseng et al., 1999).

Another key aspect of LIA involves the regulation of SMO subcellular localization by Patched. In *Drosophila*, Ptc resides at the cell surface in the absence of HH ligand, where it destabilizes SMO accumulation at the plasma membrane (Denef et al., 2000; Zhu et al., 2003). HH-binding induces Ptc internalization, leading to the stabilization of SMO at the cell surface to activate downstream signaling (Denef et al., 2000; Zhu et al., 2003). SMO molecules with activating mutations that render it refractory to Ptc-mediated inhibition are constitutively present at the cell surface even in the absence of HH ligand (Zhu et al., 2003). This reciprocal localization of PTCH1 and SMO is conserved in vertebrates with respect to the membrane of the primary cilium (Rohatgi et al., 2007; Corbit et al., 2005). The primary cilium is a microtubule-based cellular protrusion that is essential for HH signal transduction (Huangfu et al., 2003). Many HH pathway components exhibit dynamic trafficking through the ciliary compartment,

including PTCH1, SMO, SUFU, and the GLI transcription factors (Rohatgi et al., 2007; Corbit et al., 2005; Haycraft et al., 2005; Tukachinsky et al., 2010). In the absence of HH ligand, PTCH1 is present within the ciliary membrane to prevent SMO ciliary entry (Rohatgi et al., 2007). Ligand-binding prevents PTCH1 ciliary accumulation, enabling SMO to enter the primary cilium to initiate the HH signal transduction cascade (Rohatgi et al., 2007). Importantly, SMO ciliary entry is necessary, but not sufficient for HH pathway activation and likely involves a two step process including translocation to the ciliary membrane and subsequent activation (Rohatgi et al., 2009; Corbit et al., 2005; Milenkovic et al., 2009). Collectively, these data support a model for LIA where PTCH1 controls the local distribution of small molecules that are required for both SMO trafficking and activation.

*Ligand-Dependent Antagonism by Patched Limits the Magnitude and Range of Hedgehog Signaling*

*Ptc* was initially defined as a target of HH signaling in *Drosophila* (Forbes et al., 1993; Alexandre et al., 1996). Induction of vertebrate *Ptch1* by HH signaling is conserved in mice; thus, feedback up-regulation of *Patched* represents a fundamental aspect of HH signal transduction (Goodrich et al., 1996). Moreover, *Ptch1* appears to be directly regulated by HH signaling based on ChIP-Chip and ChIP-Seq studies that demonstrate binding of GLI1 and GLI3 at the *Ptch1* locus (Vokes et al., 2007; 2008; Peterson et al., 2012).

The function of Patched feedback-upregulation was first demonstrated in the *Drosophila* wing imaginal disc, where HH ligands produced in the posterior compartment induce HH target gene expression in cells within the anterior aspect of the tissue. As expected, *Ptc* mutant clones in the anterior compartment exhibited active HH signaling independent of their distance from the

HH source due to loss of SMO repression (Chen and Struhl, 1996). Strikingly, HH target genes were also inappropriately up-regulated in wildtype cells distal to these *Ptc* mutant clones (Chen and Struhl, 1996), suggesting that *Ptc* not only antagonizes SMO activity cell autonomously, but also sequesters HH ligands and prevents signaling in cells further away from the HH source. Similarly, *Smo* mutant cells were incapable of HH ligand sequestration due to loss of PTC-feedback up-regulation (Chen and Struhl, 1996). Critically, a transgene expressing constitutive, low levels of *Ptc* from the *Tubulinα1* promoter was sufficient to restore SMO inhibition in cells distal to the HH source, suggesting that the low levels of Ptc provided by the transgene are capable of antagonizing SMO activity in the absence of HH ligand (Chen and Struhl, 1996). However, this transgene failed to restore the ability of *Ptc* mutant cells to sequester HH ligand, leading to constitutive HH pathway activation throughout the anterior compartment (Chen and Struhl, 1996). Collectively, these data demonstrated two critical aspects of Ptc function: (1) that low levels of Ptc are sufficient to inhibit SMO activity, which was later confirmed by the sub-stoichiometric relationship between PTCH1 and SMO as discussed above (Taipale et al., 2002) and (2) that feedback up-regulation of Ptc plays an essential role in *Drosophila* to bind and sequester HH ligands to restrict signaling in cells distal to the HH source (Chen and Struhl, 1996). Importantly, this also established an experimental paradigm to separate LIA and LDA by Ptc.

The molecular mechanism underlying LDA by Ptc likely involves endocytosis and degradation of liganded receptor complexes, clearing HH proteins from the extracellular space. Early immunohistochemical studies demonstrated that Ptc was present at both the cell surface and within intracellular punctate structures (Tabata and Kornberg, 1994). In *Drosphila*, HH ligand induces the internalization of Ptc in a dynamin-dependent manner (Denef et al., 2000;

Martín et al., 2001; Torroja et al., 2004). The internalized Hh-Ptc complexes are destined for lysosomal degradation, a mechanism that is likely conserved in vertebrates (Torroja et al., 2004; Incardona et al., 2002). However, recent evidence suggests that PTCH1-SHH complexes can be rerouted to a recycling endocytic pathway by the LRP2 receptor to promote HH signaling in the developing forebrain (Christ et al., 2012); thus, the subcellular trafficking of Ptc/PTCH1 in response to HH ligand is likely governed in a context-specific manner.

The role of LDA to restrict HH signaling in vertebrates is less clear. A similar genetic strategy as used in *Drosophila* was developed in mice to rescue the early lethality of *Ptch1*$^{-/-}$ embryos caused by a loss of LIA (Fig. 1-4 A) (Milenkovic et al., 1999). In this model, *Ptch1* was expressed ubiquitously, at low levels from the metallothionein promoter (*MT-Ptch1*) (Milenkovic et al., 1999). Tonal expression of *Ptch1* from the transgene is sufficient to inhibit SMO activity; however, there is no feedback up-regulation of *Ptch1* in response to HH signaling in *MT-Ptch1;Ptch1*$^{-/-}$ mice, which lack *Ptch1* expression from the endogenous locus (Fig. 1-4 A). While *Ptch1*$^{-/-}$ mice die at E9.5 and exhibit constitutive HH signaling throughout the embryo (Fig. 1-4 B), *MT-Ptch1;Ptch1*$^{-/-}$ embryos demonstrate dramatic rescue of the *Ptch1*$^{-/-}$ phenotype and are nearly indistinguishable from wildtype embryos at E10.5 (Fig. 1-4, C and D). Depending on the transgenic line used in these rescue experiments, *MT-Ptch1;Ptch1*$^{-/-}$ embryos either survive to E15.5 with no apparent defects in HH-dependent patterning or perish at E12.5 and exhibit exencephaly and polydactyly, consistent with elevated HH pathway activity (Milenkovic et al., 1999). A closer examination of early ventral neural patterning in *MT-Ptch1;Ptch1*$^{-/-}$ at E10.5 demonstrated a subtle expansion of HH-dependent FOXA2+ floor plate cells and NKX2.2+ v3 interneuron progenitors, consistent with a mild increase in the magnitude and range of HH ligand activity in the developing neural tube (Jeong and McMahon, 2005). This mild

phenotype was surprising considering the constitutive de-repression of HH signaling observed in analogous experiments in the *Drosophila* wing imaginal disc, calling into question the role of PTCH1-feedback inhibition in vertebrate development.

### 1.3.2 An Expansion of Cell Surface Hedgehog Pathway Antagonists in the Vertebrate Lineage

The apparent limited role for negative feedback by PTCH1 in mice sharply contrasts with the essential role for Ptc-feedback inhibition in *Drosophila*. Unique to vertebrates are two additional cell surface HH pathway antagonists: the PTCH1-homologue, Patched 2 (PTCH2), and an unrelated membrane-anchored glycoprotein, Hedgehog interacting protein 1 (HHIP1) (Chuang and McMahon, 1999; Motoyama et al., 1998b; Carpenter et al., 1998; Koudijs et al., 2008; 2005). Like *Ptch1*, both *Ptch2* and *Hhip1* are direct targets of the HH pathway that are up-regulated in proximity to the source of HH ligand production (Fig. 1-3) (Chuang and McMahon, 1999; Vokes et al., 2008; 2007; Motoyama et al., 1998a; Peterson et al., 2012; Holtz et al., 2013). To date, no PTCH2 or HHIP1 homologues have been described in *Drosophila*; thus, one explanation for the discordance between the role of LDA in mice and flies involves compensation between PTCH1 and the vertebrate specific HH feedback inhibitors. However, the roles for PTCH2 and HHIP1 during vertebrate embryogenesis are just beginning to unravel. Moreover, the molecular and cellular mechanisms employed by the vertebrate specific antagonists remain largely unexplored. The following sections will delineate the current understanding of PTCH2 and HHIP1 in vertebrate HH signal transduction.

*PTCH2: a PTCH1-homologue induced by HH Signaling*

A second *Patched* gene was initially cloned from the adult newt eye and subsequently identified in mouse, humans, and zebrafish (Takabatake et al., 1997; Motoyama et al., 1998b; Carpenter et al., 1998; Zaphiropoulos et al., 1999; Koudijs et al., 2008; 2005). *Ptch2* is expressed in largely overlapping domains with *Ptch1*, consistent with *Ptch2* as a target of HH signaling; however, *Ptch2* is co-expressed with *Shh* in several contexts, which is not observed with *Ptch1* (Motoyama et al., 1998a; b). The direct regulation of *Ptch2* by HH was later confirmed by ChIP-Chip and Chip-Seq studies (Vokes et al., 2007; 2008; Peterson et al., 2012; Holtz et al., 2013).

PTCH2 is a 12-pass transmembrane protein that shares 56% amino acid identity with PTCH1 (Motoyama et al., 1998b; Carpenter et al., 1998). The major structural divergence between PTCH1 and PTCH2 is a truncated C-terminal tail in PTCH2. This leads to increased stability of PTCH2 compared to PTCH1, as ubiquitylation of the PTCH1 C-terminus by NEDD4- and SMURF-ubiquitin ligases targets the protein for endocytosis and degradation (Kawamura et al., 2008; Huang et al., 2013; Yue et al., 2014). Despite these structural differences, PTCH2 binds to all three mammalian HH ligands with similar affinity to PTCH1 (Carpenter et al., 1998) and can complex with PTCH1 (Rahnama et al., 2004). While PTCH2 can inhibit HH ligand-dependent signaling in cell-based assays, there are conflicting reports as to whether PTCH2 possesses the ability to directly inhibit SMO activity in *Ptch1*$^{-/-}$ mouse embryonic fibroblasts (MEFs), which exhibit high levels of ligand-independent HH pathway activity (Rahnama et al., 2004; Nieuwenhuis et al., 2006).

*Ptch2* mutant mice were generated to test the functional role for PTCH2 during vertebrate embryogenesis (Nieuwenhuis et al., 2006; Lee et al., 2006). Surpisingly, *Ptch2*$^{-/-}$ mice are viable and fertile and exhibit no apparent defects in HH-dependent organ development (Nieuwenhuis et al., 2006; Lee et al., 2006). This is in stark contrast to *Ptch1*$^{-/-}$ mutants, which die at E9.5 and

display constitutive HH signaling throughout the embryo due to a loss of LIA. While *Ptch2* mutants do display a subtle expansion of *Ptch1* and *Gli1* expression in the developing limb bud consistent with elevated HH signaling, these defects do not alter HH-dependent digit specification (Nieuwenhuis et al., 2006). Interestingly, aged *Ptch2*$^{+/-}$ and *Ptch2*$^{-/-}$ male mice develop alopecia and skin lesions characterized by epidermal and dermal hyperplasia, ulceration, and loss of hair follicles (Nieuwenhuis et al., 2006); thus, PTCH2 may perform an important role to maintain normal skin homeostasis in adulthood.

Beyond embryonic development, loss of *Ptch2* enhances tumorigenesis in *Ptch1*$^{+/-}$ mice (Lee et al., 2006). *Ptch1*$^{+/-}$ mice exposed to ionizing radiation develop tumors in several organs and have been used as a model for BCC, medulloblastoma, and rhabdomyosarcoma (Pazzaglia et al., 2002; Zurawel et al., 2000; Pazzaglia, 2006; Mancuso et al., 2004). While *Ptch2*$^{-/-}$ mice exposed to ionizing radiation are not predisposed to cancer, *Ptch2*$^{-/-}$*;Ptch1*$^{+/-}$ mice show a decreased tumor latency and decreased overall survival compared to *Ptch1*$^{+/-}$ animals after radiation exposure (Lee et al., 2006). Moreover, mutations in *Ptch2* have been linked to Gorlin's syndrome, suggesting that PTCH2 may function as a tumor suppressor in humans (Fujii et al., 2013; Fan et al., 2008). These data demonstrate that PTCH2 plays overlapping roles with PTCH1 to restrict tumorigenesis; thus, a similar functional redundancy between PTCH2 and PTCH1 may explain the lack of overt HH phenotypes in *Ptch2*$^{-/-}$ embryos. However, this idea has yet to be formally tested.

*HHIP1 plays overlapping and distinct roles with PTCH1 during vertebrate embryogenesis*

HHIP1 was first isolated in a screen to identify novel HH ligand-binding proteins (Chuang and McMahon, 1999). HHIP possesses several conserved functional domains including

an N-terminal cysteine rich domain (CRD), a 6-bladed β-propeller domain, two membrane proximal EGF repeats, a C-terminal hydrophobic region, and 4 N-linked glycosylation sites (Chuang and McMahon, 1999). This initial study described HHIP1 as a membrane-anchored protein based on its retention at the cell surface when expressed in COS-7 cells (Chuang and McMahon, 1999). Deletion of the C-terminal 22 amino acids stimulated significant secretion of HHIP from cells, suggesting that HHIP1 was a type-I transmembrane protein with a C-terminal membrane spanning helix (Chuang and McMahon, 1999). However, a subsequent report identified the presence of a secreted form of HHIP1 when overexpressed in HEK293T cells (Coulombe et al., 2004); thus, there is controversy surrounding the exact nature of the interaction between HHIP1 and the cell membrane.

HHIP1 binds to all three mammalian HH ligands with high affinity (Chuang and McMahon, 1999; Pathi et al., 2001; Bishop et al., 2009; Bosanac et al., 2009). A crystal structure of HHIP1 in complex with SHH ligand implicated the β-propeller domain as the site of HH binding (Bishop et al., 2009; Bosanac et al., 2009). Overexpression of HHIP1 in the developing mouse skeleton using the *Colα1* promoter produced shortened limbs similar to phenotypes observed in *Ihh*$^{-/-}$ embryos, demonstrating that HHIP1 can function to antagonize HH pathway activity (Chuang and McMahon, 1999). *Hhip1* was initially described as a HH target gene due to its expression near the sources of HH ligand production (Chuang and McMahon, 1999). ChIP-Chip and Chip-Seq studies demonstrated GLI binding at the *Hhip1* locus, confirming direct regulation of *Hhip1* expression by HH signaling (Vokes et al., 2007; 2008; Peterson et al., 2012); however, additional inputs that control *Hhip1* expression have been demonstrated in *Xenopus,* including the BMP, WNT, and FGF signaling pathways (Cornesse et al., 2005).

These similarities between PTCH1 and HHIP1 as membrane-associated HH pathway antagonists induced by HH signaling led to the idea that HHIP1 might cooperate with PTCH1 in LDA of HH signaling during nervous system development (Jeong and McMahon, 2005). This idea was tested in mice by examining neural patterning in embryos lacking the combined feedback activities of PTCH1 and HHIP1 (Jeong and McMahon, 2005). *Hhip1*$^{-/-}$ mice are indistinguishable from *wildtype* embryos based on the number and distribution of HH-dependent ventral neuronal cell populations (Chuang, 2003; Jeong and McMahon, 2005). While *MT-Ptch1;Ptch1*$^{-/-}$ embryos displayed a subtle increase in HH signaling in the ventral neural tube, *MT-Ptch1;Ptch1*$^{-/-}$*;Hhip1*$^{-/-}$ mice exhibited a dramatic expansion of HH-dependent ventral cell fates and a concomitant retraction of dorsal neuronal cell types at E10.5 (Jeong and McMahon, 2005). These double mutant embryos also displayed an expansion of the SHH-producing floor plate; however, this severe ventralization phenotype was also observed at E8.5 prior to the induction of floor plate *Shh* expression, suggesting that this expansion of HH signaling is not secondary to increased HH ligand production (Jeong and McMahon, 2005). These data support a model where PTCH1 and HHIP1 play overlapping roles in LDA of HH signaling during ventral neural patterning.

Interestingly, dorsal neural identity persists to an extent in *MT-Ptch1;Ptch1*$^{-/-}$*;Hhip1*$^{-/-}$ embryos. These dorsal progenitors are competent to respond to HH signaling based on the expression of high level HH target genes throughout the dorsal-ventral axis observed in *Ptch1*$^{-/-}$ and *Sufu*$^{-/-}$ embryos, which exhibit constitutive HH pathway activation downstream of HH ligand (Cooper et al., 2005; Goodrich et al., 1997). This discrepancy suggests that additional mechanisms may contribute to LDA of HH signaling during neural pattering.

While HHIP1 is functionally redundant with PTCH1 in the developing nervous system, HHIP1 does display unique requirements in different tissues during embryogenesis. Most notably, *Hhip1*$^{-/-}$ mice die at birth due to severe defects in lung branching morphogenesis resulting from unrestrained HH pathway activity in the lung mesenchyme (Chuang, 2003). During lung development, *Shh* is expressed by the lung epithelium and activates HH signaling in the underlying mesenchyme to repress expression of *Fgf10*, a key mediator if epithelial outgrowth (Bellusci et al., 1997b; a; Sekine et al., 1999; Pepicelli et al., 1998; Litingtung et al., 1998). *Shh*$^{-/-}$ embryos display a near complete absence of secondary branching morphogenesis with high levels of *Fgf10* expression (Pepicelli et al., 1998; Litingtung et al., 1998). Counterintuitively, *Fgf10* expression is maintained in the mesenchyme proximal to the growing epithelial bud tips, which are the sites of highest *Shh* expression in the lung endoderm (Bellusci et al., 1997b; a). It has been proposed that the high levels of SHH production at branch tips induces expression of *Hhip1* in the surrounding mesenchyme to inhibit HH signaling and maintain the localized expression of *Fgf10* to stimulate epithelial outgrowth (Chuang, 2003). Consistent with this model, *Hhip1*$^{-/-}$ lungs exhibit a loss of *Fgf10* expression in the lung mesenchyme (Chuang, 2003).

This unique requirement for HHIP1 during lung branching morphogenesis contrasts with the redundant role with PTCH1 in the developing nervous system. This is not simply a consequence of expression differences since *Ptch1*-feedback upregulation occurs in the lung mesenchyme (Chuang, 2003; Pepicelli et al., 1998; Bellusci et al., 1997b). These data suggest that HHIP1 performs a unique, non-redundant activity that is essential for lung branching morphogenesis that cannot be fulfilled by PTCH1; however, the features that distinguish HHIP1 from PTCH1 in this context remain unknown. Importantly, *Hhip1*$^{-/-}$ embryos also display

developmental defects in other organ systems including the pancreas, stomach, and duodenum (Kawahira et al., 2003). In the developing pancreas, loss of HHIP1 produces a decrease in organ mass and endocrine cell numbers through a reduction in *Fgf10* expression (Kawahira et al., 2003); thus, HHIP1 likely plays a key role to protect *Fgf10* expression by inhibiting HH signaling in multiple organs derived from the endoderm.

In addition to its role in lung development, HHIP1 has been implicated in a variety of human lung diseases including COPD, lung cancer, and asthma (Wilk et al., 2009; Hancock et al., 2010; Van Durme et al., 2010; Young et al., 2010; Li et al., 2011b; Zhou et al., 2012; Castaldi et al., 2014). These SNPs that associate with COPD are not found within the *Hhip1* coding sequence, but instead largely reside in a distal enhancer region upstream of the *Hhip1* gene that contributes to *Hhip1* expression (Zhou et al., 2012). Consistent with a role for HHIP1 in COPD, lung tissue from COPD patients exhibited ~50% decrease in HHIP1 protein levels compared to control samples (Zhou et al., 2012). Importantly, PTCH1 and PTCH2 have not been associated with lung disease; therefore, HHIP1 appears to play a unique role to regulate both lung morphogenesis and to maintain lung physiology in adult life. However, the role for HHIP1 in the adult lung is unknown.

*Blurring the lines: HH co-receptors play dual roles to promote and antagonize HH signaling*

In addition to feedback up-regulation of PTCH1, PTCH2, and HHIP1, another essential component of negative feedback regulation of HH ligands involves downregulation of the positive-acting cell surface HH co-receptors, CDON (CAM-related/downregulated by oncogenes), BOC (brother of CDON), and GAS1 (growth arrest-specific 1) (Tenzen et al., 2006; Lee et al., 2001a; Allen et al., 2007). *Drosophila* possess the CDON/BOC homologues, Ihog

(interference Hedgehog) and Boi (brother of Ihog); however, no GAS1 homologue as been identified in flies (Lum et al., 2003; Yao et al., 2006). While these cell surface components are largely thought to promote HH signal transduction by functioning as essential HH co-receptors, recent evidence suggests that these molecules can play dual roles as HH pathway antagonists.

CDON and BOC are transmembrane-anchored proteins within the Ig superfamily, possessing a series of Ig repeats followed by three fibronectin type III (FNIII) domains (Kang et al., 1997; 2002). In contrast, GAS1 is a GPI-anchored protein that has homology to GDNF receptor family (Cabrera et al., 2006; Stebel et al., 2000). All three proteins directly bind to HH ligands and can promote HH signaling in a ligand-dependent manner when overexpressed in the developing chicken neural tube (Tenzen et al., 2006; Lee et al., 2001a; Allen et al., 2011; 2007). GAS1, CDON, and BOC can also bind to PTCH1 and form distinct receptor complexes (Izzi et al., 2011). Importantly, *Gas1, Cdon*, and *Boc* are all under negative regulation by HH signaling (Tenzen et al., 2006; Allen et al., 2007).

The essential role for GAS1, CDON, and BOC to promote HH signaling during development was largely defined through loss-of-function studies in mice. While $Boc^{-/-}$ mice are viable and fertile, $Cdon^{-/-}$ embryos display a mild loss of HH-dependent ventral cell fates in the neural tube and develop holoprosencephaly to varying degrees depending on the genetic background, consistent with a role for CDON to promote HH signaling (Tenzen et al., 2006; Zhang et al., 2006; Allen et al., 2011; Okada et al., 2006). GAS1 was initially characterized as a HH pathway antagonist through overexpression studies in the developing somite and tooth (Lee et al., 2001a; Cobourne et al., 2004); however, $Gas1^{-/-}$ embryos display prominent loss-of-function HH phenotypes in the cerebellum, limb, eye, face, and neural tube, demonstrating a positive role for GAS1 in HH signal transduction (Lee et al., 2001b; Liu et al., 2002; 2001; Allen

et al., 2007; 2011; Izzi et al., 2011; Martinelli and Fan, 2007). Analysis of compound mutant embryos suggested that GAS, CDON, and BOC cooperate to promote HH signaling. For example, *Gas1*$^{-/-}$*;Cdon*$^{-/-}$, *Gas1*$^{-/-}$*;Boc*$^{-/-}$, and *Cdon*$^{-/-}$*;Boc*$^{-/-}$ embryos exhibit more severe loss-of-function phenotypes in the developing neural tube than loss of any single component (Tenzen et al., 2006; Allen et al., 2007; 2011). Strikingly, *Gas1;Cdon;Boc* triple mutant embryos display a near complete loss of HH signaling throughout the embryo, similar to *Smo*$^{-/-}$ animals. These data suggest that GAS1, CDON, and BOC play overlapping and essential roles to transduce HH ligand-based signaling (Allen et al., 2011; Izzi et al., 2011). Similar results were observed in *Drosophila*, where *Ihog;Boi* double mutants display a complete loss of HH signaling (Camp et al., 2010; Zheng et al., 2010).

In addition to their role to promote HH signaling, recent evidence suggest that the HH co-receptors can function to antagonize HH pathway activity in certain contexts. In the developing *Drosophila* ovary, where HH signaling stimulates the proliferation of follicle stem cells (FSC), Boi binds and sequesters HH ligands to antagonize FSC divisions in a manner analogous to Ptc (Hartman et al., 2010). Interestingly, this mechanism acts in times of nutritional deprivation to restrict FSC proliferation and can be reversed in response to feeding through S6 kinase-dependent phosphorylation of the Boi intracellular domain (Hartman et al., 2010). In zebrafish, morpholino-mediated knockdown of *Cdon* caused an expansion of HH signaling in the developing eye, suggesting that CDON can antagonize HH signaling in this context (Cardozo et al., 2014). Rescue experiments demonstrated that this antagonistic activity depends on the ability of CDON to bind to HH ligands, but was independent of PTCH1-binding (Cardozo et al., 2014). A similar tissue-specific role for BOC to antagonize HH signaling in the lower jaw of zebrafish has also been proposed (Bergeron et al., 2011).

Collectively, these data demonstrate that the role for cell surface HH pathway components can vary in a context-dependent manner. The precise mechanisms that govern these divergent activities remain elusive. This likely does not involve the mode of ligand binding, since most cell surface HH pathway components bind to overlapping domains on the surface of HH ligands (Bishop et al., 2009; Bosanac et al., 2009; McLellan et al., 2008; Whalen et al., 2013; Beachy et al., 2010). Instead, this phenomenon may be related to tissue-specific factors that govern the trafficking and assembly of distinct HH receptor complexes. Future studies will be needed to determine the molecular characteristics that define HH-binding activators and antagonists.

### 1.3.3 Heparan Sulfate Proteoglycans Play Diverse Roles in Hedgehog Signal Transduction

Another critical regulator of HH pathway activity at the cell surface involves heparan sulfate proteoglycans (HSPGs). HSPGs are proteins found at the cell surface and within the extracellular matrix (ECM) that are decorated with heparan sulfates (HS), a glycosaminoglycan (GAG) composed of repeating disaccharide units of glucuronic acid and N-acetylglucosamine (Esko and Lindahl, 2001). HS can be differentially modified through variable sulfation, deacetylation, and epimerization of glucuronic acid to iduronic acid (Esko and Lindahl, 2001). Moreover, these modifications vary between tissue types and over developmental times, producing a great diversity of HS species that can differentially influence several cell signaling pathways (Esko and Lindahl, 2001; Allen and Rapraeger, 2003). There are two major classes of cell surface HSPGs including the transmembrane-anchored syndecans and the GPI-linked glypicans while Perlecan is a secreted HSPG found in the ECM (Lin, 2004). HSPGs are key regulators of morphogen signaling during embryogenesis (Yan and Lin, 2009; Häcker et al.,

2005). Both HS and the HSPG core proteins play critical roles in the production, processing, distribution, and reception of HH ligands at the cell surface (Yan and Lin, 2009; Bandari et al., 2015). HS and several associated core proteins directly interact with HH ligands in addition to other cell surface HH pathway components (Lee et al., 1994; Bumcrot et al., 1995; Chang et al., 2011; Whalen et al., 2013; Rubin et al., 2002; Zhang et al., 2007; Capurro et al., 2008; Williams et al., 2010). Moreover, certain HSPGs function to antagonize HH signaling during embryogenesis, similar to PTCH1, PTCH2, and HHIP1 (Capurro et al., 2008).

*A critical role for HS to mediate HH ligand distribution*

The role for HS to regulate HH signaling came from an analysis of the *Drosophila tout velu* (*ttv*) mutant (Bellaiche et al., 1998). *Ttv* is the *Drosophila* homologue of the mammalian hereditary multiple exostoses (EXT) family of proteins, mutation of which causes an autosomal dominant disorder characterized by benign bone tumors (exostoses) and short stature (Ahn et al., 1995; Stickens and Evans, 1997). EXT proteins are glycosyltransferases that are essential for HS biosynthesis (Lind et al., 1998; McCormick et al., 1998). In the *Drosophila* wing imaginal disc, *ttv* was found to be required for the cell-to-cell movement of HH ligands within responding cells, but was not required to initiate the HH response in cells immediately adjacent to the source of HH production (Bellaiche et al., 1998; The et al., 1999; Han et al., 2004b). Moreover, loss of *ttv* caused retention of HH ligand within producing cells in the developing embryo (The et al., 1999). These data demonstrated that HS is required to distribute HH ligands within a target field.

Disruption of HS biosynthesis in mice causes lethality during gastrulation due to defects in FGF signaling (García-García and Anderson, 2003; Lin et al., 2000). However, a hypomorphic allele of *Ext1* bypassed this early lethality and resulted in enhanced IHH signaling in the

developing bone through an increased range of HH ligand diffusion (Koziel et al., 2004). A similar defect was observed in *Ext1*$^{+/-}$ mice (Hilton et al., 2005). In contrast to studies in *Drosophila,* these data demonstrate that HS-interactions with HH ligands can also act to restrict HH ligand diffusion within a target field. Importantly, these models only lead to a partial disruption of HS-biosynthesis; therefore, conditional ablation of *Ext* genes in the developing bone will help to determine whether the requirement for HS in the cell-to-cell movement of HH ligands is conserved from flies to mice (Mundy et al., 2011). It is also important to consider how HS modifications might affect HH ligand distribution within a target field as HS sulfation can affect HH protein production and distribution in flies, zebrafish, chickens, and mice (Danesin et al., 2006; Oustah et al., 2014; Touahri et al., 2012; Wojcinski et al., 2011).

*Glypican family members play diverse roles to regulate HH signal transduction*

Members of the glypican family of core proteins are the predominant HSPGs that regulate HH signal transduction during embryogenesis. *Drosophila* possess two glypican core proteins, Dally and Dally-like protein (Dlp), while vertebrate have an extended family of 6 glypicans (GPC1-6) (Filmus et al., 2008). Glypicans play complex and diverse roles to regulate HH signal transduction in both Hh producing and receiving cells. The role for glypicans in HH signaling was first identified in an RNAi screen to define novel regulators of the HH pathway in *Drosophila*, which demonstrated an essential role for Dlp in HH signal transduction (Lum et al., 2003). *Dlp* mutants phenocopy a loss of HH signaling in the *Drosophila* embryo (Desbordes and Sanson, 2003; Han et al., 2004a; Williams et al., 2010); however, the requirement for Dlp is less pronounced in the wing imaginal disc due to redundancy with Dally (Gallet et al., 2008; Han et al., 2004a). Interestingly, the un-modified Dlp core protein is sufficient to rescue *Dlp* mutants,

demonstrating that these effects are HS-independent and instead rely on the core protein (Williams et al., 2010; Yan et al., 2010). The exact molecular mechanism underlying this effect remains unclear. While there are conflicting reports as to whether the Dlp core protein can interact with HH ligand (Williams et al., 2010; Yan et al., 2010), Dlp does associate with Ptc and can stimulate the endocytosis of Ptc-Hh complexes to promote HH activation (Yan et al., 2010; Gallet et al., 2008). Similarly, Dally promotes HH signaling through endocytosis of Ptc in receiving cells, an activity that requires cleavage of Dally by the GPI-hydrolase, Notum (Giraldez et al., 2002; Ayers et al., 2012).

In addition to the role of glypicans in responding cells, Dally plays a distinct role in Hh-producing cells to promote the formation of a long-range apical signaling gradient in the wing imaginal disc (Ayers et al., 2012). This activity depends on cleavage of Dally by Notum and is consistent with the role for HSPG-mediated assembly of HH ligands into signaling competent, multivalent structures (Ayers et al., 2010; Vyas et al., 2008; Eugster et al., 2007). Interestingly, this mechanism is thought to promote an apical distribution of HH ligands, which produces distinct functional consequences in HH receiving cells compared to a separate, Dally-independent basolaterally-distributed pool of HH proteins (Ayers et al., 2010). In addition to packaging HH proteins into higher order structures, HS promotes the release of soluble HH ligand complexes from producing cells by promoting metalloprotease-dependent shedding of SHH *in vitro* (Dierker et al., 2009; Ohlig et al., 2012); however, the *in vivo* significance of this mechanism remains unclear.

Mammalian glypicans have also been implicated in HH signal transduction [reviewed in (Yan and Lin, 2008)]. This was first demonstrated for Glypican-3 (GPC3), which is the causative mutation underlying Simpson-Golabi-Behmel syndrome, an X-linked disorder characterized by

developmental overgrowth (tall stature) and defects in digit specification, cleft palate, cardiac defects, cystic kidneys, in addition to rib and vertebrae fusions (Pilia et al., 1996; Neri et al., 1998). Many of these phenotypes were recapitulated in a *Gpc3*$^{-/-}$ mouse model and are reminiscent of defects in HH signal transduction in multiple organ systems (Cano-Gauci et al., 1999). Consistently, *Gpc3*$^{-/-}$ mice display overactive HH signaling in multiple contexts during embryogenesis (Capurro et al., 2008; 2009); thus, GPC3 functions as an antagonist of HH signaling.

In contrast to the inhibitory activity of GPC3, Glypican-5 (GPC5) functions to promote HH signaling. This was initially defined in the context of rhabdomyosarcoma, which exhibit overexpression of GPC5 in some instances (Williamson et al., 2007). Overactive HH signaling is a potent driver of rhabdomyosarcoma in both mice and humans, leading to the idea that GPC5 may potentiate HH signaling to drive tumor growth (Hahn et al., 1998; Bridge et al., 2000; Rajurkar et al., 2014; Nitzki et al., 2011). This was formally demonstrated in rhabdomyosarcoma cell lines, where GPC5 promotes tumor proliferation in response to HH signaling (Li et al., 2011a). Moreover, GPC5 enhances HH-dependent expansion of cerebellar granule cell precursors *in vitro*, suggesting that GPC5 can promote HH signaling in several contexts (Witt et al., 2013); however, these data have yet to be confirmed in *Gpc5* knockout mouse model.

The opposing roles for GPC3 and GPC5 to antagonize and promote HH signaling, respectively, are reflected in their distinct mechanisms of action. GPC3 competes with PTCH1 for HH ligand binding at the cell surface (Capurro et al., 2008). This is mediated through direct interaction between the GPC3 core protein and SHH, while the HS-chains interact with the LRP1 receptor to promote endocytosis and degradation of GPC3-HH complexes (Capurro et al., 2008; 2012). GPC5 also binds to HH ligand in addition to interacting with PTCH1 through its HS side

chains (Li et al., 2011a). This HS-dependent interaction also promotes the localization of GPC5 to the primary cilium, suggesting that GPC5 may function as a co-receptor for HH signaling (Li et al., 2011a; Witt et al., 2013). These distinct interactions might be related to the higher degree of HS sulfation present on GPC5 compared to GPC3 (Li et al., 2011a). Intriguingly, preventing convertase-dependent cleavage of GPC3 leads to a higher degree of HS sulfation and promotes interactions with PTCH1 (Capurro et al., 2015). Surprisingly, this abolishes the antagonistic activity of GPC3, which instead promotes HH signaling similar to GPC5 (Capurro et al., 2015); therefore, the degree of HS-sulfation may determine the identity of an HSPG as an HH activator or antagonist.

Overall, these data demonstrate that vertebrate glypicans play diverse roles to regulate HH signaling; however, these data mostly focus on the role of glypicans in HH-responding cells. Conditional mouse mutants will be essential to tease out the precise roles of GPC3 and GPC5 in different developmental contexts. Moreover, preliminary evidence suggests that GPC1, GPC2, GPC4, and GPC6 can also modulate HH signaling (Williams et al., 2010; Wilson and Stoeckli, 2013); thus, it will be critical to determine the role of the entire glypican family in HH signal transduction.

*Complex interactions between HS and HH ligands*

HH ligands possess a conserved Cardin-Weintraub sequence (C-W, XBBBXXBX, where B is a basic amino acid), which is a common HS-interaction motif (Cardin and Weintraub, 1989). Mutation of basic residues within the C-W sequence in SHH reduced interactions with HS and diminished the ability of SHH to stimulate proliferation in cerebellar granule neuronal precursors (CGNPs) (Rubin et al., 2002). A knock-in mouse model mutating two of these C-W residues at

the endogenous *Shh* locus (*Shh*$^{ala/ala}$) produced mice that were viable and fertile (Chan et al., 2009). Interestingly, while HH-dependent patterning was largely preserved in *Shh*$^{ala/ala}$ mice, these animals exhibited smaller body size and reduced HH-dependent proliferative responses (Chan et al., 2009). These data suggested that the patterning and proliferative responses to HH signaling could be dissociated through proteoglycan interactions; however, these data need to be interpreted with caution since additional motifs within SHH can mediate interactions with HS (Chang et al., 2011; Whalen et al., 2013). Recently, a crystal structure of SHH in complex with different species of HS demonstrated an expanded mode of GAG binding employed by SHH and implicated a direct role for HS in the multimerization of HH ligands (Whalen et al., 2013). This may provide a mechanism to understand the role for HS to promote the assembly of higher order, multivalent HH ligand complexes (Vyas et al., 2008; Eugster et al., 2007; Whalen et al., 2013).

While most of the focus to date has been on the interactions between HS and HH ligands, additional HH pathway components interact with HS *in vitro*, including Ihog and CDON (Zhang et al., 2007); however, the functional consequences of these interactions are unknown. It will be important to determine whether additional HH pathway components associate with HS and how these interactions contribute to HH signal transduction.

### 1.4 Conclusions

Regulation of HH signaling at the cell surface is a dynamic process involving a diverse array of HH-binding proteins. These molecules precisely control the magnitude and range of HH pathway activity to ensure normal tissue development in both flies and humans. Moreover, many of these cell surface HH pathway components continue to play critical roles into adulthood to maintain proper tissue homeostasis and function as tumor suppressors in a variety of contexts. In

particular, feedback up-regulation of HH ligand-binding antagonist is a highly conserved process that plays a critical role to restrict the activity of HH ligands (Jeong and McMahon, 2005; Milenkovic et al., 1999; Chen and Struhl, 1996). This likely functions through two distinct mechanisms: (1) to cell autonomously decrease the sensitivity of cells to HH signaling by competing with productive ligand-receptor interactions at the cell surface and (2) to inhibit signaling non-cell autonomously in cells distal to the HH source by sequestering HH ligands and restricting their distribution within a tissue (Chen and Struhl, 1996; Jeong and McMahon, 2005).

While *Drosophila* Ptc is the sole feedback HH inhibitor in flies, vertebrates possess three cell surface HH antagonists that are direct targets of the pathway, including PTCH1, PTCH2, and HHIP1 (Chen and Struhl, 1996; Goodrich et al., 1996; Motoyama et al., 1998; Carpenter et al., 1998; Chuang and McMahon, 1999; Vokes et al., 2007; 2008; Holtz et al., 2013). The central focus of this dissertation involves this expansion of HH feedback inhibitors in vertebrates to include PTCH2 and HHIP1. While HHIP1 and PTCH1 play overlapping roles to restrict HH signaling during vertebrate embryogenesis, there is no described role for PTCH2 *in vivo* (Jeong and McMahon, 2005). In Chapter II, I use a combinatorial genetic approach to explore the role for PTCH2 in HH-dependent ventral neural patterning by addressing the potential redundancy between PTCH2, PTCH1, and HHIP1. Moreover, I set out to determine how all three vertebrate antagonists cooperate to restrict HH signaling by analyzing neural patterning in the complete absence of PTCH2-, HHIP1-, and PTCH1-feedback inhibition. Importantly, I also explore the cellular and molecular mechanisms of PTCH2-mediated inhibition of HH signaling including: (1) whether PTCH2 possesses similar catalytic activity as PTCH1 to directly antagonize SMO function; (2) if PTCH2 functions in the context of a receptor complex by exploring interactions

between PTCH2 and the HH co-receptors, GAS1, CDON, and BOC; and (3) whether PTCH2 localizes to the primary cilium similar to other HH pathway components.

Another key question is: why vertebrates possess additional feedback antagonists if they play largely redundant roles with PTCH1? While HHIP1 plays overlapping roles with PTCH1 in the developing nervous system, HHIP1 plays a non-redundant role to antagonize HH signaling in the developing lung (Chuang, 2003). However, the mechanisms underlying this unique activity of HHIP1 remain undefined. In Chapter III, I explore the biochemical and molecular mechanisms employed by HHIP1 to antagonize HH pathway activity that are distinct from PTCH1 and PTCH2. In particular, I define a novel role for HHIP1 as a secreted antagonist of vertebrate HH signaling. Moreover, I explore a critical interaction between HHIP1 and HS that governs the surface association and tissue distribution of HHIP1 protein. Finally, I examine whether endogenous HHIP1 protein can control the tissue distribution of HH ligands during vertebrate embryogenesis.

## 1.5 Figures

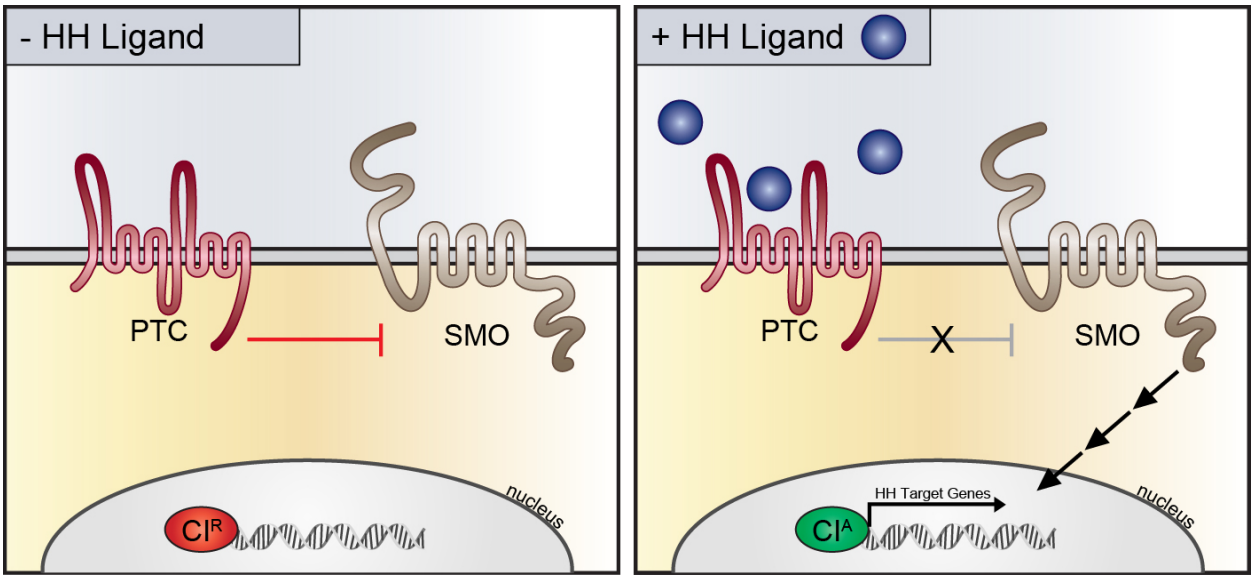


**Figure 1-1. Basic mechanisms of HH signal transduction.** (Left) In the absence of HH ligand, PTC constitutively inhibits the activity of SMO, a key transducer of the HH pathway. This leads to processing of the CI (GLIs in vertebrates) transcription factor into a repressor form that inhibits HH target gene activation. (Right) Ligand-binding to PTC relieves this inhibition enabling SMO to initiate a downstream signaling cascade leading to activation of HH target genes.

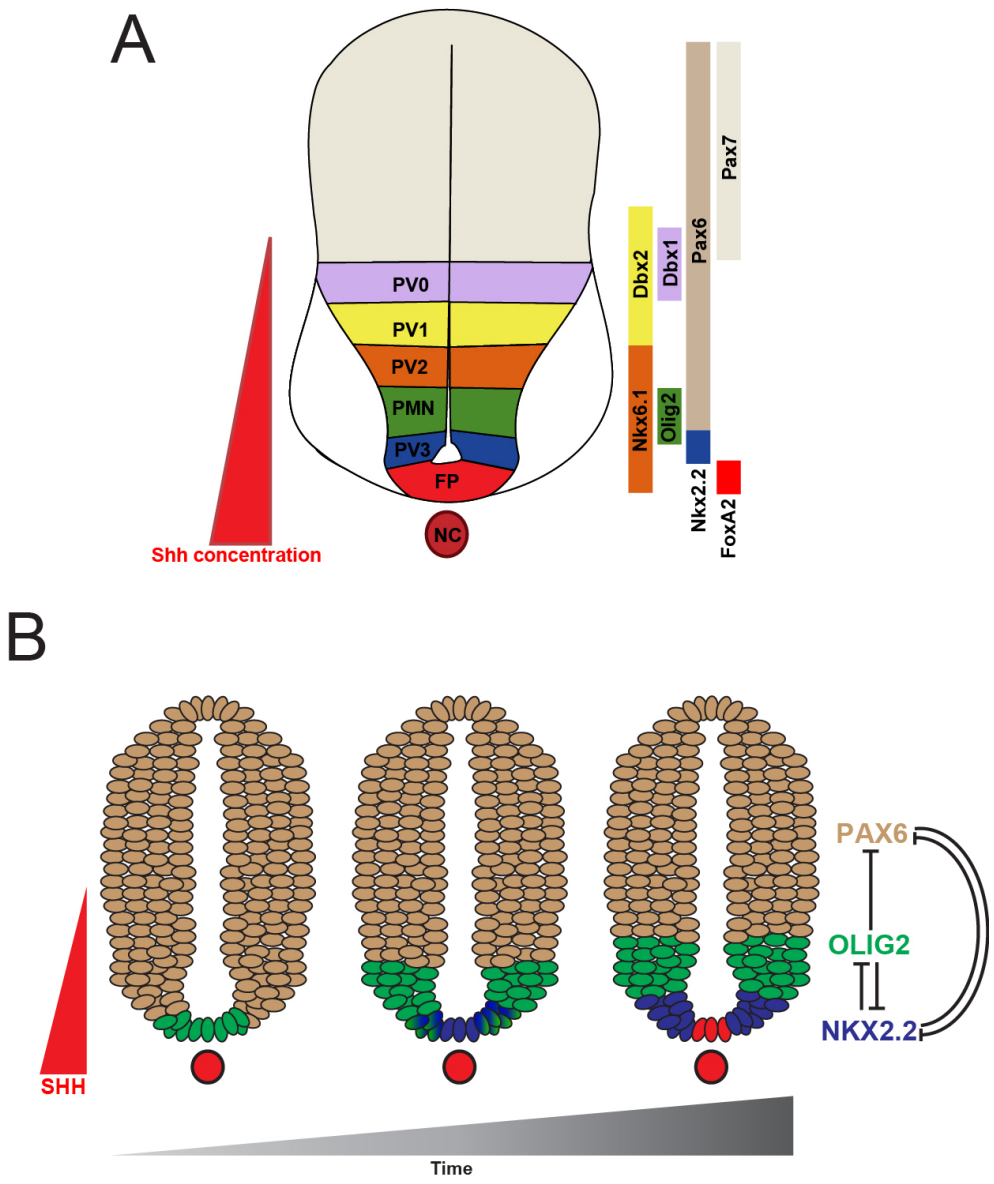


**Figure 1-2. Graded HH signaling specifies distinct neuronal progenitor domains in the ventral neural tube.** (A) In the developing spinal cord, SHH ligand produced from the notochord and floor plate establish a gradient of HH ligand within the neural tube. This gradient of HH signaling leads to the induction (Class II; *Nkx6.1, Olig2, Nkx2.2, FoxA2, Dbx1, Dbx2*) and repression (Class I; *Pax7, Pax3*) of HH target genes in a concentration-dependent manner. Combinatorial expression of these transcription factors along the dorsal-ventral axis specifies five distinct ventral neuronal progenitor domains. (B) The duration of exposure to HH signaling is also critical for HH target gene activation, with initiation of low threshold targets (*Olig2*, green) at the onset of exposure to HH ligands, while higher threshold targets (*Nkx2.2*, blue; *FoxA2,* red) are induced at later time points. Subsueqent cross-repressive interactions between transcription factors in neighboring domains establishes a complex gene regulatory network that sharpens the boundaries between progenitor domains and prevents co-expression of these fate-determinants, which is observed at earlier time points (blue-green nuclei).

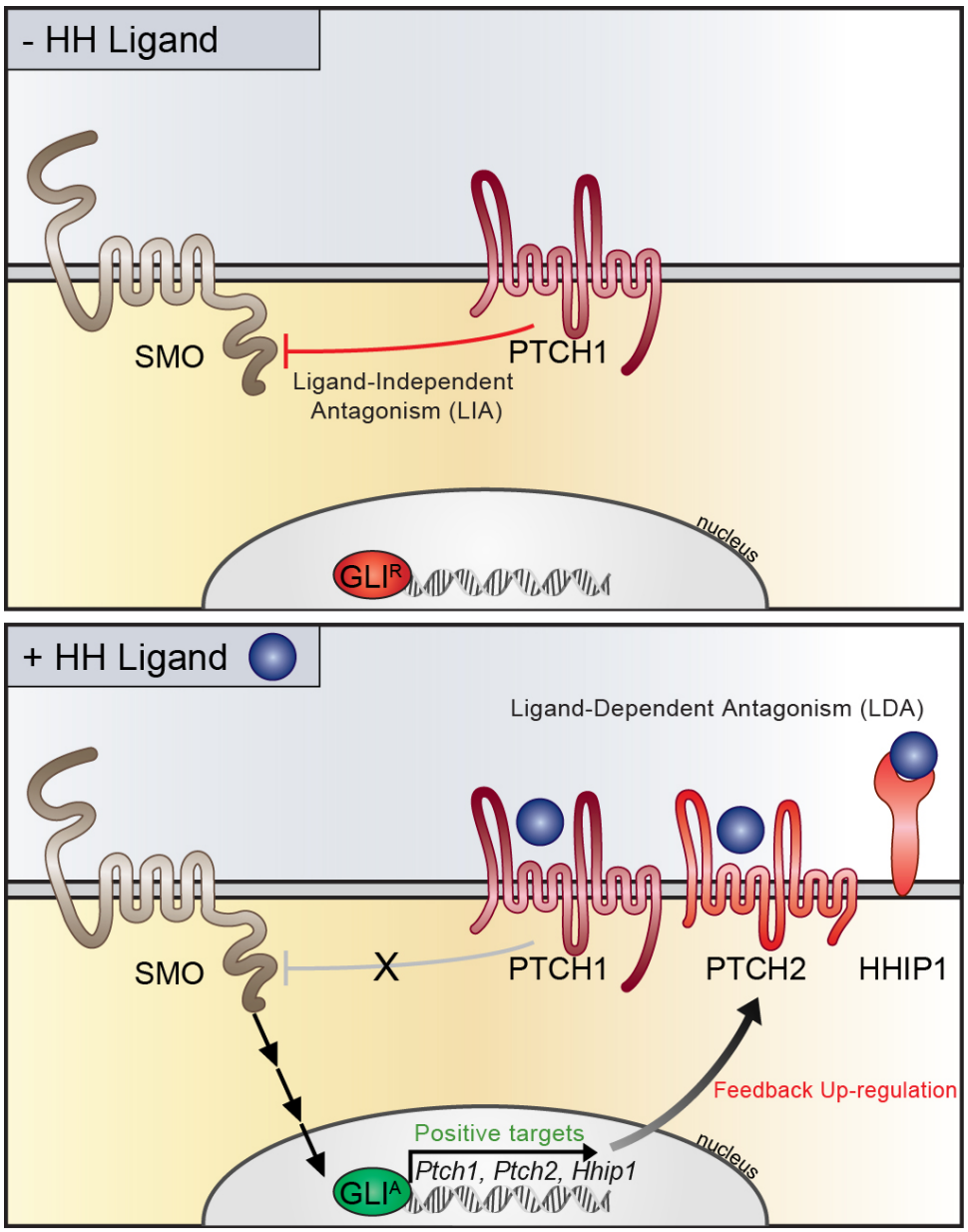


**Figure 1-3. Distinct mechanisms of HH pathway inhibition by cell surface molecules.** (Top panel) In the absence of HH ligand, PTCH1 inhibits the activity of SMO to prevent HH pathway activity in a process termed ligand-independent antagonism (LIA). (Bottom panel) Ligand-binding to PTCH1 relieves this inhibition, culminating in HH target gene expression including feedback up-regulation of *Ptch1*. High levels of PTCH1 at the cell surface binds ands sequesters HH ligands to restrict HH protein diffusion within a target field. Vertebrates possess two additional cell surface HH pathway antagonists, PTCH2 and HHIP1, that bind to HH ligands and are direct targets of the pathway.

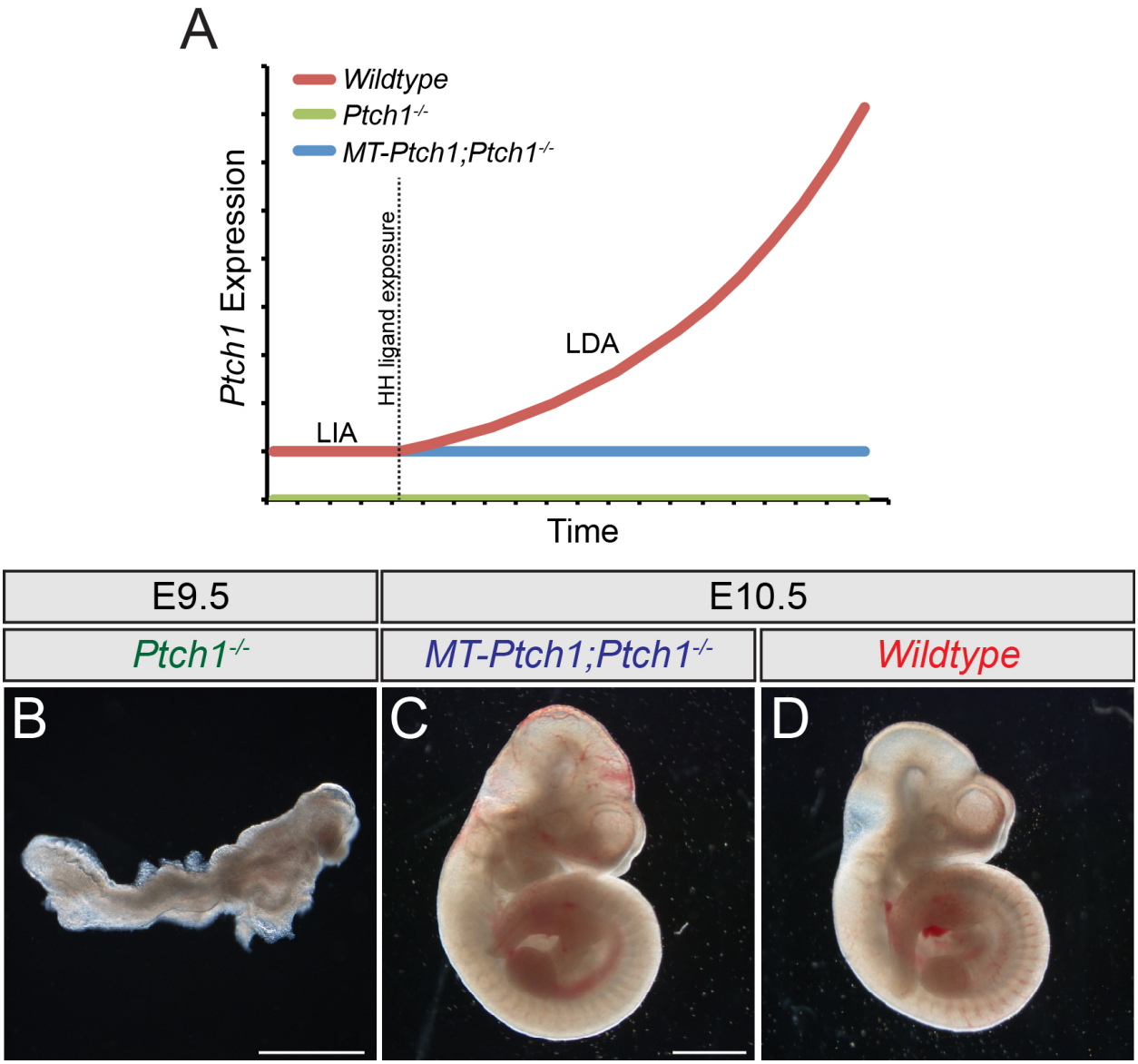


**Figure 1-4. An experimental model to dissociate LIA and LDA.** (A) A hypothetical model for the expression of *Ptch1* over time in a HH-responsive tissue during embryogenesis. (Red line) While low levels of *Ptch1* are required to inhibit SMO activity (LIA), initiation of HH signaling (dotted line) leads to feedback up-regulation of *Ptch1* to bind and sequester HH ligands (LDA). While there is no *Ptch1* expression in *Ptch1*$^{-/-}$ embryos (green line), LIA can be restored by a transgene expressing tonic levels of *Ptch1* from the metallothionein promoter (blue line). In *MT-Ptch1;Ptch1*$^{-/-}$ embryos, there are sufficient levels of *Ptch1* for LIA of SMO, but no feedback up-regulation of *Ptch1* occurs in response to HH signaling (LDA, blue line). (B-D) Whole mount images of *Ptch1*$^{-/-}$ (B), *MT-Ptch1;Ptch1*$^{-/-}$ (C), and *wildtype* embryos (D) at E9.5 (B) and E10.5 (C, D). While *Ptch1*$^{-/-}$ embryos die at E9.5 and exhibit severe developmental defects due to constitutive HH signaling (B), *MT-Ptch1;Ptch1*$^{-/-}$ animals are nearly indistinguishable from *wildtype* embryos at E10.5 (compare C, D). This demonstrates sufficient rescue of LIA by the *MT-Ptch1* transgene and suggests that LDA of HH signaling might play a limited role to restrict HH signaling in vertebrates. Image in B was provided by Irene Althaus. Scale bar (B) 1000 μm.

## 1.6 References


Aberger, F., and A. Ruiz i Altaba. 2014. Context-dependent signal integration by the GLI code: the oncogenic load, pathways, modifiers and implications for cancer therapy. *Semin. Cell Dev. Biol.* 33:93–104. doi:10.1016/j.semcdb.2014.05.003.

Adolphe, C., E. Nieuwenhuis, R. Villani, Z.J. Li, P. Kaur, C.-C. Hui, and B.J. Wainwright. 2014. Patched 1 and patched 2 redundancy has a key role in regulating epidermal differentiation. *J. Invest. Dermatol.* 134:1981–1990. doi:10.1038/jid.2014.63.

Adolphe, C., R. Hetherington, T. Ellis, and B. Wainwright. 2006. Patched1 functions as a gatekeeper by promoting cell cycle progression. *Cancer Research*. 66:2081–2088. doi:10.1158/0008-5472.CAN-05-2146.

Ahn, J., H.J. Lüdecke, S. Lindow, W.A. Horton, B. Lee, M.J. Wagner, B. Horsthemke, and D.E. Wells. 1995. Cloning of the putative tumour suppressor gene for hereditary multiple exostoses (EXT1). *Nat Genet*. 11:137–143. doi:10.1038/ng1095-137.

Alcedo, J., M. Ayzenzon, T. Von Ohlen, M. Noll, and J.E. Hooper. 1996. The Drosophila smoothened gene encodes a seven-pass membrane protein, a putative receptor for the hedgehog signal. *Cell*. 86:221–232.

Alexandre, C., A. Jacinto, and P.W. Ingham. 1996. Transcriptional activation of hedgehog target genes in Drosophila is mediated directly by the cubitus interruptus protein, a member of the GLI family of zinc finger DNA-binding proteins. *Genes & Development*. 10:2003–2013.

Allen, B.L., and A.C. Rapraeger. 2003. Spatial and temporal expression of heparan sulfate in mouse development regulates FGF and FGF receptor assembly. *J. Cell Biol.* 163:637–648. doi:10.1083/jcb.200307053.

Allen, B.L., J.Y. Song, L. Izzi, I.W. Althaus, J.-S. Kang, F. Charron, R.S. Krauss, and A.P. McMahon. 2011. Overlapping roles and collective requirement for the coreceptors GAS1, CDO, and BOC in SHH pathway function. *Dev. Cell*. 20:775–787. doi:10.1016/j.devcel.2011.04.018.

Allen, B.L., T. Tenzen, and A.P. McMahon. 2007. The Hedgehog-binding proteins Gas1 and Cdo cooperate to positively regulate Shh signaling during mouse development. *Genes & Development*. 21:1244–1257. doi:10.1101/gad.1543607.

Amakye, D., Z. Jagani, and M. Dorsch. 2013. Unraveling the therapeutic potential of the Hedgehog pathway in cancer. *Nat. Med.* 19:1410–1422. doi:10.1038/nm.3389.

Amanai, K., and J. Jiang. 2001. Distinct roles of Central missing and Dispatched in sending the Hedgehog signal. *Development*. 128:5119–5127.

Aszterbaum, M., A. Rothman, R.L. Johnson, M. Fisher, J. Xie, J.M. Bonifas, X. Zhang, M.P. Scott, and E.H. Epstein. 1998. Identification of mutations in the human PATCHED gene in sporadic basal cell carcinomas and in patients with the basal cell nevus syndrome. *J. Invest.*

*Dermatol.* 110:885–888. doi:10.1046/j.1523-1747.1998.00222.x.

Athar, M., C. Li, A.L. Kim, V.S. Spiegelman, and D.R. Bickers. 2014. Sonic hedgehog signaling in Basal cell nevus syndrome. *Cancer Research*. 74:4967–4975. doi:10.1158/0008-5472.CAN-14-1666.

Ayers, K.L., A. Gallet, L. Staccini-Lavenant, and P.P. Therond. 2010. The long-range activity of Hedgehog is regulated in the apical extracellular space by the glypican Dally and the hydrolase Notum. *Dev. Cell*. 18:605–620. doi:10.1016/j.devcel.2010.02.015.

Ayers, K.L., R. Mteirek, A. Cervantes, L. Lavenant-Staccini, P.P. Therond, and A. Gallet. 2012. Dally and Notum regulate the switch between low and high level Hedgehog pathway signalling. *Development*. 139:3168–3179. doi:10.1242/dev.078402.

Bae, G.-U., S. Domené, E. Roessler, K. Schachter, J.-S. Kang, M. Muenke, and R.S. Krauss. 2011. Mutations in CDON, encoding a hedgehog receptor, result in holoprosencephaly and defective interactions with other hedgehog receptors. *Am. J. Hum. Genet.* 89:231–240. doi:10.1016/j.ajhg.2011.07.001.

Balaskas, N., A. Ribeiro, J. Panovska, E. Dessaud, N. Sasai, K.M. Page, J. Briscoe, and V. Ribes. 2012. Gene regulatory logic for reading the sonic hedgehog signaling gradient in the vertebrate neural tube. *Cell*. 148:273–284. doi:10.1016/j.cell.2011.10.047.

Bandari, S., S. Exner, C. Ortmann, V. Bachvarova, A. Vortkamp, and K. Grobe. 2015. Sweet on hedgehogs: regulatory roles of heparan sulfate proteoglycans in hedgehog-dependent cell proliferation and differentiation. *Curr. Protein Pept. Sci.* 16:66–76.

Beachy, P.A., S.G. Hymowitz, R.A. Lazarus, D.J. Leahy, and C. Siebold. 2010. Interactions between Hedgehog proteins and their binding partners come into view. *Genes & Development*. 24:2001–2012. doi:10.1101/gad.1951710.

Bellaiche, Y., I. The, and N. Perrimon. 1998. Tout-velu is a Drosophila homologue of the putative tumour suppressor EXT-1 and is needed for Hh diffusion. *Nature*. 394:85–88. doi:10.1038/27932.

Belloni, E., M. Muenke, E. Roessler, G. Traverso, J. Siegel-Bartelt, A. Frumkin, H.F. Mitchell, H. Donis-Keller, C. Helms, A.V. Hing, H.H. Heng, B. Koop, D. Martindale, J.M. Rommens, L.C. Tsui, and S.W. Scherer. 1996. Identification of Sonic hedgehog as a candidate gene responsible for holoprosencephaly. *Nat Genet*. 14:353–356. doi:10.1038/ng1196-353.

Bellusci, S., J. Grindley, H. Emoto, N. Itoh, and B.L. Hogan. 1997a. Fibroblast growth factor 10 (FGF10) and branching morphogenesis in the embryonic mouse lung. *Development*. 124:4867–4878.

Bellusci, S., Y. Furuta, M.G. Rush, R. Henderson, G. Winnier, and B.L. Hogan. 1997b. Involvement of Sonic hedgehog (Shh) in mouse embryonic lung growth and morphogenesis. *Development*. 124:53–63.

Bergeron, S.A., O.V. Tyurina, E. Miller, A. Bagas, and R.O. Karlstrom. 2011. Brother of cdo (umleitung) is cell-autonomously required for Hedgehog-mediated ventral CNS patterning in the zebrafish. *Development*. 138:75–85. doi:10.1242/dev.057950.

Berman, D.M., S.S. Karhadkar, A. Maitra, R. Montes De Oca, M.R. Gerstenblith, K. Briggs, A.R. Parker, Y. Shimada, J.R. Eshleman, D.N. Watkins, and P.A. Beachy. 2003. Widespread requirement for Hedgehog ligand stimulation in growth of digestive tract tumours. *Nature*. 425:846–851. doi:10.1038/nature01972.

Bidet, M., O. Joubert, B. Lacombe, M. Ciantar, R. Nehmé, P. Mollat, L. Brétillon, H. Faure, R. Bittman, M. Ruat, and I. Mus-Veteau. 2011. The hedgehog receptor patched is involved in cholesterol transport. *PLoS ONE*. 6:e23834. doi:10.1371/journal.pone.0023834.

Binns, W., L.F. James, J.L. Shupe, and G. Everett. 1963. A congenital cyclopian- type malformation in lambs induced by maternal ingestion of a range plant, Veratrum californicum. *Am. J. Vet. Res.* 24:1164–1175.

Bischoff, M., A.-C. Gradilla, I. Seijo, G. Andrés, C. Rodríguez-Navas, L. González-Méndez, and I. Guerrero. 2013. Cytonemes are required for the establishment of a normal Hedgehog morphogen gradient in Drosophila epithelia. *Nat. Cell Biol.* 15:1269–1281. doi:10.1038/ncb2856.

Bishop, B., A.R. Aricescu, K. Harlos, C.A. O'Callaghan, E.Y. Jones, and C. Siebold. 2009. Structural insights into hedgehog ligand sequestration by the human hedgehog-interacting protein HHIP. *Nature Publishing Group*. 16:698–703. doi:10.1038/nsmb.1607.

Bosanac, I., H.R. Maun, S.J. Scales, X. Wen, A. Lingel, J.F. Bazan, F.J. de Sauvage, S.G. Hymowitz, and R.A. Lazarus. 2009. The structure of SHH in complex with HHIP reveals a recognition role for the Shh pseudo active site in signaling. *Nature Publishing Group*. 16:691–697. doi:10.1038/nsmb.1632.

Bosse, K., R.C. Betz, Y.A. Lee, T.F. Wienker, A. Reis, H. Kleen, P. Propping, S. Cichon, and M.M. Nöthen. 2000. Localization of a gene for syndactyly type 1 to chromosome 2q34-q36. *Am. J. Hum. Genet.* 67:492–497. doi:10.1086/303028.

Bridge, J.A., J. Liu, V. Weibolt, K.S. Baker, D. Perry, R. Kruger, S. Qualman, F. Barr, P. Sorensen, T. Triche, and R. Suijkerbuijk. 2000. Novel genomic imbalances in embryonal rhabdomyosarcoma revealed by comparative genomic hybridization and fluorescence in situ hybridization: an intergroup rhabdomyosarcoma study. *Genes Chromosomes Cancer*. 27:337–344.

Briscoe, J., A. Pierani, T.M. Jessell, and J. Ericson. 2000. A homeodomain protein code specifies progenitor cell identity and neuronal fate in the ventral neural tube. *Cell*. 101:435–445.

Briscoe, J., L. Sussel, P. Serup, D. Hartigan-O'Connor, T.M. Jessell, J.L. Rubenstein, and J. Ericson. 1999. Homeobox gene Nkx2.2 and specification of neuronal identity by graded Sonic hedgehog signalling. *Nature*. 398:622–627. doi:10.1038/19315.

Bumcrot, D.A., R. Takada, and A.P. McMahon. 1995. Proteolytic processing yields two secreted forms of sonic hedgehog. *Mol. Cell. Biol.* 15:2294–2303.

Burke, R., D. Nellen, M. Bellotto, E. Hafen, K.A. Senti, B.J. Dickson, and K. Basler. 1999. Dispatched, a novel sterol-sensing domain protein dedicated to the release of cholesterol-modified hedgehog from signaling cells. *Cell*. 99:803–815.

Cabrera, J.R., L. Sanchez-Pulido, A.M. Rojas, A. Valencia, S. Mañes, J.R. Naranjo, and B. Mellström. 2006. Gas1 is related to the glial cell-derived neurotrophic factor family receptors alpha and regulates Ret signaling. *J. Biol. Chem.* 281:14330–14339. doi:10.1074/jbc.M509572200.

Callejo, A., J. Culi, and I. Guerrero. 2008. Patched, the receptor of Hedgehog, is a lipoprotein receptor. *Proceedings of the National Academy of Sciences of the United States of America*. 105:912–917. doi:10.1073/pnas.0705603105.

Camp, D., K. Currie, A. Labbé, D.J. van Meyel, and F. Charron. 2010. Ihog and Boi are essential for Hedgehog signaling in Drosophila. *Neural Development*. 5:28. doi:10.1186/1749-8104-5-28.

Cano-Gauci, D.F., H.H. Song, H. Yang, C. McKerlie, B. Choo, W. Shi, R. Pullano, T.D. Piscione, S. Grisaru, S. Soon, L. Sedlackova, A.K. Tanswell, T.W. Mak, H. Yeger, G.A. Lockwood, N.D. Rosenblum, and J. Filmus. 1999. Glypican-3-deficient mice exhibit developmental overgrowth and some of the abnormalities typical of Simpson-Golabi-Behmel syndrome. *J. Cell Biol.* 146:255–264.

Capdevila, J., F. Pariente, J. Sampedro, J.L. Alonso, and I. Guerrero. 1994a. Subcellular localization of the segment polarity protein patched suggests an interaction with the wingless reception complex in Drosophila embryos. *Development*. 120:987–998.

Capdevila, J., M.P. Estrada, E. Sánchez-Herrero, and I. Guerrero. 1994b. The Drosophila segment polarity gene patched interacts with decapentaplegic in wing development. *EMBO J.* 13:71–82.

Capurro, M., W. Shi, T. Izumikawa, and J. Filmus. 2015. Processing by convertases is required for Glypican-3-induced inhibition of Hedgehog signaling. *J. Biol. Chem.* doi:10.1074/jbc.M114.612705.

Capurro, M.I., F. Li, and J. Filmus. 2009. Overgrowth of a mouse model of Simpson-Golabi-Behmel syndrome is partly mediated by Indian hedgehog. *EMBO Rep*. 10:901–907. doi:10.1038/embor.2009.98.

Capurro, M.I., P. Xu, W. Shi, F. Li, A. Jia, and J. Filmus. 2008. Glypican-3 inhibits Hedgehog signaling during development by competing with patched for Hedgehog binding. *Dev. Cell*. 14:700–711. doi:10.1016/j.devcel.2008.03.006.

Capurro, M.I., W. Shi, and J. Filmus. 2012. LRP1 mediates Hedgehog-induced endocytosis of the GPC3-Hedgehog complex. *J. Cell. Sci.* 125:3380–3389. doi:10.1242/jcs.098889.

Cardin, A.D., and H.J. Weintraub. 1989. Molecular modeling of protein-glycosaminoglycan interactions. *Arteriosclerosis*. 9:21–32.

Cardozo, M.J., L. Sánchez-Arrones, A. Sandonis, C. Sánchez-Camacho, G. Gestri, S.W. Wilson, I. Guerrero, and P. Bovolenta. 2014. Cdon acts as a Hedgehog decoy receptor during proximal-distal patterning of the optic vesicle. *Nat Commun*. 5:4272. doi:10.1038/ncomms5272.

Carpenter, D., D.M. Stone, J. Brush, A. Ryan, M. Armanini, G. Frantz, A. Rosenthal, and F.J. de Sauvage. 1998. Characterization of two patched receptors for the vertebrate hedgehog protein family. *Proceedings of the National Academy of Sciences of the United States of America*. 95:13630–13634.

Carstea, E.D., J.A. Morris, K.G. Coleman, S.K. Loftus, D. Zhang, C. Cummings, J. Gu, M.A. Rosenfeld, W.J. Pavan, D.B. Krizman, J. Nagle, M.H. Polymeropoulos, S.L. Sturley, Y.A. Ioannou, M.E. Higgins, M. Comly, A. Cooney, A. Brown, C.R. Kaneski, E.J. Blanchette-Mackie, N.K. Dwyer, E.B. Neufeld, T.Y. Chang, L. Liscum, J.F. Strauss, K. Ohno, M. Zeigler, R. Carmi, J. Sokol, D. Markie, R.R. O'Neill, O.P. van Diggelen, M. Elleder, M.C. Patterson, R.O. Brady, M.T. Vanier, P.G. Pentchev, and D.A. Tagle. 1997. Niemann-Pick C1 disease gene: homology to mediators of cholesterol homeostasis. *Science*. 277:228–231.

Caspary, T., M.J. García-García, D. Huangfu, J.T. Eggenschwiler, M.R. Wyler, A.S. Rakeman, H.L. Alcorn, and K.V. Anderson. 2002. Mouse Dispatched homolog1 is required for long-range, but not juxtacrine, Hh signaling. *Current Biology*. 12:1628–1632.

Castaldi, P.J., M.H. Cho, R.S.J. Estépar, M.-L.N. McDonald, N. Laird, T.H. Beaty, G. Washko, J.D. Crapo, E.K. Silverman, on behalf of the COPDGene Investigators. 2014. Genome-Wide Association Identifies Regulatory Loci Associated with Distinct Local Histogram Emphysema Patterns. *Am. J. Respir. Crit. Care Med.* doi:10.1164/rccm.201403-0569OC.

Chamoun, Z., R.K. Mann, D. Nellen, D.P. von Kessler, M. Bellotto, P.A. Beachy, and K. Basler. 2001. Skinny hedgehog, an acyltransferase required for palmitoylation and activity of the hedgehog signal. *Science*. 293:2080–2084. doi:10.1126/science.1064437.

Chan, J.A., S. Balasubramanian, R.M. Witt, K.J. Nazemi, Y. Choi, M.F. Pazyra-Murphy, C.O. Walsh, M. Thompson, and R.A. Segal. 2009. Proteoglycan interactions with Sonic Hedgehog specify mitogenic responses. *Nat. Neurosci.* 12:409–417. doi:10.1038/nn.2287.

Chang, A.L.S., and A.E. Oro. 2012. Initial assessment of tumor regrowth after vismodegib in advanced Basal cell carcinoma. *Arch Dermatol*. 148:1324–1325. doi:10.1001/archdermatol.2012.2354.

Chang, D.T., A. López, D.P. von Kessler, C. Chiang, B.K. Simandl, R. Zhao, M.F. Seldin, J.F. Fallon, and P.A. Beachy. 1994. Products, genetic linkage and limb patterning activity of a murine hedgehog gene. *Development*. 120:3339–3353.

Chang, S.-C., B. Mulloy, A.I. Magee, and J.R. Couchman. 2011. Two distinct sites in sonic Hedgehog combine for heparan sulfate interactions and cell signaling functions. *J. Biol.*

*Chem.* 286:44391–44402. doi:10.1074/jbc.M111.285361.

Chen, J.K., J. Taipale, K.E. Young, T. Maiti, and P.A. Beachy. 2002a. Small molecule modulation of Smoothened activity. *Proceedings of the National Academy of Sciences of the United States of America*. 99:14071–14076. doi:10.1073/pnas.182542899.

Chen, J.K., J. Taipale, M.K. Cooper, and P.A. Beachy. 2002b. Inhibition of Hedgehog signaling by direct binding of cyclopamine to Smoothened. *Genes & Development*. 16:2743–2748. doi:10.1101/gad.1025302.

Chen, M.-H., Y.-J. Li, T. Kawakami, S.-M. Xu, and P.-T. Chuang. 2004. Palmitoylation is required for the production of a soluble multimeric Hedgehog protein complex and long-range signaling in vertebrates. *Genes & Development*. 18:641–659. doi:10.1101/gad.1185804.

Chen, Y., and G. Struhl. 1996. Dual roles for patched in sequestering and transducing Hedgehog. *Cell*. 87:553–563.

Chiang, C., Y. Litingtung, E. Lee, K.E. Young, J.L. Corden, H. Westphal, and P.A. Beachy. 1996. Cyclopia and defective axial patterning in mice lacking Sonic hedgehog gene function. *Nature*. 383:407–413. doi:10.1038/383407a0.

Chidambaram, A., A.M. Goldstein, M.R. Gailani, B. Gerrard, S.J. Bale, J.J. DiGiovanna, A.E. Bale, and M. Dean. 1996. Mutations in the human homologue of the Drosophila patched gene in Caucasian and African-American nevoid basal cell carcinoma syndrome patients. *Cancer Research*. 56:4599–4601.

Christ, A., A. Christa, E. Kur, O. Lioubinski, S. Bachmann, T.E. Willnow, and A. Hammes. 2012. LRP2 Is an Auxiliary SHH Receptor Required to Condition the Forebrain Ventral Midline for Inductive Signals. *Dev. Cell*. 22:268–278. doi:10.1016/j.devcel.2011.11.023.

Chuang, P.T. 2003. Feedback control of mammalian Hedgehog signaling by the Hedgehog-binding protein, Hip1, modulates Fgf signaling during branching morphogenesis of the lung. *Genes & Development*. 17:342–347. doi:10.1101/gad.1026303.

Chuang, P.T., and A.P. McMahon. 1999. Vertebrate Hedgehog signalling modulated by induction of a Hedgehog-binding protein. *Nature*. 397:617–621. doi:10.1038/17611.

Cobourne, M.T., I. Miletich, and P.T. Sharpe. 2004. Restriction of sonic hedgehog signalling during early tooth development. *Development*. 131:2875–2885. doi:10.1242/dev.01163.

Cooper, A.F., K.P. Yu, M. Brueckner, L.L. Brailey, L. Johnson, J.M. McGrath, and A.E. Bale. 2005. Cardiac and CNS defects in a mouse with targeted disruption of suppressor of fused. *Development*. 132:4407–4417. doi:10.1242/dev.02021.

Cooper, M.K., C.A. Wassif, P.A. Krakowiak, J. Taipale, R. Gong, R.I. Kelley, F.D. Porter, and P.A. Beachy. 2003. A defective response to Hedgehog signaling in disorders of cholesterol biosynthesis. *Nat Genet*. 33:508–513. doi:10.1038/ng1134.

Cooper, M.K., J.A. Porter, K.E. Young, and P.A. Beachy. 1998. Teratogen-mediated inhibition of target tissue response to Shh signaling. *Science*. 280:1603–1607.

Corbit, K.C., P. Aanstad, V. Singla, A.R. Norman, D.Y.R. Stainier, and J.F. Reiter. 2005. Vertebrate Smoothened functions at the primary cilium. *Nature*. 437:1018–1021. doi:10.1038/nature04117.

Corcoran, R.B., and M.P. Scott. 2006. Oxysterols stimulate Sonic hedgehog signal transduction and proliferation of medulloblastoma cells. *Proceedings of the National Academy of Sciences of the United States of America*. 103:8408–8413. doi:10.1073/pnas.0602852103.

Cornesse, Y., T. Pieler, and T. Hollemann. 2005. Olfactory and lens placode formation is controlled by the hedgehog-interacting protein (Xhip) in Xenopus. *Developmental Biology*. 277:296–315. doi:10.1016/j.ydbio.2004.09.016.

Coulombe, J., E. Traiffort, K. Loulier, H. Faure, and M. Ruat. 2004. Hedgehog interacting protein in the mature brain: membrane-associated and soluble forms. *Molecular and Cellular Neuroscience*. 25:323–333. doi:10.1016/j.mcn.2003.10.024.

Creanga, A., T.D. Glenn, R.K. Mann, A.M. Saunders, W.S. Talbot, and P.A. Beachy. 2012. Scube/You activity mediates release of dually lipid-modified Hedgehog signal in soluble form. *Genes & Development*. 26:1312–1325. doi:10.1101/gad.191866.112.

Danesin, C., E. Agius, N. Escalas, X. Ai, C. Emerson, P. Cochard, and C. Soula. 2006. Ventral neural progenitors switch toward an oligodendroglial fate in response to increased Sonic hedgehog (Shh) activity: involvement of Sulfatase 1 in modulating Shh signaling in the ventral spinal cord. *J. Neurosci.* 26:5037–5048. doi:10.1523/JNEUROSCI.0715-06.2006.

Denef, N., D. Neubüser, L. Perez, and S.M. Cohen. 2000. Hedgehog induces opposite changes in turnover and subcellular localization of patched and smoothened. *Cell*. 102:521–531.

Desbordes, S.C., and B. Sanson. 2003. The glypican Dally-like is required for Hedgehog signalling in the embryonic epidermis of Drosophila. *Development*. 130:6245–6255. doi:10.1242/dev.00874.

Dessaud, E., L.L. Yang, K. Hill, B. Cox, F. Ulloa, A. Ribeiro, A. Mynett, B.G. Novitch, and J. Briscoe. 2007. Interpretation of the sonic hedgehog morphogen gradient by a temporal adaptation mechanism. *Nature*. 450:717–720. doi:10.1038/nature06347.

Dierker, T., R. Dreier, A. Petersen, C. Bordych, and K. Grobe. 2009. Heparan sulfate-modulated, metalloprotease-mediated sonic hedgehog release from producing cells. *J. Biol. Chem.* 284:8013–8022. doi:10.1074/jbc.M806838200.

Echelard, Y., D.J. Epstein, B. St-Jacques, L. Shen, J. Mohler, J.A. McMahon, and A.P. McMahon. 1993. Sonic hedgehog, a member of a family of putative signaling molecules, is implicated in the regulation of CNS polarity. *Cell*. 75:1417–1430.

Ericson, J., P. Rashbass, A. Schedl, S. Brenner-Morton, A. Kawakami, V. van Heyningen, T.M.

Jessell, and J. Briscoe. 1997. Pax6 controls progenitor cell identity and neuronal fate in response to graded Shh signaling. *Cell*. 90:169–180.

Erkan, M., S. Hausmann, C.W. Michalski, A.A. Fingerle, M. Dobritz, J. Kleeff, and H. Friess. 2012. The role of stroma in pancreatic cancer: diagnostic and therapeutic implications. *Nat Rev Gastroenterol Hepatol*. 9:454–467. doi:10.1038/nrgastro.2012.115.

Esko, J.D., and U. Lindahl. 2001. Molecular diversity of heparan sulfate. *J. Clin. Invest.* 108:169–173. doi:10.1172/JCI13530.

Eugster, C., D. Panáková, A. Mahmoud, and S. Eaton. 2007. Lipoprotein-heparan sulfate interactions in the Hh pathway. *Dev. Cell*. 13:57–71. doi:10.1016/j.devcel.2007.04.019.

Evans, D.G., E.J. Ladusans, S. Rimmer, L.D. Burnell, N. Thakker, and P.A. Farndon. 1993. Complications of the naevoid basal cell carcinoma syndrome: results of a population based study. *Journal of Medical Genetics*. 30:460–464.

Evans, D.G., P.A. Farndon, L.D. Burnell, H.R. Gattamaneni, and J.M. Birch. 1991. The incidence of Gorlin syndrome in 173 consecutive cases of medulloblastoma. *Br. J. Cancer*. 64:959–961.

Falkenstein, K.N., and S.A. Vokes. 2014. Transcriptional regulation of graded Hedgehog signaling. *Semin. Cell Dev. Biol.* 33:73–80. doi:10.1016/j.semcdb.2014.05.010.

Fan, Z., J. Li, J. Du, H. Zhang, Y. Shen, C.-Y. Wang, and S. Wang. 2008. A missense mutation in PTCH2 underlies dominantly inherited NBCCS in a Chinese family. *Journal of Medical Genetics*. 45:303–308. doi:10.1136/jmg.2007.055343.

Feng, J., B. White, O.V. Tyurina, B. Guner, T. Larson, H.Y. Lee, R.O. Karlstrom, and J.D. Kohtz. 2004. Synergistic and antagonistic roles of the Sonic hedgehog N- and C-terminal lipids. *Development*. 131:4357–4370. doi:10.1242/dev.01301.

Filmus, J., M. Capurro, and J. Rast. 2008. Glypicans. *Genome Biol.* 9:224. doi:10.1186/gb-2008-9-5-224.

Forbes, A.J., Y. Nakano, A.M. Taylor, and P.W. Ingham. 1993. Genetic analysis of hedgehog signalling in the Drosophila embryo. *Dev. Suppl.* 115–124.

Fujii, K., H. Ohashi, M. Suzuki, H. Hatsuse, T. Shiohama, H. Uchikawa, and T. Miyashita. 2013. Frameshift mutation in the PTCH2 gene can cause nevoid basal cell carcinoma syndrome. *Fam. Cancer*. 12:611–614. doi:10.1007/s10689-013-9623-1.

Gailani, M.R., M. Ståhle-Bäckdahl, D.J. Leffell, M. Glynn, P.G. Zaphiropoulos, C. Pressman, A.B. Undén, M. Dean, D.E. Brash, A.E. Bale, and R. Toftgård. 1996. The role of the human homologue of Drosophila patched in sporadic basal cell carcinomas. *Nat Genet*. 14:78–81. doi:10.1038/ng0996-78.

Gallet, A., L. Ruel, L. Staccini-Lavenant, and P.P. Therond. 2006. Cholesterol modification is

necessary for controlled planar long-range activity of Hedgehog in Drosophila epithelia. *Development*. 133:407–418. doi:10.1242/dev.02212.

Gallet, A., L. Staccini-Lavenant, and P.P. Therond. 2008. Cellular trafficking of the glypican Dally-like is required for full-strength Hedgehog signaling and wingless transcytosis. *Dev. Cell*. 14:712–725. doi:10.1016/j.devcel.2008.03.001.

Gallet, A., R. Rodriguez, L. Ruel, and P.P. Therond. 2003. Cholesterol modification of hedgehog is required for trafficking and movement, revealing an asymmetric cellular response to hedgehog. *Dev. Cell*. 4:191–204.

Gao, B., J. Guo, C. She, A. Shu, M. Yang, Z. Tan, X. Yang, S. Guo, G. Feng, and L. He. 2001. Mutations in IHH, encoding Indian hedgehog, cause brachydactyly type A-1. *Nat Genet*. 28:386–388. doi:10.1038/ng577.

García-García, M.J., and K.V. Anderson. 2003. Essential role of glycosaminoglycans in Fgf signaling during mouse gastrulation. *Cell*. 114:727–737.

Giraldez, A.J., R.R. Copley, and S.M. Cohen. 2002. HSPG modification by the secreted enzyme Notum shapes the Wingless morphogen gradient. *Dev. Cell*. 2:667–676.

Goodrich, L.V., L. Milenkovic, K.M. Higgins, and M.P. Scott. 1997. Altered neural cell fates and medulloblastoma in mouse patched mutants. *Science*. 277:1109–1113. doi:10.1126/science.277.5329.1109.

Goodrich, L.V., R.L. Johnson, L. Milenkovic, J.A. McMahon, and M.P. Scott. 1996. Conservation of the hedgehog/patched signaling pathway from flies to mice: induction of a mouse patched gene by Hedgehog. *Genes & Development*. 10:301–312.

Gorlin, R.J., and R.W. Goltz. 1960. Multiple nevoid basal-cell epithelioma, jaw cysts and bifid rib. A syndrome. *N. Engl. J. Med.* 262:908–912. doi:10.1056/NEJM196005052621803.

Grachtchouk, M., R. Mo, S. Yu, X. Zhang, H. Sasaki, C.C. Hui, and A.A. Dlugosz. 2000. Basal cell carcinomas in mice overexpressing Gli2 in skin. *Nat Genet*. 24:216–217. doi:10.1038/73417.

Grachtchouk, V., M. Grachtchouk, L. Lowe, T. Johnson, L. Wei, A. Wang, F. de Sauvage, and A.A. Dlugosz. 2003. The magnitude of hedgehog signaling activity defines skin tumor phenotype. *EMBO J.* 22:2741–2751. doi:10.1093/emboj/cdg271.

Hahn, H., C. Wicking, P.G. Zaphiropoulous, M.R. Gailani, S. Shanley, A. Chidambaram, I. Vorechovsky, E. Holmberg, A.B. Undén, S. Gillies, K. Negus, I. Smyth, C. Pressman, D.J. Leffell, B. Gerrard, A.M. Goldstein, M. Dean, R. Toftgård, G. Chenevix-Trench, B. Wainwright, and A.E. Bale. 1996. Mutations of the human homolog of Drosophila patched in the nevoid basal cell carcinoma syndrome. *Cell*. 85:841–851.

Hahn, H., L. Wojnowski, A.M. Zimmer, J. Hall, G. Miller, and A. Zimmer. 1998. Rhabdomyosarcomas and radiation hypersensitivity in a mouse model of Gorlin syndrome.

*Nat. Med.* 4:619–622.

Han, C., T.Y. Belenkaya, B. Wang, and X. Lin. 2004a. Drosophila glypicans control the cell-to-cell movement of Hedgehog by a dynamin-independent process. *Development*. 131:601–611. doi:10.1242/dev.00958.

Han, C., T.Y. Belenkaya, M. Khodoun, M. Tauchi, X. Lin, and X. Lin. 2004b. Distinct and collaborative roles of Drosophila EXT family proteins in morphogen signalling and gradient formation. *Development*. 131:1563–1575. doi:10.1242/dev.01051.

Hancock, D.B., M. Eijgelsheim, J.B. Wilk, S.A. Gharib, L.R. Loehr, K.D. Marciante, N. Franceschini, Y.M.T.A. van Durme, T.-H. Chen, R.G. Barr, M.B. Schabath, D.J. Couper, G.G. Brusselle, B.M. Psaty, C.M. van Duijn, J.I. Rotter, A.G. Uitterlinden, A. Hofman, N.M. Punjabi, F. Rivadeneira, A.C. Morrison, P.L. Enright, K.E. North, S.R. Heckbert, T. Lumley, B.H.C. Stricker, G.T. O'Connor, and S.J. London. 2010. Meta-analyses of genome-wide association studies identify multiple loci associated with pulmonary function. *Nat Genet*. 42:45–52. doi:10.1038/ng.500.

Hartman, T.R., D. Zinshteyn, H.K. Schofield, E. Nicolas, A. Okada, and A.M. O'Reilly. 2010. Drosophila Boi limits Hedgehog levels to suppress follicle stem cell proliferation. *J. Cell Biol.* 191:943–952. doi:10.1083/jcb.201007142.

Haycraft, C.J., B. Banizs, Y. Aydin-Son, Q. Zhang, E.J. Michaud, and B.K. Yoder. 2005. Gli2 and Gli3 localize to cilia and require the intraflagellar transport protein polaris for processing and function. *PLoS Genet.* 1:e53. doi:10.1371/journal.pgen.0010053.

Häcker, U., K. Nybakken, and N. Perrimon. 2005. Heparan sulphate proteoglycans: the sweet side of development. *Nat. Rev. Mol. Cell Biol.* 6:530–541. doi:10.1038/nrm1681.

Hettmer, S., L.A. Teot, P. van Hummelen, L. MacConaill, R.T. Bronson, C. Dall'Osso, J. Mao, A.P. McMahon, P.J. Gruber, H.E. Grier, C. Rodriguez-Galindo, C.D. Fletcher, and A.J. Wagers. 2013. Mutations in Hedgehog pathway genes in fetal rhabdomyomas. *J. Pathol.* 231:44–52. doi:10.1002/path.4229.

Hidalgo, A., and P. Ingham. 1990. Cell patterning in the Drosophila segment: spatial regulation of the segment polarity gene patched. *Development*. 110:291–301.

Hilton, M.J., L. Gutiérrez, D.A. Martinez, and D.E. Wells. 2005. EXT1 regulates chondrocyte proliferation and differentiation during endochondral bone development. *Bone*. 36:379–386. doi:10.1016/j.bone.2004.09.025.

Hoff, Von, D.D., P.M. LoRusso, C.M. Rudin, J.C. Reddy, R.L. Yauch, R. Tibes, G.J. Weiss, M.J. Borad, C.L. Hann, J.R. Brahmer, H.M. Mackey, B.L. Lum, W.C. Darbonne, J.C. Marsters, F.J. de Sauvage, and J.A. Low. 2009. Inhibition of the hedgehog pathway in advanced basal-cell carcinoma. *N. Engl. J. Med.* 361:1164–1172. doi:10.1056/NEJMoa0905360.

Hollway, G.E., J. Maule, P. Gautier, T.M. Evans, D.G. Keenan, C. Lohs, D. Fischer, C. Wicking,

and P.D. Currie. 2006. Scube2 mediates Hedgehog signalling in the zebrafish embryo. *Developmental Biology*. 294:104–118. doi:10.1016/j.ydbio.2006.02.032.

Holtz, A.M., K.A. Peterson, Y. Nishi, S. Morin, J.Y. Song, F. Charron, A.P. McMahon, and B.L. Allen. 2013. Essential role for ligand-dependent feedback antagonism of vertebrate hedgehog signaling by PTCH1, PTCH2 and HHIP1 during neural patterning. *Development*. 140:3423–3434. doi:10.1242/dev.095083.

Hooper, J.E., and M.P. Scott. 1989. The Drosophila patched gene encodes a putative membrane protein required for segmental patterning. *Cell*. 59:751–765.

Huang, S., Z. Zhang, C. Zhang, X. Lv, X. Zheng, Z. Chen, L. Sun, H. Wang, Y. Zhu, J. Zhang, S. Yang, Y. Lu, Q. Sun, Y. Tao, F. Liu, Y. Zhao, and D. Chen. 2013. Activation of Smurf E3 ligase promoted by smoothened regulates hedgehog signaling through targeting patched turnover. *PLoS Biol*. 11:e1001721. doi:10.1371/journal.pbio.1001721.

Huangfu, D., A. Liu, A.S. Rakeman, N.S. Murcia, L. Niswander, and K.V. Anderson. 2003. Hedgehog signalling in the mouse requires intraflagellar transport proteins. *Nature*. 426:83–87. doi:10.1038/nature02061.

Hui, C.-C., and S. Angers. 2011. Gli proteins in development and disease. *Annu. Rev. Cell Dev. Biol.* 27:513–537. doi:10.1146/annurev-cellbio-092910-154048.

Hutchin, M.E., M.S.T. Kariapper, M. Grachtchouk, A. Wang, L. Wei, D. Cummings, J. Liu, L.E. Michael, A. Glick, and A.A. Dlugosz. 2005. Sustained Hedgehog signaling is required for basal cell carcinoma proliferation and survival: conditional skin tumorigenesis recapitulates the hair growth cycle. *Genes & Development*. 19:214–223. doi:10.1101/gad.1258705.

Incardona, J.P., J. Gruenberg, and H. Roelink. 2002. Sonic hedgehog induces the segregation of patched and smoothened in endosomes. *Current Biology*. 12:983–995.

Ingham, P.W., A.M. Taylor, and Y. Nakano. 1991. Role of the Drosophila patched gene in positional signalling. *Nature*. 353:184–187. doi:10.1038/353184a0.

Italiano, A., A. Le Cesne, C. Bellera, S. Piperno-Neumann, F. Duffaud, N. Penel, P. Cassier, J. Domont, N. Takebe, M. Kind, J.-M. Coindre, J.-Y. Blay, and B. Bui. 2013. GDC-0449 in patients with advanced chondrosarcomas: a French Sarcoma Group/US and French National Cancer Institute Single-Arm Phase II Collaborative Study. *Ann. Oncol.* 24:2922–2926. doi:10.1093/annonc/mdt391.

Izzi, L., M. Lévesque, S. Morin, D. Laniel, B.C. Wilkes, F. Mille, R.S. Krauss, A.P. McMahon, B.L. Allen, and F. Charron. 2011. Boc and Gas1 each form distinct Shh receptor complexes with Ptch1 and are required for Shh-mediated cell proliferation. *Dev. Cell*. 20:788–801. doi:10.1016/j.devcel.2011.04.017.

Jeong, J., and A.P. McMahon. 2005. Growth and pattern of the mammalian neural tube are governed by partially overlapping feedback activities of the hedgehog antagonists patched 1 and Hhip1. *Development*. 132:143–154. doi:10.1242/dev.01566.

Johnson, J.-L.F.A., T.E. Hall, J.M. Dyson, C. Sonntag, K. Ayers, S. Berger, P. Gautier, C. Mitchell, G.E. Hollway, and P.D. Currie. 2012. Scube activity is necessary for Hedgehog signal transduction in vivo. *Developmental Biology*. 368:193–202. doi:10.1016/j.ydbio.2012.05.007.

Johnson, R.L., A.L. Rothman, J. Xie, L.V. Goodrich, J.W. Bare, J.M. Bonifas, A.G. Quinn, R.M. Myers, D.R. Cox, E.H. Epstein, and M.P. Scott. 1996. Human homolog of patched, a candidate gene for the basal cell nevus syndrome. *Science*. 272:1668–1671.

Johnson, R.L., J.K. Grenier, and M.P. Scott. 1995. patched overexpression alters wing disc size and pattern: transcriptional and post-transcriptional effects on hedgehog targets. *Development*. 121:4161–4170.

Johnson, R.L., L. Zhou, and E.C. Bailey. 2002. Distinct consequences of sterol sensor mutations in Drosophila and mouse patched homologs. *Developmental Biology*. 242:224–235. doi:10.1006/dbio.2001.0524.

Kang, J.-S., P.J. Mulieri, Y. Hu, L. Taliana, and R.S. Krauss. 2002. BOC, an Ig superfamily member, associates with CDO to positively regulate myogenic differentiation. *EMBO J.* 21:114–124. doi:10.1093/emboj/21.1.114.

Kang, J.S., M. Gao, J.L. Feinleib, P.D. Cotter, S.N. Guadagno, and R.S. Krauss. 1997. CDO: an oncogene-, serum-, and anchorage-regulated member of the Ig/fibronectin type III repeat family. *J. Cell Biol.* 138:203–213.

Kawahira, H., N.H. Ma, E.S. Tzanakakis, A.P. McMahon, P.-T. Chuang, and M. Hebrok. 2003. Combined activities of hedgehog signaling inhibitors regulate pancreas development. *Development*. 130:4871–4879. doi:10.1242/dev.00653.

Kawakami, A., Y. Nojima, A. Toyoda, M. Takahoko, M. Satoh, H. Tanaka, H. Wada, I. Masai, H. Terasaki, Y. Sakaki, H. Takeda, and H. Okamoto. 2005. The zebrafish-secreted matrix protein you/scube2 is implicated in long-range regulation of hedgehog signaling. *Current Biology*. 15:480–488. doi:10.1016/j.cub.2005.02.018.

Kawakami, T., T. Kawcak, Y.-J. Li, W. Zhang, Y. Hu, and P.-T. Chuang. 2002. Mouse dispatched mutants fail to distribute hedgehog proteins and are defective in hedgehog signaling. *Development*. 129:5753–5765.

Kawamura, S., K. Hervold, F.-A. Ramirez-Weber, and T.B. Kornberg. 2008. Two patched protein subtypes and a conserved domain of group I proteins that regulates turnover. *J. Biol. Chem.* 283:30964–30969. doi:10.1074/jbc.M806242200.

Khaliullina, H., D. Panáková, C. Eugster, F. Riedel, M. Carvalho, and S. Eaton. 2009. Patched regulates Smoothened trafficking using lipoprotein-derived lipids. *Development*. 136:4111–4121. doi:10.1242/dev.041392.

Kohtz, J.D., H.Y. Lee, N. Gaiano, J. Segal, E. Ng, T. Larson, D.P. Baker, E.A. Garber, K.P. Williams, and G. Fishell. 2001. N-terminal fatty-acylation of sonic hedgehog enhances the

induction of rodent ventral forebrain neurons. *Development*. 128:2351–2363.

Kornberg, T.B., and S. Roy. 2014. Cytonemes as specialized signaling filopodia. *Development*. 141:729–736. doi:10.1242/dev.086223.

Koudijs, M.J., M.J. den Broeder, A. Keijser, E. Wienholds, S. Houwing, E.M.H.C. van Rooijen, R. Geisler, and F.J.M. van Eeden. 2005. The zebrafish mutants dre, uki, and lep encode negative regulators of the hedgehog signaling pathway. *PLoS Genet.* 1:e19. doi:10.1371/journal.pgen.0010019.

Koudijs, M.J., M.J. den Broeder, E. Groot, and F.J. van Eeden. 2008. Genetic analysis of the two zebrafish patched homologues identifies novel roles for the hedgehog signaling pathway. *BMC Developmental Biology*. 8:15. doi:10.1186/1471-213X-8-15.

Koziel, L., M. Kunath, O.G. Kelly, and A. Vortkamp. 2004. Ext1-dependent heparan sulfate regulates the range of Ihh signaling during endochondral ossification. *Dev. Cell*. 6:801–813. doi:10.1016/j.devcel.2004.05.009.

Krauss, S., J.P. Concordet, and P.W. Ingham. 1993. A functionally conserved homolog of the Drosophila segment polarity gene hh is expressed in tissues with polarizing activity in zebrafish embryos. *Cell*. 75:1431–1444.

Lee, C.S., L. Buttitta, and C.M. Fan. 2001a. Evidence that the WNT-inducible growth arrest-specific gene 1 encodes an antagonist of sonic hedgehog signaling in the somite. *Proceedings of the National Academy of Sciences of the United States of America*. 98:11347–11352. doi:10.1073/pnas.201418298.

Lee, C.S., N.R. May, and C.M. Fan. 2001b. Transdifferentiation of the ventral retinal pigmented epithelium to neural retina in the growth arrest specific gene 1 mutant. *Developmental Biology*. 236:17–29. doi:10.1006/dbio.2001.0280.

Lee, J.D., and J.E. Treisman. 2001. Sightless has homology to transmembrane acyltransferases and is required to generate active Hedgehog protein. *Current Biology*. 11:1147–1152.

Lee, J.D., P. Kraus, N. Gaiano, S. Nery, J. Kohtz, G. Fishell, C.A. Loomis, and J.E. Treisman. 2001c. An acylatable residue of Hedgehog is differentially required in Drosophila and mouse limb development. *Developmental Biology*. 233:122–136. doi:10.1006/dbio.2001.0218.

Lee, J.J., D.P. von Kessler, S. Parks, and P.A. Beachy. 1992. Secretion and localized transcription suggest a role in positional signaling for products of the segmentation gene hedgehog. *Cell*. 71:33–50.

Lee, J.J., R.M. Perera, H. Wang, D.-C. Wu, X.S. Liu, S. Han, J. Fitamant, P.D. Jones, K.S. Ghanta, S. Kawano, J.M. Nagle, V. Deshpande, Y. Boucher, T. Kato, J.K. Chen, J.K. Willmann, N. Bardeesy, and P.A. Beachy. 2014. Stromal response to Hedgehog signaling restrains pancreatic cancer progression. *Proceedings of the National Academy of Sciences of the United States of America*. 111:E3091–100. doi:10.1073/pnas.1411679111.

Lee, J.J., S.C. Ekker, D.P. von Kessler, J.A. Porter, B.I. Sun, and P.A. Beachy. 1994. Autoproteolysis in hedgehog protein biogenesis. *Science*. 266:1528–1537.

Lee, Y., H.L. Miller, H.R. Russell, K. Boyd, T. Curran, and P.J. McKinnon. 2006. Patched2 modulates tumorigenesis in patched1 heterozygous mice. *Cancer Research*. 66:6964–6971. doi:10.1158/0008-5472.CAN-06-0505.

Lewis, P.M., M.P. Dunn, J.A. McMahon, M. Logan, J.F. Martin, B. St-Jacques, and A.P. McMahon. 2001. Cholesterol modification of sonic hedgehog is required for long-range signaling activity and effective modulation of signaling by Ptc1. *Cell*. 105:599–612.

Li, F., W. Shi, M. Capurro, and J. Filmus. 2011a. Glypican-5 stimulates rhabdomyosarcoma cell proliferation by activating Hedgehog signaling. *J. Cell Biol.* 192:691–704. doi:10.1083/jcb.201008087.

Li, X., T.D. Howard, W.C. Moore, E.J. Ampleford, H. Li, W.W. Busse, W.J. Calhoun, M. Castro, K.F. Chung, S.C. Erzurum, A.M. Fitzpatrick, B. Gaston, E. Israel, N.N. Jarjour, W.G. Teague, S.E. Wenzel, S.P. Peters, G.A. Hawkins, E.R. Bleecker, and D.A. Meyers. 2011b. Importance of hedgehog interacting protein and other lung function genes in asthma. *J. Allergy Clin. Immunol.* 127:1457–1465. doi:10.1016/j.jaci.2011.01.056.

Li, Y., H. Zhang, Y. Litingtung, and C. Chiang. 2006. Cholesterol modification restricts the spread of Shh gradient in the limb bud. *Proceedings of the National Academy of Sciences of the United States of America*. 103:6548–6553. doi:10.1073/pnas.0600124103.

Lin, X. 2004. Functions of heparan sulfate proteoglycans in cell signaling during development. *Development*. 131:6009–6021. doi:10.1242/dev.01522.

Lin, X., G. Wei, Z. Shi, L. Dryer, J.D. Esko, D.E. Wells, and M.M. Matzuk. 2000. Disruption of gastrulation and heparan sulfate biosynthesis in EXT1-deficient mice. *Developmental Biology*. 224:299–311. doi:10.1006/dbio.2000.9798.

Lind, T., F. Tufaro, C. McCormick, U. Lindahl, and K. Lidholt. 1998. The putative tumor suppressors EXT1 and EXT2 are glycosyltransferases required for the biosynthesis of heparan sulfate. *J. Biol. Chem.* 273:26265–26268.

Litingtung, Y., L. Lei, H. Westphal, and C. Chiang. 1998. Sonic hedgehog is essential to foregut development. *Nat Genet*. 20:58–61. doi:10.1038/1717.

Liu, Y., C. Liu, Y. Yamada, and C.-M. Fan. 2002. Growth arrest specific gene 1 acts as a region-specific mediator of the Fgf10/Fgf8 regulatory loop in the limb. *Development*. 129:5289–5300.

Liu, Y., N.R. May, and C.M. Fan. 2001. Growth arrest specific gene 1 is a positive growth regulator for the cerebellum. *Developmental Biology*. 236:30–45. doi:10.1006/dbio.2000.0146.

Loftus, S.K., J.A. Morris, E.D. Carstea, J.Z. Gu, C. Cummings, A. Brown, J. Ellison, K. Ohno,

M.A. Rosenfeld, D.A. Tagle, P.G. Pentchev, and W.J. Pavan. 1997. Murine model of Niemann-Pick C disease: mutation in a cholesterol homeostasis gene. *Science*. 277:232–235.

LoRusso, P.M., A. Jimeno, G. Dy, A. Adjei, J. Berlin, L. Leichman, J.A. Low, D. Colburn, I. Chang, S. Cheeti, J.Y. Jin, and R.A. Graham. 2011. Pharmacokinetic dose-scheduling study of hedgehog pathway inhibitor vismodegib (GDC-0449) in patients with locally advanced or metastatic solid tumors. *Clin. Cancer Res.* 17:5774–5782. doi:10.1158/1078-0432.CCR-11-0972.

LoRusso, P.M., S.A. Piha-Paul, M. Mita, A.D. Colevas, V. Malhi, D. Colburn, M. Yin, J.A. Low, and R.A. Graham. 2013. Co-administration of vismodegib with rosiglitazone or combined oral contraceptive in patients with locally advanced or metastatic solid tumors: a pharmacokinetic assessment of drug-drug interaction potential. *Cancer Chemother. Pharmacol.* 71:193–202. doi:10.1007/s00280-012-1996-6.

Lu, X., S. Liu, and T.B. Kornberg. 2006. The C-terminal tail of the Hedgehog receptor Patched regulates both localization and turnover. *Genes & Development*. 20:2539–2551. doi:10.1101/gad.1461306.

Lum, L., S. Yao, B. Mozer, A. Rovescalli, D. Von Kessler, M. Nirenberg, and P.A. Beachy. 2003. Identification of Hedgehog pathway components by RNAi in Drosophila cultured cells. *Science*. 299:2039–2045. doi:10.1126/science.1081403.

Ma, Y., A. Erkner, R. Gong, S. Yao, J. Taipale, K. Basler, and P.A. Beachy. 2002. Hedgehog-mediated patterning of the mammalian embryo requires transporter-like function of dispatched. *Cell*. 111:63–75.

Mancuso, M., S. Pazzaglia, M. Tanori, H. Hahn, P. Merola, S. Rebessi, M.J. Atkinson, V. Di Majo, V. Covelli, and A. Saran. 2004. Basal cell carcinoma and its development: insights from radiation-induced tumors in Ptch1-deficient mice. *Cancer Research*. 64:934–941.

Mao, J., K.L. Ligon, E.Y. Rakhlin, S.P. Thayer, R.T. Bronson, D. Rowitch, and A.P. McMahon. 2006. A novel somatic mouse model to survey tumorigenic potential applied to the Hedgehog pathway. *Cancer Research*. 66:10171–10178. doi:10.1158/0008-5472.CAN-06-0657.

Marigo, V., R.A. Davey, Y. Zuo, J.M. Cunningham, and C.J. Tabin. 1996. Biochemical evidence that patched is the Hedgehog receptor. *Nature*. 384:176–179. doi:10.1038/384176a0.

Martinelli, D.C., and C.-M. Fan. 2007. Gas1 extends the range of Hedgehog action by facilitating its signaling. *Genes & Development*. 21:1231–1243. doi:10.1101/gad.1546307.

Martizez Arias, A., N.E. Baker, and P.W. Ingham. 1988. Role of segment polarity genes in the definition and maintenance of cell states in the Drosophila embryo. *Development*. 103:157–170.

Martí, E., D.A. Bumcrot, R. Takada, and A.P. McMahon. 1995. Requirement of 19K form of Sonic hedgehog for induction of distinct ventral cell types in CNS explants. *Nature*.

375:322–325. doi:10.1038/375322a0.

Martín, V., G. Carrillo, C. Torroja, and I. Guerrero. 2001. The sterol-sensing domain of Patched protein seems to control Smoothened activity through Patched vesicular trafficking. *Current Biology*. 11:601–607.

Mathew, E., Y. Zhang, A.M. Holtz, K.T. Kane, J.Y. Song, B.L. Allen, and M. Pasca di Magliano. 2014. Dosage-dependent regulation of pancreatic cancer growth and angiogenesis by hedgehog signaling. *Cell Rep*. 9:484–494. doi:10.1016/j.celrep.2014.09.010.

McCormick, C., Y. Leduc, D. Martindale, K. Mattison, L.E. Esford, A.P. Dyer, and F. Tufaro. 1998. The putative tumour suppressor EXT1 alters the expression of cell-surface heparan sulfate. *Nat Genet*. 19:158–161. doi:10.1038/514.

McCready, M.E., E. Sweeney, A.E. Fryer, D. Donnai, A. Baig, L. Racacho, M.L. Warman, A.G.W. Hunter, and D.E. Bulman. 2002. A novel mutation in the IHH gene causes brachydactyly type A1: a 95-year-old mystery resolved. *Hum. Genet.* 111:368–375. doi:10.1007/s00439-002-0815-2.

McLellan, J.S., X. Zheng, G. Hauk, R. Ghirlando, P.A. Beachy, and D.J. Leahy. 2008. The mode of Hedgehog binding to Ihog homologues is not conserved across different phyla. *Nature*. 455:979–983. doi:10.1038/nature07358.

McMahon, A.P., P.W. Ingham, and C.J. Tabin. 2003. Developmental roles and clinical significance of hedgehog signaling. *Curr. Top. Dev. Biol.* 53:1–114.

Micchelli, C.A., I. The, E. Selva, V. Mogila, and N. Perrimon. 2002. Rasp, a putative transmembrane acyltransferase, is required for Hedgehog signaling. *Development*. 129:843–851.

Milenkovic, L., L.V. Goodrich, K.M. Higgins, and M.P. Scott. 1999. Mouse patched1 controls body size determination and limb patterning. *Development*. 126:4431–4440.

Milenkovic, L., M.P. Scott, and R. Rohatgi. 2009. Lateral transport of Smoothened from the plasma membrane to the membrane of the cilium. *J. Cell Biol.* 187:365–374. doi:10.1083/jcb.200907126.

Mohler, J., and K. Vani. 1992. Molecular organization and embryonic expression of the hedgehog gene involved in cell-cell communication in segmental patterning of Drosophila. *Development*. 115:957–971.

Motoyama, J., H. Heng, M.A. Crackower, T. Takabatake, K. Takeshima, L.C. Tsui, and C. Hui. 1998a. Overlapping and non-overlapping Ptch2 expression with Shh during mouse embryogenesis. *Mech. Dev.* 78:81–84.

Motoyama, J., T. Takabatake, K. Takeshima, and C.-C. Hui. 1998b. Ptch2, a second mouse Patched gene is co-expressed with Sonic hedgehog. *Nat Genet*. 18:104–106. doi:10.1038/ng0298-104.

Mundy, C., T. Yasuda, T. Kinumatsu, Y. Yamaguchi, M. Iwamoto, M. Enomoto-Iwamoto, E. Koyama, and M. Pacifici. 2011. Synovial joint formation requires local Ext1 expression and heparan sulfate production in developing mouse embryo limbs and spine. *Developmental Biology*. 351:70–81. doi:10.1016/j.ydbio.2010.12.022.

Myers, B.R., N. Sever, Y.C. Chong, J. Kim, J.D. Belani, S. Rychnovsky, J.F. Bazan, and P.A. Beachy. 2013. Hedgehog pathway modulation by multiple lipid binding sites on the smoothened effector of signal response. *Dev. Cell*. 26:346–357. doi:10.1016/j.devcel.2013.07.015.

Nachtergaele, S., D.M. Whalen, L.K. Mydock, Z. Zhao, T. Malinauskas, K. Krishnan, P.W. Ingham, D.F. Covey, C. Siebold, and R. Rohatgi. 2013. Structure and function of the Smoothened extracellular domain in vertebrate Hedgehog signaling. *eLife*. 2:e01340. doi:10.7554/eLife.01340.

Nachtergaele, S., L.K. Mydock, K. Krishnan, J. Rammohan, P.H. Schlesinger, D.F. Covey, and R. Rohatgi. 2012. Oxysterols are allosteric activators of the oncoprotein Smoothened. *Nat Chem Biol*. 8:211–220. doi:10.1038/nchembio.765.

Nakano, Y., I. Guerrero, A. Hidalgo, A. Taylor, J.R. Whittle, and P.W. Ingham. 1989. A protein with several possible membrane-spanning domains encoded by the Drosophila segment polarity gene patched. *Nature*. 341:508–513. doi:10.1038/341508a0.

Nanni, L., J.E. Ming, M. Bocian, K. Steinhaus, D.W. Bianchi, C. Die-Smulders, A. Giannotti, K. Imaizumi, K.L. Jones, M.D. Campo, R.A. Martin, P. Meinecke, M.E. Pierpont, N.H. Robin, I.D. Young, E. Roessler, and M. Muenke. 1999. The mutational spectrum of the sonic hedgehog gene in holoprosencephaly: SHH mutations cause a significant proportion of autosomal dominant holoprosencephaly. *Hum Mol Genet*. 8:2479–2488.

Nedelcu, D., J. Liu, Y. Xu, C. Jao, and A. Salic. 2013. Oxysterol binding to the extracellular domain of Smoothened in Hedgehog signaling. *Nat Chem Biol*. 9:557–564. doi:10.1038/nchembio.1290.

Neri, G., F. Gurrieri, G. Zanni, and A. Lin. 1998. Clinical and molecular aspects of the Simpson-Golabi-Behmel syndrome. *Am. J. Med. Genet.* 79:279–283.

Nieuwenhuis, E., J. Motoyama, P.C. Barnfield, Y. Yoshikawa, X. Zhang, R. Mo, M.A. Crackower, and C.-C. Hui. 2006. Mice with a targeted mutation of patched2 are viable but develop alopecia and epidermal hyperplasia. *Mol. Cell. Biol.* 26:6609–6622. doi:10.1128/MCB.00295-06.

Nitzki, F., A. Zibat, A. Frommhold, A. Schneider, W. Schulz-Schaeffer, T. Braun, and H. Hahn. 2011. Uncommitted precursor cells might contribute to increased incidence of embryonal rhabdomyosarcoma in heterozygous Patched1-mutant mice. *Oncogene*. 30:4428–4436. doi:10.1038/onc.2011.157.

Novitch, B.G., A.I. Chen, and T.M. Jessell. 2001. Coordinate regulation of motor neuron subtype identity and pan-neuronal properties by the bHLH repressor Olig2. *Neuron*. 31:773–789.

Nüsslein-Volhard, C., and E. Wieschaus. 1980. Mutations affecting segment number and polarity in Drosophila. *Nature*. 287:795–801.

Ohlig, S., U. Pickhinke, S. Sirko, S. Bandari, D. Hoffmann, R. Dreier, P. Farshi, M. Götz, and K. Grobe. 2012. An emerging role of Sonic hedgehog shedding as a modulator of heparan sulfate interactions. *J. Biol. Chem.* 287:43708–43719. doi:10.1074/jbc.M112.356667.

Okada, A., F. Charron, S. Morin, D.S. Shin, K. Wong, P.J. Fabre, M. Tessier-Lavigne, and S.K. McConnell. 2006. Boc is a receptor for sonic hedgehog in the guidance of commissural axons. *Nature*. 444:369–373. doi:10.1038/nature05246.

Olive, K.P., M.A. Jacobetz, C.J. Davidson, A. Gopinathan, D. McIntyre, D. Honess, B. Madhu, M.A. Goldgraben, M.E. Caldwell, D. Allard, K.K. Frese, G. Denicola, C. Feig, C. Combs, S.P. Winter, H. Ireland-Zecchini, S. Reichelt, W.J. Howat, A. Chang, M. Dhara, L. Wang, F. Rückert, R. Grützmann, C. Pilarsky, K. Izeradjene, S.R. Hingorani, P. Huang, S.E. Davies, W. Plunkett, M. Egorin, R.H. Hruban, N. Whitebread, K. McGovern, J. Adams, C. Iacobuzio-Donahue, J. Griffiths, and D.A. Tuveson. 2009. Inhibition of Hedgehog signaling enhances delivery of chemotherapy in a mouse model of pancreatic cancer. *Science*. 324:1457–1461. doi:10.1126/science.1171362.

Oustah, A.A., C. Danesin, N. Khouri-Farah, M.-A. Farreny, N. Escalas, P. Cochard, B. Glise, and C. Soula. 2014. Dynamics of Sonic hedgehog signaling in the ventral spinal cord are controlled by intrinsic changes in source cells requiring Sulfatase 1. *Development*. 141:1392–1403. doi:10.1242/dev.101717.

Özdemir, B.C., T. Pentcheva-Hoang, J.L. Carstens, X. Zheng, C.-C. Wu, T.R. Simpson, H. Laklai, H. Sugimoto, C. Kahlert, S.V. Novitskiy, A. De Jesus-Acosta, P. Sharma, P. Heidari, U. Mahmood, L. Chin, H.L. Moses, V.M. Weaver, A. Maitra, J.P. Allison, V.S. LeBleu, and R. Kalluri. 2014. Depletion of carcinoma-associated fibroblasts and fibrosis induces immunosuppression and accelerates pancreas cancer with reduced survival. *Cancer Cell*. 25:719–734. doi:10.1016/j.ccr.2014.04.005.

Pathi, S., S. Pagan-Westphal, D.P. Baker, E.A. Garber, P. Rayhorn, D. Bumcrot, C.J. Tabin, R. Blake Pepinsky, and K.P. Williams. 2001. Comparative biological responses to human Sonic, Indian, and Desert hedgehog. *Mech. Dev.* 106:107–117.

Pazzaglia, S. 2006. Ptc1 heterozygous knockout mice as a model of multi-organ tumorigenesis. *Cancer Lett.* 234:124–134. doi:10.1016/j.canlet.2005.03.047.

Pazzaglia, S., M. Mancuso, M.J. Atkinson, M. Tanori, S. Rebessi, V.D. Majo, V. Covelli, H. Hahn, and A. Saran. 2002. High incidence of medulloblastoma following X-ray-irradiation of newborn Ptc1 heterozygous mice. *Oncogene*. 21:7580–7584. doi:10.1038/sj.onc.1205973.

Pepicelli, C.V., P.M. Lewis, and A.P. McMahon. 1998. Sonic hedgehog regulates branching morphogenesis in the mammalian lung. *Current Biology*. 8:1083–1086.

Pepinsky, R.B., C. Zeng, D. Wen, P. Rayhorn, D.P. Baker, K.P. Williams, S.A. Bixler, C.M. Ambrose, E.A. Garber, K. Miatkowski, F.R. Taylor, E.A. Wang, and A. Galdes. 1998.

Identification of a palmitic acid-modified form of human Sonic hedgehog. *J. Biol. Chem.* 273:14037–14045.

Peterson, K.A., Y. Nishi, W. Ma, A. Vedenko, L. Shokri, X. Zhang, M. McFarlane, J.-M. Baizabal, J.P. Junker, A. van Oudenaarden, T. Mikkelsen, B.E. Bernstein, T.L. Bailey, M.L. Bulyk, W.H. Wong, and A.P. McMahon. 2012. Neural-specific Sox2 input and differential Gli-binding affinity provide context and positional information in Shh-directed neural patterning. *Genes & Development*. 26:2802–2816. doi:10.1101/gad.207142.112.

Pilia, G., R.M. Hughes-Benzie, A. MacKenzie, P. Baybayan, E.Y. Chen, R. Huber, G. Neri, A. Cao, A. Forabosco, and D. Schlessinger. 1996. Mutations in GPC3, a glypican gene, cause the Simpson-Golabi-Behmel overgrowth syndrome. *Nat Genet*. 12:241–247. doi:10.1038/ng0396-241.

Porter, J.A., D.P. von Kessler, S.C. Ekker, K.E. Young, J.J. Lee, K. Moses, and P.A. Beachy. 1995. The product of hedgehog autoproteolytic cleavage active in local and long-range signalling. *Nature*. 374:363–366. doi:10.1038/374363a0.

Porter, J.A., K.E. Young, and P.A. Beachy. 1996a. Cholesterol modification of hedgehog signaling proteins in animal development. *Science*. 274:255–259.

Porter, J.A., S.C. Ekker, W.J. Park, D.P. von Kessler, K.E. Young, C.H. Chen, Y. Ma, A.S. Woods, R.J. Cotter, E.V. Koonin, and P.A. Beachy. 1996b. Hedgehog patterning activity: role of a lipophilic modification mediated by the carboxy-terminal autoprocessing domain. *Cell*. 86:21–34.

Radhakrishna, U., A. Wild, K.H. Grzeschik, and S.E. Antonarakis. 1997. Mutation in GLI3 in postaxial polydactyly type A. *Nat Genet*. 17:269–271. doi:10.1038/ng1197-269.

Rahnama, F., R. Toftgård, and P.G. Zaphiropoulos. 2004. Distinct roles of PTCH2 splice variants in Hedgehog signalling. *Biochem. J.* 378:325–334. doi:10.1042/BJ20031200.

Rajurkar, M., H. Huang, J.L. Cotton, J.K. Brooks, J. Sicklick, A.P. McMahon, and J. Mao. 2014. Distinct cellular origin and genetic requirement of Hedgehog-Gli in postnatal rhabdomyosarcoma genesis. *Oncogene*. 33:5370–5378. doi:10.1038/onc.2013.480.

Rhim, A.D., P.E. Oberstein, D.H. Thomas, E.T. Mirek, C.F. Palermo, S.A. Sastra, E.N. Dekleva, T. Saunders, C.P. Becerra, I.W. Tattersall, C.B. Westphalen, J. Kitajewski, M.G. Fernandez-Barrena, M.E. Fernandez-Zapico, C. Iacobuzio-Donahue, K.P. Olive, and B.Z. Stanger. 2014. Stromal elements act to restrain, rather than support, pancreatic ductal adenocarcinoma. *Cancer Cell*. 25:735–747. doi:10.1016/j.ccr.2014.04.021.

Ribes, V., and J. Briscoe. 2009. Establishing and interpreting graded Sonic Hedgehog signaling during vertebrate neural tube patterning: the role of negative feedback. *Cold Spring Harb Perspect Biol*. 1:a002014. doi:10.1101/cshperspect.a002014.

Riddle, R.D., R.L. Johnson, E. Laufer, and C. Tabin. 1993. Sonic hedgehog mediates the polarizing activity of the ZPA. *Cell*. 75:1401–1416.

Robarge, K.D., S.A. Brunton, G.M. Castanedo, Y. Cui, M.S. Dina, R. Goldsmith, S.E. Gould, O. Guichert, J.L. Gunzner, J. Halladay, W. Jia, C. Khojasteh, M.F.T. Koehler, K. Kotkow, H. La, R.L. Lalonde, K. Lau, L. Lee, D. Marshall, J.C. Marsters, L.J. Murray, C. Qian, L.L. Rubin, L. Salphati, M.S. Stanley, J.H.A. Stibbard, D.P. Sutherlin, S. Ubhayaker, S. Wang, S. Wong, and M. Xie. 2009. GDC-0449-a potent inhibitor of the hedgehog pathway. *Bioorg. Med. Chem. Lett.* 19:5576–5581. doi:10.1016/j.bmcl.2009.08.049.

Roelink, H., A. Augsburger, J. Heemskerk, V. Korzh, S. Norlin, A. Ruiz i Altaba, Y. Tanabe, M. Placzek, T. Edlund, and T.M. Jessell. 1994. Floor plate and motor neuron induction by vhh-1, a vertebrate homolog of hedgehog expressed by the notochord. *Cell*. 76:761–775.

Roelink, H., J.A. Porter, C. Chiang, Y. Tanabe, D.T. Chang, P.A. Beachy, and T.M. Jessell. 1995. Floor plate and motor neuron induction by different concentrations of the amino-terminal cleavage product of sonic hedgehog autoproteolysis. *Cell*. 81:445–455.

Roessler, E., E. Belloni, K. Gaudenz, P. Jay, P. Berta, S.W. Scherer, L.C. Tsui, and M. Muenke. 1996. Mutations in the human Sonic Hedgehog gene cause holoprosencephaly. *Nat Genet*. 14:357–360. doi:10.1038/ng1196-357.

Roessler, E., Y.-Z. Du, J.L. Mullor, E. Casas, W.P. Allen, G. Gillessen-Kaesbach, E.R. Roeder, J.E. Ming, A. Ruiz i Altaba, and M. Muenke. 2003. Loss-of-function mutations in the human GLI2 gene are associated with pituitary anomalies and holoprosencephaly-like features. *Proceedings of the National Academy of Sciences of the United States of America*. 100:13424–13429. doi:10.1073/pnas.2235734100.

Rohatgi, R., L. Milenkovic, and M.P. Scott. 2007. Patched1 regulates hedgehog signaling at the primary cilium. *Science*. 317:372–376. doi:10.1126/science.1139740.

Rohatgi, R., L. Milenkovic, R.B. Corcoran, and M.P. Scott. 2009. Hedgehog signal transduction by Smoothened: pharmacologic evidence for a 2-step activation process. *Proceedings of the National Academy of Sciences of the United States of America*. 106:3196–3201. doi:10.1073/pnas.0813373106.

Rojas-Ríos, P., I. Guerrero, and A. González-Reyes. 2012. Cytoneme-mediated delivery of hedgehog regulates the expression of bone morphogenetic proteins to maintain germline stem cells in Drosophila. *PLoS Biol*. 10:e1001298. doi:10.1371/journal.pbio.1001298.

Rubin, J.B., Y. Choi, and R.A. Segal. 2002. Cerebellar proteoglycans regulate sonic hedgehog responses during development. *Development*. 129:2223–2232.

Rudin, C.M., C.L. Hann, J. Laterra, R.L. Yauch, C.A. Callahan, L. Fu, T. Holcomb, J. Stinson, S.E. Gould, B. Coleman, P.M. LoRusso, D.D. Von Hoff, F.J. de Sauvage, and J.A. Low. 2009. Treatment of medulloblastoma with hedgehog pathway inhibitor GDC-0449. *N. Engl. J. Med.* 361:1173–1178. doi:10.1056/NEJMoa0902903.

Ruiz i Altaba, A. 1999. Gli proteins and Hedgehog signaling: development and cancer. *Trends Genet.* 15:418–425.

Sanders, T.A., E. Llagostera, and M. Barna. 2013. Specialized filopodia direct long-range transport of SHH during vertebrate tissue patterning. *Nature*. 497:628–632. doi:10.1038/nature12157.

Scales, S.J., and F.J. de Sauvage. 2009. Mechanisms of Hedgehog pathway activation in cancer and implications for therapy. *Trends in Pharmacological Sciences*. 30:303–312. doi:10.1016/j.tips.2009.03.007.

Schuske, K., J.E. Hooper, and M.P. Scott. 1994. patched overexpression causes loss of wingless expression in Drosophila embryos. *Developmental Biology*. 164:300–311. doi:10.1006/dbio.1994.1200.

Schüller, U., V.M. Heine, J. Mao, A.T. Kho, A.K. Dillon, Y.-G. Han, E. Huillard, T. Sun, A.H. Ligon, Y. Qian, Q. Ma, A. Alvarez-Buylla, A.P. McMahon, D.H. Rowitch, and K.L. Ligon. 2008. Acquisition of granule neuron precursor identity is a critical determinant of progenitor cell competence to form Shh-induced medulloblastoma. *Cancer Cell*. 14:123–134. doi:10.1016/j.ccr.2008.07.005.

Sekine, K., H. Ohuchi, M. Fujiwara, M. Yamasaki, T. Yoshizawa, T. Sato, N. Yagishita, D. Matsui, Y. Koga, N. Itoh, and S. Kato. 1999. Fgf10 is essential for limb and lung formation. *Nat Genet*. 21:138–141. doi:10.1038/5096.

Sekulic, A., M.R. Migden, A.E. Oro, L. Dirix, K.D. Lewis, J.D. Hainsworth, J.A. Solomon, S. Yoo, S.T. Arron, P.A. Friedlander, E. Marmur, C.M. Rudin, A.L.S. Chang, J.A. Low, H.M. Mackey, R.L. Yauch, R.A. Graham, J.C. Reddy, and A. Hauschild. 2012. Efficacy and safety of vismodegib in advanced basal-cell carcinoma. *N. Engl. J. Med.* 366:2171–2179. doi:10.1056/NEJMoa1113713.

Stamataki, D., F. Ulloa, S.V. Tsoni, A. Mynett, and J. Briscoe. 2005. A gradient of Gli activity mediates graded Sonic Hedgehog signaling in the neural tube. *Genes & Development*. 19:626–641. doi:10.1101/gad.325905.

Stebel, M., P. Vatta, M.E. Ruaro, G. Del Sal, R.G. Parton, and C. Schneider. 2000. The growth suppressing gas1 product is a GPI-linked protein. *FEBS Lett.* 481:152–158.

Stickens, D., and G.A. Evans. 1997. Isolation and characterization of the murine homolog of the human EXT2 multiple exostoses gene. *Biochem. Mol. Med.* 61:16–21.

Stone, D.M., M. Hynes, M. Armanini, T.A. Swanson, Q. Gu, R.L. Johnson, M.P. Scott, D. Pennica, A. Goddard, H. Phillips, M. Noll, J.E. Hooper, F. de Sauvage, and A. Rosenthal. 1996. The tumour-suppressor gene patched encodes a candidate receptor for Sonic hedgehog. *Nature*. 384:129–134. doi:10.1038/384129a0.

Stottmann, R.W., A. Turbe-Doan, P. Tran, L.E. Kratz, J.L. Moran, R.I. Kelley, and D.R. Beier. 2011. Cholesterol metabolism is required for intracellular hedgehog signal transduction in vivo. *PLoS Genet.* 7:e1002224. doi:10.1371/journal.pgen.1002224.

Strutt, H., C. Thomas, Y. Nakano, D. Stark, B. Neave, A.M. Taylor, and P.W. Ingham. 2001.

Mutations in the sterol-sensing domain of Patched suggest a role for vesicular trafficking in Smoothened regulation. *Current Biology*. 11:608–613.

Svärd, J., K. Heby-Henricson, K.H. Henricson, M. Persson-Lek, B. Rozell, M. Lauth, A. Bergström, J. Ericson, R. Toftgård, and S. Teglund. 2006. Genetic elimination of Suppressor of fused reveals an essential repressor function in the mammalian Hedgehog signaling pathway. *Dev. Cell*. 10:187–197. doi:10.1016/j.devcel.2005.12.013.

Tabata, T., and T.B. Kornberg. 1994. Hedgehog is a signaling protein with a key role in patterning Drosophila imaginal discs. *Cell*. 76:89–102.

Tabata, T., S. Eaton, and T.B. Kornberg. 1992. The Drosophila hedgehog gene is expressed specifically in posterior compartment cells and is a target of engrailed regulation. *Genes & Development*. 6:2635–2645.

Taipale, J., J.K. Chen, M.K. Cooper, B. Wang, R.K. Mann, L. Milenkovic, M.P. Scott, and P.A. Beachy. 2000. Effects of oncogenic mutations in Smoothened and Patched can be reversed by cyclopamine. *Nature*. 406:1005–1009. doi:10.1038/35023008.

Taipale, J., M.K. Cooper, T. Maiti, and P.A. Beachy. 2002. Patched acts catalytically to suppress the activity of Smoothened. *Nature*. 418:892–897. doi:10.1038/nature00989.

Takabatake, T., M. Ogawa, T.C. Takahashi, M. Mizuno, M. Okamoto, and K. Takeshima. 1997. Hedgehog and patched gene expression in adult ocular tissues. *FEBS Lett.* 410:485–489.

Tang, J.Y., J.M. Mackay-Wiggan, M. Aszterbaum, R.L. Yauch, J. Lindgren, K. Chang, C. Coppola, A.M. Chanana, J. Marji, D.R. Bickers, and E.H. Epstein. 2012. Inhibiting the hedgehog pathway in patients with the basal-cell nevus syndrome. *N. Engl. J. Med.* 366:2180–2188. doi:10.1056/NEJMoa1113538.

Taylor, A.M., Y. Nakano, J. Mohler, and P.W. Ingham. 1993. Contrasting distributions of patched and hedgehog proteins in the Drosophila embryo. *Mech. Dev.* 42:89–96.

Teglund, S., and R. Toftgård. 2010. Hedgehog beyond medulloblastoma and basal cell carcinoma. *BBA - Reviews on Cancer*. 1805:181–208. doi:10.1016/j.bbcan.2010.01.003.

Tenzen, T., B.L. Allen, F. Cole, J.-S. Kang, R.S. Krauss, and A.P. McMahon. 2006. The cell surface membrane proteins Cdo and Boc are components and targets of the Hedgehog signaling pathway and feedback network in mice. *Dev. Cell*. 10:647–656. doi:10.1016/j.devcel.2006.04.004.

Thayer, S.P., M.P. di Magliano, P.W. Heiser, C.M. Nielsen, D.J. Roberts, G.Y. Lauwers, Y.P. Qi, S. Gysin, C. Fernández-del Castillo, V. Yajnik, B. Antoniu, M. McMahon, A.L. Warshaw, and M. Hebrok. 2003. Hedgehog is an early and late mediator of pancreatic cancer tumorigenesis. *Nature*. 425:851–856. doi:10.1038/nature02009.

The, I., Y. Bellaiche, and N. Perrimon. 1999. Hedgehog movement is regulated through tout velu-dependent synthesis of a heparan sulfate proteoglycan. *Mol. Cell*. 4:633–639.

Therond, P.P. 2012. Release and transportation of Hedgehog molecules. *Curr. Opin. Cell Biol.* 24:173–180. doi:10.1016/j.ceb.2012.02.001.

Theunissen, J.-W., and F.J. de Sauvage. 2009. Paracrine Hedgehog signaling in cancer. *Cancer Research*. 69:6007–6010. doi:10.1158/0008-5472.CAN-09-0756.

Tian, H., C.A. Callahan, K.J. DuPree, W.C. Darbonne, C.P. Ahn, S.J. Scales, and F.J. de Sauvage. 2009. Hedgehog signaling is restricted to the stromal compartment during pancreatic carcinogenesis. *Proceedings of the National Academy of Sciences of the United States of America*. 106:4254–4259. doi:10.1073/pnas.0813203106.

Tian, H., J. Jeong, B.D. Harfe, C.J. Tabin, and A.P. McMahon. 2005. Mouse Disp1 is required in sonic hedgehog-expressing cells for paracrine activity of the cholesterol-modified ligand. *Development*. 132:133–142. doi:10.1242/dev.01563.

Torroja, C., N. Gorfinkiel, and I. Guerrero. 2004. Patched controls the Hedgehog gradient by endocytosis in a dynamin-dependent manner, but this internalization does not play a major role in signal transduction. *Development*. 131:2395–2408. doi:10.1242/dev.01102.

Tostar, U., C.J. Malm, J.M. Meis-Kindblom, L.-G. Kindblom, R. Toftgård, and A.B. Undén. 2006. Deregulation of the hedgehog signalling pathway: a possible role for the PTCH and SUFU genes in human rhabdomyoma and rhabdomyosarcoma development. *J. Pathol.* 208:17–25. doi:10.1002/path.1882.

Touahri, Y., N. Escalas, B. Benazeraf, P. Cochard, C. Danesin, and C. Soula. 2012. Sulfatase 1 promotes the motor neuron-to-oligodendrocyte fate switch by activating Shh signaling in Olig2 progenitors of the embryonic ventral spinal cord. *J. Neurosci.* 32:18018–18034. doi:10.1523/JNEUROSCI.3553-12.2012.

Tseng, T.T., K.S. Gratwick, J. Kollman, D. Park, D.H. Nies, A. Goffeau, and M.H. Saier. 1999. The RND permease superfamily: an ancient, ubiquitous and diverse family that includes human disease and development proteins. *J. Mol. Microbiol. Biotechnol.* 1:107–125.

Tukachinsky, H., L.V. Lopez, and A. Salic. 2010. A mechanism for vertebrate Hedgehog signaling: recruitment to cilia and dissociation of SuFu-Gli protein complexes. *J. Cell Biol.* 191:415–428. doi:10.1083/jcb.201004108.

Tukachinsky, H., R.P. Kuzmickas, C.Y. Jao, J. Liu, and A. Salic. 2012. Dispatched and scube mediate the efficient secretion of the cholesterol-modified hedgehog ligand. *Cell Rep*. 2:308–320. doi:10.1016/j.celrep.2012.07.010.

Van Durme, Y.M.T.A., M. Eijgelsheim, G.F. Joos, A. Hofman, A.G. Uitterlinden, G.G. Brusselle, and B.H.C. Stricker. 2010. Hedgehog-interacting protein is a COPD susceptibility gene: the Rotterdam Study. *Eur. Respir. J.* 36:89–95. doi:10.1183/09031936.00129509.

Vokes, S.A., H. Ji, S. McCuine, T. Tenzen, S. Giles, S. Zhong, W.J.R. Longabaugh, E.H. Davidson, W.H. Wong, and A.P. McMahon. 2007. Genomic characterization of Gli-activator targets in sonic hedgehog-mediated neural patterning. *Development*. 134:1977–1989.

doi:10.1242/dev.001966.

Vokes, S.A., H. Ji, W.H. Wong, and A.P. McMahon. 2008. A genome-scale analysis of the cis-regulatory circuitry underlying sonic hedgehog-mediated patterning of the mammalian limb. *Genes & Development*. 22:2651–2663. doi:10.1101/gad.1693008.

Vorechovsky, I., O. Tingby, M. Hartman, B. Strömberg, M. Nister, V.P. Collins, and R. Toftgård. 1997. Somatic mutations in the human homologue of Drosophila patched in primitive neuroectodermal tumours. *Oncogene*. 15:361–366. doi:10.1038/sj.onc.1201340.

Vyas, N., D. Goswami, A. Manonmani, P. Sharma, H.A. Ranganath, K. VijayRaghavan, L.S. Shashidhara, R. Sowdhamini, and S. Mayor. 2008. Nanoscale organization of hedgehog is essential for long-range signaling. *Cell*. 133:1214–1227. doi:10.1016/j.cell.2008.05.026.

Wetmore, C., D.E. Eberhart, and T. Curran. 2000. The normal patched allele is expressed in medulloblastomas from mice with heterozygous germ-line mutation of patched. *Cancer Research*. 60:2239–2246.

Whalen, D.M., T. Malinauskas, R.J.C. Gilbert, and C. Siebold. 2013. Structural insights into proteoglycan-shaped Hedgehog signaling. *Proceedings of the National Academy of Sciences of the United States of America*. doi:10.1073/pnas.1310097110.

Wicking, C., S. Shanley, I. Smyth, S. Gillies, K. Negus, S. Graham, G. Suthers, N. Haites, M. Edwards, B. Wainwright, and G. Chenevix-Trench. 1997. Most germ-line mutations in the nevoid basal cell carcinoma syndrome lead to a premature termination of the PATCHED protein, and no genotype-phenotype correlations are evident. *Am. J. Hum. Genet.* 60:21–26.

Wijgerde, M., J.A. McMahon, M. Rule, and A.P. McMahon. 2002. A direct requirement for Hedgehog signaling for normal specification of all ventral progenitor domains in the presumptive mammalian spinal cord. *Genes & Development*. 16:2849–2864. doi:10.1101/gad.1025702.

Wilk, J.B., T.-H. Chen, D.J. Gottlieb, R.E. Walter, M.W. Nagle, B.J. Brandler, R.H. Myers, I.B. Borecki, E.K. Silverman, S.T. Weiss, and G.T. O'Connor. 2009. A genome-wide association study of pulmonary function measures in the Framingham Heart Study. *PLoS Genet.* 5:e1000429. doi:10.1371/journal.pgen.1000429.

Williams, E.H., W.N. Pappano, A.M. Saunders, M.-S. Kim, D.J. Leahy, and P.A. Beachy. 2010. Dally-like core protein and its mammalian homologues mediate stimulatory and inhibitory effects on Hedgehog signal response. *Proceedings of the National Academy of Sciences of the United States of America*. 107:5869–5874. doi:10.1073/pnas.1001777107.

Williamson, D., J. Selfe, T. Gordon, Y.-J. Lu, K. Pritchard-Jones, K. Murai, P. Jones, P. Workman, and J. Shipley. 2007. Role for amplification and expression of glypican-5 in rhabdomyosarcoma. *Cancer Research*. 67:57–65. doi:10.1158/0008-5472.CAN-06-1650.

Wilson, N.H., and E.T. Stoeckli. 2013. Sonic Hedgehog Regulates Its Own Receptor on Postcrossing Commissural Axons in a Glypican1-Dependent Manner. *Neuron*. 79:478–491.

doi:10.1016/j.neuron.2013.05.025.

Witt, R.M., M.-L. Hecht, M.F. Pazyra-Murphy, S.M. Cohen, C. Noti, T.H. van Kuppevelt, M. Fuller, J.A. Chan, J.J. Hopwood, P.H. Seeberger, and R.A. Segal. 2013. Heparan sulfate proteoglycans containing a glypican 5 core and 2-O-sulfo-iduronic acid function as Sonic Hedgehog co-receptors to promote proliferation. *J. Biol. Chem.* 288:26275–26288. doi:10.1074/jbc.M112.438937.

Wojcinski, A., H. Nakato, C. Soula, and B. Glise. 2011. DSulfatase-1 fine-tunes Hedgehog patterning activity through a novel regulatory feedback loop. *Developmental Biology*. 358:168–180. doi:10.1016/j.ydbio.2011.07.027.

Wong, S.Y., A.D. Seol, P.-L. So, A.N. Ermilov, C.K. Bichakjian, E.H. Epstein, A.A. Dlugosz, and J.F. Reiter. 2009. Primary cilia can both mediate and suppress Hedgehog pathway-dependent tumorigenesis. *Nat. Med.* 15:1055–1061. doi:10.1038/nm.2011.

Woods, I.G., and W.S. Talbot. 2005. The you gene encodes an EGF-CUB protein essential for Hedgehog signaling in zebrafish. *PLoS Biol*. 3:e66. doi:10.1371/journal.pbio.0030066.

Xie, J., M. Murone, S.M. Luoh, A. Ryan, Q. Gu, C. Zhang, J.M. Bonifas, C.W. Lam, M. Hynes, A. Goddard, A. Rosenthal, E.H. Epstein, and F.J. de Sauvage. 1998. Activating Smoothened mutations in sporadic basal-cell carcinoma. *Nature*. 391:90–92. doi:10.1038/34201.

Yan, D., and X. Lin. 2008. Opposing roles for glypicans in Hedgehog signalling. *Nat. Cell Biol.* 10:761–763. doi:10.1038/ncb0708-761.

Yan, D., and X. Lin. 2009. Shaping morphogen gradients by proteoglycans. *Cold Spring Harb Perspect Biol*. 1:a002493. doi:10.1101/cshperspect.a002493.

Yan, D., Y. Wu, Y. Yang, T.Y. Belenkaya, X. Tang, and X. Lin. 2010. The cell-surface proteins Dally-like and Ihog differentially regulate Hedgehog signaling strength and range during development. *Development*. 137:2033–2044. doi:10.1242/dev.045740.

Yang, Z.-J., T. Ellis, S.L. Markant, T.-A. Read, J.D. Kessler, M. Bourboulas, U. Schüller, R. Machold, G. Fishell, D.H. Rowitch, B.J. Wainwright, and R.J. Wechsler-Reya. 2008. Medulloblastoma can be initiated by deletion of Patched in lineage-restricted progenitors or stem cells. *Cancer Cell*. 14:135–145. doi:10.1016/j.ccr.2008.07.003.

Yao, S., L. Lum, and P. Beachy. 2006. The ihog cell-surface proteins bind Hedgehog and mediate pathway activation. *Cell*. 125:343–357. doi:10.1016/j.cell.2006.02.040.

Yauch, R.L., G.J.P. Dijkgraaf, B. Alicke, T. Januario, C.P. Ahn, T. Holcomb, K. Pujara, J. Stinson, C.A. Callahan, T. Tang, J.F. Bazan, Z. Kan, S. Seshagiri, C.L. Hann, S.E. Gould, J.A. Low, C.M. Rudin, and F.J. de Sauvage. 2009. Smoothened mutation confers resistance to a Hedgehog pathway inhibitor in medulloblastoma. *Science*. 326:572–574. doi:10.1126/science.1179386.

Yauch, R.L., S.E. Gould, S.J. Scales, T. Tang, H. Tian, C.P. Ahn, D. Marshall, L. Fu, T.

Januario, D. Kallop, M. Nannini-Pepe, K. Kotkow, J.C. Marsters, L.L. Rubin, and F.J. de Sauvage. 2008. A paracrine requirement for hedgehog signalling in cancer. *Nature*. 455:406–410. doi:10.1038/nature07275.

Yavari, A., R. Nagaraj, E. Owusu-Ansah, A. Folick, K. Ngo, T. Hillman, G. Call, R. Rohatgi, M.P. Scott, and U. Banerjee. 2010. Role of lipid metabolism in smoothened derepression in hedgehog signaling. *Dev. Cell*. 19:54–65. doi:10.1016/j.devcel.2010.06.007.

Young, R.P., C.F. Whittington, R.J. Hopkins, B.A. Hay, M.J. Epton, P.N. Black, and G.D. Gamble. 2010. Chromosome 4q31 locus in COPD is also associated with lung cancer. *Eur. Respir. J.* 36:1375–1382. doi:10.1183/09031936.00033310.

Yue, S., L.-Y. Tang, Y. Tang, Y. Tang, Q.-H. Shen, J. Ding, Y. Chen, Z. Zhang, T.-T. Yu, Y.E. Zhang, and S.Y. Cheng. 2014. Requirement of Smurf-mediated endocytosis of Patched1 in sonic hedgehog signal reception. *eLife*. 3. doi:10.7554/eLife.02555.

Zaphiropoulos, P.G., A.B. Undén, F. Rahnama, R.E. Hollingsworth, and R. Toftgård. 1999. PTCH2, a novel human patched gene, undergoing alternative splicing and up-regulated in basal cell carcinomas. *Cancer Research*. 59:787–792.

Zeng, X., J.A. Goetz, L.M. Suber, W.J. Scott, C.M. Schreiner, and D.J. Robbins. 2001. A freely diffusible form of Sonic hedgehog mediates long-range signalling. *Nature*. 411:716–720. doi:10.1038/35079648.

Zhang, F., J.S. McLellan, A.M. Ayala, D.J. Leahy, and R.J. Linhardt. 2007. Kinetic and structural studies on interactions between heparin or heparan sulfate and proteins of the hedgehog signaling pathway. *Biochemistry*. 46:3933–3941. doi:10.1021/bi6025424.

Zhang, W., J.-S. Kang, F. Cole, M.-J. Yi, and R.S. Krauss. 2006. Cdo functions at multiple points in the Sonic Hedgehog pathway, and Cdo-deficient mice accurately model human holoprosencephaly. *Dev. Cell*. 10:657–665. doi:10.1016/j.devcel.2006.04.005.

Zhang, X.M., M. Ramalho-Santos, and A.P. McMahon. 2001. Smoothened mutants reveal redundant roles for Shh and Ihh signaling including regulation of L/R asymmetry by the mouse node. *Cell*. 105:781–792.

Zheng, X., R.K. Mann, N. Sever, and P.A. Beachy. 2010. Genetic and biochemical definition of the Hedgehog receptor. *Genes & Development*. 24:57–71. doi:10.1101/gad.1870310.

Zhou, X., R.M. Baron, M. Hardin, M.H. Cho, J. Zielinski, I. Hawrylkiewicz, P. Sliwinski, C.P. Hersh, J.D. Mancini, K. Lu, D. Thibault, A.L. Donahue, B.J. Klanderman, B. Rosner, B.A. Raby, Q. Lu, A.M. Geldart, M.D. Layne, M.A. Perrella, S.T. Weiss, A.M.K. Choi, and E.K. Silverman. 2012. Identification of a chronic obstructive pulmonary disease genetic determinant that regulates HHIP. *Hum Mol Genet*. 21:1325–1335. doi:10.1093/hmg/ddr569.

Zhu, A.J., L. Zheng, K. Suyama, and M.P. Scott. 2003. Altered localization of Drosophila Smoothened protein activates Hedgehog signal transduction. *Genes & Development*. 17:1240–1252. doi:10.1101/gad.1080803.

Zurawel, R.H., C. Allen, R. Wechsler-Reya, M.P. Scott, and C. Raffel. 2000. Evidence that haploinsufficiency of Ptch leads to medulloblastoma in mice. *Genes Chromosomes Cancer*. 28:77–81.

# CHAPTER II:

## Essential role for ligand-dependent feedback antagonism of vertebrate Hedgehog signaling by PTCH1, PTCH2, and HHIP1 during neural patterning

### 2.1 Abstract

Hedgehog (HH) signaling is essential for vertebrate and invertebrate embryogenesis. In *Drosophila*, feedback up-regulation of the HH receptor, Patched (PTC; PTCH in vertebrates), is required to restrict HH signaling during development. In contrast, PTCH1 up-regulation is dispensable for early HH-dependent patterning in mice. Unique to vertebrates are two additional HH-binding antagonists that are induced by HH signaling, HHIP1 and the PTCH1 homologue, PTCH2. While HHIP1 functions semi-redundantly with PTCH1 to restrict HH signaling in the developing nervous system, a role for PTCH2 remains unresolved. Data presented here define a novel role for PTCH2 as a ciliary-localized HH pathway antagonist. While PTCH2 is dispensable for normal ventral neural patterning, combined removal of PTCH2- and PTCH1-feedback antagonism produces a significant expansion of HH-dependent ventral neural progenitors. Strikingly, complete loss of PTCH2-, HHIP1-, and PTCH1-feedback inhibition results in ectopic specification of ventral cell fates throughout the neural tube, reflecting constitutive HH pathway activation. Overall, these data reveal an essential role for ligand-dependent feedback inhibition of vertebrate HH signaling governed collectively by PTCH1, PTCH2, and HHIP1.

## 2.2 Introduction

During embryogenesis, complex gene expression patterns arise within fields of initially equivalent cells to form the tissues that comprise a fully developed organism (Perrimon and McMahon, 1999). A small number of conserved signaling pathways act via secreted ligands to establish these embryonic patterns, producing distinct cellular responses in a concentration and time dependent manner (Freeman, 2000; Ulloa and Briscoe, 2007; Kutejova et al., 2009). These pathways require precise spatial and temporal control of ligand production and distribution to preserve the requisite diversity of cellular responses and to limit signaling within the appropriate domains. Thus, feedback antagonism of secreted ligands plays a critical role in regulating the level and spatial distribution of signaling within a target field (Perrimon and McMahon, 1999; Freeman, 2000).

Hedgehog (HH) proteins are secreted molecules that play critical roles in both vertebrate and invertebrate development (McMahon et al., 2003). Negative feedback at the level of HH ligand is governed by the canonical receptor, Patched (PTC; PTCH in vertebrates) (Chen and Struhl, 1996). Seminal studies in *Drosophila* identified two distinct forms of PTC-mediated antagonism (Chen and Struhl, 1996). In the absence of ligand, PTC inhibits the activity of Smoothened (SMO) (Ingham et al., 2000), a key effector of the pathway, in a process termed ligand-independent antagonism (LIA) (Jeong and McMahon, 2005). Ligand binding to PTC relieves SMO inhibition and culminates in modulation of HH target genes, including *ptc* itself. Consequently, PTC is highly up-regulated near the source of HH production to bind and sequester ligand and limit the level and the range of signaling within a responding tissue (Hooper and Scott, 1989; Nakano et al., 1989). This negative feedback by PTC at the level of ligand is known as ligand-dependent antagonism (LDA) (Jeong and McMahon, 2005).

Evidence from *Drosophila* suggests that PTC up-regulation is dispensable for SMO inhibition (LIA), but is required to sequester HH ligand and prevent pathway activation in cells more distal to the HH source (LDA) (Chen and Struhl, 1996). Feedback up-regulation of the vertebrate PTCH1 receptor is conserved in mammals (Goodrich et al., 1996); however, similar experiments that abrogate PTCH1-feedback up-regulation in mice do not dramatically alter HH signaling during early embryogenesis (Milenkovic et al., 1999; Jeong and McMahon, 2005). In this model, tonal levels of PTCH1 are produced from a transgene using the metallothionein promoter (*MT-Ptch1*) (Milenkovic et al., 1999). In *MT-Ptch1;Ptch1*$^{-/-}$ embryos, basal levels of PTCH1 are sufficient for LIA, but surprisingly given the *Drosophila* studies, these embryos display a largely normal body plan at E10.5 with relatively minor disturbances of HH-dependent patterning (Milenkovic et al., 1999; Jeong and McMahon, 2005).

In contrast to *Drosophila*, vertebrates possess two additional cell surface HH-binding proteins that are induced by HH signaling: Hedgehog interacting protein 1 (HHIP1; (Chuang and McMahon, 1999), a membrane anchored glycoprotein, and Patched 2 (PTCH2; (Motoyama et al., 1998b), a structural homolog of PTCH1 that arose from a gene duplication event. HHIP1 acts partially redundantly with PTCH1 to antagonize HH signaling in the developing mouse central nervous system (CNS); embryos lacking both HHIP1 and PTCH1-feedback inhibition generate cell fates within the normal HH signaling domain that are more ventral than expected, and HH-responses extend into dorsal regions that do not normally exhibit active signaling (Jeong and McMahon, 2005). In comparison, mutant embryos such as *Ptch1*$^{-/-}$, where LIA is removed, and *Sufu*$^{-/-}$, where the pathway is activated downstream of ligand, have an even more ventralized phenotype with a significant extent of the neural tube adopting a Sonic HH (SHH)-secreting floorplate fate (Goodrich et al., 1997; Cooper et al., 2005). The differences in the severity of

these patterning defects suggest that other mechanisms limit ligand-dependent vertebrate HH pathway activity.

The contribution of PTCH2 in feedback antagonism during CNS patterning has not been addressed. Mouse PTCH1 and PTCH2 share 56% amino acid identity; a key difference is that PTCH2 is more stable than PTCH1 due to a truncated C-terminal region (Kawamura et al., 2008). Although PTCH2 antagonizes HH signaling in cell-based assays (Rahnama et al., 2004), *Ptch2*$^{-/-}$ mice are viable and fertile, whereas *Ptch1*$^{-/-}$ mice die at E9.5 with ectopic HH signaling throughout the embryo (Nieuwenhuis et al., 2006; Goodrich et al., 1997). *Ptch2*$^{-/-}$ embryos do, however, exhibit subtle changes in gene expression consistent with increased HH pathway activation, including a slight expansion of *Ptch1* and *Gli1* expression in the developing limb bud and the embryonic hair follicle (Nieuwenhuis et al., 2006). These transcriptional changes ultimately resolve to produce normally patterned HH-responsive tissues although aged male *Ptch2*$^{+/-}$ and *Ptch2*$^{-/-}$ mice develop epidermal hyperplasia and alopecia (Nieuwenhuis et al., 2006). That PTCH1 action may mask PTCH2 activity is a reasonable hypothesis especially given the observation that the loss of *Ptch2* enhances tumorigenesis in a *Ptch1*$^{+/-}$ background (Lee et al., 2006).

Here, we demonstrate that PTCH2 is a critical component of LDA in the developing neural tube. While embryos lacking PTCH2 alone or in combination with HHIP1 display normal neural patterning, combined loss of PTCH2 and PTCH1-feedback inhibition results in a significant expansion of SHH dependent-ventral cell populations. In addition, complete loss of PTCH2, HHIP1, and PTCH1-feedback inhibition results in a neural tube composed entirely of ventral cell populations, similar to *Ptch1*$^{-/-}$ and *Sufu*$^{-/-}$ embryos. Overall, these data demonstrate an essential role for negative feedback at the level of HH ligand during vertebrate development

and reveal a collective requirement for PTCH1, PTCH2, and HHIP1 in ligand-dependent feedback inhibition.

## 2.3 Results

*Ptch2 is a direct HH target that antagonizes SHH-mediated pathway activation in vivo.*

Genomic characterization of GLI1 and GLI3 binding profiles highlight HH pathway components, including *Ptch1*, *Ptch2* and *Hhip1*, as direct transcriptional targets of HH signaling (Vokes et al., 2008; 2007; Peterson et al., 2012). Previously, a promoter proximal GLI1 binding region (GBR) associated with *Ptch1* recapitulated the majority of *Ptch1* expression, including in the CNS (Vokes et al., 2007). Similarly, *Ptch2* possesses a conserved promoter proximal GBR (*Ptch2*$^{(-0.5kb)}$; Fig. 2-1 A); however, the regulatory potential of this region remains unexplored. To determine the enhancer activity associated with *Ptch2*$^{(-0.5kb)}$ , we isolated a highly conserved 459 base pair region and assayed reporter expression in transient transgenic mouse embryos at E10.5 (Fig. 2-1 B). The *Ptch2*$^{(-0.5kb)}$ enhancer displays a ventral distribution throughout the entire CNS consistent with *Ptch2* as a direct readout of SHH signaling (Fig. 2-1, C and D) and in line with previous reports of *Ptch2* expression in the neural tube (Motoyama et al., 1998a).

To examine PTCH2-mediated antagonism of HH signaling, and to directly compare PTCH2 to other cell surface HH pathway antagonists, we expressed PTCH2, PTCH1, and HHIP1 in HH-responsive NIH/3T3 fibroblasts. Cells transfected with a HH-responsive luciferase reporter (Chen et al., 1999) and treated with SHH show robust induction of luciferase activity compared to untreated cells (Fig. 2-1 E). Consistent with previous reports, expression of PTCH1, HHIP1, or PTCH2 inhibits NSHH-mediated pathway activation (Fig. 2-1 E; (Rahnama et al., 2004).

To extend these results, we utilized chick *in ovo* electroporations to determine whether PTCH2 could antagonize SHH-dependent ventral neural patterning. During nervous system development, a gradient of SHH directly induces (class II genes: *Nkx6.1, Nkx2.2, FoxA2,* etc.) or indirectly represses (class I genes: *Pax7, Pax3,* etc.) expression of a series of transcriptional regulators in a concentration-dependent manner (Dessaud et al., 2008). The combinatorial activity of these transcriptional determinants along the dorsal-ventral (D-V) axis specifies unique neural progenitor domains that generate distinct classes of mature neurons (Briscoe et al., 2000). These targets quantitatively readout HH pathway activity *in vivo*.

Ectopic expression of EGFP (pCIG) in the chick neural tube does not affect neural patterning (Fig. 2-1, F-I) based on expression of NKX6.1 (class II target) and PAX7 (class I target). In contrast, over-expression of either PTCH1 or PTCH2 represses NKX6.1 (Fig. 2-1, J, K, N, and O, arrows) and de-represses PAX7 expression in the ventral neural tube (Fig. 2-1, L, M, P, and Q, arrows) consistent with PTCH1 and PTCH2 acting as HH pathway antagonists. Importantly, NKX6.1 is maintained and PAX7 remains repressed in more ventral cells electroporated with either PTCH1 or PTCH2 (Fig. 2-1, J-Q, arrowheads), suggesting that Patched-mediated antagonism can be overcome by higher ligand concentrations. In contrast, a ligand-insensitive PTCH1 ($PTCH1^{\Delta L2}$) that acts as a constitutive SMO antagonist (Briscoe et al., 2001) inhibits NKX6.1 and enables PAX7 expression in a position-independent manner (Fig. 2-1, R-U). Taken together, these data are consistent with PTCH2 acting as a HH pathway antagonist.

*$Ptch2^{-/-}$ and $Ptch2^{-/-}$;$Hhip1^{-/-}$ embryos display normal ventral neural patterning*

To determine the endogenous actions of PTCH2, we analyzed SHH-dependent ventral neural patterning in *Ptch2*$^{-/-}$ embryos. Consistent with other published alleles, *Ptch2*$^{-/-}$ mice are viable and fertile (Nieuwenhuis et al., 2006) and display a grossly normal body plan at E10.5 (Fig. 2-2 A and B). As reported for *Hhip1* mutants (Jeong and McMahon, 2005), *Ptch2*$^{-/-}$ embryos exhibit no overt defects in ventral neural patterning at E10.5 (Fig. 2-3; Fig. 2-4, B and G).

To address possible redundancy between PTCH2 and HHIP1 functions, we analyzed neural patterning in *Ptch2;Hhip1* double mutant embryos at E10.5 (Fig. 2-4); however, *Ptch2*$^{-/-}$*;Hhip1*$^{-/-}$ embryos are grossly normal and exhibit no defects in ventral neural patterning at this stage (Fig. 2-2, A-C; Fig. 2-4, E and J).

*Expansion of ventral neural progenitors in embryos lacking PTCH1 and PTCH2 feedback antagonism*

Given the previously identified redundancy between PTCH1 and HHIP1, we reasoned that PTCH1-feedback inhibition is sufficient to antagonize SHH signaling in *Ptch2;Hhip1* double mutants. Thus, to uncover a role for PTCH2, we utilized an *MT-Ptch1* transgene that produces sufficient levels of PTCH1 for LIA of SMO (Milenkovic et al., 1999), to compare the phenotypes of *MT-Ptch1;Ptch1*$^{-/-}$ embryos that lack PTCH1-mediated LDA with *MT-Ptch1;Ptch1*$^{-/-}$*;Ptch2*$^{-/-}$ embryos, incapable of both PTCH1 and PTCH2-dependent LDA.

As previously reported, *MT-Ptch1;Ptch1*$^{-/-}$ embryos display a grossly normal body plan at E10.5 (Fig. 2-2 D) (Milenkovic et al., 1999; Jeong and McMahon, 2005), although a subtle expansion of ventral cell identities is detected when compared to wildtype embryos at E10.5 (Fig. 2-5, A, B, E, and F). This is in stark contrast to analogous experiments performed in

*Drosophila*, where removal of PTC-feedback inhibition completely abrogates receptor-mediated feedback antagonism (Chen and Struhl, 1996). Intriguingly, *MT-Ptch1;Ptch1*$^{-/-}$*;Ptch2*$^{-/-}$ embryos exhibit midbrain and hindbrain exencephaly (Fig. 2-2 E)– similar to mutants lacking GLI3 repressor activity (Hui and Joyner, 1993) and consistent with overactive HH pathway activity. Compared to *MT-Ptch1;Ptch1*$^{-/-}$ embryos, *MT-Ptch1;Ptch1*$^{-/-}$*;Ptch2*$^{-/-}$ embryos also exhibit significant expansion of SHH-dependent NKX6.1 (Fig. 2-5 D), FOXA2, NKX2.2, and OLIG2 (Fig. 2-5 H) expression at E10.5 indicative of an increased range of HH signaling in the absence of PTCH2. In particular, NKX2.2+ cells, which require a high threshold for induction (Ericson et al., 1997), are dorsally extended in *MT-Ptch1;Ptch1*$^{-/-}$*;Ptch2*$^{-/-}$ embryos (Fig. 2-5 H, arrows, see insets). The ventral expansion is accompanied by retraction of the dorsal PAX3+ domain in *MT-Ptch1;Ptch1*$^{-/-}$*;Ptch2*$^{-/-}$ embryos (Fig. 2-5 D). Quantitation demonstrates a significant increase in FOXA2+ floorplate cells (Fig. 2-5 I), NKX2.2+ v3 interneuron progenitors (Fig. 2-5 J), and the proportion of the neural tube that is NKX6.1+ in *MT-Ptch1;Ptch1*$^{-/-}$*;Ptch2*$^{-/-}$ embryos compared to *MT-Ptch1;Ptch1*$^{-/-}$ animals (Fig. 2-5 K).

These results, in combination with previous studies (Jeong and McMahon, 2005), demonstrate that PTCH2 and HHIP1 functionally compensate for the absence of PTCH1-feedback inhibition during ventral neural patterning. To determine whether transcriptional up-regulation of *Ptch2* or *Hhip1* occurs in the absence of PTCH1-mediated LDA, we examined *Ptch2* and *Hhip1* expression patterns in the neural tube of *MT-Ptch1;Ptch1*$^{-/-}$ embryos using RNA *in situ* hybridization (Fig. 2-6). Both *Hhip1* and *Ptch2* are transcriptionally up-regulated in the ventral neural tube of *MT-Ptch1;Ptch1*$^{-/-}$ compared to wildtype embryos at E9.5 and E10.5 (Fig. 2-6). We also observe significant up-regulation of *Hhip1* transcripts in the paraxial mesoderm in embryos lacking PTCH1-feedback inhibition (Fig. 2-6, M-P).

Together the data suggest that PTCH1, PTCH2 and HHIP1 all contribute to LDA of SHH signaling. Further, when PTCH2 or HHIP1 is absent, the normal patterning response is dependent on PTCH1-mediated LDA.

*Severe neural tube ventralization in E10.5 embryos lacking combined PTCH1, PTCH2 and HHIP1 feedback antagonism*

In both *MT-Ptch1;Ptch1*$^{-/-}$*;Ptch2*$^{-/-}$ and *MT-Ptch1;Ptch1*$^{-/-}$*;Hhip1*$^{-/-}$ embryos, a persistent PAX3+; NKX6.1- dorsal domain suggests that SHH signaling is largely absent from the dorsal neural tube (Fig. 2-5; Fig. 2-7, B and J). The cells in this region are HH-responsive, as evident from *Ptch1*$^{-/-}$ embryos where NKX6.1 extends the length of the D-V axis and only a small number of PAX3+ cells remain (Goodrich et al., 1997). This disparity could be explained by the residual functions of HHIP1 or PTCH2 in *MT-Ptch1;Ptch1*$^{-/-}$*;Ptch2*$^{-/-}$ or *MT-Ptch1;Ptch1*$^{-/-}$*;Hhip1*$^{-/-}$ embryos, respectively.

To test this, we reduced the gene dosage of *Hhip1* in *MT-Ptch1;Ptch1*$^{-/-}$*;Ptch2*$^{-/-}$ embryos. Consistent with this view, *MT-Ptch1;Ptch1*$^{-/-}$*;Ptch2*$^{-/-}$*;Hhip1*$^{+/-}$ embryos display a more severe expansion of ventral cell populations than *MT-Ptch1;Ptch1*$^{-/-}$*;Ptch2*$^{-/-}$ embryos (Fig. 2-7, B, F, C, and G). Additionally, *MT-Ptch1;Ptch1*$^{-/-}$*;Hhip1*$^{-/-}$*;Ptch2*$^{+/-}$ embryos exhibit a further expansion of ventral cell identities compared to *MT-Ptch1;Ptch1*$^{-/-}$*;Hhip1*$^{-/-}$ embryos (Fig. 2-7, J, K, N, and O). Thus, both HHIP1 and PTCH2 play significant roles when PTCH1/PTCH2 or PTCH1/HHIP1 feedback responses are removed, respectively. Of note, there is significant variability in the degree of patterning defects in these embryos, which likely reflects the large effects from fluctuations in near threshold levels of dorsal SHH signals (Fig. 2-7, K and O, insets). Interestingly, we also observed significant mixing amongst different cell populations indicating

that LDA is essential to generate discrete boundaries between progenitor domains (Fig. 2-7, F and G, arrows).

These data support the notion that PTCH1, PTCH2, and HHIP1 together comprise a feedback network of cell surface HH antagonists. To test this hypothesis, we generated embryos that completely lack cell surface feedback antagonism (*MT-Ptch1;Ptch1*$^{-/-}$*;Ptch2*$^{-/-}$*;Hhip1*$^{-/-}$).

Grossly, triple mutant embryos display severe exencephaly throughout most of the anterior-posterior axis, CNS overgrowth, craniofacial abnormalities, and enlarged somites (Fig. 2-2 G). Remarkably, *MT-Ptch1;Ptch1*$^{-/-}$*;Ptch2*$^{-/-}$*;Hhip1*$^{-/-}$ embryos exhibit neural patterning defects comparable to those described in *Ptch1*$^{-/-}$ embryos (Fig. 2-7, D, H, L, and P) (Goodrich et al., 1997): a small dorsal midline cluster of PAX3+ cells, NKX6.1 expression along the entire D-V axis (Fig. 2-7, D and L), OLIG2+ motor neuron progenitors confined to the dorsal neural tube, and NKX2.2+ v3 progenitors extending to the dorsal limits of the neuraxis (Fig. 2-7, H and P; Fig. 2-8).

FOXA2 is critical for induction of SHH at the ventral midline and its activation there requires the highest level of HH signaling (Roelink et al., 1995; Ribes et al., 2010). In *MT-Ptch1;Ptch1*$^{-/-}$*;Ptch2*$^{-/-}$*;Hhip1*$^{-/-}$ embryos, FOXA2 production extends throughout the D-V axis with high levels of expression ventrally and low levels dorsally (Fig. 2-7, H and P; Fig. 2-8), resulting in a dramatically enlarged SHH producing floorplate (Fig. 2-7, Q-U). However, persistent NKX2.2 expression in these cells demonstrates incomplete floorplate maturation (Fig. 2-7, H and P; Fig. 2-8).

As an expected outcome of progenitor misspecification, we also observed a severe reduction in post-mitotic descendants of specific progenitor classes in the absence of all LDA, including motor neurons (ISL1 and MNR2), V1 interneurons (EN1), and V0 interneurons

(EVX1; Fig. 2-9). Overall, these data demonstrate a collective requirement for PTCH2, HHIP1, and PTCH1-feedback inhibition to restrict HH signaling in order to ensure the appropriate diversity of both ventral and dorsal neural progenitor types.

Beyond the severe neural patterning defects observed in the embryos, we also detected significant deficits in the size and cellularity of *MT-Ptch1;Ptch1*$^{-/-}$*;Ptch2*$^{-/-}$*;Hhip1*$^{-/-}$ neural tubes as well as aberrant neuroepithelial outgrowths (Fig. 2-10, A-E, arrows) and cells budding off of the epithelium into the lumen (Fig 2-10, F-J, arrowheads). These morphologic defects are accompanied by reduced proliferation and increased apoptosis, as assessed by Phospho-Histone H3 (PH3) and Cleaved Caspase-3 (CC3) staining, respectively, in triple mutants (Fig. 2-11). Notably, apoptotic cells are most prominent in the paraxial mesoderm surrounding the neural tube (Fig. 2-11) and the distal extent of apoptotic mesodermal cells from the notochord increases with the severity of the LDA mutations, suggesting that the cell death is dependent on SHH ligand. Additionally, the loss of paraxial mesoderm could contribute to the lack of mature neurons (Fig. 2-9) due to compromised retinoic acid production from the somites, which is required for neuronal differentiation in the neural tube (Diez del Corral et al., 2003; Novitch et al., 2003; Sockanathan et al., 2003).

*Severe neural tube ventralization in E8.5 MT-Ptch1;Ptch1*$^{-/-}$*;Ptch2*$^{-/-}$*;Hhip1*$^{-/-}$ *embryos is independent of floorplate-derived SHH*

The extended SHH domain in *MT-Ptch1;Ptch1*$^{-/-}$*;Ptch2*$^{-/-}$*;Hhip1*$^{-/-}$ embryos raises the possibility that the observed patterning defects are secondary to enhanced SHH ligand production rather than due to a direct deficiency of LDA. To resolve these conflicting interpretations, we examined neural patterning at E8.5, where SHH-dependent ventral patterning

derives solely from notochord-expressed ligand. While FOXA2 expression begins around the 8-somite stage, floorplate SHH expression does not initiate until the 16-somite stage (Jeong and McMahon, 2005). Thus, patterning defects prior to this time reflect direct readouts of the loss of LDA uncomplicated by ectopic SHH from an expanded floorplate.

In *Ptch2*$^{-/-}$*;Hhip1*$^{-/-}$ embryos at E8.5, neural patterning is normal as indicated by the dorsal restriction of PAX3, and NKX6.1 expression in the ventral neural tube (Fig. 2-12, A and F). In addition, FOXA2 expression initiates in the ventral midline with SHH synthesis limited to the notochord (Fig. 2-12 K). As expected, *MT-Ptch1;Ptch1*$^{-/-}$ embryos exhibit a slight expansion of NKX6.1 and FOXA2 compared to *Ptch2*$^{-/-}$*;Hhip1*$^{-/-}$ embryos (Fig. 2-12, B, G, and L). However, *MT-Ptch1;Ptch1*$^{-/-}$*;Ptch2*$^{-/-}$ embryos demonstrate a dramatic expansion of NKX6.1 and FOXA2 expression compared to *MT-Ptch1;Ptch1*$^{-/-}$ embryos (Fig. 2-12, C, H, and M) at E8.5. Interestingly, the magnitude of this early difference is more marked than at E10.5, with FOXA2 expression at the dorsal most extent of the neural tube in E8.5 *MT-Ptch1;Ptch1*$^{-/-}$*;Ptch2*$^{-/-}$ and *MT-Ptch1;Ptch1*$^{-/-}$*;Ptch2*$^{-/-}$*;Hhip1*$^{+/-}$ embryos (Fig. 2-12, M and N, arrows), a phenotype never observed at E10.5. In some instances, we also observed reduced PAX3 (Fig. 2-12, H and I) and induction of FOXA2 (Fig. 2-12, M and N) in the somites of LDA mutants at E8.5, suggesting that ligand-mediated feedback antagonism also functions to restrain HH signaling in other HH-responsive tissues. Finally, *MT-Ptch1;Ptch1*$^{-/-}$*;Ptch2*$^{-/-}$*;Hhip1*$^{-/-}$ embryos exhibit severe neural tube ventralization nearly indistinguishable from *Ptch1*$^{-/-}$ embryos at E8.5 (Fig. 2-12, J and O). In each instance, immunostaining for SHH confirmed that the patterning defects arise solely from notochord-derived ligand (Fig. 2-12, K-O). Collectively, these results are consistent with a direct requirement for LDA in neural progenitors to limit HH signaling at the onset of ventral neural patterning.

*PTCH2 is a ciliary-localized SMO antagonist*

While the ectopic signaling observed in *MT-Ptch1;Ptch1*$^{-/-}$*;Ptch2*$^{-/-}$*;Hhip1*$^{-/-}$ embryos is likely ligand-dependent, loss of inhibition downstream of ligand could also contribute to this phenotype. To address this, we tested whether PTCH1, PTCH2 or HHIP1 could antagonize signaling downstream of SMO. In NIH/3T3 cells, co-transfection of PTCH1, PTCH2, or HHIP1 with constitutively active SMOM2 (Xie et al., 1998) does not reduce HH pathway activity compared to cells transfected with SMOM2 alone (Fig. 2-13 A); thus, these cell surface molecules act upstream of SMO.

We next explored whether PTCH1, PTCH2, and HHIP1 can directly antagonize SMO activity (LIA). Towards this end, we employed mouse embryonic fibroblasts (MEFs) isolated from *Ptch1*$^{-/-}$ embryos that lack LIA and exhibit high levels of HH signaling. While PTCH1 can directly inhibit SMO, there are conflicting reports concerning LIA by PTCH2 (Rahnama et al., 2004; Nieuwenhuis et al., 2006). As previously reported, expression of PTCH1 in *Ptch1*$^{-/-}$ MEFs causes robust inhibition of HH-responsive luciferase reporter activity even at low concentrations of transfected DNA (Fig. 2-13 B; (Taipale et al., 2002). While PTCH1 and PTCH2 function equivalently at high DNA concentrations, PTCH2 displays significantly reduced activity at lower concentrations, even though PTCH2 protein is highly stable compared to PTCH1 (Fig. 2-13 B; (Kawamura et al., 2008). In contrast, HHIP1 is unable to inhibit SMO at any DNA concentration tested (Fig. 2-13 B). Overall, these results suggest that PTCH2 is capable of LIA of SMO but that PTCH2 activity is weaker than PTCH1.

PTCH1 and PTCH2 are structurally related to the RND permease superfamily, which consists of 12-pass transmsembrane proteins that function by proton-antiport to efflux small molecules across lipid bilayers (Tseng et al., 1999). This transporter activity is dependent on a

conserved RND domain and missense mutations within the PTCH1 RND motif result in impaired LIA, consistent with PTCH1 functioning catalytically as an RND transporter (Tseng et al., 1999; Taipale et al., 2002). To determine whether LIA by PTCH2 involves a similar catalytic activity, we generated two analogous PTCH2 RND mutants: PTCH2G465V and PTCH2D469Y. As previously reported, PTCH1G495V and PTCH1D499Y exhibit reduced ability to inhibit SMO in *Ptch1*$^{-/-}$ MEFs (Fig. 2-13 C). Similarly, PTCH2G465V and PTCH2D469Y display impaired LIA at all concentrations tested (Fig. 2-13 D), consistent with PTCH2 functioning as an RND permease. PTCH2 binds all three mammalian HH ligands with similar affinity as PTCH1 (Carpenter et al., 1998); however, previous work suggested that PTCH2-mediated inhibition of SMO is only relieved after treatment with Desert Hedgehog (DHH) ligand and does not respond to SHH (Rahnama et al., 2004). We next determined whether PTCH2 could respond to SHH in *Ptch1*$^{-/-}$ MEFs. Interestingly, both PTCH1- and PTCH2-mediated inhibition of SMO is partially relieved upon treatment with SHH (Fig. 2-13 E), suggesting that PTCH2 is responsive to SHH ligand. In contrast, a ligand-insensitive PTCH1 construct (PTCH1$^{\Delta L2}$) is refractory to SHH treatment (Fig. 2-13 E).

During vertebrate embryogenesis, the HH co-receptors GAS1, CDON, and BOC are collectively required to initiate HH ligand-mediated responses (Allen et al., 2011). *Gas1;Cdon;Boc* triple mutant embryos are nearly identical to *Smo*$^{-/-}$ mutants (Allen et al., 2011), yet HH signaling can be activated downstream of ligand using small molecule SMO agonists in co-receptor deficient cerebellar granule neuron precursors (Izzi et al., 2011). Consistent with their role in mediating HH ligand-dependent signaling, GAS1, CDON, and BOC interact with PTCH1 and can form distinct receptor complexes (Bae et al., 2011; Izzi et al., 2011). Based on the ability of PTCH2 to respond to SHH, we assessed whether PTCH2 interacts with the HH co-

receptors by co-immunoprecipitation. Similar to PTCH1, HA-tagged PTCH2 interacts with GAS1, CDON, and BOC in COS7 cells (Fig. 2-13 F), suggesting that PTCH2 can also form complexes with the HH co-receptors.

SMO transduces the HH signal at the primary cilium, an organelle critical for vertebrate HH signal transduction (Corbit et al., 2005; Huangfu et al., 2003). In the absence of ligand, PTCH1 localizes to the primary cilium to prevent SMO ciliary accumulation and activation. Ligand-binding to PTCH1 delocalizes LIA from the ciliary membrane, enabling downstream signaling through SMO (Rohatgi et al., 2007). To determine whether PTCH2 and HHIP1 also localize to the primary cilium, we expressed HA-tagged PTCH2 and HHIP1 in NIH/3T3 cells to examine co-labeling of HA with the ciliary marker, Acetylated Tubulin (ACTUB). Consistent with previous studies, PTCH1 localizes to the primary cilium (Fig. 2-13, G-I). Strikingly, we also detect PTCH2 within the ciliary membrane of transfected cells (Fig. 2-13, J-L). This localization is not dependent on a physical interaction with endogenous PTCH1 as PTCH2::HA also localizes to the primary cilium in *Ptch1*$^{-/-}$ MEFs (Fig. 2-13, J-L, insets). In contrast, HHIP1::HA does not localize to the primary cilium (Fig. 2-13, M-O). Taken together these data suggest that ciliary localization is a shared feature between PTCH1 and PTCH2, but that ciliary localization is not a universal requirement for ligand-dependent HH pathway antagonism.

## 2.4 Discussion

*A novel role for PTCH2 as a HH pathway antagonist during vertebrate neural patterning*

While initial studies suggested that PTCH2 plays little to no role in antagonizing HH signaling *in vivo* (Nieuwenhuis et al., 2006), data presented here support an important role for PTCH2 in restricting HH pathway activity during vertebrate embryogenesis. First, embryos

lacking both PTCH1 and PTCH2 feedback inhibition (*MT-Ptch1;Ptch1$^{-/-}$;Ptch2$^{-/-}$*) display more severe patterning defects than those lacking only PTCH1 feedback antagonism (*MT-Ptch1;Ptch1$^{-/-}$*). This inhibitory role is most evident at E8.5, when HH-dependent ventral patterning initially occurs unopposed by antagonistic roof plate signals, including Wnts and BMPs (Parr et al., 1993; Dudley and Robertson, 1997). Second, the severe ventralization observed in *MT-Ptch1;Ptch1$^{-/-}$;Ptch2$^{-/-}$;Hhip1$^{-/-}$* embryos compared to *MT-Ptch1;Ptch1$^{-/-}$;Hhip1$^{-/-}$* animals suggests that PTCH2 limits HH activity in the absence of both HHIP1 and PTCH1 LDA. Lastly, chick electroporation studies and cell signaling assays confirm that PTCH2 directly antagonizes HH ligand function. This finding is particularly important in light of the potential role for PTCH2 in human cancers and congenital disorders (Fan et al., 2008; 2009).

We also present evidence that both PTCH1 and PTCH2 restrict HH signaling using similar molecular mechanisms. Like PTCH1, PTCH2 can antagonize ligand-dependent HH pathway activation and directly inhibit SMO activity. Moreover, PTCH2-mediated LIA depends on a conserved RND motif, implicating PTCH2 as a novel RND-permease within the HH pathway. Emerging evidence suggests that the cell surface HH machinery functions in the context of a complex interaction network (Izzi et al., 2011; Bae et al., 2011). Similar to PTCH1, data presented here show that PTCH2 may function as a receptor complex with the obligate HH co-receptors, GAS1, CDON, and BOC. This is consistent with the ability of PTCH2 to respond to SHH ligand, but future studies will be needed to define the functional significance of these interactions and to determine how HHIP1 participates in the cell surface HH interactome.

PTCH1 is thought to function within the membrane of the primary cilium to prevent ciliary entry and subsequent activation of SMO (Rohatgi et al., 2007). Consistent with this idea, we detect PTCH2 within primary cilium, implicating PTCH2 as a novel, ciliary localized HH

pathway component. However, the lack of ciliary localized HHIP1 suggests that ciliary localization is not a general requirement for ligand-dependent HH pathway antagonism, and that diverse mechanisms exist to restrict the activity of HH ligands during embryogenesis.

*Collective requirement for PTCH2, HHIP1, and PTCH1 during feedback antagonism of vertebrate HH signaling*

Our data support a model where PTCH2, HHIP1, and PTCH1 comprise a semi-redundant feedback network of cell surface antagonists that collectively act to restrict ligand-dependent HH pathway activity (LDA). Removal of any single cell surface antagonist produces little to no defects in ventral cell specification, while combined removal of PTCH1-feedback inhibition and either PTCH2 or HHIP1 produces a significant expansion of ventral cell populations. Intriguingly, complete loss of feedback inhibition by all three cell surface antagonists yields a neural tube composed entirely of ventral cell populations, including expression of the highest-level HH targets, NKX2.2 and FOXA2, throughout the D-V axis.

Patterning defects of this magnitude have thus far only been described for mutations that activate HH signaling downstream of ligand, such as *Ptch1*$^{-/-}$ and *Sufu*$^{-/-}$ embryos (Goodrich et al., 1997; Cooper et al., 2005). In contrast, the severe ventralization observed in *MT-Ptch1;Ptch1*$^{-/-}$*;Ptch2*$^{-/-}$*;Hhip1*$^{-/-}$ embryos likely results from loss of inhibition at the level of HH ligand (LDA) and not simply from loss of SMO inhibition (LIA). First, only PTCH1 and PTCH2 are capable of LIA; thus, the lack of ectopic signaling in the dorsal neural tube of *MT-Ptch1;Ptch1*$^{-/-}$*;Ptch2*$^{-/-}$ embryos confirms that PTCH1 levels provided by the *MT-Ptch1* transgene are sufficient for LIA. Since HHIP1 is incapable of LIA, the severe ventralization observed upon further removal of HHIP1 likely results from enhanced ligand-dependent signaling. That HHIP1

is indirectly required for LIA is unlikely due to the normal patterning observed in *Hhip1*$^{-/-}$ and *Ptch2*$^{-/-}$*;Hhip1*$^{-/-}$ embryos. Collectively, these results suggest an essential role for negative feedback at the level of HH ligand to restrict HH signaling during ventral neural patterning. Of note, this mechanism is likely more global as we also observe defects in somite patterning and craniofacial development.

Despite the overall similarities in patterning defects, there are some clear differences between *MT-Ptch1;Ptch1*$^{-/-}$*;Ptch2*$^{-/-}$*;Hhip1*$^{-/-}$ (total LDA mutant) and *Ptch1*$^{-/-}$ (complete or near complete LIA mutant) embryos. The floorplate, as demarcated by the highest levels of FOXA2 and SHH synthesis, extends to the dorsal limits of the latter, but only to mid regions of the neural tube in the former. This may reflect the importance of timing in HH-dependent patterning (Dessaud et al., 2008; Balaskas et al., 2012; Dessaud et al., 2007). In *Ptch1*$^{-/-}$ embryos, ectopic signaling occurs once cells gain competence to initiate a HH response. Conversely, the ectopic pathway activity observed in complete LDA mutants is dependent on the kinetics of SHH ligand production and distribution. Dorsal progenitors in LDA mutants ultimately experience high levels of SHH as evident by FOXA2 and NKX2.2 expression; however dorsal cells may not receive this signal within the narrow early competence window required for definitive floorplate specification (Ribes et al., 2010). Lastly, additional HH binding proteins may limit the time and range of SHH ligand-based responses, including the HH co-receptors GAS1, CDON, and BOC (Allen et al., 2011; Izzi et al., 2011), glypicans (Capurro et al., 2008; Li et al., 2011), megalin (LRP2) (Christ et al., 2012), or other cell surface proteins.

*Feedback regulation of SHH is required to establish discrete neural progenitor domain boundaries*

At the onset of ventral neural patterning, the SHH gradient induces or represses expression of transcriptional determinants along the D-V axis to establish distinct progenitor fates. This initial pattern established by SHH ligand is thought to be inherently disorganized and must be refined by cross-repressive interactions between transcription factors expressed in neighboring domains, resulting in sharp boundaries between neural progenitor populations (Briscoe et al., 1999; Briscoe et al., 2000; Ericson et al., 1997). In fact, mathematical models of the downstream gene regulatory network (GRN) initiated by HH signaling can recapitulate the graded and discrete patterns established in the ventral neural tube independent of threshold responses to HH ligand (Balaskas et al., 2012). This suggests that precise interpretation of a SHH gradient is not required to establish distinct progenitor domains in the ventral neural tube (Balaskas et al., 2012). However, our observation of significant mixing of pV3 and pMN populations in embryos with compromised LDA demonstrates the importance of feedback inhibition at the level of HH ligand to produce sharp boundaries between progenitor populations and suggests that the downstream GRN is not sufficient to properly pattern the ventral neural tube in the context of deregulated HH ligand.

A recent study in zebrafish suggests that the initial noisy pattern established by HH ligand is corrected by dramatic cell rearrangements. These migratory events lead to clustering and positioning of neural progenitors to establish discrete boundaries between domains (Xiong et al., 2013). Strikingly, ectopic motor neurons induced in the zebrafish neural tube migrate into the appropriate region independent of their initial position (Xiong et al., 2013). Conservation of this mechanism in mice would predict that ectopic ventral progenitors in embryos with disrupted LDA should migrate into their appropriate positions and produce discrete boundaries. However, this is not the case as our analysis reveals significant mixing of ectopic pMN and pV3 cells. This

discrepancy suggests that mouse and zebrafish could have fundamentally different mechanisms to achieve HH-dependent ventral patterning. Alternatively, the ectopic progenitors in LDA mutants could have been specified after cells are epithelialized and therefore unable to migrate. One intriguing possibility is that the proper regulation of HH ligands is required to direct these coordinated cell movements, despite an apparent lack of a role for downstream signaling in this process (Xiong et al., 2013).

*Complexity of cell surface regulation of HH signaling during vertebrate embryogenesis*

Together, the data presented here demonstrate that *Drosophila* and mammals have fundamentally similar feedback responses, though the unique role of *Drosophila* PTC has been distributed amongst three partially redundant proteins in mammals (PTCH1, PTCH2 and HHIP1), each of which are direct transcriptional targets of the SHH pathway and each of which participates in direct LDA of SHH signaling (Fig. 2-14). The presence of additional antagonists may provide essential robustness to HH-dependent patterning processes during vertebrate development, where HH ligands act over significantly larger distances and greater developmental times in a broader variety of tissue contexts than during invertebrate embryogenesis.

Notably, the collective action of PTCH1, PTCH2, and HHIP1 to restrict HH pathway activity is analogous to the general requirement for the HH co-receptors, GAS1, CDON, and BOC, to activate HH signaling (Allen et al., 2011; Izzi et al., 2011). Similarly, removal of a single co-receptor produces only minor defects in ventral neural patterning while combined removal of GAS1, CDON, and BOC reveals their collective requirement in ligand-mediated HH pathway activation (Allen et al., 2011). The results presented in this study define an equally important network of cell surface antagonists that are collectively required to antagonize ligand-

dependent HH signaling. However, it remains unclear what characteristics distinguish GAS1, CDON, and BOC as HH pathway activators compared to the HH pathway antagonists examined in this study. Future studies will be needed to elucidate the mechanisms that regulate the balance between HH pathway activation and inhibition at the cell surface in different HH-responsive tissues during embryogenesis, organ homeostasis, and HH-dependent disease processes.

## 2.5 Materials and Methods

*Mice*

*Ptch2* mice were generated and provided by Curis. The absence of *Ptch2* mRNA was confirmed by expression analysis in the testes, the highest site of *Ptch2* expression (Carpenter et al., 1998). *Hhip1* (Chuang, 2003), *Ptch1* (Goodrich et al., 1997), and *MtPtch1* (Milenkovic et al., 1999) mice have all been previously described. For timed pregnant analyses, noon of the day on which a vaginal plug was detected was considered E0.5. Precise embryo staging was achieved by assessment of somite number at the time of dissection. For each analysis, a minimum of 3 embryos were analyzed and representative images are shown.

For transgenic analysis of the *Ptch2* enhancer, the *Ptch2* enhancer region (chr4:116,768,296-116,768,754) was PCR amplified from C57Bl/6J genomic DNA, sequence verified and cloned upstream of a modified Hsp68-lacZ reporter construct containing a single copy of the chicken beta-globin insulator. Transient transgenics were generated via pronuclear injection and collected at E10.5. PCR genotyping and X-gal staining were performed as previously described (Vokes et al., 2007).

*Chick in ovo neural tube electroporations*

Electroporations were performed as previously described (Allen et al., 2011). In brief, DNA (1.0 μg/μl) was injected into the neural tubes of Hamburger-Hamilton stage 10-12 chicken embryos with 50 ng/μl Fast Green. Embryos were dissected after 48 hours and fixed in 4% PFA for immunofluorescent analysis.

*Immunofluorescence*

Immunofluorescence was performed essentially as previously described (Allen et al., 2011). Neural patterning analysis was performed at the forelimb level in E9.5 and E10.5 embryos. The following antibodies were used: mouse IgG1 anti-NKX6.1 (1:20, Developmental Studies Hybridoma Bank [DSHB]), mouse IgG2a anti-PAX3 (1:20, DSHB), rabbit IgG anti-DBX1 (1:1000, gift from Dr. Yasushi Nagakawa), mouse IgG1 anti-FOXA2 (1:20, DSHB), rabbit IgG anti-FOXA2 (1:500, Cell Signaling), mouse IgG2b anti-NKX2.2 (1:20, DSHB), rabbit IgG anti-OLIG2 (1:1000, Millipore), mouse IgG1 anti-SHH (1:20, DSHB), rabbit IgG anti-Cleaved Caspase-3 (1:200, Cell Signaling), rabbit IgG anti-Phospho-Histone H3 (1:1000, Millipore), mouse IgG1 anti-MNR2 (1:20, DSHB), mouse IgG2b anti-ISL1 (1:20, DSHB), mouse IgG2a anti-EVX1 (1:20, DSHB), and mouse IgG1 anti-EN1 (1:20, DSHB). Nuclei were visualized with DAPI (1:30,000, Molecular Probes). Alexa 488, 555, and 633 secondary antibodies (1:500, Molecular Probes) were visualized on a Leica upright SP5X confocal microscope.

*Cellular localization of HH pathway components*

NIH/3T3 fibroblasts were plated at 150,000 cells/well on coverslips and transfected 16-24 hours later. 6 hours post-transfection, cells were placed into low serum (0.5%) media and fixed 48 hours later in 4% PFA for immunofluorescent analysis.

*Luciferase assays*

Luciferase assays were adapted from a previously published protocol (Nybakken et al., 2005). Mouse NIH/3T3 fibroblasts were plated at 25,000 cells/well on gelatinized 24-well plates and transfected 16-24 hours later with 150ng of a ptcΔ136-GL3 luciferase reporter (Nybakken et al., 2005; Chen et al., 1999), 50ng of pSV-β-galactosidase (Promega), and 100 ng of control (*pCIG*) or experimental constructs using Lipofectamine 2000 (Invitrogen). After 48 hours, cells were placed in low serum (0.5%) media with 25µl of conditioned media from control (*pCDNA3*) or NSHH transfected (*NShh-pCDNA3*) COS7 cells. Luciferase (Luciferase Assay System kit, Promega) and β-galactosidase (BetaFluor β-galactosidase Assay Kit, Novagen) activity were measured after 48 hours. Luciferase values were normalized to β-galactosidase activity and expressed as fold induction relative to control treated cells.

Signaling assays in *Ptch1*$^{-/-}$ MEFs (a gift from Dr. M.P. Scott) were performed as described with the following modifications. *Ptch1*$^{-/-}$ MEFs were plated at 50,000 cells per well and secreted placental alkaline phosphatase was used as a transfection control (Alkaline Phosphatase Yellow pNPP Liquid Substrate for ELISA, Sigma-Aldrich).

*Immunoprecipitation*

COS7 cells were plated at 1x$10^6$ cells/100 mm-dish and transfected the next day with expression plasmids for the indicated proteins. Immunoprecipitations and western blot analyses were performed as previously described (Okada et al., 2006) In brief, PTCH::HA proteins were immunoprecipitated using a mouse anti-HA antibody (SIGMA H3663). Western blot analyses were then performed using mouse anti-HA, rabbit anti-GFP (Molecular Probes A11122), goat

anti-Gas1 (R&D AF2644), and mouse anti-Actin (SIGMA A5441) to reveal the input and IP levels.

*In situ hybridization*

In situ hybridization was performed essentially as described (Wilkinson, 1992) using digoxigenin labeled probes on 20μm sections collected at the forelimb level of E9.5 and E10.5 embryos.

## 2.6 Acknowledgements

This chapter has been published in *Development* (see citation below) and has been included in this dissertation with permission from the journal editors.

Holtz, A.M., K.A. Peterson, Y. Nishi, S. Morin, J.Y. Song, F. Charron, A.P. McMahon, and B.L. Allen. 2013. Essential role for ligand-dependent feedback antagonism of vertebrate hedgehog signaling by PTCH1, PTCH2 and HHIP1 during neural patterning. *Development*. 140:3423–3434. doi:10.1242/dev.095083.

We thank Dr. M.P. Scott (Stanford University) for the *MT-Ptch1* and *Ptch1* mutant mice and the *Ptch1*$^{-/-}$ MEFs. We also acknowledge Dr. D.A. Bumcrot (Curis) for the *Ptch2* mutant mice. We would like to thank Dr. Y. Nagakawa (University of Minnesota) for the DBX1 antibody. The NKX6.1, PAX3, FOXA2, NKX2.2, SHH, MNR2, ISL1, EVC1, and EN1 antibodies were obtained from the Developmental Studies Hybridoma Bank developed under the auspices of the NICHD and maintained by The University of Iowa, Department of Biological Sciences, Iowa City, IA. Confocal microscopy was performed in the Microscopy and Image Analysis Laboratory (MIL) at the University of Michigan. A.M.H. was supported by the University of Michigan MSTP training grant T32 GM007863. J.S. is supported by a research team grant through The

University of Michigan Center For Organogenesis. B.L.A. is supported by startup funds from The University of Michigan Biological Sciences Scholars Program, Endowment for Basic Sciences and the Department of Cell and Developmental Biology.

## 2.7 Figures

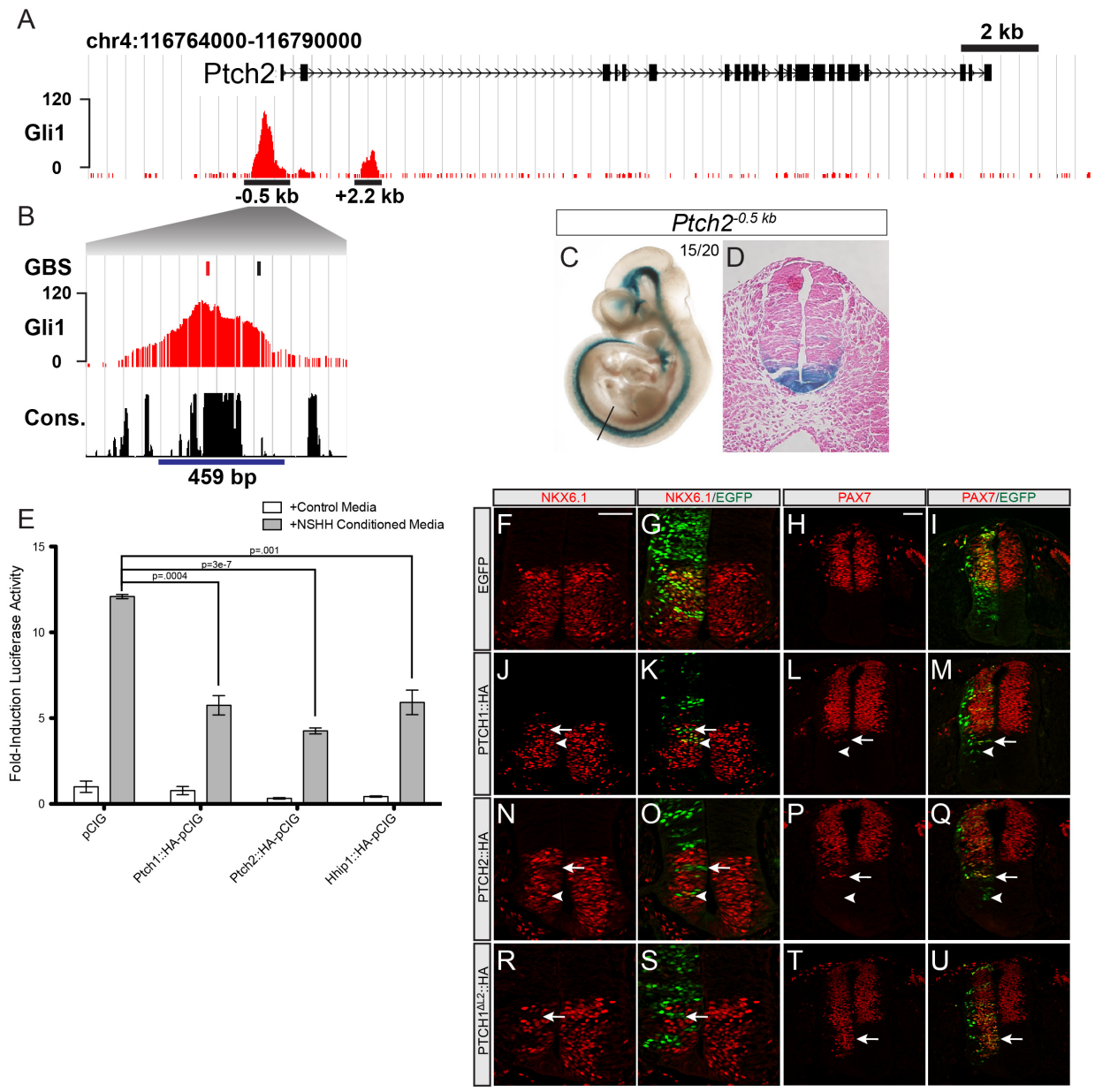


**Figure 2-1**. **PTCH2 is a direct transcriptional target that antagonizes HH signaling in NIH/3T3 cells and in the developing chick neural tube.** (A) *Ptch2* regulatory landscape highlighting two discrete Gli1 binding events positioned at -0.5 kb and +2.2 kb relative to TSS. (B) Zoom in view of -0.5 kb region assayed for enhancer activity (blue bar). Computationally predicted Gli binding sites (GBS) are shown in black (nonconserved) and red (conserved). Multi-species conservation (cons.) is shown below. (C) Transient transgenic analysis of *Ptch2*$^{(-0.5\ kb)}$ regulatory region shows neural specific activity at E10.5. The number of embryos expressing transgene out of total transgenic positives is shown in upper right hand corner. (D) Transverse section taken from region indicated in (C, black bar) shows reporter activity restricted to the ventral neural tube. (E) HH-responsive luciferase reporter activity measured in NIH/3T3

fibroblasts stimulated with either control media (white bars) or NSHH-conditioned media (grey bars), and co-transfected with the indicated constructs. Each condition was performed in triplicate and data are represented as mean +/- SEM (representative assay shown), p-values measured by two-tailed Student's *t*-test. (F-U) Hamburger-Hamilton stage 19-22 chick neural tubes electroporated with *pCIG* (F-I), *Ptch1::HA-pCIG* (J-M), *Ptch2::HA-pCIG* (N-Q), and *Ptch1*$^{\Delta L2}$*::HA-pCIG* (R-U) sectioned at the wing level and stained with antibodies raised against NKX6.1 (red, F, G, J, K, N, O, R, S) or PAX7 (red, H, I, L, M, P, Q, T, U). Nuclear EGFP expression (G, I, K, M, O, Q, S, U) labels electroporated cells. Arrows indicate repression of NKX6.1 expression (J, K, N, O, R, S) or ectopic expression of PAX7 (L, M, P, Q, T, U). Arrowheads indicate ventrally located electroporated cells that maintain NKX6.1 expression (J, K, N, O) or lack ectopic PAX7 expression (L, M, P, Q). Scale bars: (F, H) 50μm.

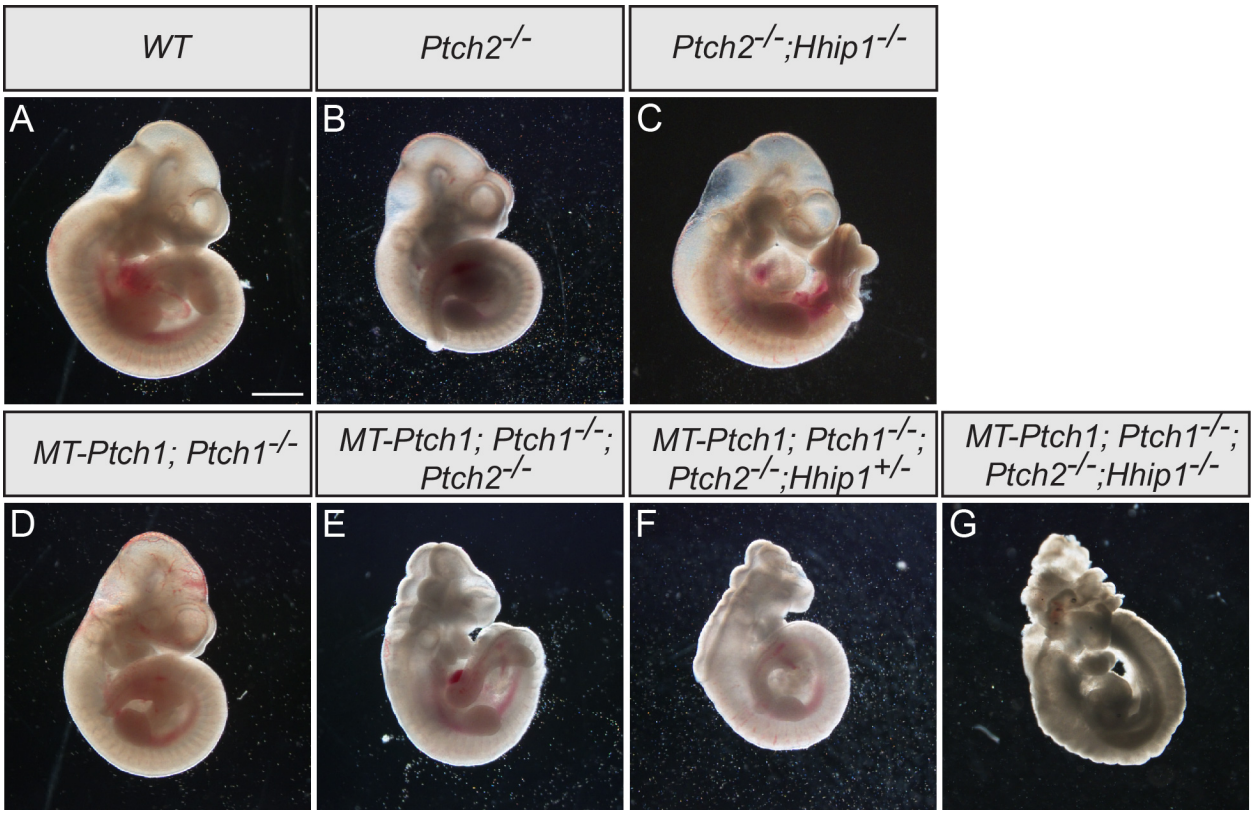


**Figure 2-2. Gross morphology of E10.5 embryos defective in ligand-dependent feedback inhibition of HH signaling.** Whole mount images of wiltype (A), *Ptch2*$^{-/-}$ (B), *Ptch2*$^{-/-}$*;Hhip1*$^{-/-}$ (C), *MT-Ptch1;Ptch1*$^{-/-}$ (D), *MT-Ptch1;Ptch1*$^{-/-}$*;Ptch2*$^{-/-}$ (E), *MT-Ptch1;Ptch1*$^{-/-}$*;Ptch2*$^{-/-}$*;Hhip1*$^{+/-}$ (F), and *MT-Ptch1;Ptch1*$^{-/-}$*;Ptch2*$^{-/-}$*;Hhip1*$^{-/-}$ (G) embryos at E10.5. Note the exencephaly present in embryos lacking both *Ptch2* and *Ptch1* (E-G). Scale bar: (A) 1mm.

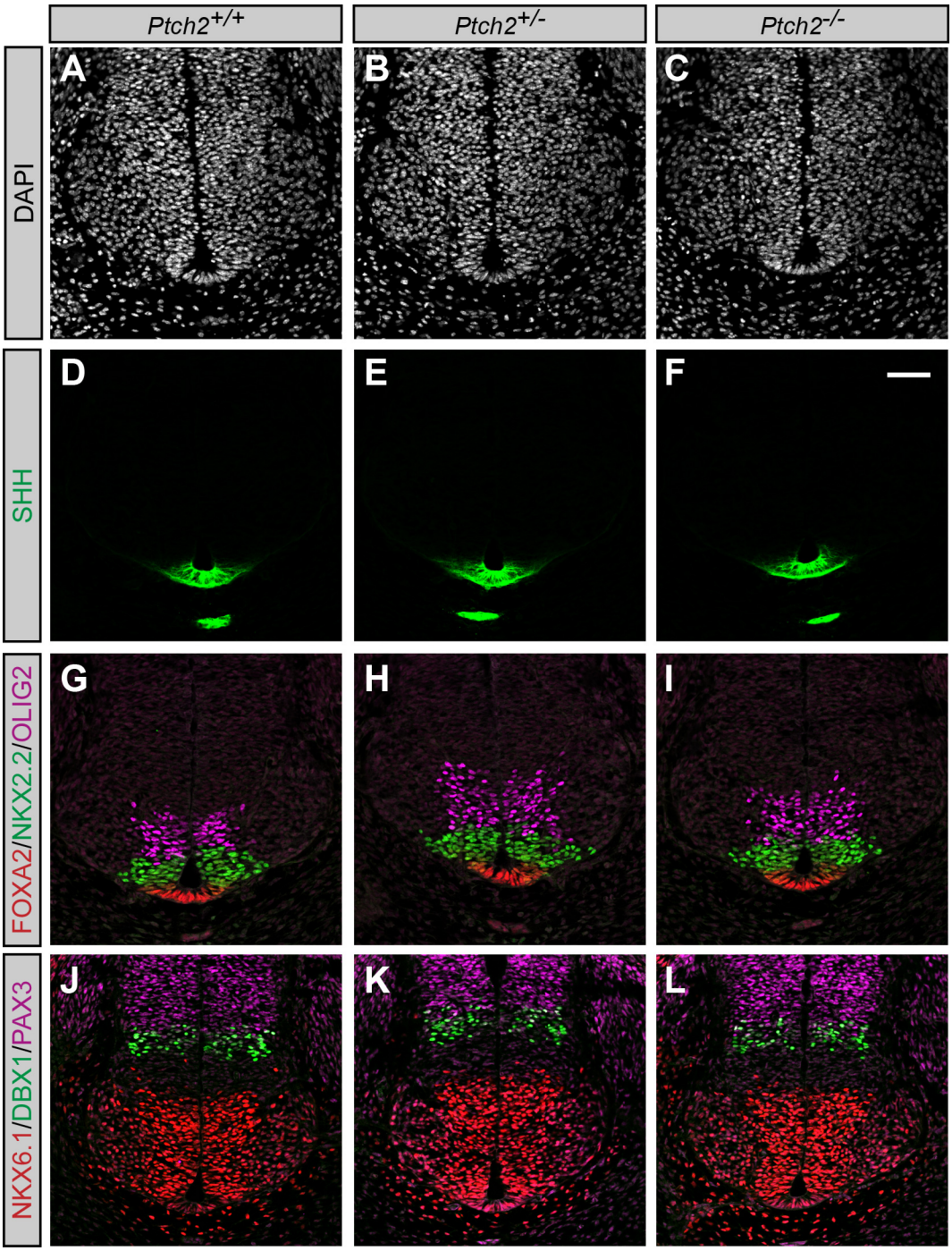


**Figure 2-3. Normal SHH-mediated ventral neural patterning in *Ptch2*$^{-/-}$ embryos.** DAPI staining (A-C) and neural patterning analysis of E10.5 embryos sectioned at the forelimb level detects expression of SHH (green; D-F), FOXA2, NKX2.2, OLIG2 (red, green, and magenta respectively; G-I), NKX6.1, DBX1, and PAX3 (red, green, and magenta; respectively; J-L) in *Ptch2*$^{+/+}$ (A, D, G, J), *Ptch2*$^{+/-}$ (B, E, H, K), and *Ptch2*$^{-/-}$ (C, F, I, L) embryos. Scale bar: (F) 50μm.

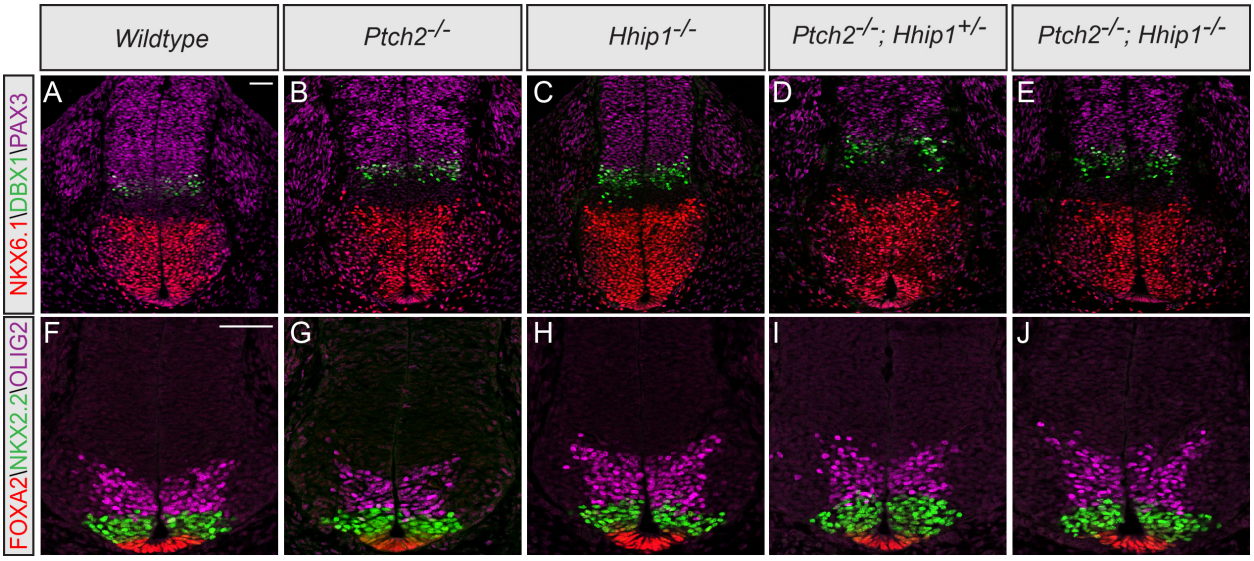


**Figure 2-4. Normal SHH-mediated ventral neural patterning in E10.5 *Ptch2*$^{-/-}$;*Hhip1*$^{-/-}$ mouse embryos.** Immunofluorescent analysis of neural patterning in E10.5 mouse forelimb sections detects expression of NKX6.1, DBX1, PAX3 (red, green and magenta, respectively; A-E), FOXA2, NKX2.2, and OLIG2 (red, green and magenta, respectively; F-J) in wildtype (A, F), *Ptch2*$^{-/-}$ (B, G), *Hhip1*$^{-/-}$ (C, H), *Ptch2*$^{-/-}$;*Hhip1*$^{+/-}$ (D, I), and *Ptch2*$^{-/-}$,*Hhip1*$^{-/-}$ (E, J) embryos. Scale bars: (A, F) 50μm.

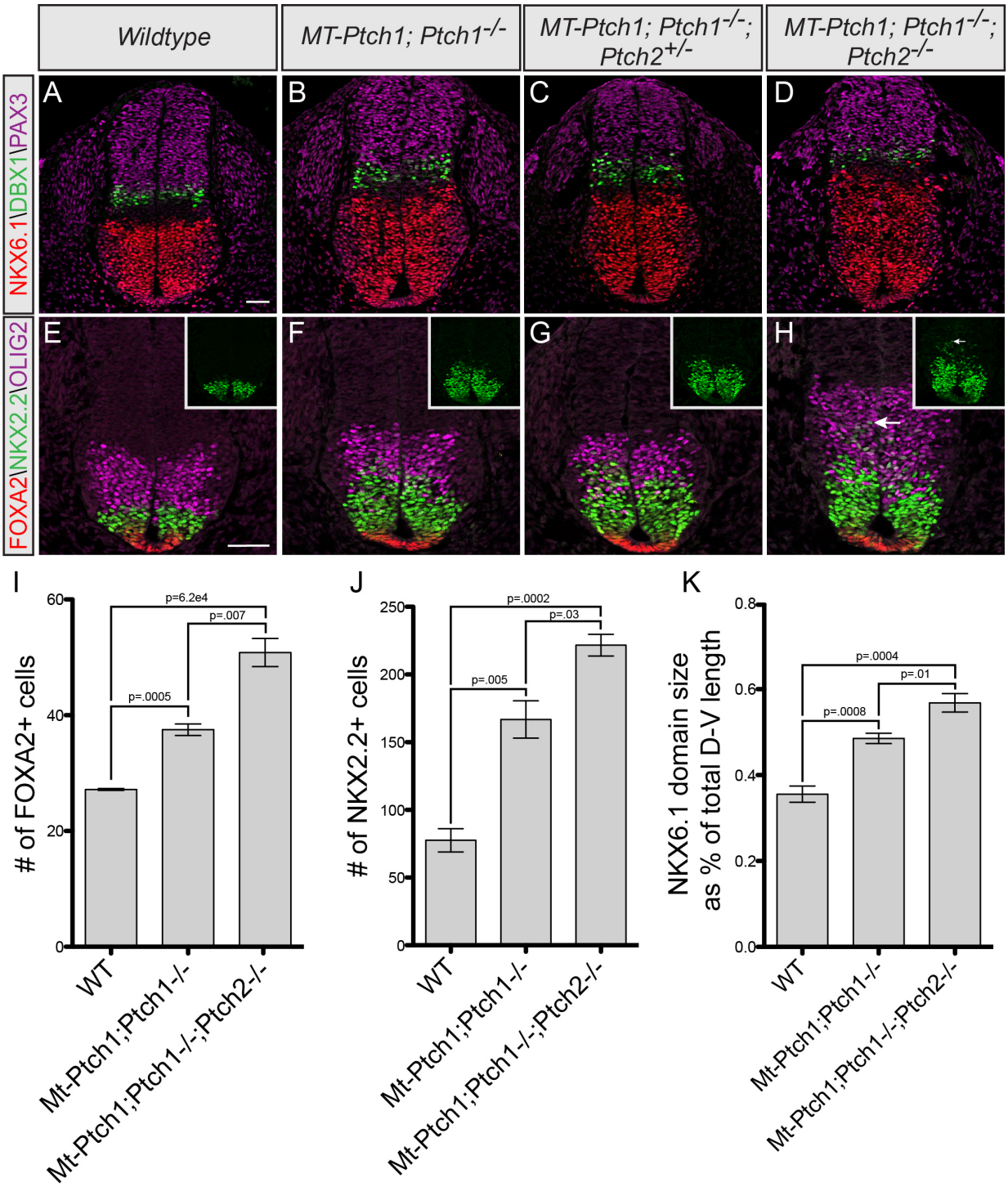


**Figure 2-5. Expansion of SHH-dependent ventral progenitor domains in E10.5 mouse embryos lacking both PTCH2 and PTCH1 feedback antagonism.** (A-H) Neural patterning analysis in E10.5 forelimb sections using antibodies against NKX6.1, DBX1, PAX3 (red, green and magenta, respectively; A-D), FOXA2, NKX2.2, and OLIG2 (red, green and magenta, respectively; E-H) in wildtype (A, E), *MT-Ptch1;Ptch1*$^{-/-}$ (B, F), *MtPtch1;Ptch1*$^{-/-}$*;Ptch2*$^{+/-}$ (C,

G), and *MT-Ptch1;Ptch1*$^{-/-}$*;Ptch2*$^{-/-}$ (D, H) embryos. Insets show NKX2.2 channel alone (E-H). Arrows indicate dorsal expansion of NKX2.2+ cells in *MT-Ptch1;Ptch1*$^{-/-}$*;Ptch2*$^{-/-}$ embryos (H). (I-K) Quantitation of FOXA2+ cell number (I), NKX2.2+ cell number (J), and NKX6.1 domain size as a % of total D-V neural tube length (K). Data are represented as mean +/- SEM calculated from at least three embryos per genotype. P-value determined by two-tailed Student's *t*-test. Scale bars: (A, E) 50μm.

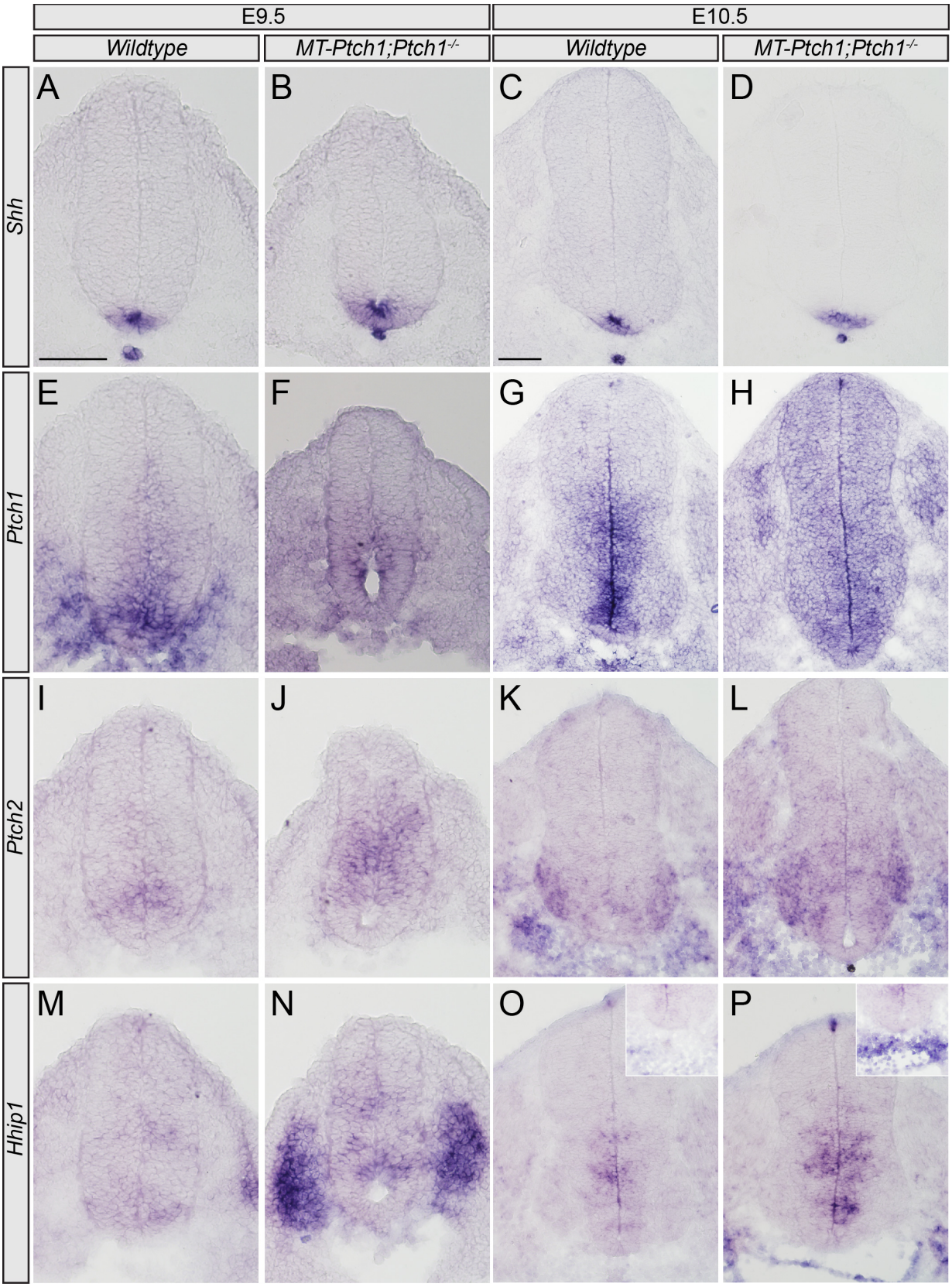
E9.5
E10.5
Wildtype
MT-Ptch1;Ptch1-/-
Wildtype
MT-Ptch1;Ptch1-/-
Shh
Ptch1
Ptch2
Hhip1
A
B
C
D
E
F
G
H
I
J
K
L
M
N
O
P

**Figure 2-6. *Ptch2* and *Hhip1* transcripts are up-regulated in the absence of PTCH1-feedback inhibition.** RNA *in situ* hybridization detects expression of *Shh* (A-D), *Ptch1* (E-H), *Ptch2* (I-L), and *Hhip1* (M-P) transcripts at the forelimb level of wildtype (A,C,E,G,I,K,M,O) and *MT-Ptch1;Ptch1*$^{-/-}$ (B,D,F,H,J,L,N,P) embryos at E9.5 (A,B,E,F,I,J,M,N) and E10.5 (C,D,G,H,K,L,O,P). The *Shh* expression domain is expanded in *MT-Ptch1;Ptch1*$^{-/-}$ (B,D) compared to wildtype (A,C) embryos. The wildtype gradient of *Ptch1* expression (E,G) is lost in *MT-Ptch1;Ptch1*$^{-/-}$ embryos (F,H), where low *Ptch1* expression is detected from the *MT-Ptch1* transgene. Note the dorsal expansion and greater intensity of *Ptch2* and *Hhip1* expression in the neural tube of *MT-Ptch1;Ptch1*$^{-/-}$ (J,L and N,P, respectively) compared to wildtype (I,K and M,O, respectively) embryos. Insets in O,P highlight increased *Hhip1* expression in the paraxial mesoderm surrounding the notochord of *MT-Ptch1;Ptch1*$^{-/-}$ embryos. Scale bar: (A,C) 200μm.

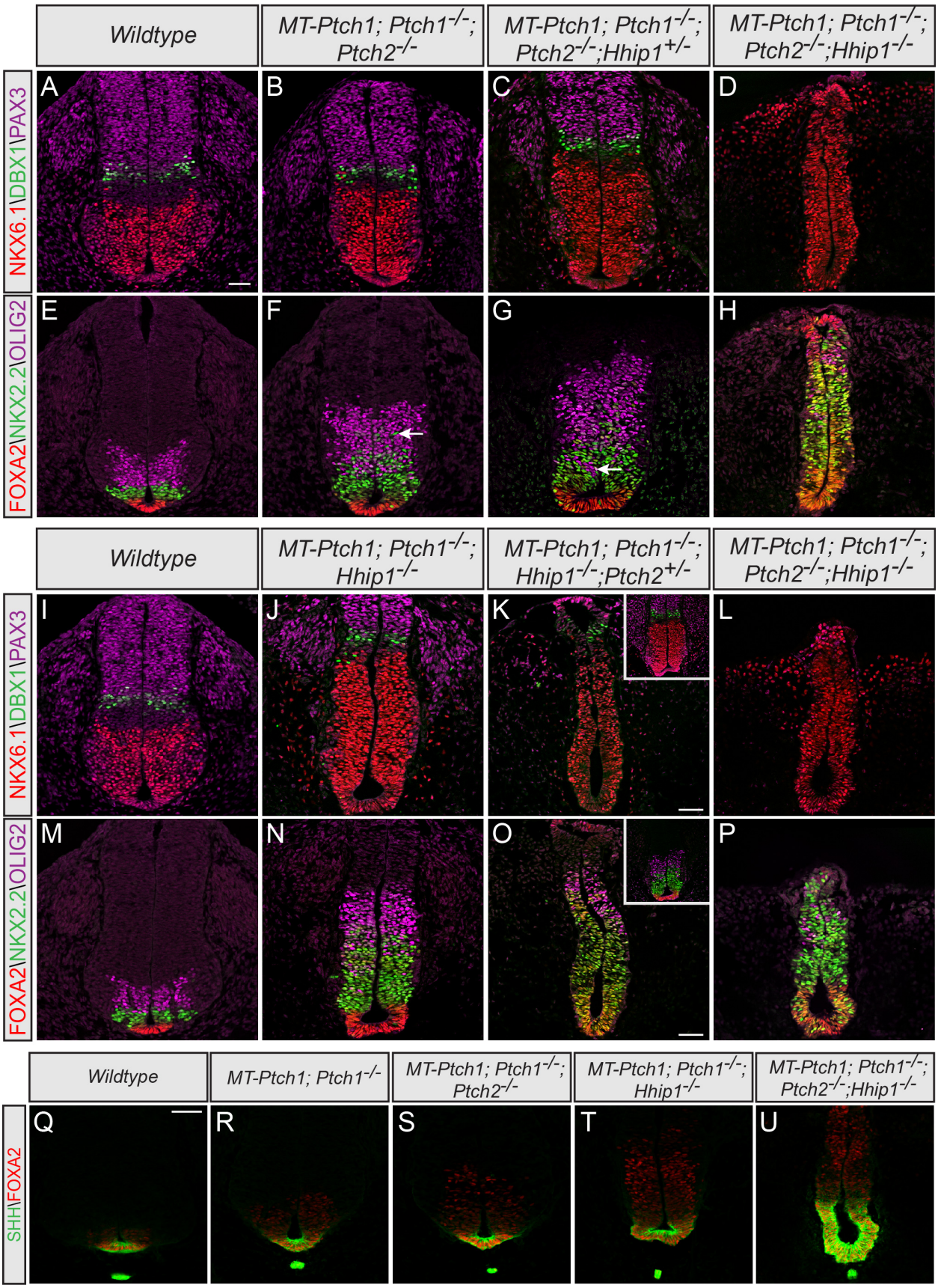
Wildtype
MT-Ptch1; Ptch1-/-; Ptch2-/-
MT-Ptch1; Ptch1-/-; Ptch2-/-;Hhip1+/-
MT-Ptch1; Ptch1-/-; Ptch2-/-;Hhip1-/-
NKX6.1\DBX1\PAX3
FOXA2\NKX2.2\OLIG2
A
B
C
D
E
F
G
H
Wildtype
MT-Ptch1; Ptch1-/-; Hhip1-/-
MT-Ptch1; Ptch1-/-; Hhip1-/-;Ptch2+/-
MT-Ptch1; Ptch1-/-; Ptch2-/-;Hhip1-/-
NKX6.1\DBX1\PAX3
FOXA2\NKX2.2\OLIG2
I
J
K
L
M
N
O
P
Wildtype
MT-Ptch1; Ptch1-/-
MT-Ptch1; Ptch1-/-; Ptch2-/-
MT-Ptch1; Ptch1-/-; Hhip1-/-
MT-Ptch1; Ptch1-/-; Ptch2-/-;Hhip1-/-
SHH\FOXA2
Q
R
S
T
U

**Figure 2-7. Severe neural tube ventralization in E10.5 *MT-Ptch1;Ptch1$^{-/-}$;Ptch2$^{-/-}$;Hhip1$^{-/-}$* embryos.** Antibody detection of NKX6.1, DBX1, PAX3 (red, green, and magenta respectively; A-D, I-L), FOXA2, NKX2.2, OLIG2 (red, green, and magenta respectively; E-H, M-P), SHH (5E1) and FOXA2 (green and red respectively; Q-U) in E10.5 forelimb sections from wildtype (A, E, I, M, Q), *MT-Ptch1;Ptch1$^{-/-}$* (R), *MT-Ptch1;Ptch1$^{-/-}$;Ptch2$^{-/-}$* (B, F, S), *MT-Ptch1;Ptch1$^{-/-}$;Hhip1$^{-/-}$* (J, N, T), *MT-Ptch1;Ptch1$^{-/-}$;Ptch2$^{-/-}$;Hhip1$^{+/-}$* (C, G), *MT-Ptch1;Ptch1$^{-/-}$;Hhip1$^{-/-}$;Ptch2$^{+/-}$* (K, O), and *MT-Ptch1;Ptch1$^{-/-}$;Ptch2$^{-/-}$;Hhip1$^{-/-}$* (D, H, L, P, U) embryos. Arrows indicate NKX2.2+ cells within the OLIG2 domain (F) and OLIG2+ cells in the NKX2.2 domain (G). Insets are representative of less severe phenotypes that are observed in *MT-Ptch1;Ptch1$^{-/-}$;Hhip1$^{-/-}$;Ptch2$^{+/-}$* embryos (K, O). Scale bars: (A, K, O) 50μm.

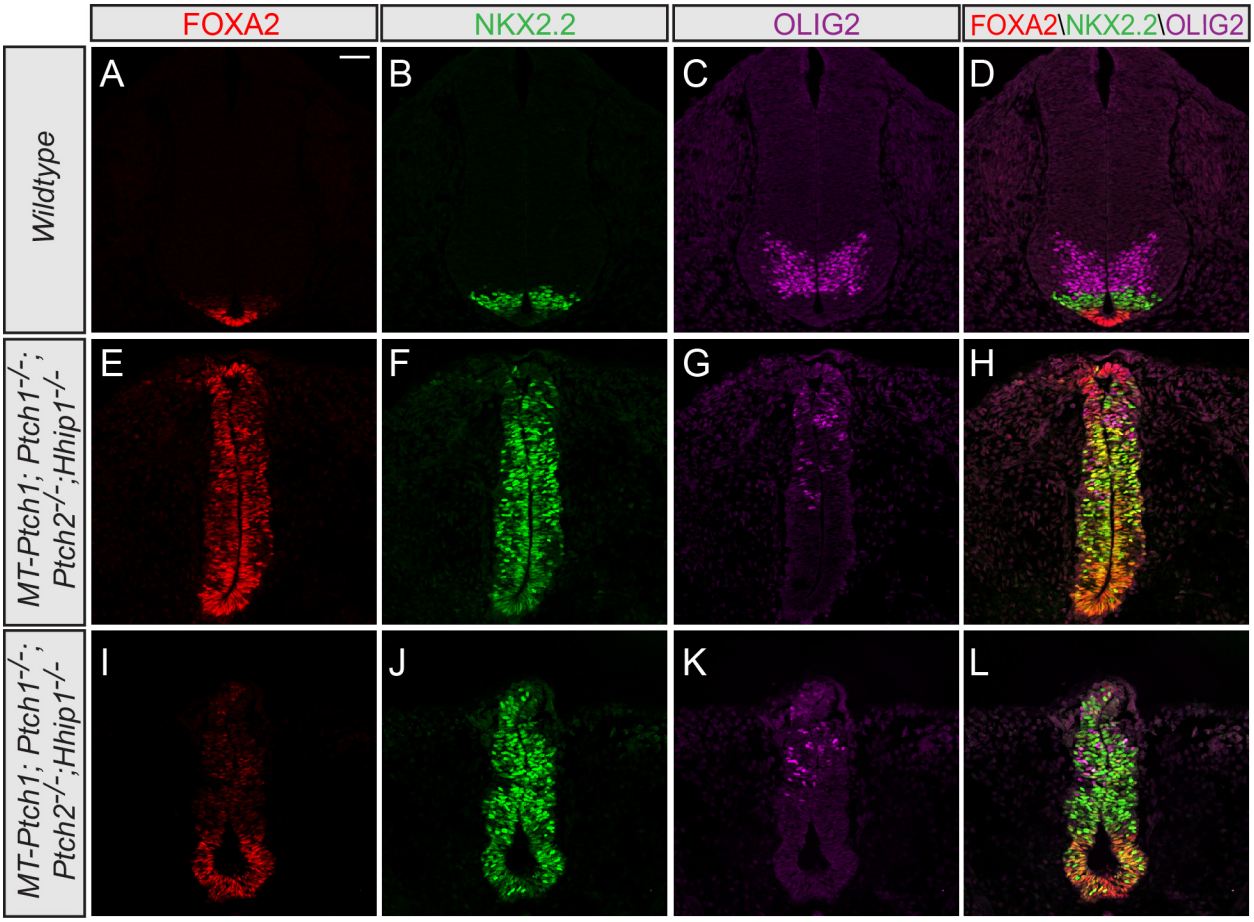


**Figure 2-8. Ubiquitous expression of FOXA2 and NKX2.2 and dorsal restriction of OLIG2 expression in E10.5 *MT-Ptch1;Ptch1$^{-/-}$;Ptch2$^{-/-}$;Hhip1$^{-/-}$* embryos.** Antibody detection of FOXA2 (red; A, D, E, H, I, L), NKX2.2 (green; B, D, F, H, J, L), and OLIG2 (magenta; C, D, G, H, K, L) in E10.5 forelimb sections from wildtype (A-D) and *MT-Ptch1;Ptch1$^{-/-}$;Ptch2$^{-/-}$;Hhip1$^{-/-}$* (E-L) embryos. Merged images are shown in D-L. Scale bar: (A) 50μm.

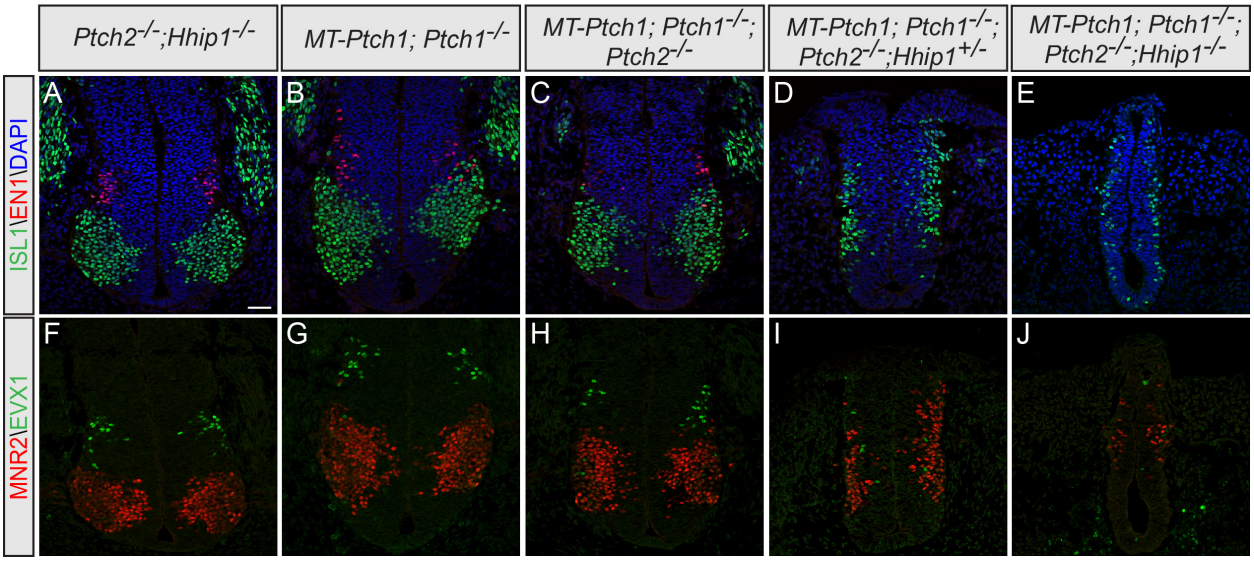


**Figure 2-9. Severe reduction of mature neuronal populations in E10.5 *MT-Ptch1;Ptch1$^{-/-}$;Ptch2$^{-/-}$;Hhip1$^{-/-}$* embryos.** Immunofluorescent analysis of neural patterning in E10.5 mouse forelimb sections detects expression of ISL1, EN1 (green and red respectively; A-E), MNR2, and EVX1 (red and green respectively; F-J) in *Ptch2$^{-/-}$;Hhip1$^{-/-}$* (A, F), *MT-Ptch1;Ptch1$^{-/-}$* (B, G), *MT-Ptch1;Ptch1$^{-/-}$;Ptch2$^{-/-}$* (C, H), *MT-Ptch1;Ptch1$^{-/-}$;Ptch2$^{-/-}$;Hhip1$^{+/-}$* (D, I), and *MT-Ptch1;Ptch1$^{-/-}$;Ptch2$^{-/-}$;Hhip1$^{-/-}$* (E, J) embryos. DAPI staining (blue) is included in A-E. Scale bar: (A) 50μm.

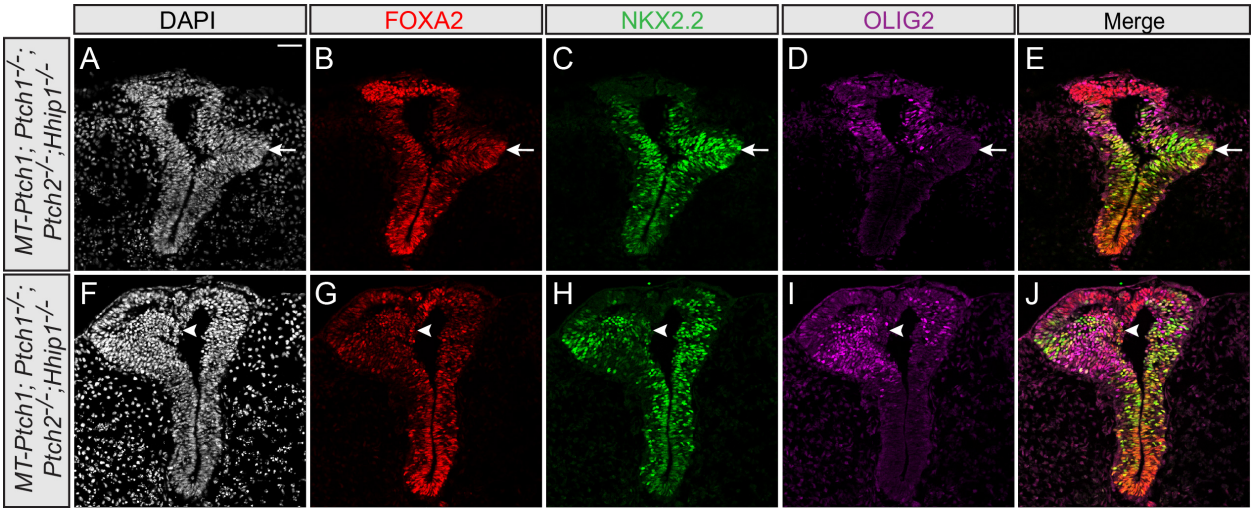


**Figure 2-10. Altered neural tube morphology in E10.5 embryos lacking PTCH2, HHIP1, and PTCH1-feedback inhibition.** DAPI staining (A, F) and antibody detection of FOXA2 (red; B, E, G, J), NKX2.2 (green; C, E, H, J), and OLIG2 (magenta; D, E, I, J) in E10.5 forelimb sections from *MT-Ptch1;Ptch1$^{-/-}$;Ptch2$^{-/-}$;Hhip1$^{-/-}$* embryos. Merged images shown in E, J. Arrows denote abnormal neural tube invaginations (A-E) and arrowheads indicate cells that have budded off of the neuroepithelium and into the luminal space (F-J). Scale bar: (A) 50μm.

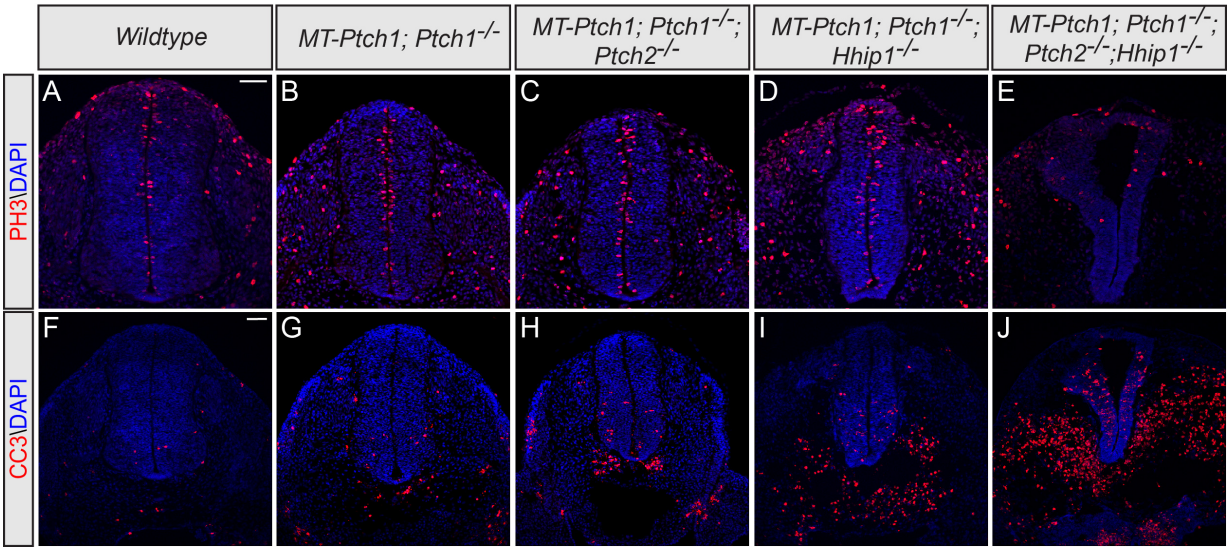


**Figure 2-11. Loss of PTCH2, HHIP1, and PTCH1-feedback antagonism decreases neural progenitor proliferation and increases apoptosis.** Immunostaining using antibodies raised against Phospho-histone H3 (PH3; A-E) and Cleaved Caspase 3 (CC3; F-J) in E10.5 forelimb sections collected from wildtype (A, F), *MT-Ptch1;Ptch1*$^{-/-}$ (B, G), *MT-Ptch1;Ptch1*$^{-/-}$*;Ptch2*$^{-/-}$ (C, H), *MT-Ptch1;Ptch1*$^{-/-}$*;Hhip1*$^{-/-}$ (D, I), and *MT-Ptch1;Ptch1*$^{-/-}$*;Ptch2*$^{-/-}$*;Hhip1*$^{-/-}$ (E, J) embryos. DAPI staining is shown in blue (A-J). Note the decreased proliferation in the ventral neural tube (E) and increased apoptosis outside the neural tube (J) in embryos lacking HH feedback inhibition. Scale bars: (A, F) 50μm.

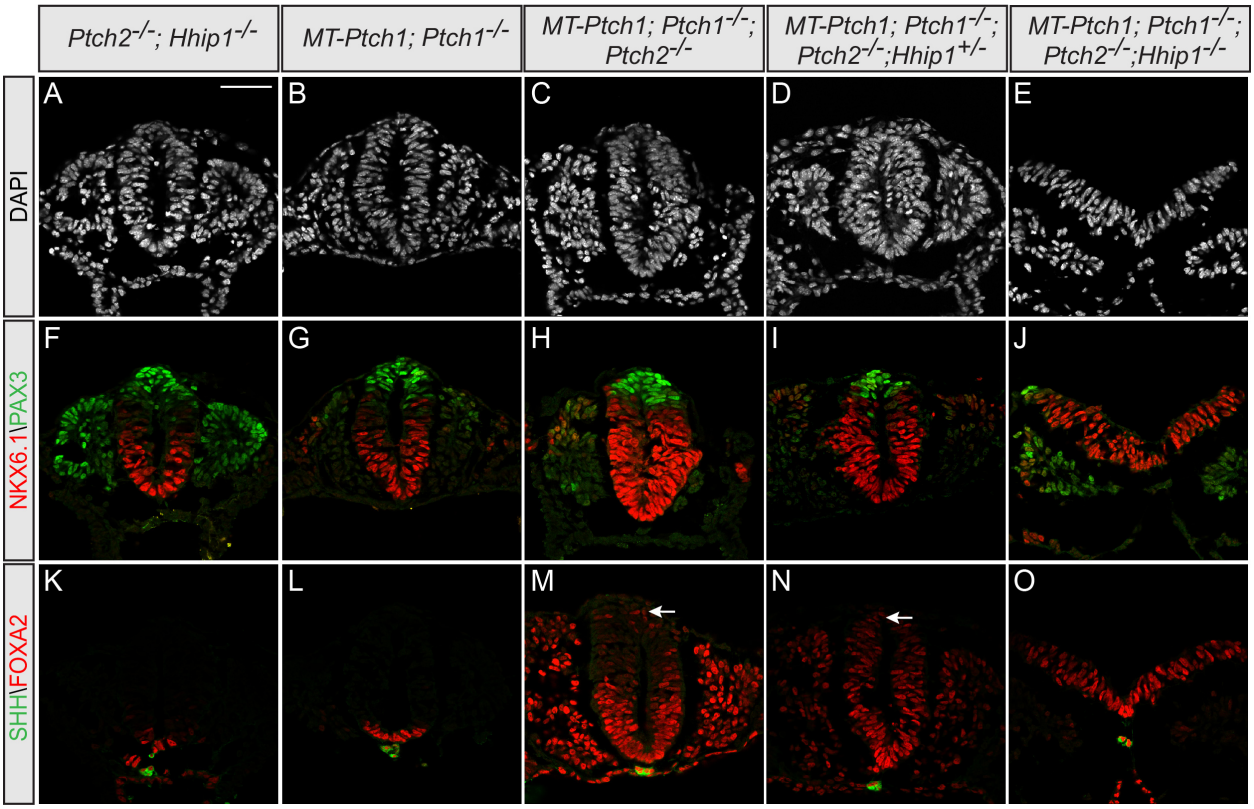


**Figure 2-12. Expansion of ventral progenitor domains occurs prior to floorplate expression of SHH in E8.5 LDA mutants.** DAPI staining (A-E) and neural patterning analysis of E8.5 embryos (9-12 somites) detects expression of NKX6.1, PAX3 (red, green respectively; F-J), FOXA2, and SHH (red, green respectively; K-O) in *Ptch2*$^{-/-}$*;Hhip1*$^{-/-}$ (F, K), *MT-Ptch1;Ptch1*$^{-/-}$ (G, L), *MT-Ptch1;Ptch1*$^{-/-}$*;Ptch2*$^{-/-}$ (H, M), *MT-Ptch1;Ptch1*$^{-/-}$*;Ptch2*$^{-/-}$*;Hhip1*$^{+/-}$ (I, N), and *MT-Ptch1;Ptch1*$^{-/-}$*;Ptch2*$^{-/-}$*;Hhip1*$^{-/-}$ (J, O) embryos. Arrows indicate FOXA2 expression at the dorsal-most region of the neural tube (M, N). Scale bars: (A) 50μm.

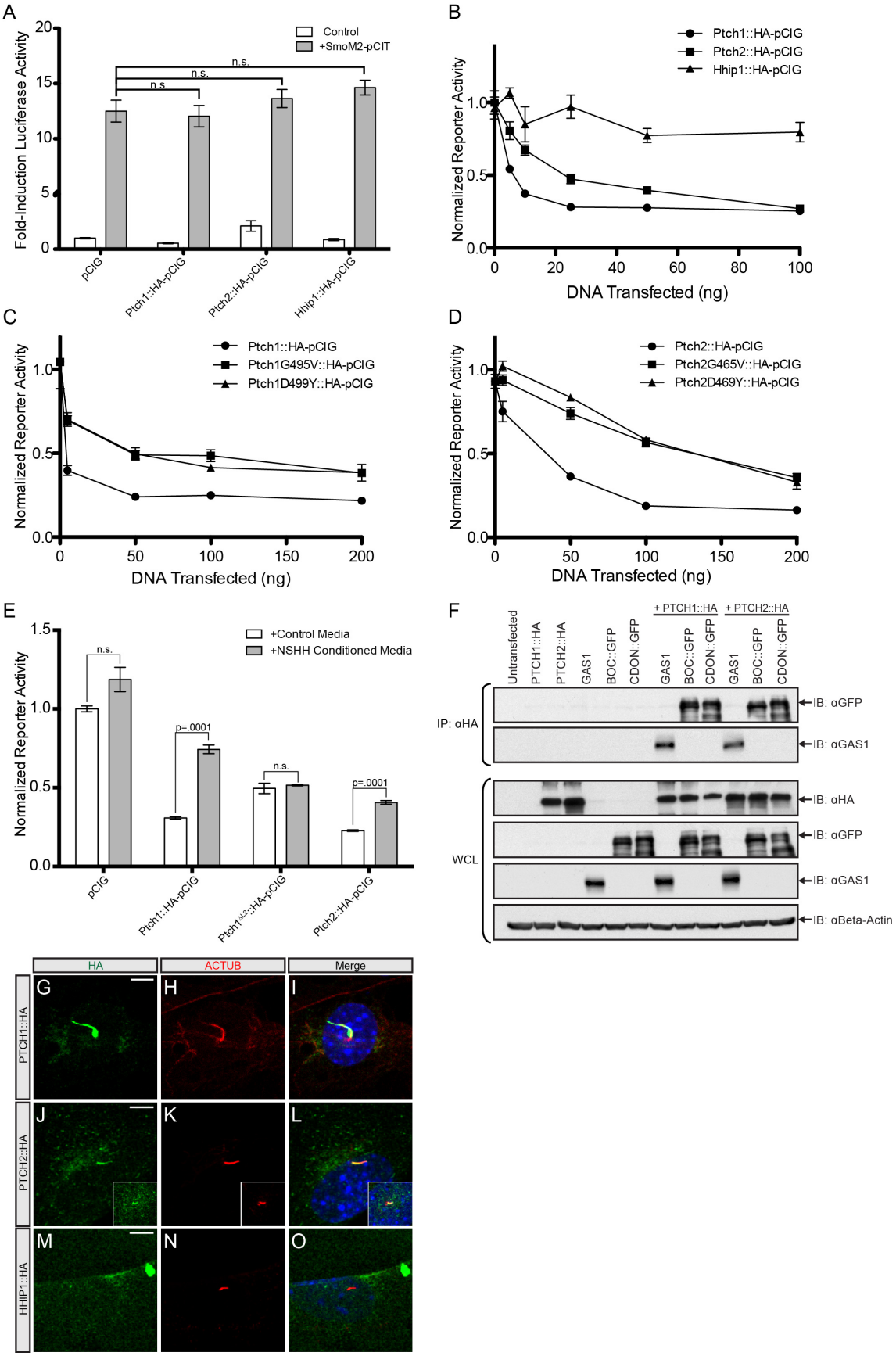
A
Fold-Induction Luciferase Activity
Control
+SmoM2-pCIT
n.s.
pCIG
Ptch1::HA-pCIG
Ptch2::HA-pCIG
Hhip1::HA-pCIG
B
Normalized Reporter Activity
Ptch1::HA-pCIG
Ptch2::HA-pCIG
Hhip1::HA-pCIG
DNA Transfected (ng)
C
Ptch1::HA-pCIG
Ptch1G495V::HA-pCIG
Ptch1D499Y::HA-pCIG
DNA Transfected (ng)
D
Ptch2::HA-pCIG
Ptch2G465V::HA-pCIG
Ptch2D469Y::HA-pCIG
DNA Transfected (ng)
E
+Control Media
+NSHH Conditioned Media
p=.0001
HA
ACTUB
Merge
PTCH1::HA
PTCH2::HA
HHIP1::HA
F
+ PTCH1::HA
+ PTCH2::HA
Untransfected
PTCH1::HA
PTCH2::HA
GAS1
BOC::GFP
CDON::GFP
IP: αHA
IB: αGFP
IB: αGAS1
WCL
IB: αHA
IB: αBeta-Actin

**Figure 2-13. Overlapping and distinct mechanisms of HH pathway antagonism by PTCH1, PTCH2, and HHIP1.** (A) HH-responsive luciferase reporter activity measured from NIH/3T3 fibroblasts stimulated with constitutively active SmoM2 and co-transfected with the indicated constructs. Each condition was performed in triplicate and data are represented as mean +/- SEM (n.s., not significant, P>.05 two-tailed Student's *t*-test, representative assay shown). (B-E) HH-responsive luciferase reporter activity measured from *Ptch1*$^{-/-}$ mouse embryonic fibroblasts (MEFs) transfected with the indicated constructs. Each condition was performed in triplicate and data expressed as luciferase reporter activity normalized to cells transfected with empty vector alone (*pCIG*) and represented as mean +/- SEM. Treatment with control- (white bars) or SHH-conditioned media (grey bars) is indicated in (E). (F) COS7 cells were transfected with the indicated constructs and lysates were immunoprecipitated with anti-HA antibody and blotted with anti-GFP or anti-GAS1 antibodies. (G-O) Immunofluorescent detection of HA (green; G, J, M) and Acetylated Tubulin (ACTUB, red; H, K, N) in NIH/3T3 cells expressing PTCH1::HA (G-I), PTCH2::HA (J-L), and HHIP1::HA (M-O). Merged images with DAPI staining (blue) shown in (I, L, O). Insets show ciliary localization of PTCH2::HA in *Ptch1*$^{-/-}$ MEFs (J-L). Scale bars: (G, J, M) 5μm.

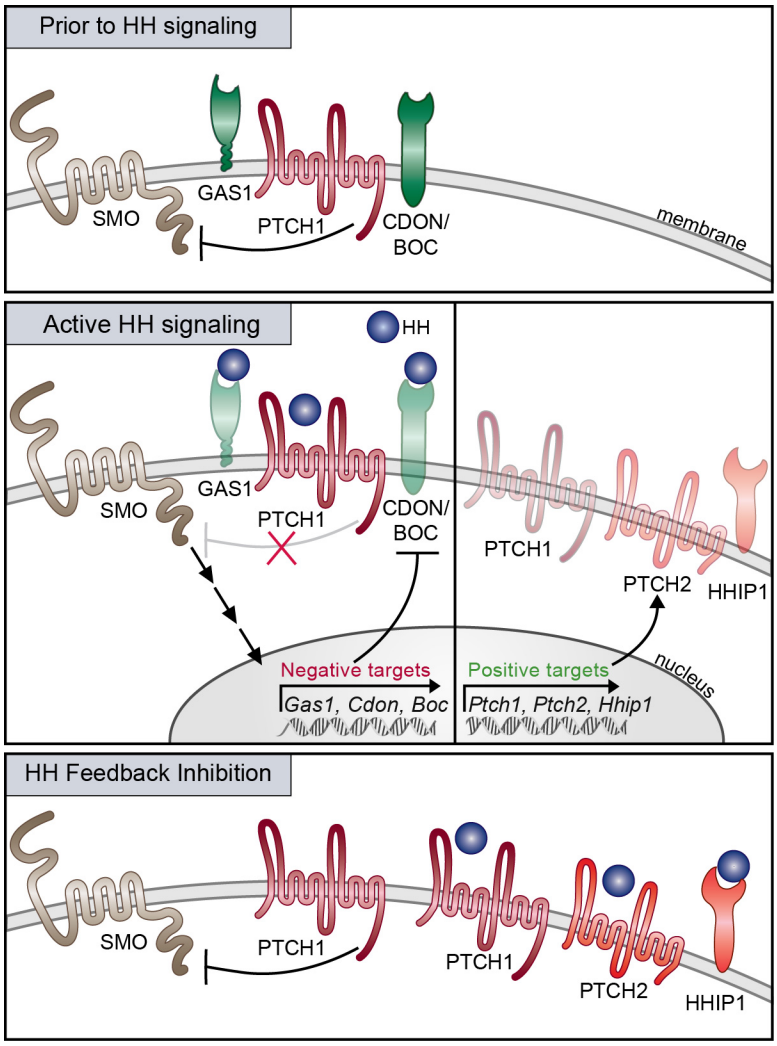


**Figure 2-14. Model of cell surface regulation of HH signaling.** In the absence of HH ligands (top panel) PTCH1 represses SMO activity (LIA). At the onset of HH signaling (middle panel), HH binding to PTCH1 and to the obligate HH co-receptors GAS1, CDON and BOC results in de-repression of SMO function and initiation of a signal transduction cascade that culminates in GLI-mediated modulation of transcriptional targets. This initiates a negative feedback mechanism at the cell surface that includes the down-regulation of *Gas1*, *Cdon* and *Boc*, and up-regulation of *Ptch1*, *Ptch2* and *Hhip1*. PTCH1, PTCH2 and HHIP1 binding to HH ligands (bottom panel) competes with productive ligand-receptor interactions to alter the balance between bound and unbound PTCH1 resulting in cell autonomous modulation of SMO activity. Additionally, ligand sequestration by cell surface HH antagonists results in non-cell autonomous HH pathway inhibition in cells distal to the HH source (LDA).

## 2.8 References


Allen, B.L., J.Y. Song, L. Izzi, I.W. Althaus, J.-S. Kang, F. Charron, R.S. Krauss, and A.P. McMahon. 2011. Overlapping roles and collective requirement for the coreceptors GAS1, CDO, and BOC in SHH pathway function. *Dev. Cell*. 20:775–787. doi:10.1016/j.devcel.2011.04.018.

Bae, G.-U., S. Domené, E. Roessler, K. Schachter, J.-S. Kang, M. Muenke, and R.S. Krauss. 2011. Mutations in CDON, encoding a hedgehog receptor, result in holoprosencephaly and defective interactions with other hedgehog receptors. *Am. J. Hum. Genet.* 89:231–240. doi:10.1016/j.ajhg.2011.07.001.

Balaskas, N., A. Ribeiro, J. Panovska, E. Dessaud, N. Sasai, K.M. Page, J. Briscoe, and V. Ribes. 2012. Gene regulatory logic for reading the sonic hedgehog signaling gradient in the vertebrate neural tube. *Cell*. 148:273–284. doi:10.1016/j.cell.2011.10.047.

Briscoe, J., A. Pierani, T.M. Jessell, and J. Ericson. 2000. A homeodomain protein code specifies progenitor cell identity and neuronal fate in the ventral neural tube. *Cell*. 101:435–445.

Briscoe, J., Y. Chen, T.M. Jessell, and G. Struhl. 2001. A hedgehog-insensitive form of patched provides evidence for direct long-range morphogen activity of sonic hedgehog in the neural tube. *Mol. Cell*. 7:1279–1291.

Capurro, M.I., P. Xu, W. Shi, F. Li, A. Jia, and J. Filmus. 2008. Glypican-3 inhibits Hedgehog signaling during development by competing with patched for Hedgehog binding. *Dev. Cell*. 14:700–711. doi:10.1016/j.devcel.2008.03.006.

Carpenter, D., D.M. Stone, J. Brush, A. Ryan, M. Armanini, G. Frantz, A. Rosenthal, and F.J. de Sauvage. 1998. Characterization of two patched receptors for the vertebrate hedgehog protein family. *Proceedings of the National Academy of Sciences of the United States of America*. 95:13630–13634.

Chen, C.H., D.P. von Kessler, W. Park, B. Wang, Y. Ma, and P.A. Beachy. 1999. Nuclear trafficking of Cubitus interruptus in the transcriptional regulation of Hedgehog target gene expression. *Cell*. 98:305–316.

Chen, Y., and G. Struhl. 1996. Dual roles for patched in sequestering and transducing Hedgehog. *Cell*. 87:553–563.

Christ, A., A. Christa, E. Kur, O. Lioubinski, S. Bachmann, T.E. Willnow, and A. Hammes. 2012. LRP2 Is an Auxiliary SHH Receptor Required to Condition the Forebrain Ventral Midline for Inductive Signals. *Dev. Cell*. 22:268–278. doi:10.1016/j.devcel.2011.11.023.

Chuang, P.T. 2003. Feedback control of mammalian Hedgehog signaling by the Hedgehog-binding protein, Hip1, modulates Fgf signaling during branching morphogenesis of the lung. *Genes & Development*. 17:342–347. doi:10.1101/gad.1026303.

Chuang, P.T., and A.P. McMahon. 1999. Vertebrate Hedgehog signalling modulated by

induction of a Hedgehog-binding protein. *Nature*. 397:617–621. doi:10.1038/17611.

Cooper, A.F., K.P. Yu, M. Brueckner, L.L. Brailey, L. Johnson, J.M. McGrath, and A.E. Bale. 2005. Cardiac and CNS defects in a mouse with targeted disruption of suppressor of fused. *Development*. 132:4407–4417. doi:10.1242/dev.02021.

Corbit, K.C., P. Aanstad, V. Singla, A.R. Norman, D.Y.R. Stainier, and J.F. Reiter. 2005. Vertebrate Smoothened functions at the primary cilium. *Nature*. 437:1018–1021. doi:10.1038/nature04117.

Dessaud, E., A.P. McMahon, and J. Briscoe. 2008. Pattern formation in the vertebrate neural tube: a sonic hedgehog morphogen-regulated transcriptional network. *Development*. 135:2489–2503. doi:10.1242/dev.009324.

Dessaud, E., L.L. Yang, K. Hill, B. Cox, F. Ulloa, A. Ribeiro, A. Mynett, B.G. Novitch, and J. Briscoe. 2007. Interpretation of the sonic hedgehog morphogen gradient by a temporal adaptation mechanism. *Nature*. 450:717–720. doi:10.1038/nature06347.

Dudley, A.T., and E.J. Robertson. 1997. Overlapping expression domains of bone morphogenetic protein family members potentially account for limited tissue defects in BMP7 deficient embryos. *Dev. Dyn.* 208:349–362. doi:10.1002/(SICI)1097-0177(199703)208:3<349::AID-AJA6>3.0.CO;2-I.

Ericson, J., P. Rashbass, A. Schedl, S. Brenner-Morton, A. Kawakami, V. van Heyningen, T.M. Jessell, and J. Briscoe. 1997. Pax6 controls progenitor cell identity and neuronal fate in response to graded Shh signaling. *Cell*. 90:169–180.

Fan, Z., J. Du, H. Liu, H. Zhang, A.A. Dlugosz, C.-Y. Wang, M. Fan, Y. Shen, and S. Wang. 2009. A susceptibility locus on 1p32-1p34 for congenital macrostomia in a Chinese family and identification of a novel PTCH2 mutation. *Am. J. Med. Genet. A*. 149A:521–524. doi:10.1002/ajmg.a.32647.

Fan, Z., J. Li, J. Du, H. Zhang, Y. Shen, C.-Y. Wang, and S. Wang. 2008. A missense mutation in PTCH2 underlies dominantly inherited NBCCS in a Chinese family. *Journal of Medical Genetics*. 45:303–308. doi:10.1136/jmg.2007.055343.

Freeman, M. 2000. Feedback control of intercellular signalling in development. *Nature*. 408:313–319. doi:10.1038/35042500.

Goodrich, L.V., L. Milenkovic, K.M. Higgins, and M.P. Scott. 1997. Altered neural cell fates and medulloblastoma in mouse patched mutants. *Science*. 277:1109–1113. doi:10.1126/science.277.5329.1109.

Goodrich, L.V., R.L. Johnson, L. Milenkovic, J.A. McMahon, and M.P. Scott. 1996. Conservation of the hedgehog/patched signaling pathway from flies to mice: induction of a mouse patched gene by Hedgehog. *Genes & Development*. 10:301–312.

Hooper, J.E., and M.P. Scott. 1989. The Drosophila patched gene encodes a putative membrane

protein required for segmental patterning. *Cell*. 59:751–765.

Huangfu, D., A. Liu, A.S. Rakeman, N.S. Murcia, L. Niswander, and K.V. Anderson. 2003. Hedgehog signalling in the mouse requires intraflagellar transport proteins. *Nature*. 426:83–87. doi:10.1038/nature02061.

Hui, C.C., and A.L. Joyner. 1993. A mouse model of greig cephalopolysyndactyly syndrome: the extra-toesJ mutation contains an intragenic deletion of the Gli3 gene. *Nat Genet*. 3:241–246. doi:10.1038/ng0393-241.

Ingham, P.W., S. Nystedt, Y. Nakano, W. Brown, D. Stark, M. van den Heuvel, and A.M. Taylor. 2000. Patched represses the Hedgehog signalling pathway by promoting modification of the Smoothened protein. *Current Biology*. 10:1315–1318.

Izzi, L., M. Lévesque, S. Morin, D. Laniel, B.C. Wilkes, F. Mille, R.S. Krauss, A.P. McMahon, B.L. Allen, and F. Charron. 2011. Boc and Gas1 each form distinct Shh receptor complexes with Ptch1 and are required for Shh-mediated cell proliferation. *Dev. Cell*. 20:788–801. doi:10.1016/j.devcel.2011.04.017.

Jeong, J., and A.P. McMahon. 2005. Growth and pattern of the mammalian neural tube are governed by partially overlapping feedback activities of the hedgehog antagonists patched 1 and Hhip1. *Development*. 132:143–154. doi:10.1242/dev.01566.

Kawamura, S., K. Hervold, F.-A. Ramirez-Weber, and T.B. Kornberg. 2008. Two patched protein subtypes and a conserved domain of group I proteins that regulates turnover. *J. Biol. Chem.* 283:30964–30969. doi:10.1074/jbc.M806242200.

Kutejova, E., J. Briscoe, and A. Kicheva. 2009. Temporal dynamics of patterning by morphogen gradients. *Curr. Opin. Genet. Dev.* 19:315–322. doi:10.1016/j.gde.2009.05.004.

Lee, Y., H.L. Miller, H.R. Russell, K. Boyd, T. Curran, and P.J. McKinnon. 2006. Patched2 modulates tumorigenesis in patched1 heterozygous mice. *Cancer Research*. 66:6964–6971. doi:10.1158/0008-5472.CAN-06-0505.

Li, F., W. Shi, M. Capurro, and J. Filmus. 2011. Glypican-5 stimulates rhabdomyosarcoma cell proliferation by activating Hedgehog signaling. *J. Cell Biol.* 192:691–704. doi:10.1083/jcb.201008087.

McMahon, A.P., P.W. Ingham, and C.J. Tabin. 2003. Developmental roles and clinical significance of hedgehog signaling. *Curr. Top. Dev. Biol.* 53:1–114.

Milenkovic, L., L.V. Goodrich, K.M. Higgins, and M.P. Scott. 1999. Mouse patched1 controls body size determination and limb patterning. *Development*. 126:4431–4440.

Motoyama, J., H. Heng, M.A. Crackower, T. Takabatake, K. Takeshima, L.C. Tsui, and C. Hui. 1998a. Overlapping and non-overlapping Ptch2 expression with Shh during mouse embryogenesis. *Mech. Dev.* 78:81–84.

Motoyama, J., T. Takabatake, K. Takeshima, and C.-C. Hui. 1998b. Ptch2, a second mouse Patched gene is co-expressed with Sonic hedgehog. *Nat Genet*. 18:104–106. doi:10.1038/ng0298-104.

Nakano, Y., I. Guerrero, A. Hidalgo, A. Taylor, J.R. Whittle, and P.W. Ingham. 1989. A protein with several possible membrane-spanning domains encoded by the Drosophila segment polarity gene patched. *Nature*. 341:508–513. doi:10.1038/341508a0.

Nieuwenhuis, E., J. Motoyama, P.C. Barnfield, Y. Yoshikawa, X. Zhang, R. Mo, M.A. Crackower, and C.-C. Hui. 2006. Mice with a targeted mutation of patched2 are viable but develop alopecia and epidermal hyperplasia. *Mol. Cell. Biol.* 26:6609–6622. doi:10.1128/MCB.00295-06.

Nybakken, K., S.A. Vokes, T.-Y. Lin, A.P. McMahon, and N. Perrimon. 2005. A genome-wide RNA interference screen in Drosophila melanogaster cells for new components of the Hh signaling pathway. *Nat Genet*. 37:1323–1332. doi:10.1038/ng1682.

Parr, B.A., M.J. Shea, G. Vassileva, and A.P. McMahon. 1993. Mouse Wnt genes exhibit discrete domains of expression in the early embryonic CNS and limb buds. *Development*. 119:247–261.

Perrimon, N., and A.P. McMahon. 1999. Negative feedback mechanisms and their roles during pattern formation. *Cell*. 97:13–16.

Peterson, K.A., Y. Nishi, W. Ma, A. Vedenko, L. Shokri, X. Zhang, M. McFarlane, J.-M. Baizabal, J.P. Junker, A. van Oudenaarden, T. Mikkelsen, B.E. Bernstein, T.L. Bailey, M.L. Bulyk, W.H. Wong, and A.P. McMahon. 2012. Neural-specific Sox2 input and differential Gli-binding affinity provide context and positional information in Shh-directed neural patterning. *Genes & Development*. 26:2802–2816. doi:10.1101/gad.207142.112.

Rahnama, F., R. Toftgård, and P.G. Zaphiropoulos. 2004. Distinct roles of PTCH2 splice variants in Hedgehog signalling. *Biochem. J.* 378:325–334. doi:10.1042/BJ20031200.

Ribes, V., N. Balaskas, N. Sasai, C. Cruz, E. Dessaud, J. Cayuso, S. Tozer, L.L. Yang, B. Novitch, E. Martí, and J. Briscoe. 2010. Distinct Sonic Hedgehog signaling dynamics specify floor plate and ventral neuronal progenitors in the vertebrate neural tube. *Genes & Development*. 24:1186–1200. doi:10.1101/gad.559910.

Roelink, H., J.A. Porter, C. Chiang, Y. Tanabe, D.T. Chang, P.A. Beachy, and T.M. Jessell. 1995. Floor plate and motor neuron induction by different concentrations of the amino-terminal cleavage product of sonic hedgehog autoproteolysis. *Cell*. 81:445–455.

Rohatgi, R., L. Milenkovic, and M.P. Scott. 2007. Patched1 regulates hedgehog signaling at the primary cilium. *Science*. 317:372–376. doi:10.1126/science.1139740.

Taipale, J., M.K. Cooper, T. Maiti, and P.A. Beachy. 2002. Patched acts catalytically to suppress the activity of Smoothened. *Nature*. 418:892–897. doi:10.1038/nature00989.

Tseng, T.T., K.S. Gratwick, J. Kollman, D. Park, D.H. Nies, A. Goffeau, and M.H. Saier. 1999. The RND permease superfamily: an ancient, ubiquitous and diverse family that includes human disease and development proteins. *J. Mol. Microbiol. Biotechnol.* 1:107–125.

Ulloa, F., and J. Briscoe. 2007. Morphogens and the control of cell proliferation and patterning in the spinal cord. *Cell Cycle*. 6:2640–2649.

Vokes, S.A., H. Ji, S. McCuine, T. Tenzen, S. Giles, S. Zhong, W.J.R. Longabaugh, E.H. Davidson, W.H. Wong, and A.P. McMahon. 2007. Genomic characterization of Gli-activator targets in sonic hedgehog-mediated neural patterning. *Development*. 134:1977–1989. doi:10.1242/dev.001966.

Vokes, S.A., H. Ji, W.H. Wong, and A.P. McMahon. 2008. A genome-scale analysis of the cis-regulatory circuitry underlying sonic hedgehog-mediated patterning of the mammalian limb. *Genes & Development*. 22:2651–2663. doi:10.1101/gad.1693008.

Xie, J., M. Murone, S.M. Luoh, A. Ryan, Q. Gu, C. Zhang, J.M. Bonifas, C.W. Lam, M. Hynes, A. Goddard, A. Rosenthal, E.H. Epstein, and F.J. de Sauvage. 1998. Activating Smoothened mutations in sporadic basal-cell carcinoma. *Nature*. 391:90–92. doi:10.1038/34201.

Xiong, F., A.R. Tentner, P. Huang, A. Gelas, K.R. Mosaliganti, L. Souhait, N. Rannou, I.A. Swinburne, N.D. Obholzer, P.D. Cowgill, A.F. Schier, and S.G. Megason. 2013. Specified neural progenitors sort to form sharp domains after noisy shh signaling. *Cell*. 153:550–561. doi:10.1016/j.cell.2013.03.023.

# CHAPTER III:

## Secreted HHIP1 interacts with heparan sulfate and regulates Hedgehog ligand distribution and function

### 3.1 Abstract

Vertebrate Hedgehog (HH) signaling is controlled by several ligand-binding antagonists including PTCH1, PTCH2, and Hedgehog-interacting protein 1 (HHIP1), whose collective action is essential for proper HH pathway activity. However, the molecular mechanisms employed by these inhibitors remain poorly understood. Here we investigate the mechanisms underlying HHIP1 antagonism of HH signaling. Strikingly, we find that HHIP1 non-cell autonomously inhibits HH-dependent neural progenitor patterning and proliferation. We further demonstrate that this non-cell autonomous antagonism of HH signaling results from the secretion of HHIP1 that is modulated by cell type-specific interactions with heparan sulfate (HS). These interactions are mediated by an HS-binding motif in the cysteine rich domain of HHIP1 that is required for its localization to the neuroepithelial basement membrane to effectively antagonize HH pathway function. Finally, we show that endogenous, secreted HHIP1 localization to HS-containing basement membranes regulates HH ligand distribution. Overall, the secreted activity of HHIP1 represents a novel mechanism to regulate HH ligand localization and function during embryogenesis.

## 3.2 Introduction

Hedgehog (HH) signaling is indispensible for embryogenesis (McMahon et al., 2003). Secreted HH ligands act over long distances to produce distinct cellular responses, depending on both the concentration and duration of HH ligand exposure (McMahon et al., 2003; Dessaud et al., 2007; Martí et al., 1995; Ericson et al., 1997). HH pathway activity is tightly controlled by complex feedback mechanisms involving a diverse array of cell surface-associated ligand-binding proteins, including the HH co-receptors GAS1, CDON, and BOC and the HH pathway antagonists PTCH1, PTCH2, and HHIP1 (Tenzen et al., 2006; Allen et al., 2011; Jeong and McMahon, 2005; Holtz et al., 2013; Beachy et al., 2010). These molecules constitute a complex feedback network that controls the magnitude and range of HH signaling (Holtz et al., 2013; Chen and Struhl, 1996; Jeong and McMahon, 2005; Milenkovic et al., 1999; Tenzen et al., 2006; Allen et al., 2007).

The canonical HH receptor Patched (PTC in *Drosophila*; PTCH1 in vertebrates) is a direct transcriptional HH pathway target (Goodrich et al., 1996; Forbes et al., 1993; Alexandre et al., 1996; Agren et al., 2004; Vokes et al., 2007). In *Drosophila*, PTC accumulation at the cell surface binds and sequesters HH ligands, limiting signaling in cells distal to the HH source (Chen and Struhl, 1996). In vertebrates, HH-dependent patterning requires not only PTCH1, but two additional, vertebrate-specific feedback antagonists: the PTCH1-homologue, PTCH2, and HH-interacting protein 1 (HHIP1) (Chuang and McMahon, 1999; Motoyama et al., 1998; Carpenter et al., 1998; Koudijs et al., 2008; 2005). PTCH1 and PTCH2 act redundantly in multiple cells and tissues, including the developing skin (Adolphe et al., 2014; Alfaro et al., 2014). while, HH-dependent ventral neural patterning is severely disrupted following the combined removal of PTCH2, HHIP1, and PTCH1-feedback inhibition (Holtz et al., 2013; Jeong

and McMahon, 2005; Milenkovic et al., 1999). These data suggest that PTCH1, PTCH2, and HHIP1 play overlapping and essential roles to limit HH ligand signaling during embryonic development.

While PTCH2 and HHIP1 perform overlapping functions with PTCH1 in the developing nervous system, they exhibit distinct requirements in different tissues. For example, *Ptch2*$^{-/-}$ mice are viable and fertile, yet aged adult males develop significant alopecia and epidermal hyperplasia (Nieuwenhuis et al., 2006). Additionally, *Hhip1*$^{-/-}$ mice die at birth due to severe defects in lung branching morphogenesis that results from unrestrained HH pathway activity in the developing lung mesenchyme (Chuang, 2003). Despite *Ptch1* and *Ptch2* expression in the embryonic lung (Bellusci et al., 1997b; Pepicelli et al., 1998), these molecules fail to compensate for the absence of HHIP1 as occurs during ventral neural patterning. Moreover, *Hhip1*$^{-/-}$ embryos display developmental defects in the pancreas, spleen, and stomach (Kawahira et al., 2003). These observations argue that PTCH2 and HHIP1 are not simply redundant with PTCH1, but that they perform distinct functions to fulfill essential, tissue-specific roles within the vertebrate lineage. However, the mechanisms that account for these non-redundant activities, especially with regard to HHIP1, remain largely unknown.

*Hhip1* is a direct transcriptional HH pathway target that encodes for a cell surface-associated protein which binds all three mammalian HH ligands with high affinity (Chuang and McMahon, 1999; Pathi et al., 2001; Bishop et al., 2009; Bosanac et al., 2009; Vokes et al., 2007). HHIP1 possesses several conserved functional domains including an N-terminal Cysteine Rich Domain (CRD), a 6-bladed β-propeller region, two membrane-proximal EGF repeats, and a C-terminal hydrophobic motif (Chuang and McMahon, 1999). Crystallographic studies identified the β-propeller domain of HHIP1 as the HH ligand-binding domain (Bosanac et al., 2009;

Bishop et al., 2009). HHIP1 is proposed to act as a membrane-bound competitive inhibitor of HH signaling (Chuang and McMahon, 1999; Bishop et al., 2009); however, both PTCH1 and PTCH2 share this activity. Thus, the molecular features that distinguish HHIP1 from PTCH1 and PTCH2 have yet to be discerned.

Here we investigate the molecular mechanisms of HHIP1 function in HH pathway inhibition. Strikingly, we find that, in contrast to PTCH1 and PTCH2, HHIP1 uniquely induces non-cell autonomous inhibition of HH-dependent neural progenitor patterning and proliferation. Further, we demonstrate that HHIP1 secretion underlies these long-range effects. Using biochemical approaches, we define HHIP1 as a secreted HH antagonist that is retained at the cell surface through cell type-specific interactions between heparan sulfate (HS) and the N-terminal CRD of HHIP1. Importantly, we show that HS-binding promotes long-range HH pathway inhibition by localizing HHIP1 to the neuroepithelial basement membrane. Finally we demonstrate that endogenous HHIP1 is a secreted protein whose association with HS-containing basement membranes regulates HH ligand distribution. Overall, these data redefine HHIP1 as a secreted, HS-binding HH pathway antagonist that utilizes a novel and distinct mechanism to restrict HH ligand function.

## 3.3 Results

*HHIP1 non-cell autonomously inhibits HH-dependent neural progenitor specification*

To interrogate PTCH1-, PTCH2- and HHIP1-mediated antagonism of HH signal transduction, we utilized a gain-of-function approach in the developing chicken neural tube to investigate their effects on HH-dependent ventral neural patterning (Fig. 3-1). Nuclear EGFP expression from a bicistronic *IRES-EGFP*$^{NLS}$ construct (*pCIG*) labels electroporated cells,

providing spatial resolution when analyzing the effects of a given protein on HH-dependent neural patterning. Expression of EGFP alone (*pCIG*) does not affect neural patterning as assessed by antibody detection of the positive HH target, NKX6.1, and the negative HH target PAX7 (Fig. 3-1, A-E) in embryos collected 24 hours post electroporation (24hpe). Similar to previous results, electroporation of *Ptch2* or *Ptch1*$^{\Delta L2}$, a ligand-insensitive construct that functions as a constitutive repressor (Briscoe et al., 2001), results in cell autonomous loss of NKX6.1 (Fig. 3-1, F-H and K-M, arrows) and ectopic PAX7 expression (Fig. 3-1, I-J and N-O, arrows), indicative of reduced HH signaling (Holtz et al., 2013). *Hhip1* electroporation also represses NKX6.1 expression in ventral progenitors (Fig. 3-1, P-R) and induces ectopic PAX7 expression (Fig. 3-1, S-T) at 24hpe. Strikingly, these effects arise non-cell autonomously; most ventral progenitors that lose NKX6.1 expression are not EGFP+ (Fig. 3-1, P-R, white line). Additionally, many ectopic PAX7+ cells do not co-express EGFP and are found ventral to the EGFP+, HHIP1-expressing cells (Fig. 3-1, S-T, arrowhead). This contrasts with the strictly cell autonomous inhibition produced by PTCH2 and PTCH1$^{\Delta L2}$ expression (Fig. 3-1, A-O).

Analysis of neural patterning at 48hpe indicates that both PTCH2 and PTCH1$^{\Delta L2}$ cell autonomously repress NKX6.1 (Fig. 3-2, F-H and K-M, arrows) and induce ventral expansion of PAX7 (Fig. 3-2, I-J and N-O). In contrast, *Hhip1* electroporation causes a significant growth defect that is most evident in the ventral neural tube, leading to a significant reduction in the number of ventral, but not dorsal progenitors compared to *Ptch2*- and *Ptch1*$^{\Delta L2}$-electroporated embryos (Fig. 3-2, P-R, brackets; and Fig. 3-2, U-V). Thus, HHIP1 antagonizes both HH-dependent neural patterning and ventral neural tube growth in a non-cell autonomous manner.

*HHIP1 inhibits neural progenitor proliferation in a non-cell autonomous manner*

To determine the cause of this HHIP1-mediated growth defect, we examined apoptosis and proliferation in neural progenitors, processes that are regulated by HH signaling (Cayuso et al., 2006; Charrier et al., 2001; Saade et al., 2013; Thibert et al., 2003). While both PTCH1$^{\Delta L2}$ and HHIP1 expression transiently induce apoptosis to similar extents at 24hpe (Fig. 3-3, E-F and I-J), *Hhip1* electroporation significantly reduces the number of mitotic, phospho-histone H3+ (PH3+) cells on the electroporated side of the neural tube at both 24hpe and 48hpe compared to *pCIG* and *Ptch1*$^{\Delta L2}$ (Fig. 3-4). Strikingly, while most HHIP1-electroporated cells are found in the dorsal neural tube, we observe the greatest reduction in proliferation ventrally (Fig. 3-4, I-L, brackets; quantified in Fig. 3-4 N). Thus, HHIP1 expression inhibits both neural progenitor patterning and proliferation in a non-cell autonomous manner.

*Cell autonomous activation of HH signaling does not block the non-cell autonomous effects of HHIP1*

To further investigate the non-cell autonomous effects of HHIP1 expression, we co-electroporated *Hhip1* with a constitutively active *Smo* construct, *SmoM2* (Xie et al., 1998). Since SMOM2 is downstream and refractory to HHIP1 inhibition, we reasoned that this would rescue any cell autonomous HH inhibition caused by HHIP1 (Holtz et al., 2013). Indeed, *SmoM2* electroporation cell autonomously induces ectopic NKX6.1+ cells (Fig. 3-5, B and C, yellow arrows) and represses PAX7 expression (Fig. 3-5, D and E, yellow arrows) at 48hpe.

Co-electroporation of *Hhip1* with *SmoM2* also induces ectopic NKX6.1 and represses PAX7 expression (Fig. 3-5, G-J, yellow arrows), indicating cell autonomous rescue of HHIP1 inhibition. However, we also detected a significant, non-cell autonomous loss of NKX6.1 and a ventral expansion of PAX7 expression in the ventral neural tube at 24hpe and 48hpe (Fig. 3-5,

G-J; Fig. 3-6, A-E, white line), which does not occur in embryos co-electroporated with *Ptch2* and *SmoM2* (Fig. 3-6, P-T). These data support the notion that HHIP1 non-cell autonomously inhibits HH signaling in the chicken neural tube.

*HHIP1 is a secreted protein*

To determine how HHIP1 expression produces non-cell autonomous effects, we investigated whether HHIP1 functions as a secreted HH antagonist. Previous studies using COS7 cells classified HHIP1 as a type-I transmembrane protein with a C-terminal 22 amino acid transmembrane domain (Chuang and McMahon, 1999). However, a subsequent report identified the presence of overexpressed HHIP1 in cell supernatants (Coulombe et al., 2004). Surprisingly, we observed significant accumulation of N-terminally HA-tagged HHIP1 (HA::HHIP1) in supernatants when expressed in HH-responsive NIH/3T3 fibroblasts (Fig. 3-7 A). In contrast, a HHIP1 chimera in which the putative C-terminal membrane anchor is replaced with the transmembrane domain from the CD4 protein (HA::HHIP1::CD4) is not secreted (Maddon et al., 1985)(Fig. 3-7 A). Thus, the CD4 transmembrane domain is sufficient to anchor HHIP1 to the cell surface. As a positive control, we also detected secreted CDON protein (HA::CDON$^{\Delta TMCD}$) in NIH/3T3 cell supernatants (Fig. 3-7 A). These data suggest that HHIP1 can be secreted from cells.

*Membrane anchoring abrogates the non-cell autonomous effects of HHIP1*

To test whether the non-cell autonomous effects of HHIP1 in the neural tube result from HHIP1 secretion, we compared the activity of secreted HHIP1 protein, and membrane-tethered HHIP1::CD4. Importantly, HHIP1 and HHIP1::CD4 function equivalently to antagonize HH-

mediated pathway activation in NIH/3T3 cells (Fig. 3-7 B); thus, membrane anchoring of HHIP1 does not compromise its cell autonomous inhibitory activity.

We next analyzed neural patterning in embryos electroporated with either *Hhip1* or *Hhip1::CD4* at 24hpe. HHIP1 non-cell autonomously inhibits NKX6.1 and induces ectopic PAX7 expression at 24hpe (Fig. 3-7, I-L, white lines). In contrast, HHIP1::CD4 antagonizes NKX6.1 and induces PAX7 expression exclusively in a cell autonomous manner at 24hpe (Fig. 3-7, N-Q, arrows). At 48hpe, the most prominent effect of HHIP1 expression is a significant growth defect in the ventral neural tube; however, membrane anchoring of HHIP1 partially rescues the growth of ventral neural progenitors at 48hpe based on gross tissue morphology (Fig. 3-8, G and L) and quantitation of PH3+ cells at 24hpe (Fig. 3-8 A). Further, HHIP1::CD4 cell autonomously inhibits expression of the high-level HH target, NKX2.2 (Fig. 3-8, M-N, arrows) and induces persistent ectopic expression of PAX7 at 48hpe (Fig. 3-8, O-P, arrows), demonstrating effective antagonism of HH signaling. Overall, these data suggest that the non-cell autonomous effects of HHIP1 on both patterning and proliferation of neural progenitors arise from HHIP1 secretion.

*HHIP1 associates with the cell surface through cell type-specific interactions with heparan sulfate*

To resolve our data demonstrating HHIP1 secretion in NIH/3T3 cells with previously published data showing cellular retention of HHIP1 in COS7 cells (Chuang and McMahon, 1999), we directly compared HA::HHIP1 secretion from NIH/3T3 and COS-7 cells. HA::HHIP1 robustly accumulates in NIH/3T3 cell supernatants (Fig. 3-9 A). However, HA::HHIP1 secretion is significantly reduced in supernatants collected from COS-7 cells, despite increased

HA::HHIP1 expression (Fig. 3-9, A and B). In fact, in some instances we failed to detect significant HA::HHIP1 secretion from COS-7 cells (Fig. 6 F). Consistent with previous reports, a HHIP1 protein lacking the putative C-terminal 22 amino acid membrane spanning helix, HA::HHIP1$^{\Delta C22}$, accumulates in COS-7 cell supernatants (Fig. 3-9, A and B) (Chuang and McMahon, 1999). Importantly, COS-7 cells are not generally defective in protein secretion based on the robust secretion of HA::CDON$^{\Delta TMCD}$ (Fig. 3-9 A). Overall, these data suggest that the balance between membrane retention and release of HHIP1 depends on the cellular context.

To test whether HHIP1 was proteolytically cleaved in NIH/3T3 cells, we generated dual-tagged HHIP1 constructs that possess an N-terminal HA tag and either a C-terminal MYC or V5 epitope (Fig. 3-9 C). Both HA::HHIP1::MYC and HA::HHIP1::V5 accumulate in NIH/3T3 cell supernatants as full-length proteins based on western blot detection of HA and MYC/V5 (Fig. 3-9, D-F), demonstrating that proteolytic cleavage of HHIP1 is not a requirement for secretion. HHIP1 has also been implicated as a glycosylphosphatidylinositol (GPI)-anchored protein (Bosanac et al., 2009); however, phosphatidylinositol phospholipase C (PI-PLC) treatment fails to release HA::HHIP1 or HA::HHIP1::CD4 from the cell surface of COS-7 cells while a GPI-anchored version of the HH co-receptor CDON (HA::CDON::GPI), is effectively released from the cell surface by PI-PLC treatment (Fig. 3-10).

To examine whether HHIP1 is retained at the cell surface through ionic interactions we treated COS-7 cells expressing HA::HHIP1 with buffers possessing increasing NaCl concentrations. Surprisingly, we detected HA::HHIP1 release from COS-7 cells with as little as 300mM NaCl, which increases substantially after incubation with 500mM NaCl (Fig. 3-11 A). As a control, HA::HHIP1::CD4 remains associated with the cell pellet at all NaCl concentrations

tested (Fig. 3-11 A). These data are consistent with HHIP1 being anchored to the cell surface through intermolecular interactions.

To identify the binding partner responsible for membrane retention of HHIP1, we first sought to determine whether HHIP1 is retained at the cell surface through interactions with heparan sulfate (HS), an abundant glycosaminoglycan (GAG) that has been implicated in multiple aspects of HH signal transduction (Häcker et al., 2005; Lin, 2004; Perrimon and Bernfield, 2000). First, we attempted to disrupt HHIP1 retention at the cell surface in COS-7 cells using heparin, a structural analog of HS (Esko and Lindahl, 2001). Incubation with as little as 100nM heparin effectively competes HA::HHIP1 from the cell surface of COS-7 cells, while HA::HHIP1::CD4 is refractory to competition with up to 10μM heparin (Fig. 3-11 B). This effect is specific to heparin as we only achieved minimal HHIP1 release with a 1000-fold excess of Chondroitin Sulfate A or a 100-fold excess of Dermatan Sulfate (Fig. 3-11, C and D).

To determine whether HHIP1 membrane retention is affected by cell type-specific modifications in HS composition, which vary between cell types and over developmental time, we isolated HS from both NIH/3T3 and COS-7 cells to perform cell surface competition assays (Allen and Rapraeger, 2003; Esko and Lindahl, 2001; Rubin et al., 2002). Since COS-7 cells largely retain HHIP1 we reasoned that COS-7 HS would preferentially bind and thus more effectively compete HHIP1 from the cell surface than HS isolated from NIH/3T3 cells. As expected, COS-7 GAGs more effectively compete HHIP1 from the cell surface than NIH/3T3 GAGs (Fig. 3-11 E). After enriching for HS by Chondroitinase ABC treatment, we observed HHIP1 release with as little as 2μg/ml of COS-7 HS, which is more effective than a 10-fold excess of NIH/3T3 HS (Fig. 3-11 F). Collectively, these data suggest that HHIP1 is retained at the cell surface through cell type-specific interactions with HS.

*HHIP1 binds to HS through basic amino acids in the N-terminal CRD*

To determine the HS-binding motif in HHIP1, we initially focused on the HHIP1 C-terminus, which was previously implicated in HHIP1 surface retention (Chuang and McMahon, 1999) (Fig. 3-9 A). Molecular modeling of the C-terminal 30 amino acids identifies a putative HS-binding site comprised of 4 arginine residues (R671, R673, R674, R678) (Fig. 3-12, A and B). Interestingly, this analysis also revealed that the C-terminal helix is amphipathic, and is thus unlikely to form a transmembrane domain (Fig. 3-12 A).

We performed heparin-agarose chromatography to investigate HHIP1-HS interactions. HA::HHIP1 binds to heparin-agarose with a peak elution of 550mM NaCl (Fig. 3-12 C). Deletion of the C-terminal 30 amino acids ($HHIP1^{\Delta C30}$), containing the potential HS-binding motif, shifts the elution peak to 450mM NaCl, indicating reduced heparin binding (Fig. 3-12 C). However, site-directed mutagenesis of the 4 arginines to alanines ($HA::HHIP1^{C4R->4A}$) does not affect heparin binding (Fig. 3-12 D). Additionally, replacing the C-terminus with a heterologous transmembrane domain (HA::HHIP1::CD4) restores heparin binding (Fig. 3-12 E). These data suggest that additional motifs are required for HS-binding and surface retention.

The EGF domains and the β-propeller region are largely dispensable for heparin binding (Fig. 3-12, F and G). However, deletion of the N-terminal CRD of HHIP1 ($HA::HHIP1^{\Delta CRD}$) shifts the elution peak to 400 mM NaCl (Fig. 3-12 H). Importantly, Surface Plasmon Resonance (SPR) studies confirm a direct interaction between purified HHIP1 with heparin ($K_d$=100nM) that is reduced 50-fold upon deletion of the N-terminal CRD ($K_d$=5000nM) (Fig. 3-13, A and B). Similar results are observed with SPR analysis of HHIP1 and HS interactions (Fig. 3-13, D and E). Additionally, the purified HHIP1 CRD directly binds both heparin and HS (Fig. 3-13, C and F). Molecular modeling of the CRD domain reveals a positively charged region at the surface

(Fig. 3-14 A), including a potential HS-binding site comprised of several basic arginine and lysine residues (Fig. 3-14 B). Based on this model, we investigated two clusters of basic amino acids that comprise the putative HS-binding moiety (Fig. 3-14, C and D). Mutation of 4 arginines to alanines in the first basic cluster (HA::HHIP1$^{\Delta HS1}$) shifts the heparin elution peak to 450mM NaCl (Fig. 3-14 E). Additionally, replacing the central KRR motif of cluster 2 with alanine residues (HA::HHIP1$^{\Delta HS2}$) weakens heparin binding and produces an elution peak of 400mM NaCl (Fig. 3-14 F). A double mutant construct, HA::HHIP1$^{\Delta HS1/2}$, (Fig. 3-14 D), elutes at a peak of 350mM NaCl (Fig. 3-14 G), suggesting that these two motifs cooperate to bind HS. Strikingly, HA::HHIP1$^{\Delta HS1}$, HA::HHIP1$^{\Delta HS2}$, and HA::HHIP1$^{\Delta HS1/2}$ proteins accumulate in COS-7 cell supernatants (Fig. 3-14 H). Collectively, these data suggest that HHIP1 is retained at the cell surface through interactions between HS and basic amino acids present within the HHIP1-CRD.

*HHIP1 interactions with HS promote basement membrane localization and HH pathway antagonism in the chicken neural tube*

To determine the functional role of the HHIP1-HS interaction, we assessed signaling in NIH/3T3 cells. HHIP1$^{\Delta HS1/2}$ antagonizes Sonic HH (SHH)-mediated pathway activity in NIH/3T3 cells equivalently to wildtype HHIP1 (Fig. 3-14 I). Surprisingly, HHIP1$^{\Delta HS1/2}$ expression in the developing chicken neural tube produces limited non-cell autonomous inhibition of SHH signaling (Fig. 3-15, G-J, white lines). Additionally, at 48hpe HHIP1$^{\Delta HS1/2}$ expression does not alter ventral neural tube growth as assessed by DAPI staining and the size of the NKX6.1+ domain (Fig. 3-15, P-R). HHIP1$^{\Delta HS1/2}$ does not affect neural progenitor proliferation at 24hpe and 48hpe (Fig. 3-15, U and V), but does induce cell death similar to HHIP1 (Fig. 3-16, D-F).

Since HHIP1 and HHIP1$^{\Delta HS1/2}$ function equivalently in cell-based assays, we reasoned that HS-binding might control the tissue localization of HHIP1 in the neural tube to promote long-range HH inhibition. Towards this end, we stained embryos electroporated with *Hhip1* and *Hhip1*$^{\Delta HS1/2}$ with an anti-HHIP1 antibody that does not detect the endogenous chicken HHIP1 protein (Fig. 3-17, A-E). Intriguingly, HHIP1 protein primarily localizes to the basal side of the neuroepithelium when expressed in the chicken neural tube and co-localizes with the basement membrane (BM) component Laminin (Fig. 3-17, F-J, arrowheads). We also observe co-localization between HHIP1 and Laminin in the surface ectoderm (Fig. 3-17, F-J, arrows, insets). Strikingly, HHIP1$^{\Delta HS1/2}$ fails to localize to the basal side of the epithelium and surface ectoderm and remains associated with electroporated cells (Fig. 3-17, K-O), similar to the localization of membrane-anchored HHIP1::CD4 (Fig. 3-17, P-T). Quantitation of these data demonstrate that while HHIP1 and HHIP1$^{\Delta HS1,}$ are expressed at equal levels, HHIP1$^{\Delta HS1,2}$ is significantly less enriched in the BM compared to HHIP1 (Fig. 3-17, U and V) Collectively, these data indicate that HS-binding mediates HHIP1 localization to the neural tube BM and is required to promote long-range inhibition of HH signaling.

*Endogenous HHIP1 protein is secreted and associates with the basement membrane in the developing neuroepithelium*

We next sought to determine the localization of endogenous HHIP1 protein in the neural tube. Using whole mount X-Gal staining of *Hhip1*$^{+/-}$ mouse embryos, which express a *lacZ* reporter from the endogenous *Hhip1* locus, we initially detect *Hhip1* expression in the developing heart and body wall at E8.5 (Fig. 3-18 A, red arrow). At E9.5, we observe *Hhip1* expression in several locations including the paraxial mesoderm, lung, and intestine, consistent

with published *Hhip1* expression data (Fig. 3-18 B) (Chuang and McMahon, 1999; Chuang, 2003). Our group and others have previously published in situ hybridization data showing low levels of *Hhip1* expression within ventral neural progenitors in the embryonic spinal cord at E10.5 (Chuang and McMahon, 1999; Holtz et al., 2013). Interestingly, while *Hhip1* expression in ventral neuronal cells is too low to detect by X-gal stain, we do observe reporter expression in the roof plate of the developing spinal cord at E10.5 and E11.5 (Fig. 3-18 C and D, red arrowheads; Fig. 3-20 A, red arrows), consistent with previously published data in *Xenopus* (Cornesse et al., 2005). Using in situ hybridization, we validated *Hhip1* expression within the paraxial mesoderm and roof plate, and also detected weaker expression in ventral neural progenitors at E10.5 (Fig. 3-18 E, arrow, red arrowhead, and black arrowhead, respectively). Interestingly, the membrane-bound HH antagonist, PTCH2, is not expressed in the developing roof plate (Fig. 3-18 F). While we confirm the roof plate expression of *Hhip1* by immunofluorescence, we do not detect HHIP1 protein by immunofluorescence at this axial level at E10.5 and E11.5 (Fig. 3-19, arrows).

Interestingly, we detect strong *Hhip1* expression in the developing diencephalon at E10.5 and E11.5 (Fig. 3-18 C, black arrow; Fig. 3-20, A and B, arrows and arrowheads). HH signaling plays a critical role in the growth and patterning of the developing midbrain and mutations in the HH pathway produce diencephalic defects in humans (Ishibashi and McMahon, 2002; Szabó et al., 2009; Ericson et al., 1995; Roessler et al., 2003; Dale et al., 1997; Zhao et al., 2012; Treier et al., 2001). At the level of Rathke's Pouch, *Hhip1* is expressed in more dorsal regions of the diencephalon (Fig. 3-20, A-C, arrowheads), and at the midline caudal to the developing pituitary (Fig. 3-20, A, B, and D, arrows). In wildtype embryos, HHIP1 protein is not readily observed within the neuroepithelium of the dorsal diencephalon, but instead accumulates basally at a

significant distance from its site of production (Fig. 3-20, E-H, arrows). Importantly, HHIP1 signal is not detected in *Hhip1*$^{-/-}$ embryos, confirming antibody specificity (Fig. 3-20, I-L). Consistent with our analysis in the chicken neural tube, endogenous HHIP1 protein co-localizes with Laminin in the BM (Fig. 3-20, M and N, arrows). Strikingly, we also observe an association between HHIP1 and the HS-decorated BM protein, Perlecan (HSPG2; Fig. 3-20, O and P, arrows). Importantly, HHIP1 does not associate with axonal projections as assessed by labeling with TUJ1 (Fig. 3-21, A-C, arrows).

To validate the distribution of secreted HHIP1 protein, we generated a novel HHIP1 antibody. Notably, this reagent also specifically detects HHIP1 protein in the neuroepithelial BM near the source of SHH ligand production in the ventral diencephalon (Fig. 3-20, Q-X, arrows). Interestingly, we observed accumulation of SHH ligand within the BM at a distance from the SHH source that co-localizes with HHIP1 in discrete puncta (Fig. 3-20, S-T; Fig. 3-22, A-D, arrows). Strikingly, this accumulation of SHH is lost in *Hhip1*$^{-/-}$ embryos, demonstrating that HHIP1 can interact with and affect the distribution of SHH ligand in the neuroeptihelial BM (Fig. 3-20, W-X; Fig. 3-22, E-H). Collectively, these data demonstrate that endogenous HHIP1 protein is secreted and associates with HS-containing BM of the developing neuroepithelium.

*Endogenous HHIP1 is produced and secreted by lung mesenchymal fibroblasts*

To determine whether endogenous HHIP1 protein is secreted and associates with BM outside of the neuroepithelium, we investigated HHIP1 distribution in the developing lung, where HHIP1 is critical for branching morphogenesis (Chuang, 2003). *Hhip1*$^{-/-}$ lungs collected at E12.5 and E14.5 possess only two rudimentary lung lobes instead of the normal five and largely fail to undergo secondary branching morphogenesis (Fig. 3-23, A-D) (Chuang, 2003). Consistent

with previous reports, *Hhip1* is exclusively expressed by mesenchymal fibroblasts proximal to the lung epithelium, but is excluded from the epithelium itself as determined by β-Galactosidase (β-Gal) expression in *Hhip1*$^{+/-}$ lungs (Fig. 3-23, E-H, arrows) (Chuang, 2003). HHIP1 protein co-localizes with β-Gal in the lung mesenchyme; however, we also detect HHIP1 protein on the basal side of epithelial cells that does not co-localize with β-Gal (Fig. 3-23 E-H, arrowheads). This signal is specific for HHIP1 as it is absent in *Hhip1*$^{-/-}$ embryos (Fig. 3-23, I-L). The epithelial HHIP1 protein staining co-localizes with the BM markers Laminin and Perlecan (Fig. 3-23, M-T, arrowheads). Interestingly, HHIP1 is only detected in regions where Perlecan is present (Fig. 3-23, Q-T, arrows). Taken together, these data indicate that endogenous HHIP1 protein is produced and secreted by lung mesenchymal fibroblasts and accumulates in the HS-containing BM of the lung epithelium.

## 3.4 Discussion

*HHIP1 is a secreted antagonist of vertebrate Hedgehog signaling*

Secreted, ligand-binding antagonists are common components of morphogen signaling pathways, including Noggin and Chordin in the BMP pathway (Zimmerman et al., 1996; Smith and Harland, 1992; Smith et al., 1993; Piccolo et al., 1996); Lefty inhibition of Nodal signaling (Meno et al., 1996; Chen and Shen, 2004); WIF-1 and a large family of secreted frizzled receptors that function as WNT pathway antagonists (Wang et al., 1997; Leyns et al., 1997; Cruciat and Niehrs, 2013; Hsieh et al., 1999); and Cerberus, which binds to and antagonizes the activity of BMP, Nodal, and WNT ligands (Piccolo et al., 1999; Bouwmeester et al., 1996). Thus, it is surprising that the ligand-binding HH pathway antagonists described to date act exclusively as membrane bound inhibitors (Chuang and McMahon, 1999; Carpenter et al., 1998; Marigo et

al., 1996; Stone et al., 1996). Here we present functional and biochemical evidence to redefine HHIP1, previously thought to be a transmembrane-anchored protein, as a secreted antagonist of vertebrate HH signaling. Importantly, this is supported by a recent, complementary study demonstrating that HHIP1 acts as a secreted HH pathway inhibitor (Kwong et al., 2014).

*Heparan sulfate regulation of HH pathway activity*

HS regulates the activity of numerous key developmental signaling pathways including, FGF, WNT, BMP, and HH (Yan and Lin, 2009). Following genetic studies in flies that identified a role for HS in the trafficking of HH ligands (Bellaiche et al., 1998; The et al., 1999), subsequent work demonstrated multiple and complex roles for HS in HH ligand trafficking; proteolytic processing and release of HH ligands; and HH signal transduction (Gallet et al., 2003; Desbordes and Sanson, 2003; Rubin et al., 2002; Lum et al., 2003; Han et al., 2004; Dierker et al., 2009; Ohlig et al., 2012). To this point studies have been restricted to direct interactions of HH ligands with HS (Whalen et al., 2013), which affects neural progenitor proliferation in flies (Park et al., 2003) and mice (Rubin et al., 2002; Chan et al., 2009; Witt et al., 2013), as well as oligodendrocyte specification in the developing spinal cord (Danesin et al., 2006; Oustah et al., 2014; Touahri et al., 2012).

Our study identifies a novel role for HS in HH signaling through its interactions with HHIP1. Further, our data suggest that HS acts to regulate the extracellular distribution of HHIP1 as mutagenesis of the HS-binding site stimulates significant release of HHIP1 from the cell surface. Importantly, and counterintuitively, interference of HHIP1-HS interactions limits long-range inhibition of HH signaling in the chicken neural tube. Interactions with HS are not required for HHIP1 activity in cell culture; instead, we find that HS-binding is required to localize HHIP1

to the BM of the neuroepithelium to promote long-range inhibition of HH signaling. This role for HS in regulating the tissue distribution of HHIP1 is consistent with previous studies in *Drosphila*, where disruption of HS biosynthesis prevents the distribution of HH ligands away from their source of production in the wing imaginal disc and in the developing embryo (Bellaiche et al., 1998; The et al., 1999). Our data suggest that HS regulates both HHIP1 and HH ligand diffusion within a target field. Alternatively, HS may stabilize and concentrate HHIP1 in the BM to reach the threshold levels required for effective antagonism (Lin, 2004).

HHIP1 interacts with HS with high affinity compared to SHH ligand (HHIP1 $K_d$ 622nM vs. SHH $K_d$ 14.5 μM) (Whalen et al., 2013). The weaker SHH-HS affinity is consistent with a "rolling" interaction that promotes the establishment of the HH morphogen gradient. The strong HHIP1-HS interaction indicates that HHIP1 is likely to become fixed within an HS-rich environment, consistent with our observation of endogenous HHIP1sequestration of SHH ligand within the neuroepithelial BM. However, the diversity of HS across cell types and tissues suggests that these interactions will vary in a tissue- and context-specific manner. Importantly, the role of HS in regulating HH-dependent signaling in vertebrates must now be considered in the context of effects on both HH ligand and HHIP1 distribution within a tissue.

*Secreted HHIP1 association with HS-containing BM in multiple organs during embryogenesis*

In exploring the molecular properties of HHIP1, we determined the extracellular distribution of endogenous, secreted HHIP1 protein within the BM of the developing neuroepithelium and lung. The functional route utilized by HH ligands during vertebrate tissue development is largely unexplored. In *Drosophila*, both apical and basal gradients of HH ligand produce distinct functional consequences in receiving cells (Ayers et al., 2012; 2010). In

vertebrates, HH ligands have been visualized in the neuroepithelial BM by antibody detection (Allen et al., 2007; Gritli-Linde et al., 2001) and by using a *Shh::GFP* fusion knock-in allele (Chamberlain et al., 2008). The presence of HHIP1 within this tissue compartment and the redistribution of SHH observed in *Hhip1*$^{-/-}$ embryos implicates the BM as one functional route utilized by HH ligands to distribute within the neural tube. Notably, the roof plate expression of *Hhip1* in the spinal cord is analogous to notochord expression of the BMP antagonists *Noggin*, *Chordin* and *Follistatin* (McMahon et al., 1998; Liem at al., 2000), consistent with a role for secreted antagonists in the regulation of morphogen function during neural patterning.

In addition to the neuroepithelium, we also observed HHIP1 accumulation in the BM of the developing lung endoderm. This suggests that HHIP1 localization to the BM is a general strategy to antagonize HH pathway activity during embryogenesis. Notably, in both cases, HHIP1 distributes towards the source of HH ligand production. The strong HHIP1-HH ligand interaction in addition to the unique HS-rich environment of the BM may provide the driving forces for the tissue distribution of HHIP1.

Interestingly, the unique requirement for HHIP1 during lung development compared to PTCH1/2 may reflect the need for a secreted HH antagonist to orchestrate lung branching morphogenesis (Chuang, 2003). In the embryonic lung, epithelial-derived HH ligands traverse the basement membrane to signal to the underlying mesenchyme, resulting in repression of *Fgf10* expression, a key mediator of epithelial outgrowth (Pepicelli et al., 1998; Litingtung et al., 1998; Chuang, 2003; Sekine et al., 1999; Bellusci et al., 1997a; Min et al., 1998). Paradoxically, *Fgf10* expression is maintained within the mesenchyme adjacent to the sites of highest *Shh* expression at growing bud tips due to the induction of *Hhip1* expression (Chuang, 2003; Bellusci et al., 1997b; Bitgood and McMahon, 1995; Urase et al., 1996). HHIP1 protein localization

within the lung BM may restrict SHH ligand exit from the epithelial compartment, thus preserving *Fgf10* expression in the adjacent mesenchyme, providing a molecular mechanism to explain the unique genetic requirement for *Hhip1* in lung branching morphogenesis.

These data also have implications for understanding human lung diseases as HHIP1 has also been implicated in a wide variety of human lung pathologies including chronic obstructive pulmonary disease (COPD), emphysema, asthma, and lung cancer; thus, HH pathway inhibition by secreted HHIP1 might also have significant implications for the regulation of HH signaling in adult tissues, and in human lung pathologies (Pillai et al., 2009; Van Durme et al., 2010; Zhou et al., 2012; Young et al., 2010; Li et al., 2011; Castaldi et al., 2014).

## 3.5 Materials and Methods

*Chicken in ovo neural tube electroporations*

Electroporations were performed as previously described (Holtz et al., 2013; Tenzen et al., 2006). In brief, DNA (1.0 μg/μl) mixed with Fast Green (50 ng/μl) was injected into Hamburger-Hamilton stage 11-13 embryos. Embryos were dissected 24 and 48 hours post electroporation (hpe), fixed in 4% PFA, and processed for immunofluorescent analysis. Electroporated cells were marked by constructs expressing either nuclear-localized EGFP (*pCIG*) *or* tdTomato (*pCIT*). *mPtch2*, *mPtch1*$^{\Delta L2}$, and all *mHhip1* constructs were cloned into pCIG. *SmoM2* cDNA (Xie et al., 1998) was cloned into *pCIT*. For co-electroporations, each construct was injected at a concentration of 0.5 μg/μl. PH3+ cells were quantified from 3 or more sections isolated from at least 4 separate embryos per condition.

*HHIP1 constructs*

All *Hhip1* constructs were derived from a full-length mouse *Hhip1* cDNA (generously provided by Dr. Pao-Tien Chuang, UCSF). *Hhip1*$^{\Delta C22}$ encodes for a protein that lacks aa A679-V700 of full-length HHIP1, while HHIP1::CD4 replaced these resides with aa V394-C417 of the mouse CD4 protein (Maddon et al., 1985). An N-terminal HA tag (YPYDVPDYA) was inserted between residues F25 and G26 preceded by a residual ClaI site. For the dual-tagged *Hhip1* constructs, C-terminal MYC (EQKLISEEDL) and V5 (GKPIPNPLLGLDST) tags were added following a flexible linker (GSG) to enhance visualization by western blot analysis. *Hhip1* deletion constructs and HS-binding mutants were generated using the QuikChange II XL Site-Directed Mutagenesis Kit (Agilent).

*Immunofluorescence*

Immunofluorescent analysis of neural patterning was performed at the wing bud axial level at both 24hpe and 48 hpe (Holtz et al., 2013). The following antibodies were used: mouse IgG1 anti-NKX6.1 (1:20, Developmental Studies Hybridoma Bank [DSHB]), mouse IgG1 anti-PAX7 (1:20, DSHB), rabbit IgG anti-cleaved caspase-3 (1:200, Cell Signaling), rabbit IgG anti-phospho-Histone H3 (1:1000, Millipore), mouse IgG2b anti-NKX2.2 (1:20, DSHB), goat IgG anti-HHIP1 (1:200, R&D Systems), rabbit IgG anti-Laminin (1:500, Abcam), rabbit IgG anti-β-Gal (1:5,000, MP Biomedicals), rabbit IgG, mouse IgG1 anti-SHH (1:20, DSHB), rat IgG anti-HSPG2 (1:500, Millipore) and mouse IgG anti-E-Cadherin (1:500, BD Laboratories). Nuclei were visualized with DAPI (1:30,000, Molecular Probes). Alexa 488, 555, and 633 secondary antibodies (1:500, Molecular Probes) were used to detect protein localization. Slides were mounted in Shandon Immu-Mount (Thermo Scientific). Images were captured on a Leica upright SP5X confocal microscope at room temperature using the LAS AF software. Leica 63x (Type:

HC PL APO CS2; N.A.: 1.2) and 25x (Type: HCX IRAPO L; N.A.: .95) water immersion objectives were used. Fluorescent intensities were quantified using ImageJ from data isolated under identical imaging conditions. Two sections from at least three embryos were analyzed in each condition. Total HHIP1 fluorescent intensity was normalized to GFP fluorescence to control for electroporation efficiency. Direct comparisons of endogenous HHIP1 protein stains between *Hhip1*$^{+/+}$, *Hhip1*$^{+/-}$, and *Hhip1*$^{-/-}$ embryos were collected under identical imaging conditions.

*Luciferase assays*

Luciferase reporter assays to read out HH pathway activity were performed as previously described (Holtz et al., 2013; Nybakken et al., 2005). In brief, NIH/3T3 cells were seeded onto 24-well plates and transfected 16-24 h later with a ptcΔ136-GL3 luciferase reporter construct (Chen et al., 1999; Nybakken et al., 2005), pSV-β-galactosidase (Promega), and either empty vector or experimental constructs. After 48 h, cells were placed in low serum media in addition to either control- or NSHH-conditioned medium. Luciferase activity (Luciferase Assay System kit, Promega) was read 48 h later and normalized to β-galactosidase activity (BetaFluor β-galactosidase Assay Kit, Novagen). Data were expressed as fold induction relative to control treated cells.

*Western Blot Analysis*

Western blot analysis was performed according to standard methods. Briefly, cells were lysed 48 hours post-transfection in RIPA buffer (50mM Tris-HCl [pH 7.2], 150mM NaCl, 0.1% TX-100, 1% sodium deoxycholate, 5mM EDTA) containing Complete Mini Protease Inhibitor Cocktail

(Roche), centrifuged at 20,000 x g for 30 min at 4°C, and analyzed by SDS-PAGE. Proteins were transferred to PVDF and probed with the following antibodies: mouse IgG1 anti-HA (1:1000, Covance), rabbit IgG anti-MYC (1:5000, Bethyl Labs), and rabbit IgG anti-V5 (1:1000, Bethyl Labs). Cell supernatants and washes from HHIP1 cell surface competition experiments were centrifuged at 20,000 x g for 5 min at room temperature prior to SDS-PAGE. NaCl washes from cell surface competition experiments underwent buffer exchange into RIPA buffer and washes from GAG competition experiments were concentrated 4-fold prior to SDS-PAGE using Nanosep 30K Omega columns (PALL Life Sciences). Western blot intensities were quantified using ImageJ.

*Glycosaminoglycan isolation*

GAG preparations were performed as previously described (Karlsson and Björnsson, 2001; Allen and Rapraeger, 2003). COS-7 and NIH/3T3 cells were grown to confluency, washed with 1x PBS, and incubated with 0.25% Trypsin-EDTA for 30 min at 37°C. Cell-trypsin mixtures were boiled for 30 min and centrifuged at 1,500 x g for 5 min at room temperature. Supernatants were isolated and proteins were precipitated in 6% TCA for 1 h on ice. Proteins were pelleted by centrifugation at 10,000 x g for 30 min at 4°C. GAGs were precipitated from the remaining supernatant by overnight incubation with 5 volumes of ethanol at -20°C and pelleted by centrifugation at 10,000 x g for 30 min at 4°C. GAG pellets were resuspended in 50mM Tris-HCl (pH 8.0) and GAGs were quantified by alcian blue precipitation (Karlsson and Björnsson, 2001). To enrich for heparan sulfate, GAGs were incubated with 0.25 units of Chondroitinase ABC (Sigma) overnight at 37°C followed by alcian blue quantitation.

*Heparin-agarose chromatography*

COS-7 cells expressing HA-tagged *Hhip1* constructs were lysed in column buffer (50mM Tris-HCl [pH 7.2], 150mM NaCl, 5mM EDTA) with 1% NP-40 containing complete mini protease inhibitor cocktail (Roche) and clarified by centrifugation at 20,000 x g for 30 min at 4°C. Columns were loaded with 2 ml of heparin-agarose (Sigma) and equilibrated with 10 ml of column buffer. Lysates were diluted 1:25 in column buffer and loaded onto the column. The column was washed with 10 ml of column buffer and HHIP1 proteins were eluted in a step gradient (4 ml per elution) of column buffer possessing increasing concentrations of NaCl. Eluates were assayed for the presence of HA-tagged HHIP1 protein by dot blot analysis. The intensity of each dot was quantified using Image J software and plotted as the relative amount of signal compared to the total intensity measured for all elutions.

*Molecular modeling and structural analysis*

Models of the C-terminal 30 residues (residues 671-700) and the N-terminal 196 residues (residues 18-213) of human HHIP1, respectively, were generated using the Full-chain Protein Structure Prediction Server ROBETTA with the default RosettaCM protocol (Raman et al., 2009). Electrostatic potentials were calculated with APBS (Baker et al., 2001) and structure representations were drawn with PYMOL (The PyMOL Molecular Graphics System, Version 1.7.0.3 Schrödinger, LLC.).

*Expression and purification of HHIP1 constructs*

Human *HHIP1* constructs (UniProt ID: Q96QV1) consisting of the N-terminal domain (HHIPN; 39-209), β-propeller and EGF repeats (217-670; (Bishop et al., 2009) and ΔC-helix full-length (18-670) were fused C-terminally with either a hexa-histidine or a BirA recognition sequence

and cloned into the pHLsec vector (Aricescu et al., 2006). Expression was performed by transient transfection in HEK-293T cells (using a semi-automated procedure (Zhao et al., 2011) in the presence of the class I α-mannosidase inhibitor, kifunensine (Chang et al., 2007). 3-4 days post-transfection, conditioned medium was harvested, buffer exchanged into PBS and purified by immobilized metal affinity chromatography using TALON beads (ClonTech). Proteins were then further purified using size-exclusion chromatography (Superdex 16/60 column, GE Healthcare) in a buffer of 10 mM HEPES pH 7.5, 150 mM NaCl.

*Hhip1 antibody generation*

Rabbits were immunized against human HHIP1 protein (aa212-670) that was purified as described above. Injections, animal husbandry, and serum production was performed at the Pocono Rabbit Farm & Laboratory (Canadensis, PA) using the 70 day antibody production package. Polyclonal HHIP1 antibodies were purified from serum using Protein-A agarose chromatography.

*HHIP1-GAG Surface Plasmon Resonance Binding Studies*

Surface Plasmon Resonance (SPR) experiments were performed using a Biacore T200 machine (GE Healthcare) in 10 mM HEPES pH 7.5, 120 mM NaCl, 0.05% (v/v) polysorbate 20, at 25 °C. Proteins were buffer exchanged into running buffer and concentrations calculated from the absorbance at 280 nm using molar extinction coefficient values. Heparin (Iduron; average molecular weight >9,000 Da) and heparan sulfate (HS) from porcine mucosa (Iduron) were biotinylated using EZ-link Biotin-LC-Hydrazide (Thermo Fisher Scientific) as described previously (Malinauskas et al., 2011) Biotinylated GAGs were immobilized upon a CM5 sensor chip to which 3,000 RU of streptavidin were coupled via primary amines. After each binding

experiment, the chip was regenerated with 1.5 M NaCl at 30 ul/min for 120s. HHIP1 proteins were injected at a flow rate of 5 μL/min for binding studies. The signal from experimental flow cells was processed, and corrected by subtraction of a blank and reference signal from a blank flow cell. In all experiments, the experimental trace returned to baseline after each regeneration. All data were analysed using SCRUBBER2 (Biologic) and GraphPad Prism Version 6.04 (GraphPad Software, La Jolla California USA). Best-fit binding curves were calculated using non-linear curve fitting of a one-site - total binding model (Y = Bmax*X / (Kd+X) + NS*X + Background, where X is analyte concentration and the amount of non-specific binding is assumed to be proportional to the concentration of analyte, hence NS is the slope of non-specific binding). The background value was constrained to zero as the data had been previously referenced. Bmax and Kd values reported are determined for the specific binding component only.

### 3.6 Acknowledgements

We thank the members of the Allen lab for productive discussions throughout the course of this study. We also thank Yevgeniya A. Mironova, Katherine T. Baldwin, Briana R. Dye, and Jason R. Spence for expert technical assistance and experimental advice. Confocal microscopy was performed in the Microscopy and Image Analysis Laboratory (MIL) at the University of Michigan. NKX6.1, PAX7, and NKX2.2 antibodies were obtained from the Developmental Studies Hybridoma Bank developed under the auspices of the NICHD and maintained by The University of Iowa, Department of Biological Sciences, Iowa City, IA. A.M.H. was supported by the University of Michigan MSTP training grant (T32 GM007863), the Cellular and Molecular Biology Training grant (T32 GM007315), and an NIH predoctoral fellowship (1F31 NS081806).

B.L.A. is supported by a Research Team Grant from the University of Michigan Center for Organogenesis, a Scientist Development Grant (11SDG638000) from the American Heart Association and funding from the National Institutes of Health (R21 CA167122 and R01 DC014428). C.S is supported by Cancer Research UK.

## 3.7 Figures

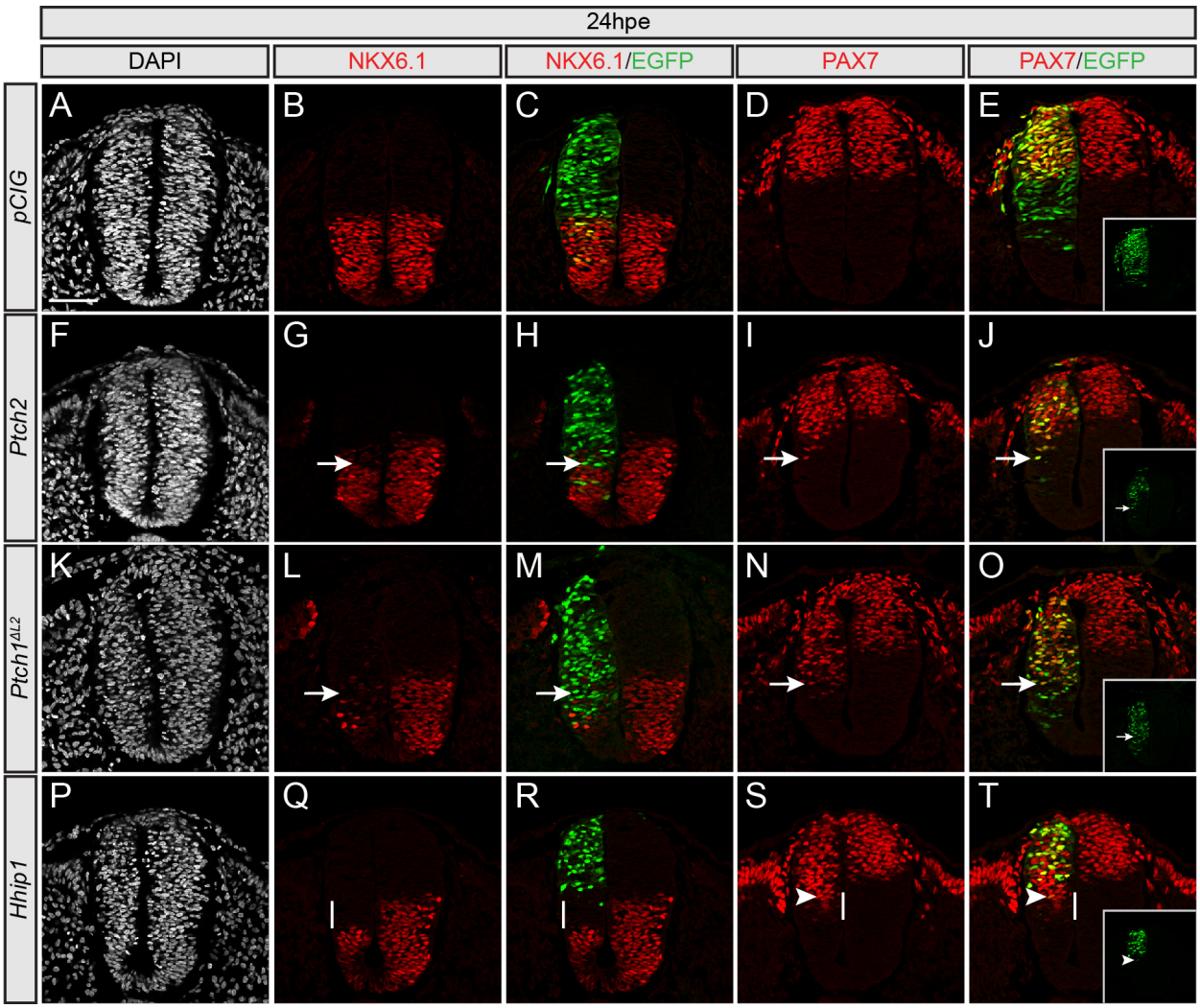


**Figure 3-1. Ectopic HHIP1 expression non-cell autonomously inhibits neural progenitor patterning.** Embryonic chicken neural tubes electroporated at Hamburger-Hamilton stage 11-13 with *pCIG* (A-E), *mPtch2-pCIG* (F-J), *mPtch1$^{\Delta L2}$-pCIG* (K-O), or *mHhip1-pCIG* (P-T) and dissected 24 hours post electroporation (hpe). Transverse sections from the wing axial level were stained with antibodies directed against NKX6.1 (red; B, C, G, H, L, M, Q, R) and PAX7 (red; D, E, I, J, N, O, S, T). Nuclei are stained with DAPI (grey; A, F, K, P). Nuclear EGFP expression labels electroporated cells (green; C, E, H, J, M, O, R, T). Arrows indicate repression of NKX6.1 expression (G, H, L, M) or ectopic PAX7 expression (I, J, N, O). Insets show individual green channels (E, J, O, T). White lines highlight non-cell autonomous NKX6.1 repression (Q, R) and ectopic PAX7 expression (S, T). Arrowheads demarcate the ventral most electroporated cell (S, T). Scale bars (A), 50μm.

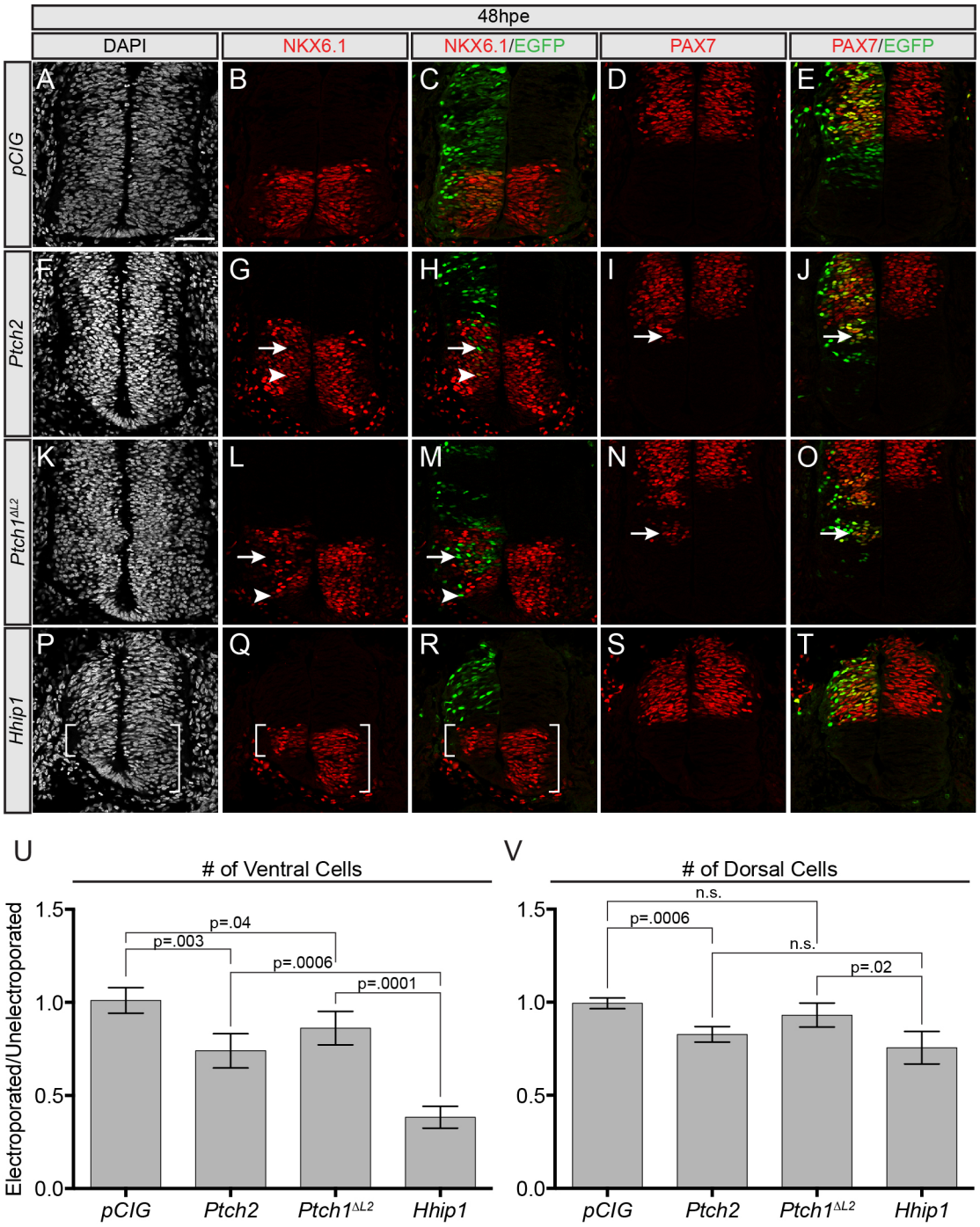


**Figure 3-2. Ectopic HHIP1 expression causes significant neural tube growth defects.** Embryonic chicken neural tubes electroporated at Hamburger-Hamilton stage 11-13 with *pCIG* (A-E), *mPtch2-pCIG* (F-J), *mPtch1*$^{\Delta L2}$*-pCIG* (K-O), or *mHhip1-pCIG* (P-T) and dissected 48 hours post electroporation (hpe). Transverse sections from the wing axial level were stained with antibodies directed against NKX6.1 (red; B, C, G, H, L, M, Q, R) and PAX7 (red; D, E, I, J, N, O, S, T). Nuclei are stained with DAPI (grey; A, F, K, P). Nuclear EGFP expression labels electroporated cells (green; C, E, H, J, M, O, R, T). Arrows indicate repression of NKX6.1 expression (G, H, L, M) or ectopic expression of PAX7 (I, J, N, O). Arrowheads denote ventrally

electroporated cells that maintain (*Ptch2*; G-H) or repress (*Ptch1*$^{\Delta L2}$; L-M) NKX6.1 expression. Brackets highlight ventral neural tube size in embryos electroporated with *Hhip1* (P-R). (U-V) Quantitation of cell numbers in the ventral (U) and dorsal (V) neural tubes of embryos electroporated with the indicated constructs and expressed as the relative number of cells on the electroporated compared to the unelectroporated side of the tissue. Data are presented as mean +/- SEM. P-values determined by two-tailed student's *t*-test. Scale bar (A), 50μm.

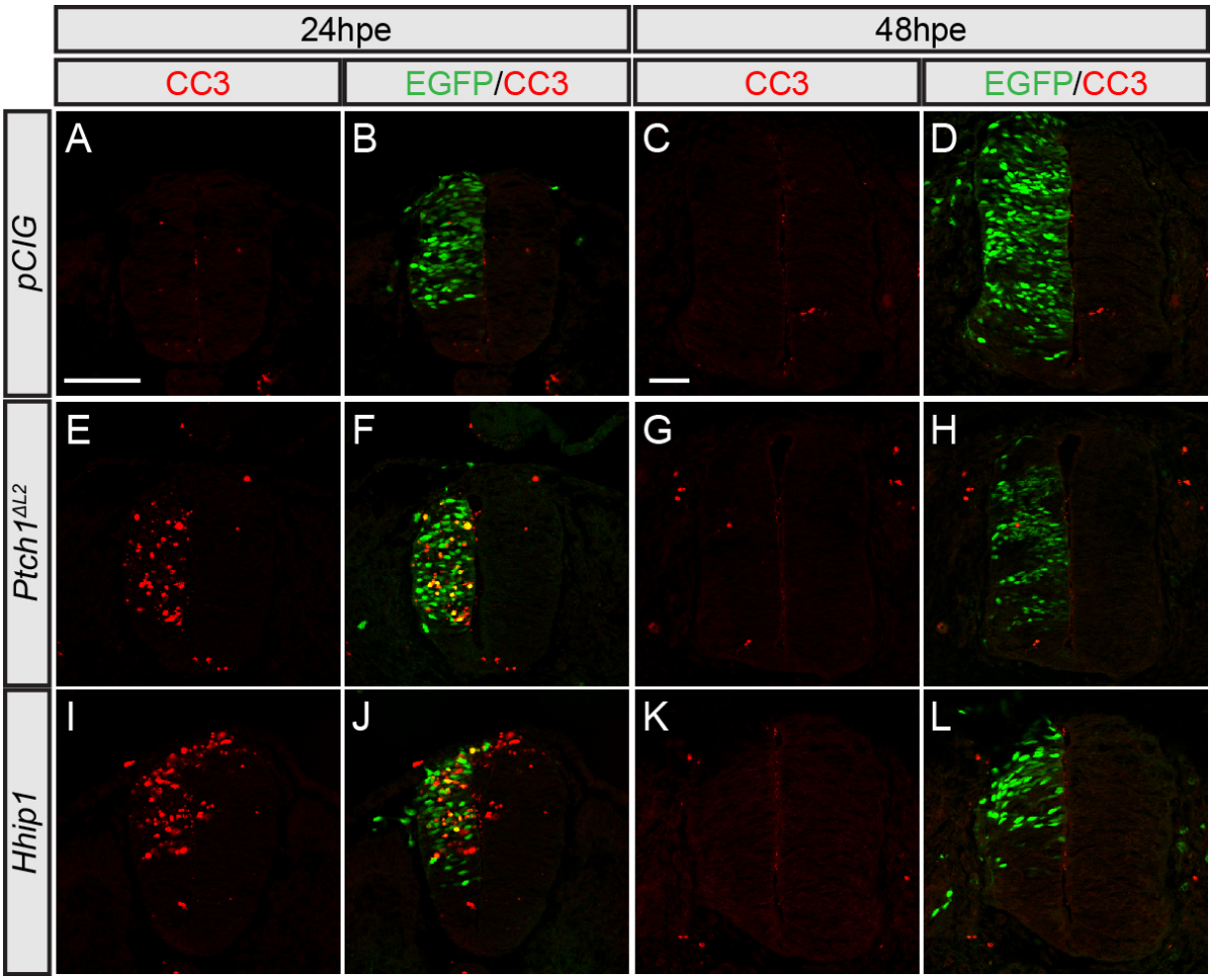


**Figure 3-3. PTCH1$^{\Delta L2}$ and HHIP1 expression transiently induce apoptosis in the neural tube.** Chicken embryos electroporated at stage 11-13 with *pCIG* (A-D), *mPtch1*$^{\Delta L2}$*-pCIG* (E-H), and *mHhip1-pCIG* (I-L) and collected at 24hpe (A, B, E, F, I, J) or 48hpe (C, D, G, H, K, L) were sectioned at the wing axial level and stained with cleaved caspase-3 (CC3, red; A-L). Electroporated cells are labeled with nuclear EGFP (green; B, D, F, H, J, L).

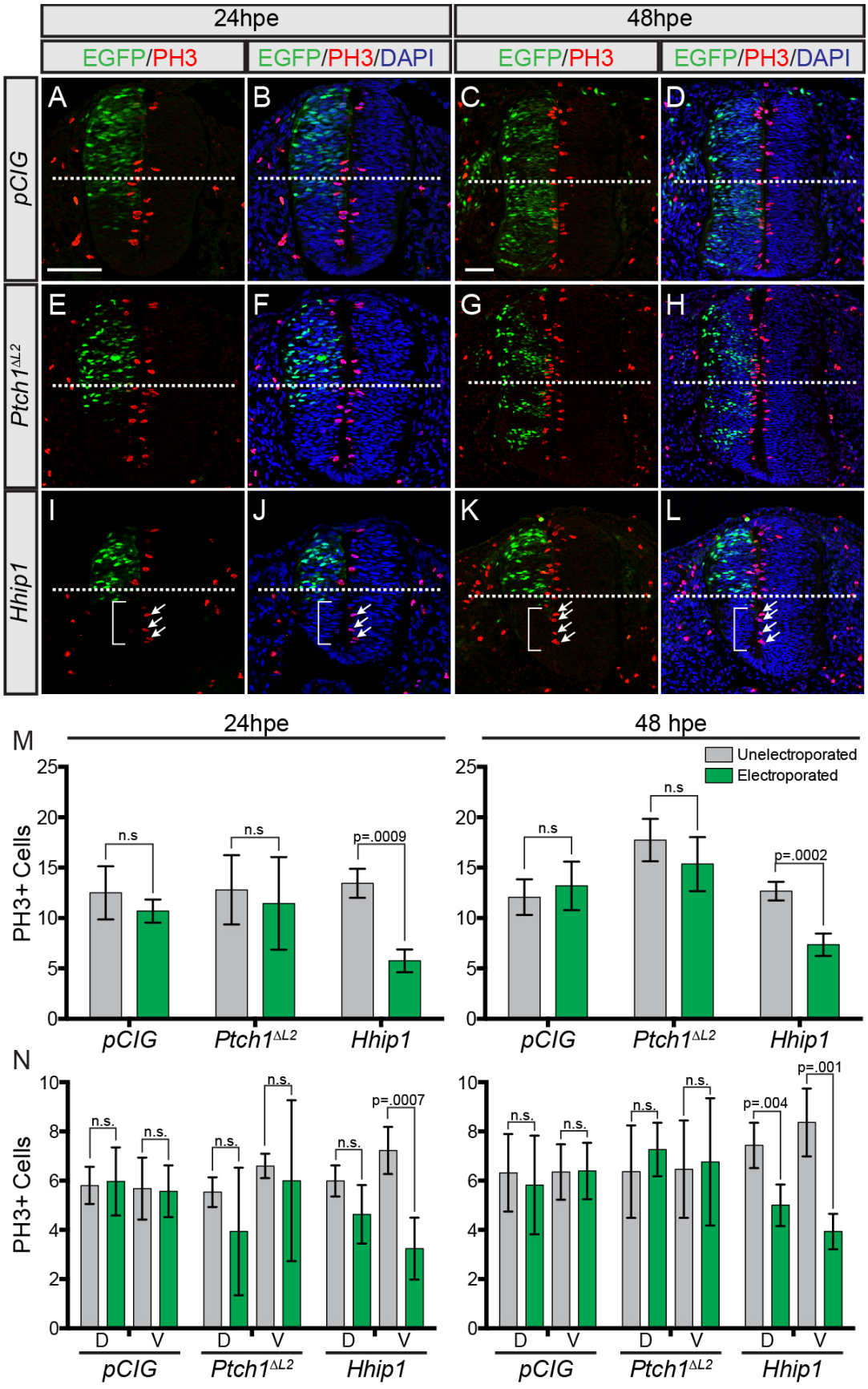
24hpe
48hpe
EGFP/PH3
EGFP/PH3/DAPI
EGFP/PH3
EGFP/PH3/DAPI
pCIG
Ptch1ΔL2
Hhip1
A
B
C
D
E
F
G
H
I
J
K
L
M
24hpe
48 hpe
Unelectroporated
Electroporated
PH3+ Cells
n.s
p=.0009
p=.0002
pCIG
Ptch1ΔL2
Hhip1
N
n.s.
p=.0007
p=.004
p=.001
D
V

**Figure 3-4. HHIP1 expression inhibits HH-dependent neuronal progenitor proliferation in a non-cell autonomous manner.** Electroporation of *pCIG* (A-D), *mPtch1*$^{\Delta L2}$*-pCIG* (E-H), or *mHhip1-pCIG* (I-L) in HH stage 11-13 chicken embryos. Embryos were dissected 24 hours post electroporation (hpe), sectioned at the wing axial level, and stained with a Phospho-histone H3 antibody (PH3, red; A-L). Nuclear EGFP expression labels electroporated cells (green; A-L). DAPI staining reveals nuclei (blue; B, D, F, H, J, and L). Dotted lines (A-L) bisect the neural tube into dorsal and ventral halves. Arrows (I-L) highlight PH3+ cells on the unelectroporated side of the neural tube while brackets (I-L) denote the lack of PH3+ cells resulting from HHIP1 expression. (M-N) Quantitation of total PH3+ cells (M) or PH3+ cells binned into either the dorsal or ventral half of the tissue (N) at 24hpe and 48hpe. Data are presented as mean +/- SEM. P-values determined by two-tailed student's *t*-test. (A, C), 50µm.

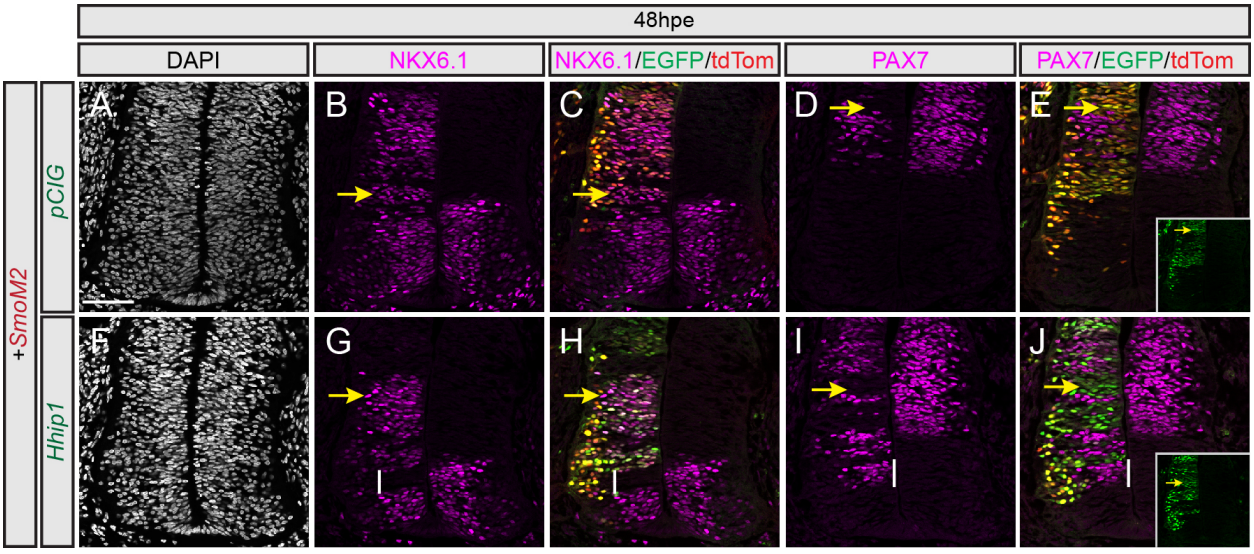


**Figure 3-5. HHIP1 non-cell autonomously inhibits HH-dependent neural patterning when co-expressed with SMOM2.** (A-J) Immunofluorescent analysis of neural patterning in chicken embryos electroporated at stage 11-13 with *SmoM2-pCIT* (A-J) and co-electroporated with either *pCIG* (A-E) or *mHhip1-pCIG* (F-J). Transverse sections collected at the wing axial level were stained with NKX6.1 (magenta; B, C, G, H) and PAX7 (magenta; D, E, I, J). DAPI stains nuclei (grey; A, F). Electroporated cells are labeled with nuclear EGFP and tdTomato (tdTom; C, E, H, J). Insets (E, J) show individual green channels (EGFP). Yellow arrows denote ectopic NKX6.1 expression (B, C, G, H) or repression of PAX7 (D, E, I, J) resulting from SMOM2 expression. Vertical lines denote non-cell autonomous inhibition of NKX6.1 expression (G, H) or ectopic PAX7 expression (I, J). Scale bar (A), 50µm.

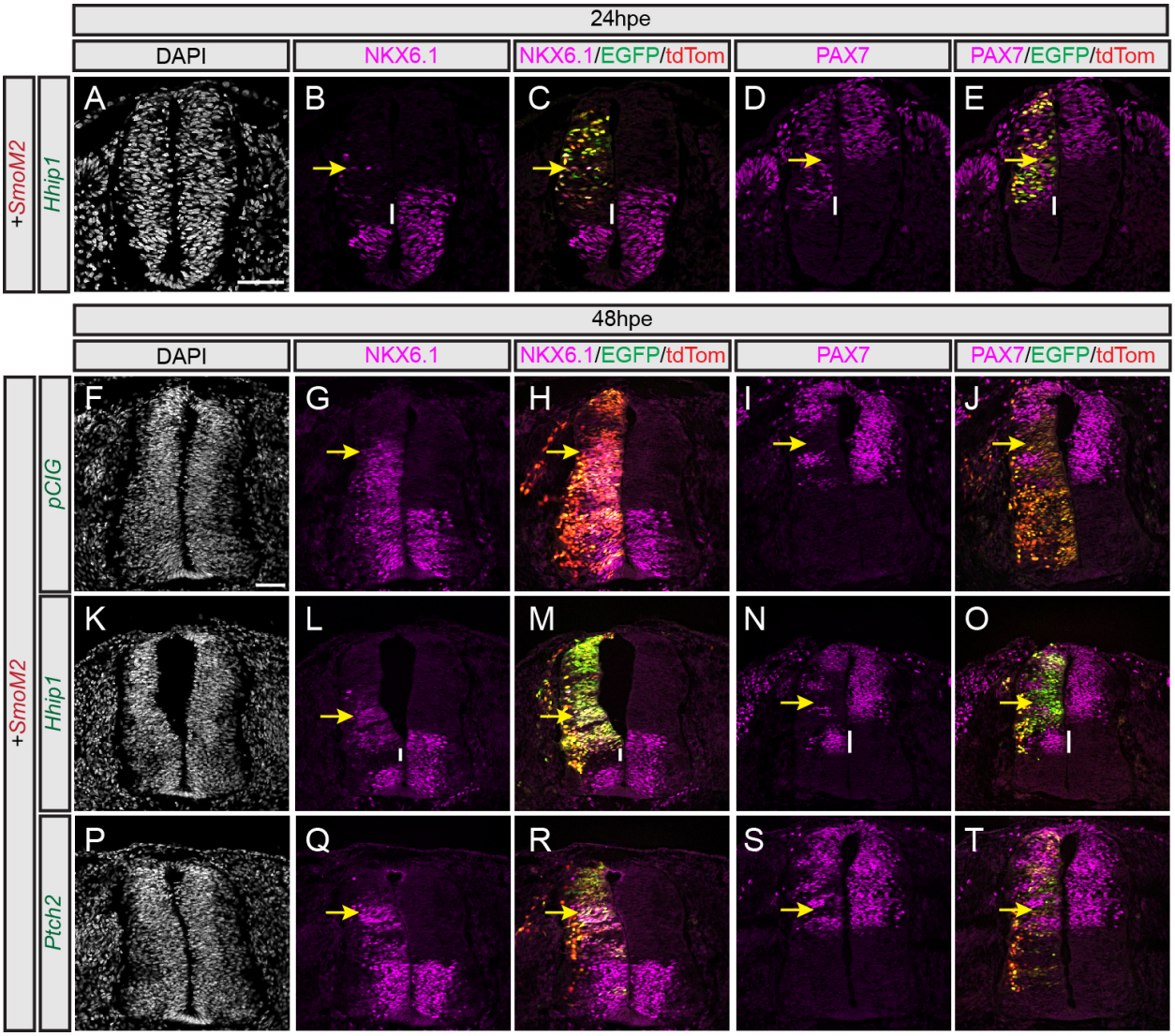


**Figure 3-6. PTCH2 does not induce non-cell autonomous inhibition of HH-dependent neural patterning when co-electroporated with SMOM2.** Chicken embryos co-electroporated at stage 11-13 with either *pCIG* (F-J), *mHhip1-pCIG* (A-E, K-O) or *mPtch2-pCIG* (P-T) and co-electroporated with *SmoM2-pCIT* (A-T) were collected at 24hpe (A-E) and 48hpe (F-T). Transverse sections at the wing axial level were stained with antibodies raised against NKX6.1 (magenta; B, C, G, H, K, M, Q, R) and PAX7 (magenta; D, E, I, J, N, O, S, T). Electroporated cells are labeled with EGFP and tdTomato (tdTom; C, E, H, J, M, O, R, T). DAPI staining labels nuclei (grey; A, F, K, P). Yellow arrows indicate cell autonomous expansion of NKX6.1 (B, C, G, H, L, M, Q, R) or repression of PAX7 (D, E, I, J, N, O, S, T) resulting from SMOM2 expression. White lines indicate non-cell autonomous repression of NKX6.1 (B, C, L, M) or expansion of PAX7 expression (D, E, N, O). Scale bars (A, F), 50μm.

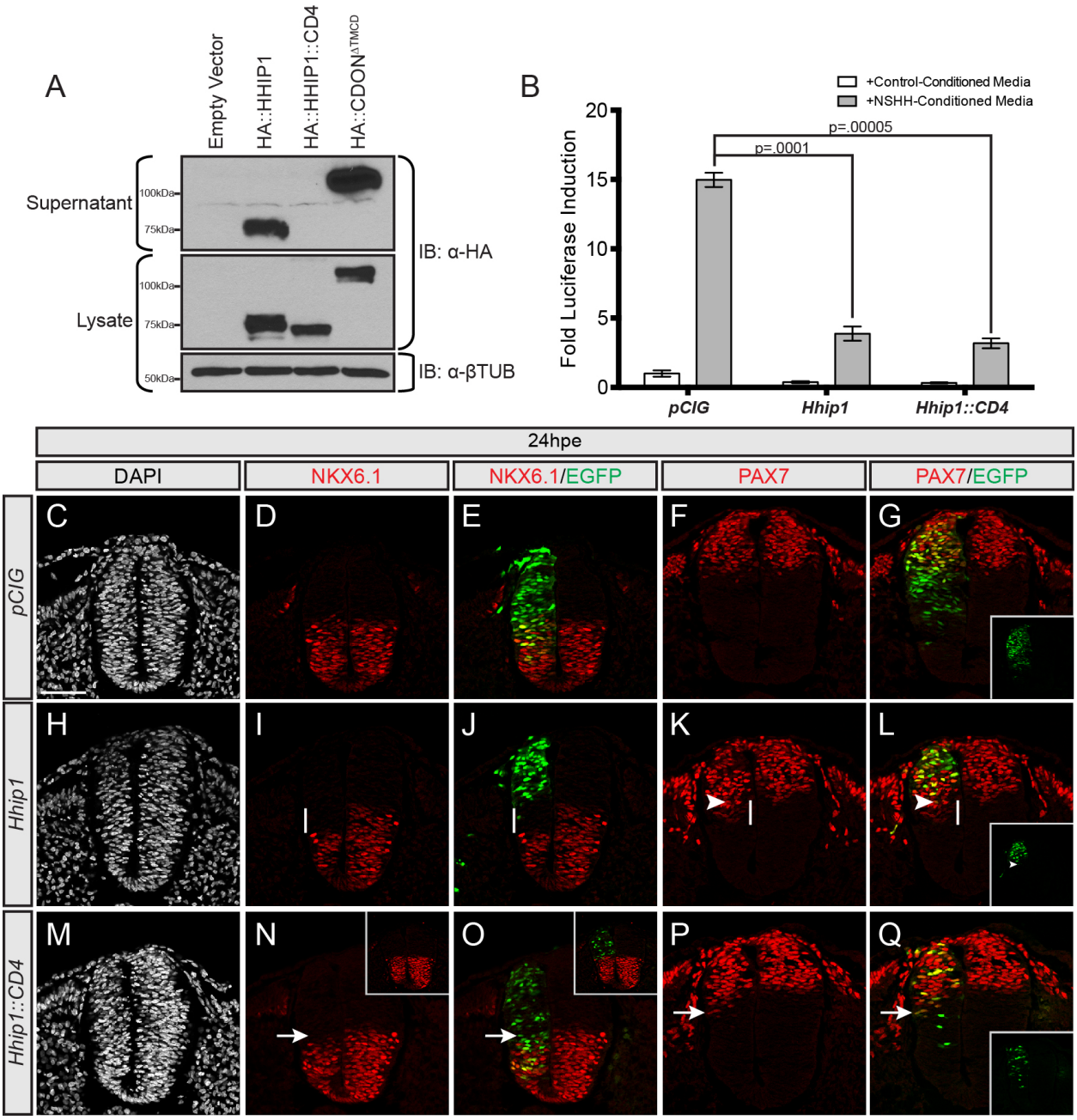


**Figure 3-7. HHIP1 secretion mediates its non-cell autonomous effects in the developing neural tube.** (A) Western blot analysis of cell lysates (bottom panels) and supernatants (top panel) collected from NIH/3T3 fibroblasts expressing HA-tagged HHIP1 proteins and probed with an anti-HA antibody. HA::CDON$^{\Delta TMCD}$ is included as a secreted protein control. Anti-β-tubulin (βTUB) is used as a loading control. (B) HH-responsive luciferase reporter activity measured in NIH/3T3 cells stimulated with either control-conditioned media (white bars) or NSHH-conditioned media (grey bars) and transfected with the indicated constructs. Data are presented as mean +/- SEM. P-values are determined by two-tailed student's *t*-tests. (C-Q) Neural patterning analysis of chicken embryos electroporated at stage 11-13 with *pCIG* (C-G), *mHhip1-pCIG* (H-L), and *mHhip1::CD4-pCIG* (M-Q) and collected at 24hpe. Embryos were

sectioned at the wing axial level and stained with antibodies against NKX6.1 (red; D, E, I, J, N, O) and PAX7 (red; F, G, K, L, P, Q). DAPI staining detects nuclei (grey; C, H, M). Electroporated cells are labeled with nuclear EGFP (E, G, J, L, O, Q). Insets show individual green channels (G, L, Q). White lines highlight non-cell autonomous NKX6.1 repression (I, J) and ectopic PAX7 expression (K, L). Arrowheads demarcate the ventral most electroporated cell (K, L). White arrows indicate cell autonomous inhibition of NKX6.1 expression (N, O), and ectopic PAX7 expression (P, Q) resulting from mHHIP1::CD4 expression. Insets in (N, O) represent embryos with dorsally restricted HHIP1::CD4 expression. Scale bar (C), 50μm.

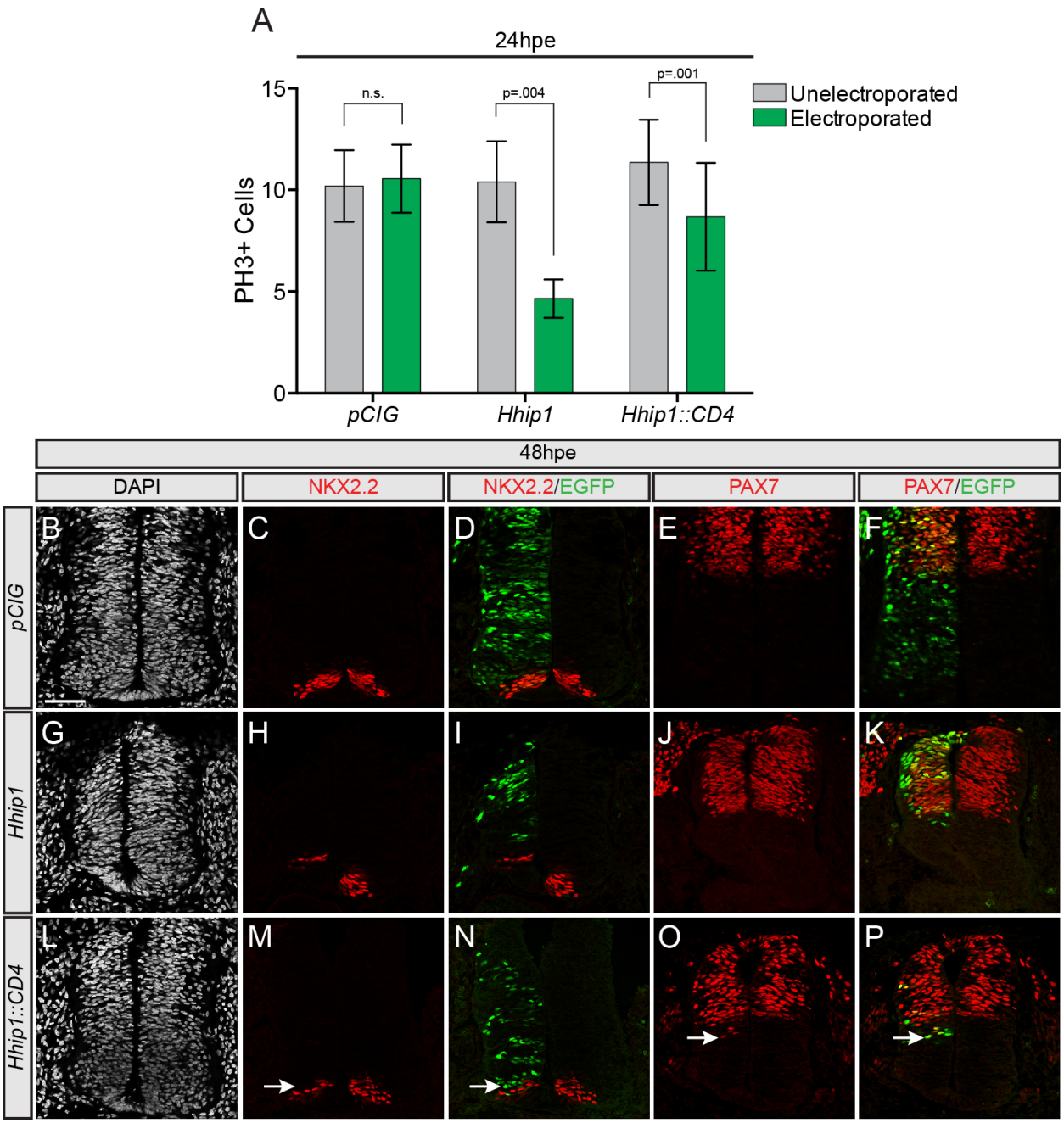


**Figure 3-8. Membrane anchoring of HHIP1 limits long-range inhibition of HH-dependent patterning at 48hpe.** (A) Quantitation of PH3+ cells in embryos electroporated with the indicated constructs at stage 11-13 and collected at 24hpe. Data are presented as mean +/- SEM. P-values calculated using Student's two-tailed *t*-test. (B-P) Transverse sections at the wing axial level from chicken embryos electroporated with *pCIG* (B-F), *mHhip1-pCIG* (G-K) and *mHhip1::CD4-pCIG* (L-P) and collected at 48hpe. Sections were immunostained to detect expression of NKX2.2 (red; C, D, H, I, M, N) and PAX7 (red; E, F, J, K, O, P). DAPI staining marks nuclei (grey; P, G, L). Nuclear EGFP expression identifies electroporated cells (D, F, I, K, N, P). Arrows indicate cell autonomous repression of NKX2.2 (M, N) or expansion of PAX7 expression (O, P). Scale bar (B), 50µm.

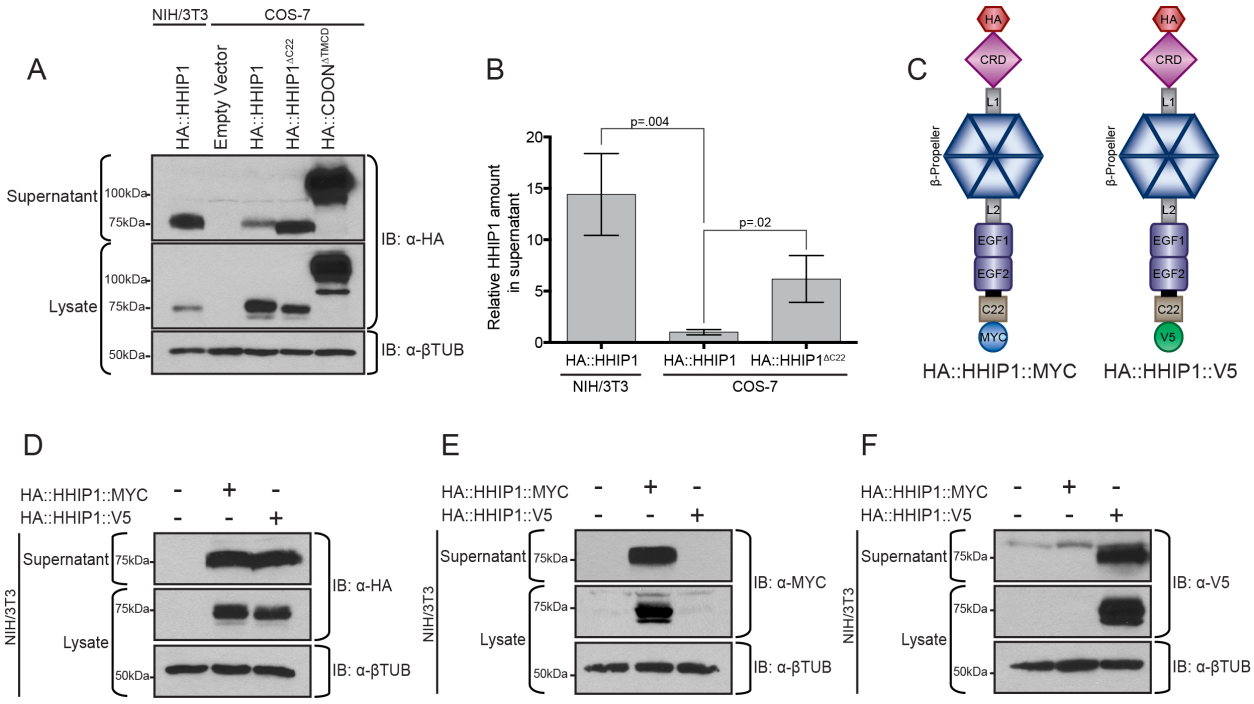


**Figure 3-9. HHIP1 is secreted in a cell-type specific manner independent of proteolytic cleavage.** (A) Western blot analysis of cell lysates (bottom panels) and supernatants (top panel) collected from NIH/3T3 and COS-7 cells expressing HA-tagged HHIP1 protein. HA::CDON$^{\Delta TMCD}$ is included as a secreted protein control. (B) Quantitation of HHIP1 secretion from NIH/3T3 and COS-7 cells. Data are presented as mean +/- SEM. P-values determined by two-tailed Student's *t*-test. (C) Schematic of dual-tagged HHIP1 constructs. (D-F) Immunoblot detection of dual-tagged HHIP1 constructs in supernatants (top panel) and lysates (bottom panels) collected from NIH/3T3 cells and probed with anti-HA (D), anti-MYC (E), and anti-V5 (F) antibodies.

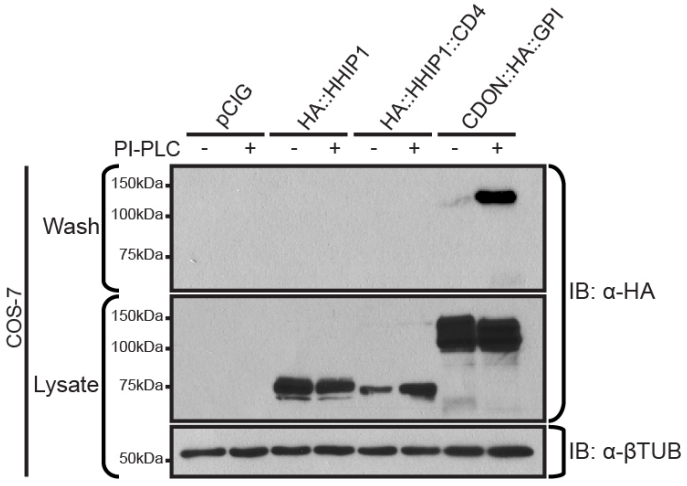


**Figure 3-10. HHIP1 is not a GPI-anchored protein.** COS-7 cells expressing the indicated HA-tagged constructs were treated with PI-PLC for 20 minutes. Both the lysates (bottom panels) and washes (top panel) were analyzed by western blot using an anti-HA antibody. Note that PI-PLC

treatment releases CDON::HA::GPI from cells while HA::HHIP1 and HA::HHIP1::CD4 remain associated with cells.

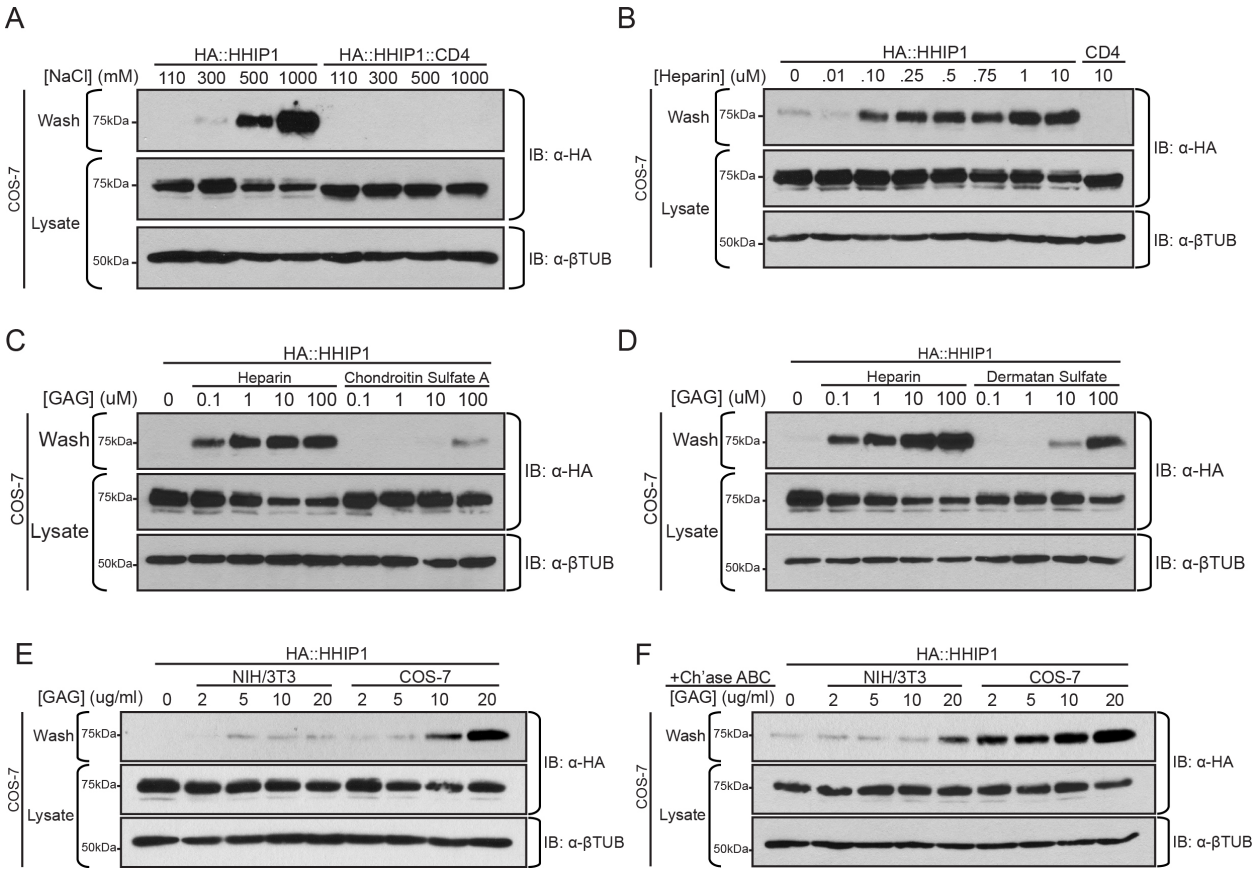


**Figure 3-11. HHIP1 is retained at the cell surface through cell-type specific interactions with heparan sulfate.** (A) COS-7 cells expressing HA::HHIP1 were washed for 20 minutes with solutions containing increasing NaCl concentrations. Both the washes (top panel) and cell lysates (bottom panels) were assayed by western blot analysis for HHIP1 expression. (B-D) As in (A), except using washes containing increasing Heparin (B), Chondroitin Sulfate A (C), or Dermatan Sulfate (D) concentrations. (E, F) As in (A-D), except using washes containing glycosaminoglycans isolated from NIH/3T3 and COS-7 cells pre- (E) and post- (F) Chondroitinase ABC (Ch'ase ABC) treatment. Anti-β-tubulin (βTUB) is used as a loading control (bottom panels, A-F).

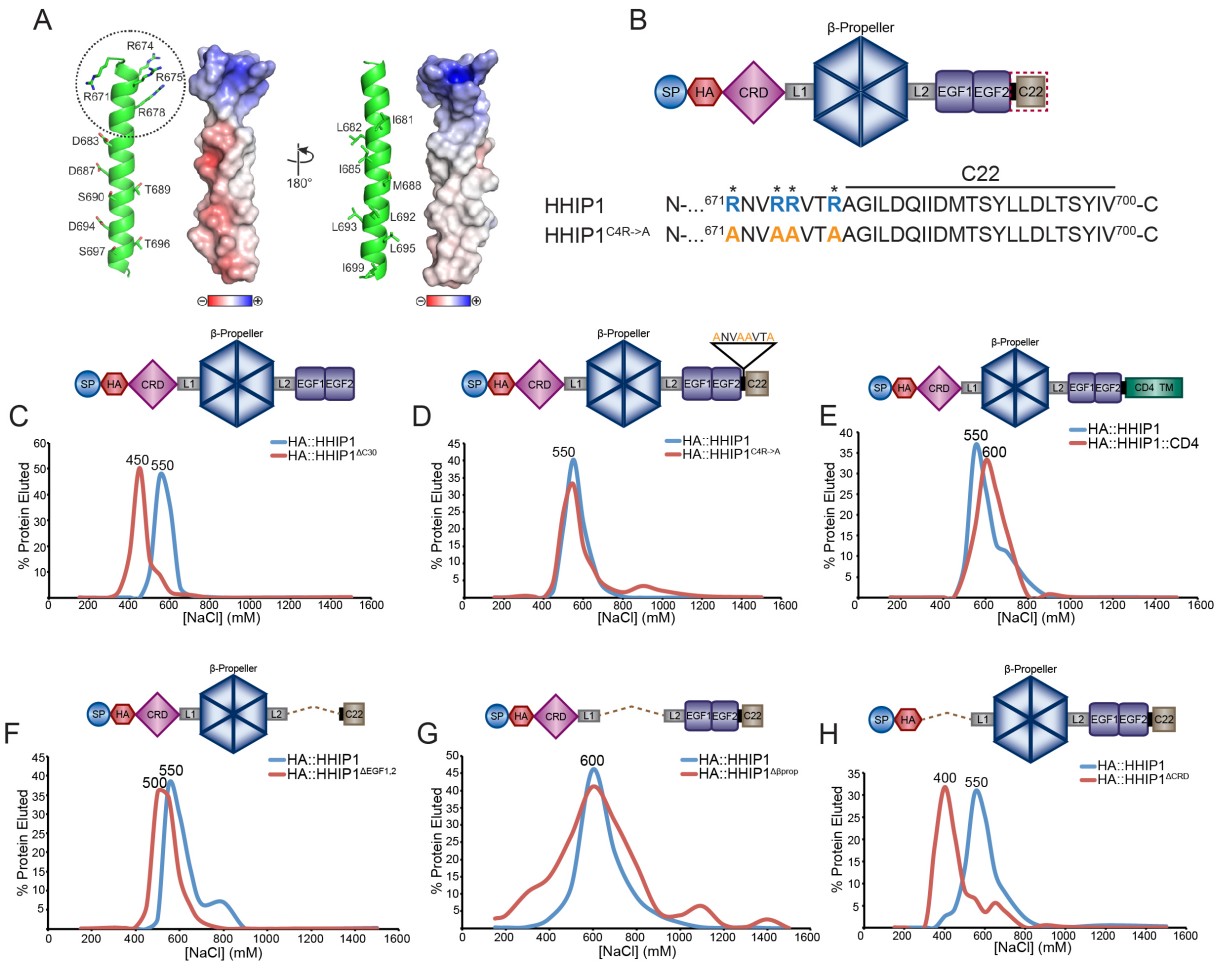


**Figure 3-12. HHIP1 associates with HS through the N-terminal CRD.** (A) Representative structural model of the HHIP1 C-terminal 30 residues shown as ribbons (left) and electrostatic potential (right). Four N-terminal arginines are highlighted (dotted circle). Electrostatic potential is calculated from -10 kbT/ec (red, acidic) to 10 kbT/ec (blue, basic). Selected residues are depicted in stick representation. (B) Cartoon depiction of HA::HHIP1 (top). Sequence analysis identifies a cluster of basic residues (blue) in the C-terminal 30 amino acids that were mutagenized to alanines (orange) to generate HHIP1$^{C4R-4A}$ (bottom). (C-H) Heparin-agarose chromatography was used to measure heparin-binding affinities for HA::HHIP1 (C-H), HA::HHIP1$^{\Delta C30}$ (C) HA::HHIP1$^{C4R->4A}$ (D), HA::HHIP1::CD4 (E), HA::HHIP1$^{\Delta EGF1,2}$ (F), and HA::HHIP1$^{\Delta\beta prop}$ (G), and HA::HHIP1$^{\Delta CRD}$ (H). NaCl concentrations (in mM) corresponding to elution peaks are indicated above each curve.

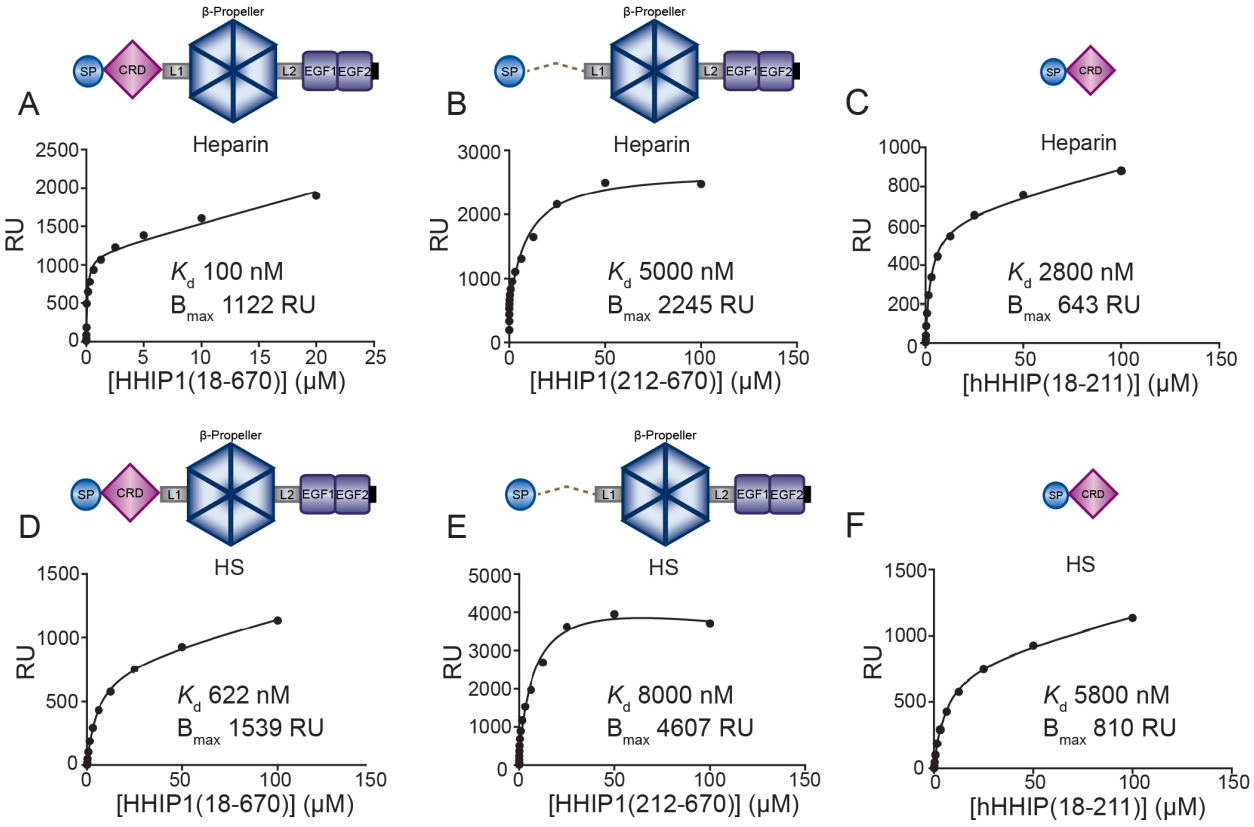


**Figure 3-13. The HHIP1-CRD directly interacts with Heparin and HS.** Representative surface plasmon resonance (SPR) binding experiments demonstrating direct interactions between HHIP1$^{(18\text{-}670)}$ (A, D), HHIP1$^{(212\text{-}670)}$ (B, E), and HHIP1$^{(18\text{-}211)}$ (C, F) with Heparin (A-C) and HS (D-F). Cartoon depictions of each construct are presented above each dataset.

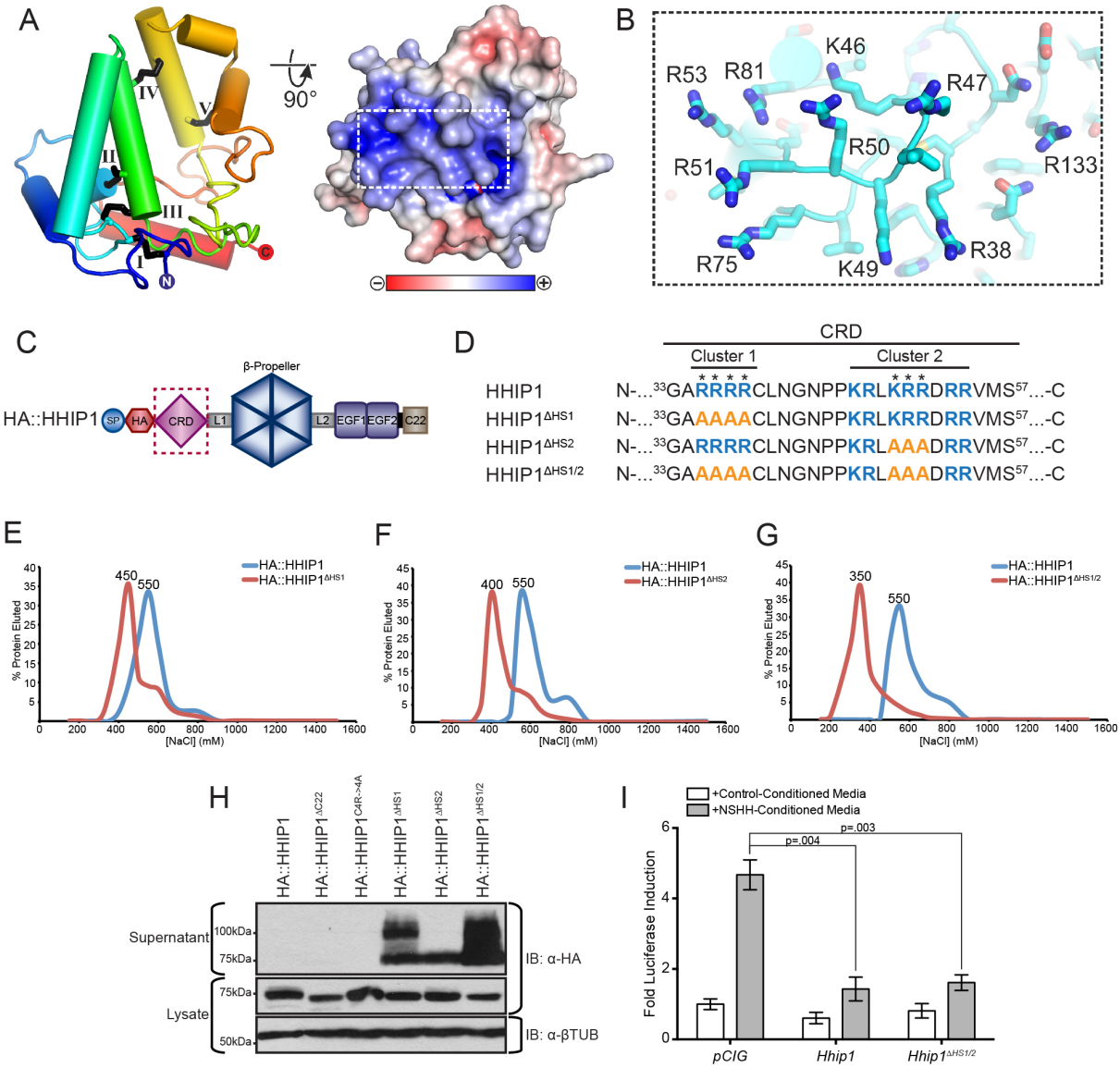


**Figure 3-14. Identification of specific residues that mediate HS-binding and cell surface retention of HHIP1.** (A) Representative model of the HHIP1 CRD. Left panel: ribbon representation in rainbow coloring from blue (N-terminus) to red (C-terminus). Potential disulphide bridges are shown in Roman numerals. Right: electrostatic potential from -10 kbT/ec (red, acidic) to 10 kbT/ec (blue, basic). (B) Close-up view of the potential HHIP1-CRD HS-binding site shown in stick representation in atomic coloring (carbon: cyan, nitrogen: blue, oxygen: red, sulfur: yellow). (C) Cartoon depiction of HA::HHIP1. (D) Sequence analysis identifies two clusters of basic residues (blue) in the CRD that were mutagenized to alanines (orange) to generate HA::HHIP1$^{\Delta HS1}$, HA::HHIP1$^{\Delta HS2}$, and HA::HHIP1$^{\Delta HS1/2}$. (E-G) Heparin-binding of HA::HHIP1 (E-G), HA::HHIP1$^{\Delta HS1}$ (E), HA::HHIP1$^{\Delta HS2}$ (F), and HA::HHIP1$^{\Delta HS1/2}$ (G) was assessed by heparin-agarose chromatography. NaCl elution peaks (in mM) are indicated above each curve. (H) Immunoblot analysis of COS-7 cell lysates (bottom panels) and supernatants (top panels) expressing HA-tagged HHIP1 HS-binding mutants. Of note, in addition to the expected 75kDa HHIP1 band, we also observe the presence of a 100kDa form in some of

the HS-binding mutants. (I) HH-responsive luciferase reporter activity measured from NIH/3T3 cells stimulated with either control-conditioned media (white bars) or NSHH-conditioned media (grey bars) and transfected with the indicated constructs. Data are presented as mean +/- SEM. P-value is determined by two-tailed Student's *t*-test.

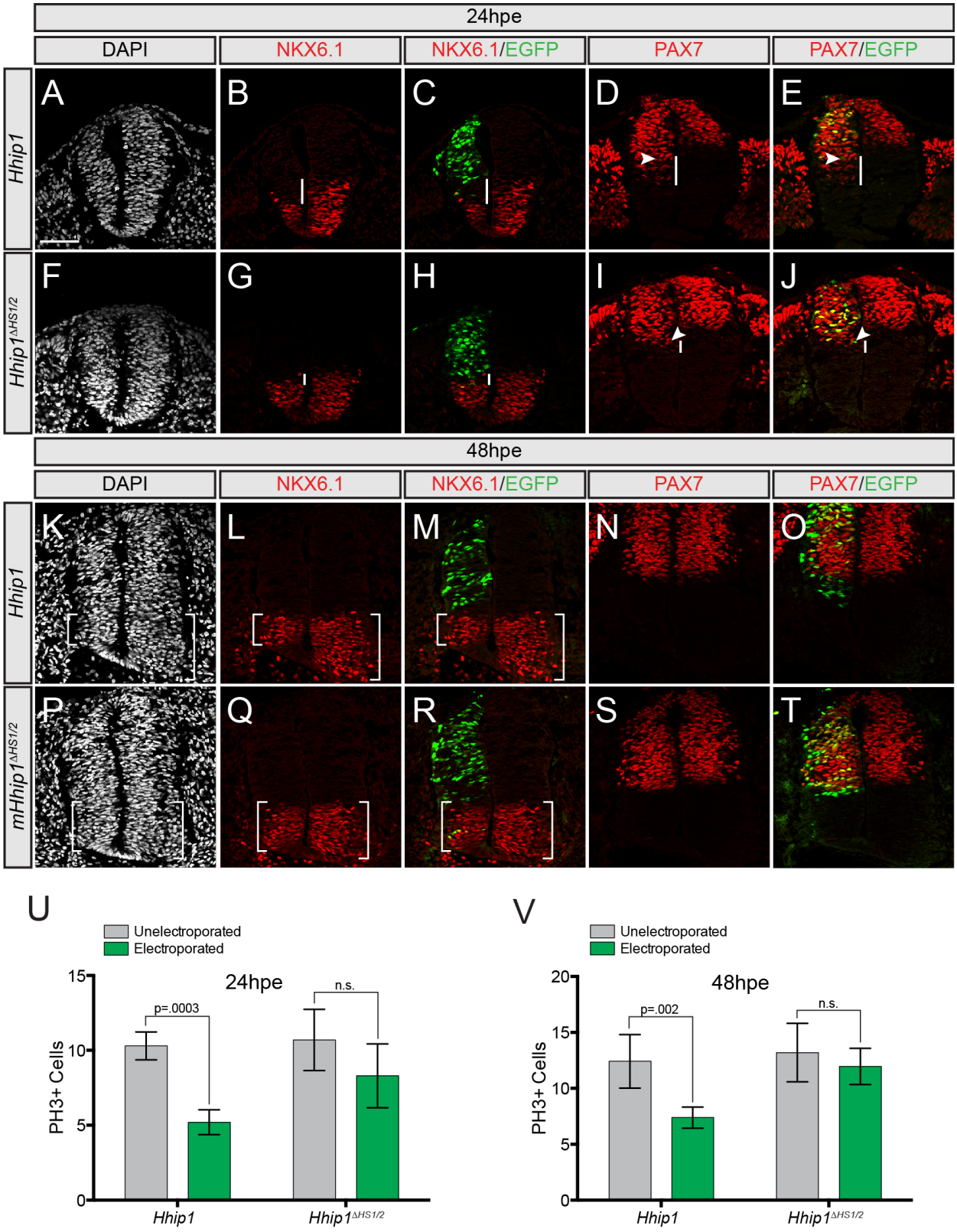


**Figure 3-15. HHIP1-HS interaction promotes long-range inhibition of HH-dependent patterning and proliferation.** (A-T) Hamburger-Hamilton stage 11-13 chicken embryos

electroporated with *mHhip1-pCIG* (A-E, K-O) and *mHhip1*$^{\Delta HS1/2}$*-pCIG* (F-J, P-T) were collected at 24hpe (A-J) and 48hpe (K-T), sectioned at the wing axial level, and immunostained with antibodies raised against NKX6.1 (red; B, C, G, H, L, M, Q, R) and PAX7 (red; D, E, I, J, N, O, S, T). Electroporated cells express nuclear EGFP (green; C, E, H, J, M, O, R, T). DAPI stains nuclei (grey; A, F, K, P). White lines indicate non-cell autonomous repression of NKX6.1 expression (B, C, G, H) and ectopic expansion of PAX7 (D, E, I, J). White arrowheads demarcate the ventral most electroporated cell (D, E, I, J). Brackets in (K-M, P-R) denote the size of the NKX6.1+ domain. (U, V) Quantitation of PH3+ cells in embryos electroporated with the indicated constructs and collected at 24hpe (U) and 48hpe (V). Data are presented as mean +/- SEM. P-values determined by Student's two-tailed *t*-test. Scale bar (A), 50μm.

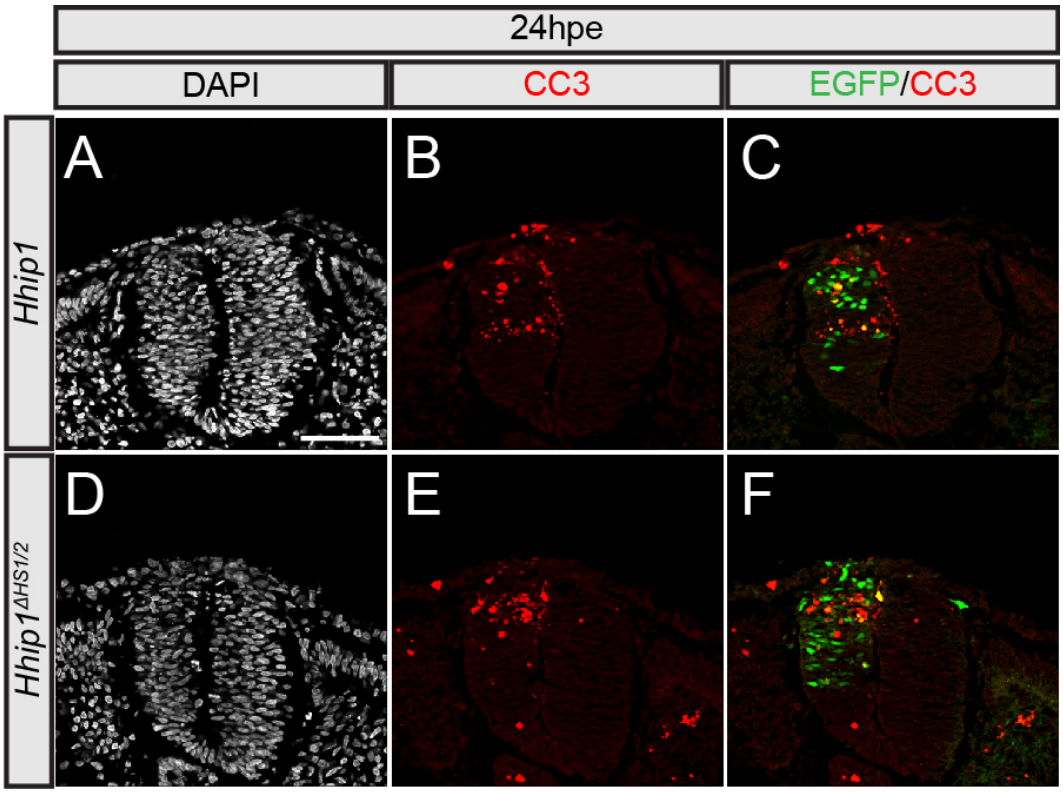


**Figure 3-16. Ectopic HHIP1$^{\Delta HS1/2}$ expression induces neuronal progenitor apoptosis.** Immunofluorescent staining with antibodies against cleaved caspase 3 (CC3) (red; B, C, E, F) in chicken embryos electroporated at HH stage 11-13 with *mHhip1-pCIG* (A-C) and *mHhip1*$^{\Delta HS1/2}$*-pCIG* (D-F) and collected at 24hpe. Embryos were sectioned at the wing bud axial level. Nuclear EGFP labels electroporated cells (green; C, F). DAPI staining reveals nuclei (grey; A, D).

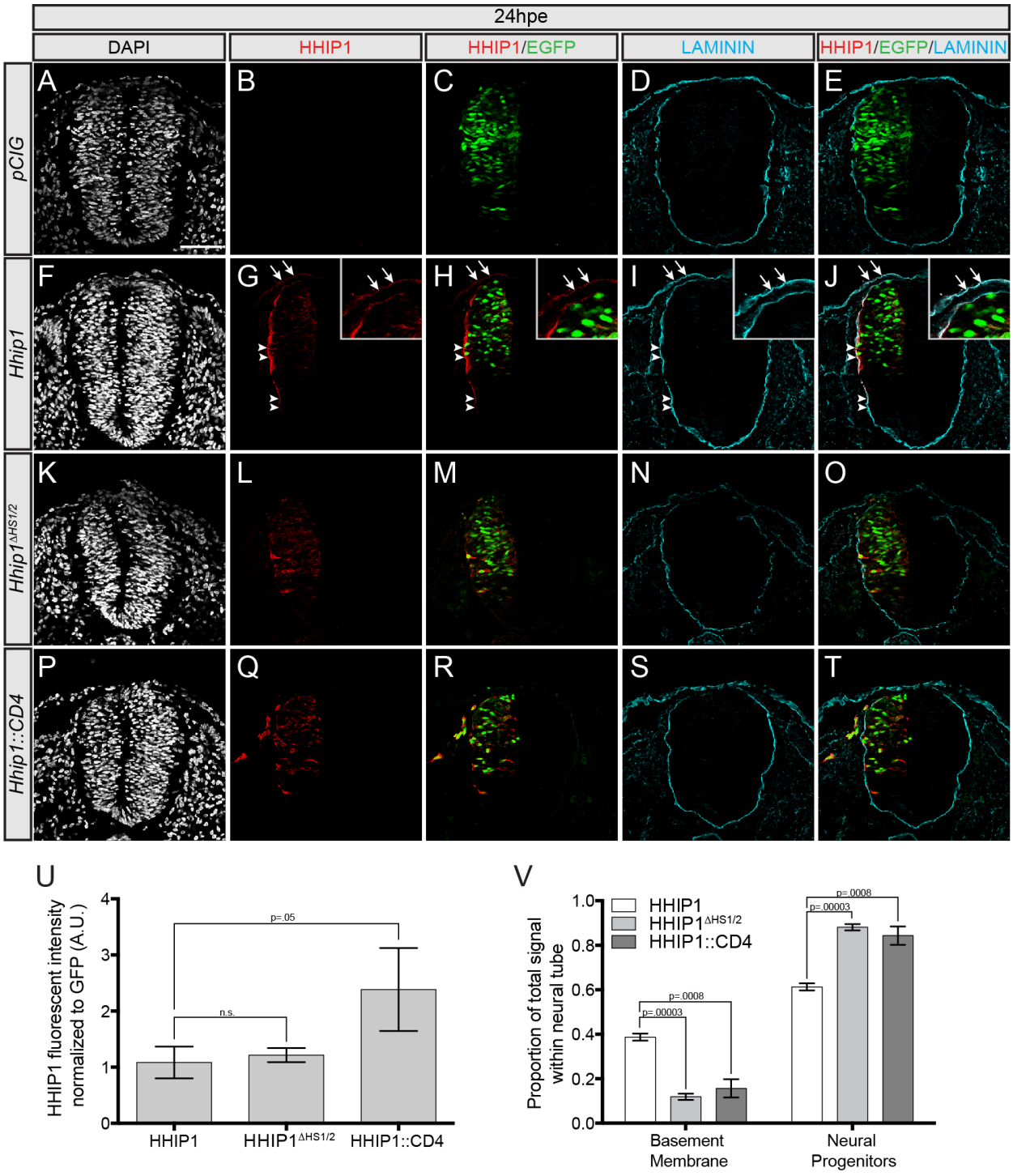


**Figure 3-17. HS-binding is required to localize HHIP1 to the neuroepithelial basement membrane.** Immunofluorescent detection of HHIP1 (red; B, C, E, G, H, J, L, M, O, Q, R, T) and Laminin (cyan; D, E, I, J, N, O, S, T) in embryos electroporated with *pCIG* (A-E), *mHhip1-pCIG* (F-J), *mHhip1*$^{\Delta HS1/2}$*-pCIG* (K-O), and *mHhip1::CD4-pCIG* (P-T) and isolated 24hpe. DAPI stains nuclei (grey; A, F, K, P). Nuclear EGFP labels electroporated cells (green; C, E, H, J, M, O, R, T). (G-J) Note HHIP1 co-localization with Laminin in the neural tube (arrowheads) and

surface ectoderm (arrows, insets). (U) Quantitation of HHIP1 fluorescent intensity normalized to GFP expression. (V) Data in U binned into signal measured within the basement membrane or neural progenitors. Data is presented as mean +/- SEM. P-values determined by Student's two-tailed *t*-test. Scale bar (A), 50µm.

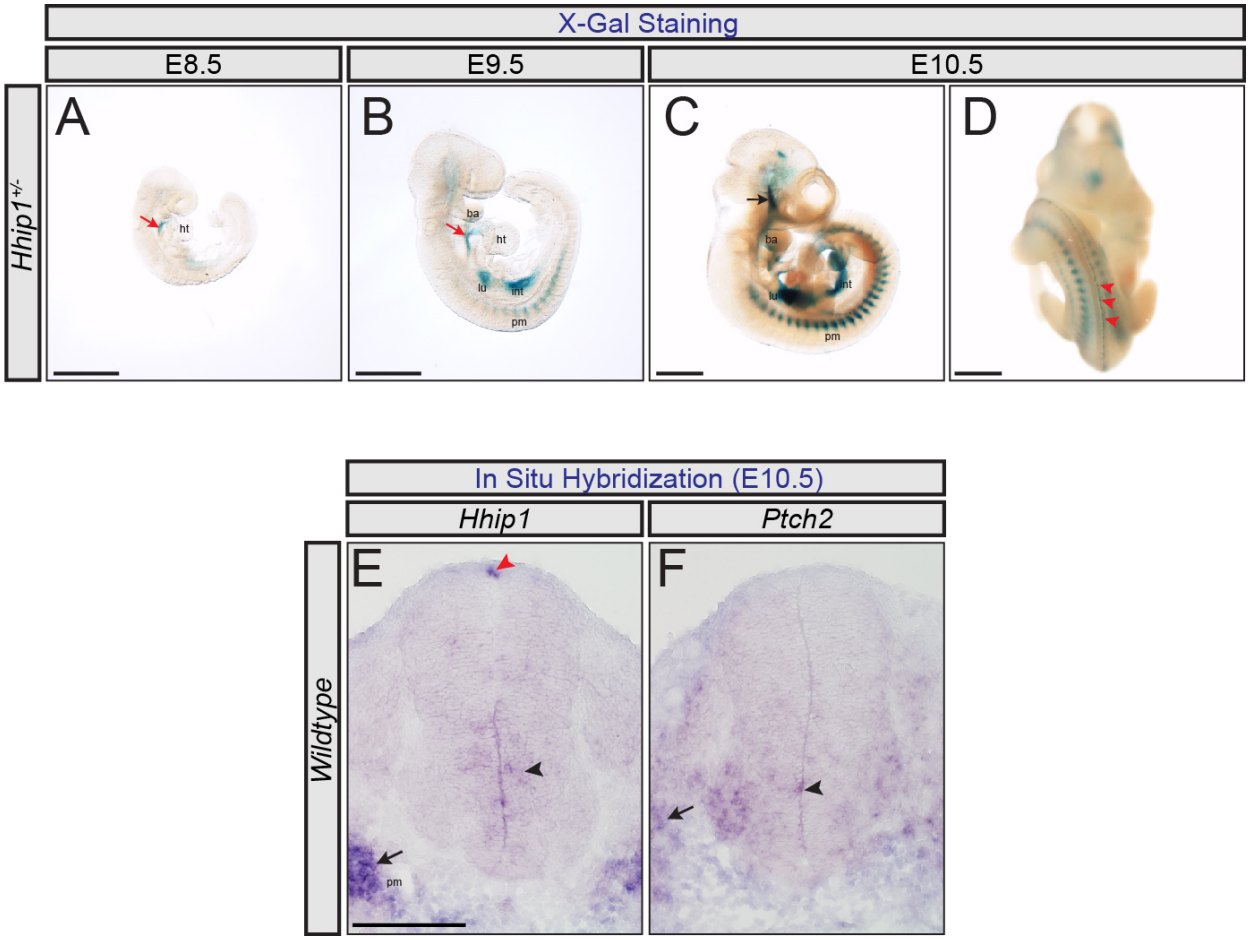


**Figure 3-18. Spatial and temporal analysis of *Hhip1* expression in mouse embryos.** (A-D) Whole mount X-gal staining of *Hhip1*$^{+/-}$ embryos collected at E8.5 (A), E9.5 (B), and E10.5 (C, D). (E, F) RNA in situ hybridization detects expression of *Hhip1* (E) and *Ptch2* (F) transcripts in E10.5 wildtype mouse embryos sectioned at the forelimb level. Red arrows (A, B) indicate *Hhip1* expression in the developing heart and body wall. Black arrow (C) demonstrate reporter expression in the diencephalon. Red arrowheads (D, E) demarcate *Hhip1* expression in the roof plate. Black arrows (E, F) indicate *Hhip1* (G) and *Ptch2* (H) expression in the paraxial mesoderm. ht, heart; ba, branchial arch; lu, lung; int, intestine; pm, paraxial mesoderm. Scale bars (A-D), 1mm. Scale bar (E), 200µm.

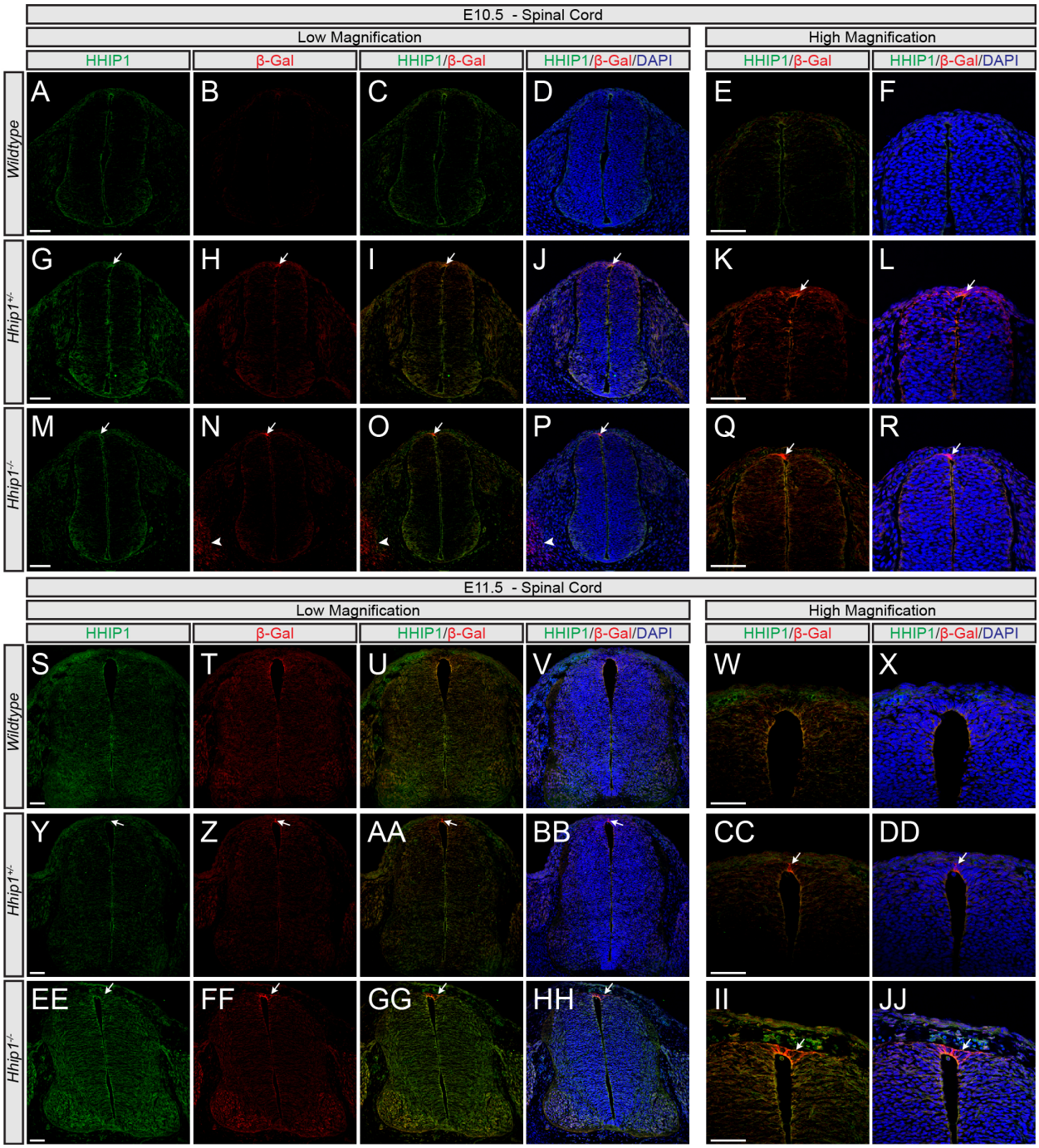


**Figure 3-19. *Hhip1* is expressed in the roof plate of the developing mouse spinal cord.** Mouse embryos isolated at E10.5 (A-R) and E11.5 (S-JJ) sectioned at the forelimb axial level and stained with antibodies to detect HHIP1 (green; A, C-F, G, I-L, M, O-R, S, U-X, Y, AA-DD, EE, GG-JJ) and β-Galactosidase (β-Gal, red; B-F, H-L, N-R, T-X, Z-DD, FF-JJ). DAPI staining reveals nuclei (blue; D, F, J, L, P, R, V, X, BB, DD, HH, JJ). Arrows (G-R, Y-JJ) denote the site of *Hhip1* expression in the roof plate. Arrowheads (N-P) highlight β-Gal expression in the paraxial mesoderm. Scale bars (A, E, G, K, M, Q, S, W, Y, CC, EE, II), 50μm.

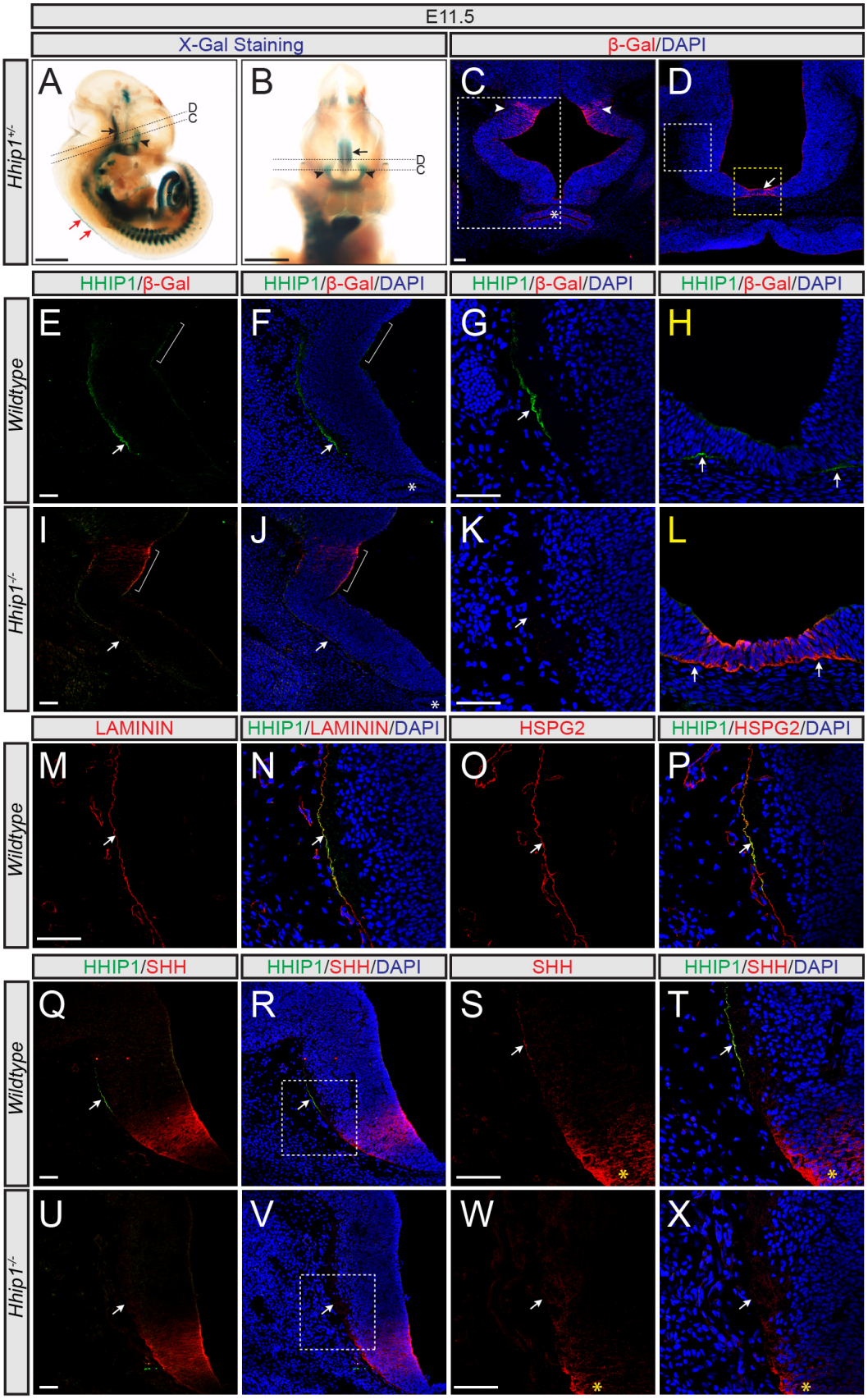
E11.5
X-Gal Staining
β-Gal/DAPI
Hhip1+/-
A
B
C
D
D
C
HHIP1/β-Gal
HHIP1/β-Gal/DAPI
HHIP1/β-Gal/DAPI
HHIP1/β-Gal/DAPI
Wildtype
E
F
G
H
Hhip1-/-
I
J
K
L
LAMININ
HHIP1/LAMININ/DAPI
HSPG2
HHIP1/HSPG2/DAPI
Wildtype
M
N
O
P
HHIP1/SHH
HHIP1/SHH/DAPI
SHH
HHIP1/SHH/DAPI
Wildtype
Q
R
S
T
Hhip1-/-
U
V
W
X

**Figure 3-20. Endogenous HHIP1 protein is secreted and accumulates in the basement membrane of the developing diencephalon.** (A, B) Whole mount X-gal staining of E11.5 *Hhip1*$^{+/-}$ mouse embryos. (C-X) Immunofluorescent detection of β-Galactosidase (β-Gal, red; C-L), HHIP1 (green; E-X), Laminin (red; M, N), HSPG2 (red; O, P), and SHH (red; Q-X) in E11.5 *Hhip1*$^{+/+}$ (E-H, M-P, Q-T), *Hhip1*$^{+/-}$ (C, D), and *Hhip1*$^{-/-}$ (I-L, U-X) mouse embryos sectioned at the axial level of the diencephalon. DAPI reveals nuclei (blue; C, D, F-H, J-L, N, P, R, T, V, X). Arrows (A, B, D) indicate *Hhip1* expression in the ventral diencephalon. Arrowheads (A-C) demarcate HHIP1 production in more dorsal regions of the diencephalon. Dashed lines (A, B) represent axial level of images depicted in C, D. White box (C) corresponds to area analyzed in panels E, F, I, J. White box (D) demonstrates region presented in G, K, M-P, Q-X. Yellow box (D) denotes area analyzed in H, L. Asterisks (C, F, J) demarcates Rathke's pouch. Brackets (E, F, I, J) highlight area of HHIP1 production. Arrows (E-H, M-P, Q-T) depict the presence of HHIP1 protein in the neuroepithelial basement membrane that co-localizes with Laminin (M, N), HSPG2 (O, P), and SHH (Q-T). HHIP1 protein signal is absent in *Hhip1*$^{-/-}$ embryos (arrows, I-L, U-X). Note the accumulation of SHH in the neuroepithelial basement membrane (arrows, S, T) that is absent in *Hhip1*$^{-/-}$ embryos (W, X). White boxes (R, V) demonstrate area of higher magnification presented in S, T, W, X. Yellow asterisks (S, T, W, X) highlight region of SHH production. A commercial HHIP1 antibody (R&D) was used in E-P while a newly developed HHIP1 antibody was used in Q-X. Scale bars (A, B), 1mm. Scale bars (C, E, G, I, K, M, Q, S, U, W), 50μm.

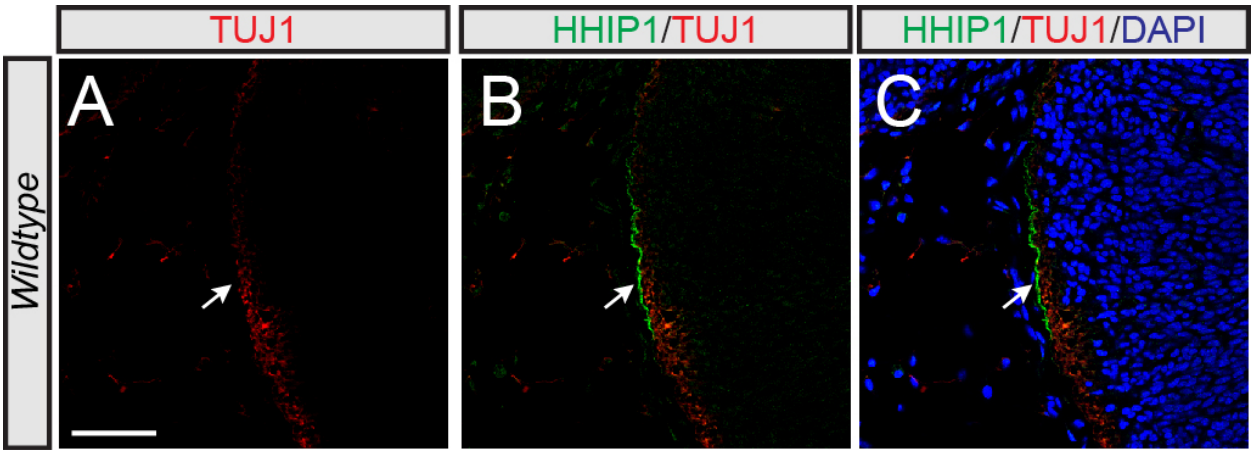


**Figure 3-21. HHIP1 does not co-loclaize with axonal processes.** E11.5 *wildtype* mouse embryos sectioned at the axial level of the diencephalon and stained with antibodies against HHIP1 (green; B, C) and TUJ1 (red; A-C). DAPI labels nuclei (blue; C). Arrows (A-C) demonstrate lack of overlap between HHIP1 and TUJ1. Scale bar (A), 50µm.

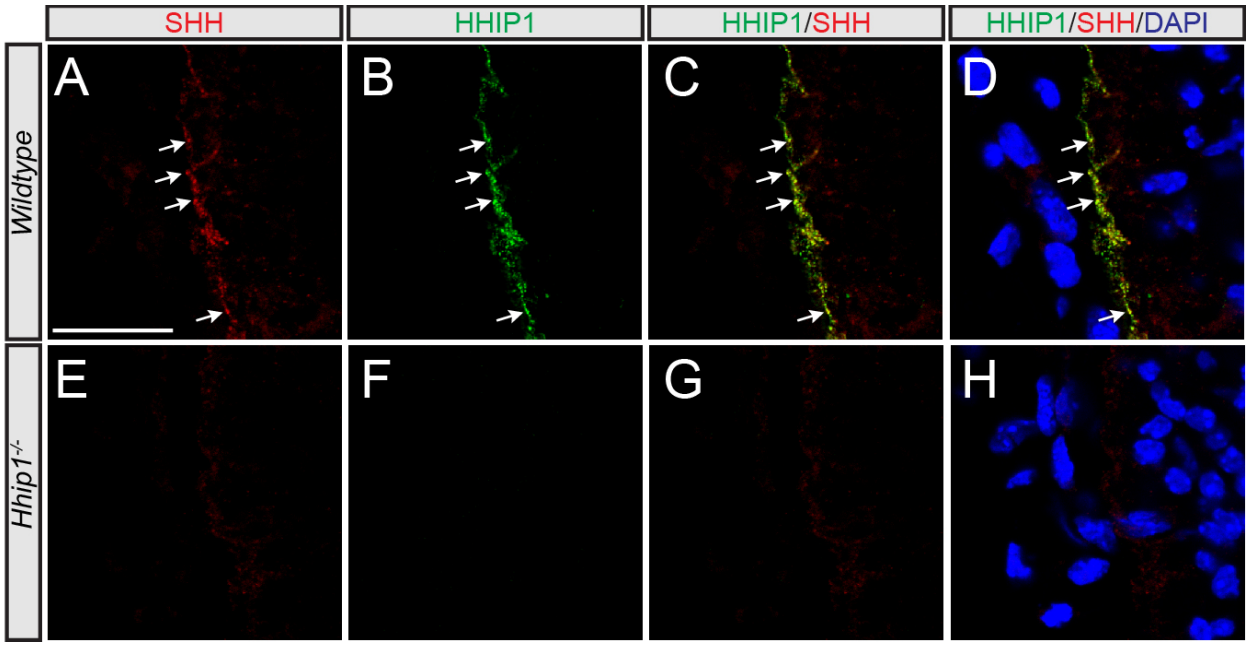


**Figure 3-22. HHIP1 co-localizes with SHH in discrete puncta in the neuroepithelial BM.** Immunofluorescent detection of SHH (red; A, C, D, E, G, H) and HHIP1 (green; B-D, F-H) in the diencephalon of E11.5 *wildtype* (A-D) and *Hhip1*$^{-/-}$ (E-H) mouse embryos. DAPI labels nuclei (blue; D, H). Arrows (A-D) depict co-localization of HHIP1 and SHH in puncta within the neuroepithelial basement membrane. Scale bar (A), 20µm.

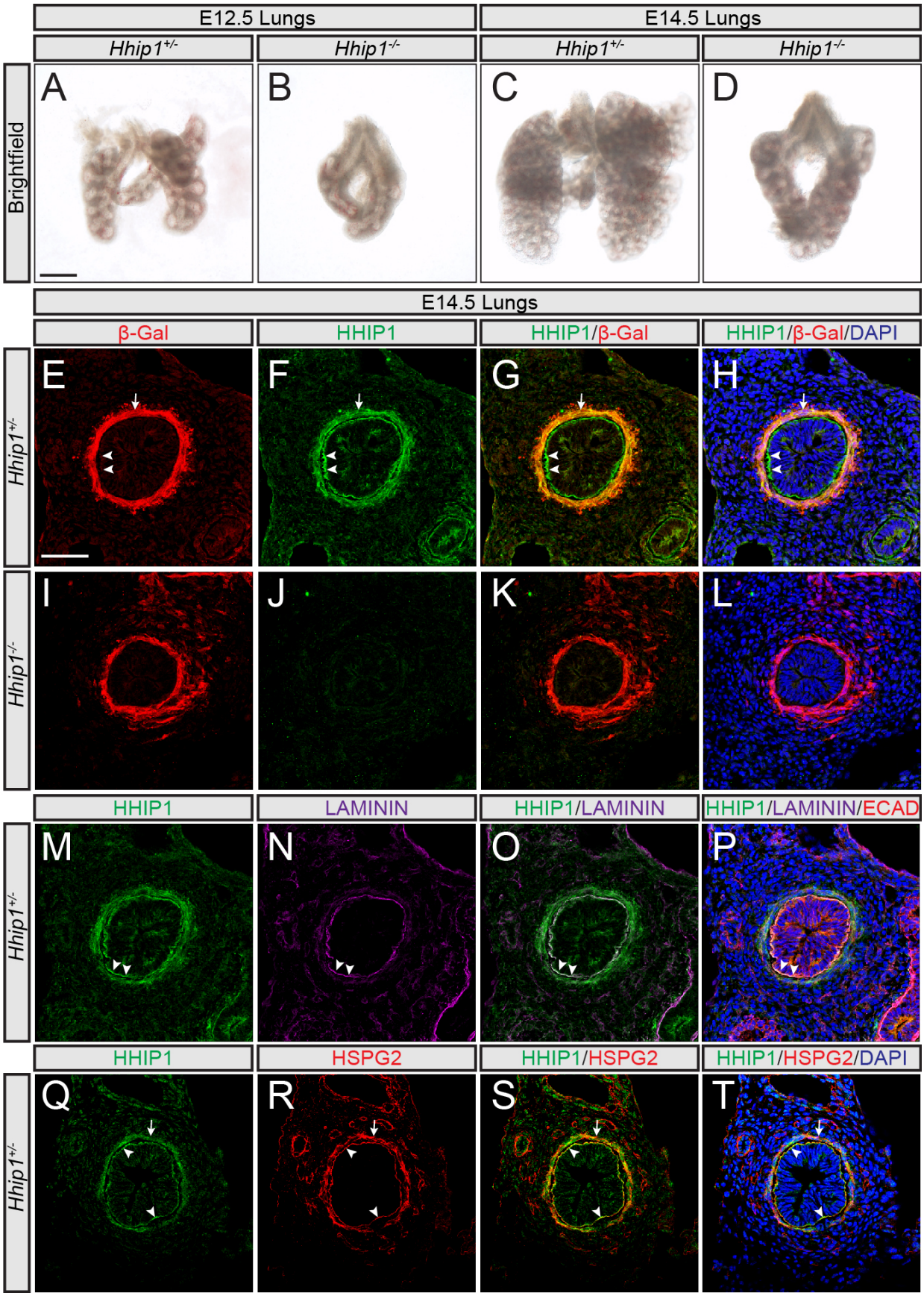
E12.5 Lungs
E14.5 Lungs
Hhip1+/-
Hhip1-/-
Hhip1+/-
Hhip1-/-
Brightfield
A
B
C
D
E14.5 Lungs
β-Gal
HHIP1
HHIP1/β-Gal
HHIP1/β-Gal/DAPI
Hhip1+/-
E
F
G
H
Hhip1-/-
I
J
K
L
HHIP1
LAMININ
HHIP1/LAMININ
HHIP1/LAMININ/ECAD
Hhip1+/-
M
N
O
P
HHIP1
HSPG2
HHIP1/HSPG2
HHIP1/HSPG2/DAPI
Hhip1+/-
Q
R
S
T

**Figure 3-23. Endogenous HHIP1 protein is secreted and accumulates in the epithelial basement membrane in the embryonic lung.** (A-D) Wholemount images of E12.5 (A-B) and E14.5 (C-D) mouse lungs isolated from *Hhip1*$^{+/-}$ (A, C) and *Hhip1*$^{-/-}$ (B, D) embryos. (E-T) Immunofluorescent detection of β-Galactosidase (β-Gal, red; E, G, H, I, K, L), HHIP1 (green; F-H, J-L, M, O, P, Q, S, T), Laminin (magenta; N-P), E-Cadherin (ECAD, red; P), and HSPG2 (red; R-T) in sections isolated from E14.5 *Hhip1*$^{+/-}$ (E-H, M-T) and *Hhip1*$^{-/-}$ (I-L) lungs. DAPI staining reveals nuclei (blue; H, L, P, T). Arrows demonstrate overlap between HHIP1 and β-Gal (E-H) or HSPG2 (Q-T) protein expression in the lung mesenchyme. Arrowheads highlight HHIP1 protein staining in the epithelial basement membrane (E-H, M-T). A commercial HHIP1 antibody (R&D) was used in E-P while a newly developed HHIP1 antibody was used in Q-T. Scale bars (A), 500μm, (E), 50μm.

### 3.8 References


Adolphe, C., E. Nieuwenhuis, R. Villani, Z.J. Li, P. Kaur, C.-C. Hui, and B.J. Wainwright. 2014. Patched 1 and patched 2 redundancy has a key role in regulating epidermal differentiation. *J. Invest. Dermatol.* 134:1981–1990. doi:10.1038/jid.2014.63.

Agren, M., P. Kogerman, M.I. Kleman, M. Wessling, and R. Toftgård. 2004. Expression of the PTCH1 tumor suppressor gene is regulated by alternative promoters and a single functional Gli-binding site. *Gene*. 330:101–114. doi:10.1016/j.gene.2004.01.010.

Alexandre, C., A. Jacinto, and P.W. Ingham. 1996. Transcriptional activation of hedgehog target genes in Drosophila is mediated directly by the cubitus interruptus protein, a member of the GLI family of zinc finger DNA-binding proteins. *Genes & Development*. 10:2003–2013.

Alfaro, A.C., B. Roberts, L. Kwong, M.F. Bijlsma, and H. Roelink. 2014. Ptch2 mediates the Shh response in Ptch1-/- cells. *Development*. 141:3331–3339. doi:10.1242/dev.110056.

Allen, B.L., and A.C. Rapraeger. 2003. Spatial and temporal expression of heparan sulfate in mouse development regulates FGF and FGF receptor assembly. *J. Cell Biol.* 163:637–648. doi:10.1083/jcb.200307053.

Allen, B.L., J.Y. Song, L. Izzi, I.W. Althaus, J.-S. Kang, F. Charron, R.S. Krauss, and A.P. McMahon. 2011. Overlapping roles and collective requirement for the coreceptors GAS1, CDO, and BOC in SHH pathway function. *Dev. Cell*. 20:775–787. doi:10.1016/j.devcel.2011.04.018.

Allen, B.L., T. Tenzen, and A.P. McMahon. 2007. The Hedgehog-binding proteins Gas1 and Cdo cooperate to positively regulate Shh signaling during mouse development. *Genes & Development*. 21:1244–1257. doi:10.1101/gad.1543607.

Aricescu, A.R., W. Lu, and E.Y. Jones. 2006. A time- and cost-efficient system for high-level protein production in mammalian cells. *Acta Crystallogr. D Biol. Crystallogr.* 62:1243–1250. doi:10.1107/S0907444906029799.

Ayers, K.L., A. Gallet, L. Staccini-Lavenant, and P.P. Therond. 2010. The long-range activity of Hedgehog is regulated in the apical extracellular space by the glypican Dally and the hydrolase Notum. *Dev. Cell*. 18:605–620. doi:10.1016/j.devcel.2010.02.015.

Ayers, K.L., R. Mteirek, A. Cervantes, L. Lavenant-Staccini, P.P. Therond, and A. Gallet. 2012. Dally and Notum regulate the switch between low and high level Hedgehog pathway signalling. *Development*. 139:3168–3179. doi:10.1242/dev.078402.

Baker, N.A., D. Sept, S. Joseph, M.J. Holst, and J.A. McCammon. 2001. Electrostatics of nanosystems: application to microtubules and the ribosome. *Proceedings of the National Academy of Sciences of the United States of America*. 98:10037–10041. doi:10.1073/pnas.181342398.

Beachy, P.A., S.G. Hymowitz, R.A. Lazarus, D.J. Leahy, and C. Siebold. 2010. Interactions

between Hedgehog proteins and their binding partners come into view. *Genes & Development*. 24:2001–2012. doi:10.1101/gad.1951710.

Bellaiche, Y., I. The, and N. Perrimon. 1998. Tout-velu is a Drosophila homologue of the putative tumour suppressor EXT-1 and is needed for Hh diffusion. *Nature*. 394:85–88. doi:10.1038/27932.

Bellusci, S., J. Grindley, H. Emoto, N. Itoh, and B.L. Hogan. 1997a. Fibroblast growth factor 10 (FGF10) and branching morphogenesis in the embryonic mouse lung. *Development*. 124:4867–4878.

Bellusci, S., Y. Furuta, M.G. Rush, R. Henderson, G. Winnier, and B.L. Hogan. 1997b. Involvement of Sonic hedgehog (Shh) in mouse embryonic lung growth and morphogenesis. *Development*. 124:53–63.

Bishop, B., A.R. Aricescu, K. Harlos, C.A. O'Callaghan, E.Y. Jones, and C. Siebold. 2009. Structural insights into hedgehog ligand sequestration by the human hedgehog-interacting protein HHIP. *Nature Publishing Group*. 16:698–703. doi:10.1038/nsmb.1607.

Bitgood, M.J., and A.P. McMahon. 1995. Hedgehog and Bmp genes are coexpressed at many diverse sites of cell-cell interaction in the mouse embryo. *Developmental Biology*. 172:126–138. doi:10.1006/dbio.1995.0010.

Bosanac, I., H.R. Maun, S.J. Scales, X. Wen, A. Lingel, J.F. Bazan, F.J. de Sauvage, S.G. Hymowitz, and R.A. Lazarus. 2009. The structure of SHH in complex with HHIP reveals a recognition role for the Shh pseudo active site in signaling. *Nature Publishing Group*. 16:691–697. doi:10.1038/nsmb.1632.

Bouwmeester, T., S. Kim, Y. Sasai, B. Lu, and E.M. De Robertis. 1996. Cerberus is a head-inducing secreted factor expressed in the anterior endoderm of Spemann's organizer. *Nature*. 382:595–601. doi:10.1038/382595a0.

Briscoe, J., Y. Chen, T.M. Jessell, and G. Struhl. 2001. A hedgehog-insensitive form of patched provides evidence for direct long-range morphogen activity of sonic hedgehog in the neural tube. *Mol. Cell*. 7:1279–1291.

Carpenter, D., D.M. Stone, J. Brush, A. Ryan, M. Armanini, G. Frantz, A. Rosenthal, and F.J. de Sauvage. 1998. Characterization of two patched receptors for the vertebrate hedgehog protein family. *Proceedings of the National Academy of Sciences of the United States of America*. 95:13630–13634.

Castaldi, P.J., M.H. Cho, R.S.J. Estépar, M.-L.N. McDonald, N. Laird, T.H. Beaty, G. Washko, J.D. Crapo, E.K. Silverman, on behalf of the COPDGene Investigators. 2014. Genome-Wide Association Identifies Regulatory Loci Associated with Distinct Local Histogram Emphysema Patterns. *Am. J. Respir. Crit. Care Med.* doi:10.1164/rccm.201403-0569OC.

Cayuso, J., F. Ulloa, B. Cox, J. Briscoe, and E. Martí. 2006. The Sonic hedgehog pathway independently controls the patterning, proliferation and survival of neuroepithelial cells by

regulating Gli activity. *Development*. 133:517–528. doi:10.1242/dev.02228.

Chamberlain, C.E., J. Jeong, C. Guo, B.L. Allen, and A.P. McMahon. 2008. Notochord-derived Shh concentrates in close association with the apically positioned basal body in neural target cells and forms a dynamic gradient during neural patterning. *Development*. 135:1097–1106. doi:10.1242/dev.013086.

Chan, J.A., S. Balasubramanian, R.M. Witt, K.J. Nazemi, Y. Choi, M.F. Pazyra-Murphy, C.O. Walsh, M. Thompson, and R.A. Segal. 2009. Proteoglycan interactions with Sonic Hedgehog specify mitogenic responses. *Nat. Neurosci.* 12:409–417. doi:10.1038/nn.2287.

Chang, V.T., M. Crispin, A.R. Aricescu, D.J. Harvey, J.E. Nettleship, J.A. Fennelly, C. Yu, K.S. Boles, E.J. Evans, D.I. Stuart, R.A. Dwek, E.Y. Jones, R.J. Owens, and S.J. Davis. 2007. Glycoprotein structural genomics: solving the glycosylation problem. *Structure*. 15:267–273. doi:10.1016/j.str.2007.01.011.

Charrier, J.B., F. Lapointe, N.M. Le Douarin, and M.A. Teillet. 2001. Anti-apoptotic role of Sonic hedgehog protein at the early stages of nervous system organogenesis. *Development*. 128:4011–4020.

Chen, C., and M.M. Shen. 2004. Two modes by which Lefty proteins inhibit nodal signaling. *Current Biology*. 14:618–624. doi:10.1016/j.cub.2004.02.042.

Chen, C.H., D.P. von Kessler, W. Park, B. Wang, Y. Ma, and P.A. Beachy. 1999. Nuclear trafficking of Cubitus interruptus in the transcriptional regulation of Hedgehog target gene expression. *Cell*. 98:305–316.

Chen, Y., and G. Struhl. 1996. Dual roles for patched in sequestering and transducing Hedgehog. *Cell*. 87:553–563.

Chuang, P.T. 2003. Feedback control of mammalian Hedgehog signaling by the Hedgehog-binding protein, Hip1, modulates Fgf signaling during branching morphogenesis of the lung. *Genes & Development*. 17:342–347. doi:10.1101/gad.1026303.

Chuang, P.T., and A.P. McMahon. 1999. Vertebrate Hedgehog signalling modulated by induction of a Hedgehog-binding protein. *Nature*. 397:617–621. doi:10.1038/17611.

Cornesse, Y., T. Pieler, and T. Hollemann. 2005. Olfactory and lens placode formation is controlled by the hedgehog-interacting protein (Xhip) in Xenopus. *Developmental Biology*. 277:296–315. doi:10.1016/j.ydbio.2004.09.016.

Coulombe, J., E. Traiffort, K. Loulier, H. Faure, and M. Ruat. 2004. Hedgehog interacting protein in the mature brain: membrane-associated and soluble forms. *Molecular and Cellular Neuroscience*. 25:323–333. doi:10.1016/j.mcn.2003.10.024.

Cruciat, C.-M., and C. Niehrs. 2013. Secreted and transmembrane wnt inhibitors and activators. *Cold Spring Harb Perspect Biol*. 5:a015081. doi:10.1101/cshperspect.a015081.

Dale, J.K., C. Vesque, T.J. Lints, T.K. Sampath, A. Furley, J. Dodd, and M. Placzek. 1997. Cooperation of BMP7 and SHH in the induction of forebrain ventral midline cells by prechordal mesoderm. *Cell*. 90:257–269.

Danesin, C., E. Agius, N. Escalas, X. Ai, C. Emerson, P. Cochard, and C. Soula. 2006. Ventral neural progenitors switch toward an oligodendroglial fate in response to increased Sonic hedgehog (Shh) activity: involvement of Sulfatase 1 in modulating Shh signaling in the ventral spinal cord. *J. Neurosci.* 26:5037–5048. doi:10.1523/JNEUROSCI.0715-06.2006.

Desbordes, S.C., and B. Sanson. 2003. The glypican Dally-like is required for Hedgehog signalling in the embryonic epidermis of Drosophila. *Development*. 130:6245–6255. doi:10.1242/dev.00874.

Dessaud, E., L.L. Yang, K. Hill, B. Cox, F. Ulloa, A. Ribeiro, A. Mynett, B.G. Novitch, and J. Briscoe. 2007. Interpretation of the sonic hedgehog morphogen gradient by a temporal adaptation mechanism. *Nature*. 450:717–720. doi:10.1038/nature06347.

Dierker, T., R. Dreier, A. Petersen, C. Bordych, and K. Grobe. 2009. Heparan sulfate-modulated, metalloprotease-mediated sonic hedgehog release from producing cells. *J. Biol. Chem.* 284:8013–8022. doi:10.1074/jbc.M806838200.

Ericson, J., J. Muhr, M. Placzek, T. Lints, T.M. Jessell, and T. Edlund. 1995. Sonic hedgehog induces the differentiation of ventral forebrain neurons: a common signal for ventral patterning within the neural tube. *Cell*. 81:747–756.

Ericson, J., P. Rashbass, A. Schedl, S. Brenner-Morton, A. Kawakami, V. van Heyningen, T.M. Jessell, and J. Briscoe. 1997. Pax6 controls progenitor cell identity and neuronal fate in response to graded Shh signaling. *Cell*. 90:169–180.

Esko, J.D., and U. Lindahl. 2001. Molecular diversity of heparan sulfate. *J. Clin. Invest.* 108:169–173. doi:10.1172/JCI13530.

Forbes, A.J., Y. Nakano, A.M. Taylor, and P.W. Ingham. 1993. Genetic analysis of hedgehog signalling in the Drosophila embryo. *Dev. Suppl.* 115–124.

Gallet, A., R. Rodriguez, L. Ruel, and P.P. Therond. 2003. Cholesterol modification of hedgehog is required for trafficking and movement, revealing an asymmetric cellular response to hedgehog. *Dev. Cell*. 4:191–204.

Goodrich, L.V., R.L. Johnson, L. Milenkovic, J.A. McMahon, and M.P. Scott. 1996. Conservation of the hedgehog/patched signaling pathway from flies to mice: induction of a mouse patched gene by Hedgehog. *Genes & Development*. 10:301–312.

Gritli-Linde, A., P. Lewis, A.P. McMahon, and A. Linde. 2001. The whereabouts of a morphogen: direct evidence for short- and graded long-range activity of hedgehog signaling peptides. *Developmental Biology*. 236:364–386. doi:10.1006/dbio.2001.0336.

Han, C., T.Y. Belenkaya, B. Wang, and X. Lin. 2004. Drosophila glypicans control the cell-to-

cell movement of Hedgehog by a dynamin-independent process. *Development*. 131:601–611. doi:10.1242/dev.00958.

Häcker, U., K. Nybakken, and N. Perrimon. 2005. Heparan sulphate proteoglycans: the sweet side of development. *Nat. Rev. Mol. Cell Biol.* 6:530–541. doi:10.1038/nrm1681.

Holtz, A.M., K.A. Peterson, Y. Nishi, S. Morin, J.Y. Song, F. Charron, A.P. McMahon, and B.L. Allen. 2013. Essential role for ligand-dependent feedback antagonism of vertebrate hedgehog signaling by PTCH1, PTCH2 and HHIP1 during neural patterning. *Development*. 140:3423–3434. doi:10.1242/dev.095083.

Hsieh, J.C., L. Kodjabachian, M.L. Rebbert, A. Rattner, P.M. Smallwood, C.H. Samos, R. Nusse, I.B. Dawid, and J. Nathans. 1999. A new secreted protein that binds to Wnt proteins and inhibits their activities. *Nature*. 398:431–436. doi:10.1038/18899.

Ishibashi, M., and A.P. McMahon. 2002. A sonic hedgehog-dependent signaling relay regulates growth of diencephalic and mesencephalic primordia in the early mouse embryo. *Development*. 129:4807–4819.

Jeong, J., and A.P. McMahon. 2005. Growth and pattern of the mammalian neural tube are governed by partially overlapping feedback activities of the hedgehog antagonists patched 1 and Hhip1. *Development*. 132:143–154. doi:10.1242/dev.01566.

Karlsson, M., and S. Björnsson. 2001. Quantitation of proteoglycans in biological fluids using Alcian blue. *Methods Mol. Biol.* 171:159–173. doi:10.1385/1-59259-209-0:159.

Kawahira, H., N.H. Ma, E.S. Tzanakakis, A.P. McMahon, P.-T. Chuang, and M. Hebrok. 2003. Combined activities of hedgehog signaling inhibitors regulate pancreas development. *Development*. 130:4871–4879. doi:10.1242/dev.00653.

Koudijs, M.J., M.J. den Broeder, A. Keijser, E. Wienholds, S. Houwing, E.M.H.C. van Rooijen, R. Geisler, and F.J.M. van Eeden. 2005. The zebrafish mutants dre, uki, and lep encode negative regulators of the hedgehog signaling pathway. *PLoS Genet.* 1:e19. doi:10.1371/journal.pgen.0010019.

Koudijs, M.J., M.J. den Broeder, E. Groot, and F.J. van Eeden. 2008. Genetic analysis of the two zebrafish patched homologues identifies novel roles for the hedgehog signaling pathway. *BMC Developmental Biology*. 8:15. doi:10.1186/1471-213X-8-15.

Kwong, L., M.F. Bijlsma, and H. Roelink. 2014. Shh-mediated degradation of Hhip allows cell autonomous and non-cell autonomous Shh signalling. *Nat Commun*. 5:4849. doi:10.1038/ncomms5849.

Leyns, L., T. Bouwmeester, S.H. Kim, S. Piccolo, and E.M. De Robertis. 1997. Frzb-1 is a secreted antagonist of Wnt signaling expressed in the Spemann organizer. *Cell*. 88:747–756.

Li, X., T.D. Howard, W.C. Moore, E.J. Ampleford, H. Li, W.W. Busse, W.J. Calhoun, M. Castro, K.F. Chung, S.C. Erzurum, A.M. Fitzpatrick, B. Gaston, E. Israel, N.N. Jarjour, W.G.

Teague, S.E. Wenzel, S.P. Peters, G.A. Hawkins, E.R. Bleecker, and D.A. Meyers. 2011. Importance of hedgehog interacting protein and other lung function genes in asthma. *J. Allergy Clin. Immunol.* 127:1457–1465. doi:10.1016/j.jaci.2011.01.056.

Liem, K.F., T.M. Jessell, and J. Briscoe. 2000. Regulation of the neural patterning activity of sonic hedgehog by secreted BMP inhibitors expressed by notochord and somites. *Development*. 127:4855–4866.

Lin, X. 2004. Functions of heparan sulfate proteoglycans in cell signaling during development. *Development*. 131:6009–6021. doi:10.1242/dev.01522.

Litingtung, Y., L. Lei, H. Westphal, and C. Chiang. 1998. Sonic hedgehog is essential to foregut development. *Nat Genet*. 20:58–61. doi:10.1038/1717.

Lum, L., S. Yao, B. Mozer, A. Rovescalli, D. Von Kessler, M. Nirenberg, and P.A. Beachy. 2003. Identification of Hedgehog pathway components by RNAi in Drosophila cultured cells. *Science*. 299:2039–2045. doi:10.1126/science.1081403.

Maddon, P.J., D.R. Littman, M. Godfrey, D.E. Maddon, L. Chess, and R. Axel. 1985. The isolation and nucleotide sequence of a cDNA encoding the T cell surface protein T4: a new member of the immunoglobulin gene family. *Cell*. 42:93–104.

Malinauskas, T., A.R. Aricescu, W. Lu, C. Siebold, and E.Y. Jones. 2011. Modular mechanism of Wnt signaling inhibition by Wnt inhibitory factor 1. *Nature Publishing Group*. 18:886–893. doi:10.1038/nsmb.2081.

Marigo, V., R.A. Davey, Y. Zuo, J.M. Cunningham, and C.J. Tabin. 1996. Biochemical evidence that patched is the Hedgehog receptor. *Nature*. 384:176–179. doi:10.1038/384176a0.

Martí, E., D.A. Bumcrot, R. Takada, and A.P. McMahon. 1995. Requirement of 19K form of Sonic hedgehog for induction of distinct ventral cell types in CNS explants. *Nature*. 375:322–325. doi:10.1038/375322a0.

McMahon, A.P., P.W. Ingham, and C.J. Tabin. 2003. Developmental roles and clinical significance of hedgehog signaling. *Curr. Top. Dev. Biol.* 53:1–114.

McMahon, J.A., S. Takada, L.B. Zimmerman, C.M. Fan, R.M. Harland, and A.P. McMahon. 1998. Noggin-mediated antagonism of BMP signaling is required for growth and patterning of the neural tube and somite. *Genes & Development*. 12:1438–1452.

Meno, C., Y. Saijoh, H. Fujii, M. Ikeda, T. Yokoyama, M. Yokoyama, Y. Toyoda, and H. Hamada. 1996. Left-right asymmetric expression of the TGF beta-family member lefty in mouse embryos. *Nature*. 381:151–155. doi:10.1038/381151a0.

Milenkovic, L., L.V. Goodrich, K.M. Higgins, and M.P. Scott. 1999. Mouse patched1 controls body size determination and limb patterning. *Development*. 126:4431–4440.

Min, H., D.M. Danilenko, S.A. Scully, B. Bolon, B.D. Ring, J.E. Tarpley, M. DeRose, and W.S.

Simonet. 1998. Fgf-10 is required for both limb and lung development and exhibits striking functional similarity to Drosophila branchless. *Genes & Development*. 12:3156–3161.

Motoyama, J., T. Takabatake, K. Takeshima, and C.-C. Hui. 1998. Ptch2, a second mouse Patched gene is co-expressed with Sonic hedgehog. *Nat Genet*. 18:104–106. doi:10.1038/ng0298-104.

Nieuwenhuis, E., J. Motoyama, P.C. Barnfield, Y. Yoshikawa, X. Zhang, R. Mo, M.A. Crackower, and C.-C. Hui. 2006. Mice with a targeted mutation of patched2 are viable but develop alopecia and epidermal hyperplasia. *Mol. Cell. Biol.* 26:6609–6622. doi:10.1128/MCB.00295-06.

Nybakken, K., S.A. Vokes, T.-Y. Lin, A.P. McMahon, and N. Perrimon. 2005. A genome-wide RNA interference screen in Drosophila melanogaster cells for new components of the Hh signaling pathway. *Nat Genet*. 37:1323–1332. doi:10.1038/ng1682.

Ohlig, S., U. Pickhinke, S. Sirko, S. Bandari, D. Hoffmann, R. Dreier, P. Farshi, M. Götz, and K. Grobe. 2012. An emerging role of Sonic hedgehog shedding as a modulator of heparan sulfate interactions. *J. Biol. Chem.* 287:43708–43719. doi:10.1074/jbc.M112.356667.

Oustah, A.A., C. Danesin, N. Khouri-Farah, M.-A. Farreny, N. Escalas, P. Cochard, B. Glise, and C. Soula. 2014. Dynamics of Sonic hedgehog signaling in the ventral spinal cord are controlled by intrinsic changes in source cells requiring Sulfatase 1. *Development*. 141:1392–1403. doi:10.1242/dev.101717.

Park, Y., C. Rangel, M.M. Reynolds, M.C. Caldwell, M. Johns, M. Nayak, C.J.R. Welsh, S. McDermott, and S. Datta. 2003. Drosophila perlecan modulates FGF and hedgehog signals to activate neural stem cell division. *Developmental Biology*. 253:247–257.

Pathi, S., S. Pagan-Westphal, D.P. Baker, E.A. Garber, P. Rayhorn, D. Bumcrot, C.J. Tabin, R. Blake Pepinsky, and K.P. Williams. 2001. Comparative biological responses to human Sonic, Indian, and Desert hedgehog. *Mech. Dev.* 106:107–117.

Pepicelli, C.V., P.M. Lewis, and A.P. McMahon. 1998. Sonic hedgehog regulates branching morphogenesis in the mammalian lung. *Current Biology*. 8:1083–1086.

Perrimon, N., and M. Bernfield. 2000. Specificities of heparan sulphate proteoglycans in developmental processes. *Nature*. 404:725–728. doi:10.1038/35008000.

Piccolo, S., E. Agius, L. Leyns, S. Bhattacharyya, H. Grunz, T. Bouwmeester, and E.M. De Robertis. 1999. The head inducer Cerberus is a multifunctional antagonist of Nodal, BMP and Wnt signals. *Nature*. 397:707–710. doi:10.1038/17820.

Piccolo, S., Y. Sasai, B. Lu, and E.M. De Robertis. 1996. Dorsoventral patterning in Xenopus: inhibition of ventral signals by direct binding of chordin to BMP-4. *Cell*. 86:589–598.

Pillai, S.G., D. Ge, G. Zhu, X. Kong, K.V. Shianna, A.C. Need, S. Feng, C.P. Hersh, P. Bakke, A. Gulsvik, A. Ruppert, K.C. Lødrup Carlsen, A. Roses, W. Anderson, S.I. Rennard, D.A.

Lomas, E.K. Silverman, D.B. Goldstein, ICGN Investigators. 2009. A genome-wide association study in chronic obstructive pulmonary disease (COPD): identification of two major susceptibility loci. *PLoS Genet.* 5:e1000421. doi:10.1371/journal.pgen.1000421.

Raman, S., R. Vernon, J. Thompson, M. Tyka, R. Sadreyev, J. Pei, D. Kim, E. Kellogg, F. DiMaio, O. Lange, L. Kinch, W. Sheffler, B.-H. Kim, R. Das, N.V. Grishin, and D. Baker. 2009. Structure prediction for CASP8 with all-atom refinement using Rosetta. *Proteins*. 77 Suppl 9:89–99. doi:10.1002/prot.22540.

Roessler, E., Y.-Z. Du, J.L. Mullor, E. Casas, W.P. Allen, G. Gillessen-Kaesbach, E.R. Roeder, J.E. Ming, A. Ruiz i Altaba, and M. Muenke. 2003. Loss-of-function mutations in the human GLI2 gene are associated with pituitary anomalies and holoprosencephaly-like features. *Proceedings of the National Academy of Sciences of the United States of America*. 100:13424–13429. doi:10.1073/pnas.2235734100.

Rubin, J.B., Y. Choi, and R.A. Segal. 2002. Cerebellar proteoglycans regulate sonic hedgehog responses during development. *Development*. 129:2223–2232.

Saade, M., I. Gutiérrez-Vallejo, G. Le Dréau, M.A. Rabadán, D.G. Miguez, J. Buceta, and E. Martí. 2013. Sonic Hedgehog Signaling Switches the Mode of Division in the Developing Nervous System. *Cell Rep*. doi:10.1016/j.celrep.2013.06.038.

Sekine, K., H. Ohuchi, M. Fujiwara, M. Yamasaki, T. Yoshizawa, T. Sato, N. Yagishita, D. Matsui, Y. Koga, N. Itoh, and S. Kato. 1999. Fgf10 is essential for limb and lung formation. *Nat Genet*. 21:138–141. doi:10.1038/5096.

Smith, W.C., A.K. Knecht, M. Wu, and R.M. Harland. 1993. Secreted noggin protein mimics the Spemann organizer in dorsalizing Xenopus mesoderm. *Nature*. 361:547–549. doi:10.1038/361547a0.

Smith, W.C., and R.M. Harland. 1992. Expression cloning of noggin, a new dorsalizing factor localized to the Spemann organizer in Xenopus embryos. *Cell*. 70:829–840.

Stone, D.M., M. Hynes, M. Armanini, T.A. Swanson, Q. Gu, R.L. Johnson, M.P. Scott, D. Pennica, A. Goddard, H. Phillips, M. Noll, J.E. Hooper, F. de Sauvage, and A. Rosenthal. 1996. The tumour-suppressor gene patched encodes a candidate receptor for Sonic hedgehog. *Nature*. 384:129–134. doi:10.1038/384129a0.

Szabó, N.-E., T. Zhao, M. Cankaya, T. Theil, X. Zhou, and G. Álvarez-Bolado. 2009. Role of neuroepithelial Sonic hedgehog in hypothalamic patterning. *J. Neurosci.* 29:6989–7002. doi:10.1523/JNEUROSCI.1089-09.2009.

Tenzen, T., B.L. Allen, F. Cole, J.-S. Kang, R.S. Krauss, and A.P. McMahon. 2006. The cell surface membrane proteins Cdo and Boc are components and targets of the Hedgehog signaling pathway and feedback network in mice. *Dev. Cell*. 10:647–656. doi:10.1016/j.devcel.2006.04.004.

The, I., Y. Bellaiche, and N. Perrimon. 1999. Hedgehog movement is regulated through tout

velu-dependent synthesis of a heparan sulfate proteoglycan. *Mol. Cell*. 4:633–639.

Thibert, C., M.-A. Teillet, F. Lapointe, L. Mazelin, N.M. Le Douarin, and P. Mehlen. 2003. Inhibition of neuroepithelial patched-induced apoptosis by sonic hedgehog. *Science*. 301:843–846. doi:10.1126/science.1085405.

Touahri, Y., N. Escalas, B. Benazeraf, P. Cochard, C. Danesin, and C. Soula. 2012. Sulfatase 1 promotes the motor neuron-to-oligodendrocyte fate switch by activating Shh signaling in Olig2 progenitors of the embryonic ventral spinal cord. *J. Neurosci.* 32:18018–18034. doi:10.1523/JNEUROSCI.3553-12.2012.

Treier, M., S. O'Connell, A. Gleiberman, J. Price, D.P. Szeto, R. Burgess, P.T. Chuang, A.P. McMahon, and M.G. Rosenfeld. 2001. Hedgehog signaling is required for pituitary gland development. *Development*. 128:377–386.

Urase, K., T. Mukasa, H. Igarashi, Y. Ishii, S. Yasugi, M.Y. Momoi, and T. Momoi. 1996. Spatial expression of Sonic hedgehog in the lung epithelium during branching morphogenesis. *Biochem. Biophys. Res. Commun.* 225:161–166. doi:10.1006/bbrc.1996.1147.

Van Durme, Y.M.T.A., M. Eijgelsheim, G.F. Joos, A. Hofman, A.G. Uitterlinden, G.G. Brusselle, and B.H.C. Stricker. 2010. Hedgehog-interacting protein is a COPD susceptibility gene: the Rotterdam Study. *Eur. Respir. J.* 36:89–95. doi:10.1183/09031936.00129509.

Vokes, S.A., H. Ji, S. McCuine, T. Tenzen, S. Giles, S. Zhong, W.J.R. Longabaugh, E.H. Davidson, W.H. Wong, and A.P. McMahon. 2007. Genomic characterization of Gli-activator targets in sonic hedgehog-mediated neural patterning. *Development*. 134:1977–1989. doi:10.1242/dev.001966.

Wang, S., M. Krinks, K. Lin, F.P. Luyten, and M. Moos. 1997. Frzb, a secreted protein expressed in the Spemann organizer, binds and inhibits Wnt-8. *Cell*. 88:757–766.

Whalen, D.M., T. Malinauskas, R.J.C. Gilbert, and C. Siebold. 2013. Structural insights into proteoglycan-shaped Hedgehog signaling. *Proceedings of the National Academy of Sciences of the United States of America*. doi:10.1073/pnas.1310097110.

Witt, R.M., M.-L. Hecht, M.F. Pazyra-Murphy, S.M. Cohen, C. Noti, T.H. van Kuppevelt, M. Fuller, J.A. Chan, J.J. Hopwood, P.H. Seeberger, and R.A. Segal. 2013. Heparan sulfate proteoglycans containing a glypican 5 core and 2-O-sulfo-iduronic acid function as Sonic Hedgehog co-receptors to promote proliferation. *J. Biol. Chem.* 288:26275–26288. doi:10.1074/jbc.M112.438937.

Xie, J., M. Murone, S.M. Luoh, A. Ryan, Q. Gu, C. Zhang, J.M. Bonifas, C.W. Lam, M. Hynes, A. Goddard, A. Rosenthal, E.H. Epstein, and F.J. de Sauvage. 1998. Activating Smoothened mutations in sporadic basal-cell carcinoma. *Nature*. 391:90–92. doi:10.1038/34201.

Yan, D., and X. Lin. 2009. Shaping morphogen gradients by proteoglycans. *Cold Spring Harb Perspect Biol*. 1:a002493. doi:10.1101/cshperspect.a002493.

Young, R.P., C.F. Whittington, R.J. Hopkins, B.A. Hay, M.J. Epton, P.N. Black, and G.D. Gamble. 2010. Chromosome 4q31 locus in COPD is also associated with lung cancer. *Eur. Respir. J.* 36:1375–1382. doi:10.1183/09031936.00033310.

Zhao, L., S.E. Zevallos, K. Rizzoti, Y. Jeong, R. Lovell-Badge, and D.J. Epstein. 2012. Disruption of SoxB1-Dependent Sonic hedgehog Expression in the HypothalamusCauses Septo-optic Dysplasia. *Dev. Cell*. 22:585–596. doi:10.1016/j.devcel.2011.12.023.

Zhao, Y., B. Bishop, J.E. Clay, W. Lu, M. Jones, S. Daenke, C. Siebold, D.I. Stuart, E.Y. Jones, and A.R. Aricescu. 2011. Automation of large scale transient protein expression in mammalian cells. *J. Struct. Biol.* 175:209–215. doi:10.1016/j.jsb.2011.04.017.

Zhou, X., R.M. Baron, M. Hardin, M.H. Cho, J. Zielinski, I. Hawrylkiewicz, P. Sliwinski, C.P. Hersh, J.D. Mancini, K. Lu, D. Thibault, A.L. Donahue, B.J. Klanderman, B. Rosner, B.A. Raby, Q. Lu, A.M. Geldart, M.D. Layne, M.A. Perrella, S.T. Weiss, A.M.K. Choi, and E.K. Silverman. 2012. Identification of a chronic obstructive pulmonary disease genetic determinant that regulates HHIP. *Hum Mol Genet*. 21:1325–1335. doi:10.1093/hmg/ddr569.

Zimmerman, L.B., J.M. De Jesús-Escobar, and R.M. Harland. 1996. The Spemann organizer signal noggin binds and inactivates bone morphogenetic protein 4. *Cell*. 86:599–606.

# CHAPTER IV:

## Discussion and Future Directions

### 4.1 A Collective Requirement for PTCH2-, HHIP1-, and PTCH1-Feedback Inhibition During Vertebrate Embryogenesis

#### 4.1.1 Summary of Key Findings

Data presented in Chapter II demonstrate that PTCH2 plays overlapping roles with PTCH1 and HHIP1 to antagonize HH signaling during vertebrate development. Importantly, recent reports support these findings in other experimental systems. In one study, neuralized embryoid bodies (NEBs) generated from *Ptch1*$^{-/-}$;*Ptch2*$^{-/-}$ embryonic stem cells (ESCs) demonstrated greater HH pathway activation than NEBs produced from *Ptch1*$^{-/-}$ ESCs (Alfaro et al., 2014). Overlapping roles for PTCH2 and PTCH1 were also recently demonstrated in the context of skin development and tumorigenesis. In mouse models with conditional inactivation of *Ptch1* (*Ptch1*$^{f/f}$) in the skin using a *K14-Cre* or a *K5-Cre* transgene, further loss of *Ptch2* lead to more severe defects in hair follicle (HF) morphogenesis and epidermal differentiation than conditional deletion of *Ptch1* alone (Adolphe et al., 2014). Moreover, *K14-CreER*$^{T2}$*;Ptch1*$^{f/f}$*;Ptch2*$^{-/-}$ adult animals treated with tamoxifen to delete *Ptch1* in the skin developed more advanced BCC-like lesions than *K14-CreER*$^{T2}$*;Ptch1*$^{f/f}$ mice (Adolphe et al., 2014). A separate study similarly demonstrated overlapping roles for PTCH1 and PTCH2 during limb development. In this context, *Prx1-Cre;Ptch1*$^{f/-}$*;Ptch2*$^{-/-}$ mice exhibited greater HH pathway

activation and more severe defects in limb outgrowth than *Prx1-Cre;Ptch1*$^{f/-}$ animals (Zhulyn et al., 2015). Taken together, these studies present compelling evidence that PTCH2 plays overlapping roles with PTCH1 to restrict HH signaling in multiple contexts during embryogenesis and tissue homeostasis, demonstrating that redundancy between the Patched receptors is likely a global mechanism to regulate HH pathway activity in vertebrates.

The most striking result from my analysis in the developing spinal cord is the severe neural tube ventralization observed in *MT-Ptch1;Ptch1*$^{-/-}$*;Ptch2*$^{-/-}$*;Hhip1*$^{-/-}$ embryos. In this context, the highest-level HH targets, FOXA2 and NKX2.2, are expressed throughout the dorsal-ventral axis of the tissue, reflecting constitutive HH pathway activation within the neural tube. This suggests that PTCH1, PTCH2, and HHIP1 comprise an essential network of cell surface HH pathway antagonists that are collectively required to inhibit ligand-dependent HH signaling during vertebrate embryogenesis. Thus, the activity of PTC-feedback inhibition in *Drosophila* has been distributed amongst three partially redundant feedback antagonists in vertebrates. These observations resolve the conflicting reports as to the requirement for LDA of HH signaling during *Drosophila* and mouse tissue patterning.

These data are reminiscent of the collective requirement for GAS1, CDON, and BOC to promote ligand-dependent HH signaling during vertebrate embryogenesis (Allen et al., 2011; Izzi et al., 2011). While loss of any single co-receptor produces little to no defects in HH-dependent ventral neural patterning, *Gas1;Cdon;Boc* triple mutants display a near complete loss of HH signaling, comparable to *Smo* mutant embryos (Allen et al., 2011). Similarly, while loss of feedback up-regulation of any single antagonist results in, at most, a subtle expansion of HH-dependent ventral cell fates, combined loss of PTCH2-, HHIP1-, and PTCH1-feedback inhibition results in constitutive HH pathway activity throughout the neural tube. Collectively, these results

define two sets of essential, yet opposing cell surface HH-binding receptors that are required to precisely regulate ligand-dependent HH signaling during vertebrate embryogenesis.

Mechanistically, I present evidence that PTCH2 utilizes similar molecular mechanisms as PTCH1 to restrict HH pathway activity. First, PTCH2 acts upstream of SMO to antagonize ligand-dependent HH pathway activity (LDA) when expressed in NIH/3T3 cells. Moreover, PTCH2 can directly antagonize SMO activity (LIA) when expressed in *Ptch1*$^{-/-}$ MEFs, albeit with reduced activity compared to PTCH1. Moreover, PTCH2 is responsive to SHH ligand in this context. Consistent with this, PTCH2 can interact with the HH co-receptors GAS1, CDON, and BOC. Finally, PTCH2 localizes to the primary cilium similar to PTCH1 and more recent evidence demonstrates that PTCH2 can prevent the ciliary accumulation of SMO (Zhulyn et al., 2015).

### 4.1.2 Future Directions

*A Role for PTCH2 to Inhibit SMO Activity During Early Embryogenesis*

The ability of PTCH2 to antagonize SMO activity is surprising considering the constitutive activation of HH signaling observed in *Ptch1*$^{-/-}$ embryos (Goodrich et al., 1997). Moreover, I have not detected any differences between *Ptch1*$^{-/-}$ and *Ptch1*$^{-/-}$*;Ptch2*$^{-/-}$ embryos isolated at E9.5, suggesting that PTCH2 possesses a limited capacity to antagonize SMO activity during early development (data not shown). This may reflect a difference in timing, as *Ptch2* may not be induced early enough to counteract the severe HH pathway activation observed in *Ptch1*$^{-/-}$ embryos. It would be interesting to analyze the role of PTCH2 in neural patterning upon conditional deletion of *Ptch1* in the spinal cord at later stages of HH dependent ventral neural patterning using a tamoxifen inducible Cre recombinase, similar to the approach used in the

developing limb (Zhulyn et al., 2015). This may bypass the need to use the *MT-Ptch1* transgene and could help to determine whether PTCH2 does indeed function to antagonize SMO activity in this context. Nevertheless, the *MT-Ptch1;Ptch1*$^{-/-}$ model does provide a powerful tool to test the role of candidate molecules to antagonize HH signal transduction. This sensitized background could be used to test whether other HH-interacting components, loss of which may not produce overt phenotypes on their own, also participate to restrict HH pathway activity in the ventral neural tube, similar to PTCH2 and HHIP1.

*Structure-Function Analysis of PTCH1 and PTCH2*

Throughout my dissertation, I have taken advantage of several assays to dissect the molecular and cellular mechanisms employed by cell surface HH pathway antagonists. These tools provide a unique opportunity to dissect the structural requirements underlying the ability of PTCH1 and PTCH2 to inhibit ligand-dependent HH signaling (LDA); to antagonize SMO activity (LIA); to respond to HH ligands; to localize to the primary cilium; and to interact with the HH co-receptors. This analysis is particularly important considering that the RND motif is the only known functional domain that is linked with PTCH1/2-mediated inhibition of SMO (Taipale et al., 2002; Holtz et al., 2013; Alfaro et al., 2014).

During the course of my studies, I have performed a preliminary structure-function analysis of the PTCH1 C-terminus (Fig. 4-1). While the C-terminal tail of PTCH1 is involved in protein turnover (Kawamura et al., 2008; Xingwu Lu, 2006), it is thought that this region is largely dispensable for HH pathway inhibition in vertebrates. This is due to the viability of the spontaneous *Mesenchymal Dysplasia* (*Mes*) mouse mutant, which was mapped to the PTCH1 C-terminal tail, truncating this region from 273 to 50 amino acids (Makino, 2001). Surprisingly, my

preliminary data shows that complete truncation of the C-terminus renders PTCH1 incapable of SMO inhibition, demonstrating the requirement for this region in LIA (Fig. 4-1, A and B). I have narrowed this region down to a 28 amino acid region stretch in the C-terminal tail (Fig. 4-1 A). Moreover, truncation of the C-terminal tail results in a compromised response to SHH ligand (Fig. 4-1 C), which could be related to enhanced stability of these constructs. Further work is needed to map this functional domain in greater detail and to determine the role of this region in regards to other aspects of PTCH1 function. In the future, a similar approach could be used to interrogate other structural requirements within PTCH1 and PTCH2, including the N-terminus, the third large intracellular loop, etc.

Another important question involves the mechanism and functional significance of ciliary localization of PTCH1/2. The current model assumes that PTCH1 acts within the membrane of the primary cilium to prevent SMO ciliary accumulation and activation (Rohatgi et al., 2007); however, this has yet to be tested functionally. A variety of cilia localization sequences (CLS) can target membrane proteins to the primary cilium (Nachury et al., 2010). Of these CLS motifs, PTCH1 and PTCH2 possess two A/Q boxes [defined as AxA/SxQ (Berbari et al., 2008)], the first of which is conserved with *Drosphila* PTC, which does not localize to the cilium when expressed in NIH/3T3 cells compared to PTCH1 and PTCH2 (Fig. 4-2, A-I). Interestingly, mutagenesis of the second A/Q box in PTCH1 ($PTCH1^{\Delta CLS}$) compromises trafficking to the primary cilium (Fig. 4-2, J-L). Surprisingly, $PTCH1^{\Delta CLS}$ maintains the ability to antagonize SMO with slightly reduced activity, but is incapable of antagonizing ligand-dependent HH signaling in NIH/3T3 cells (Fig. 4-2, M and N). These results suggest that ciliary localization of PTCH1 may play a role to inhibit ligand-dependent HH signaling. Since current models suggest that

productive HH ligand-receptor interactions occur in the ciliary membrane (Rohatgi et al., 2007), proximity to the primary cilium could be a critical aspect of LDA.

This idea is supported by an in-depth analysis of the PTCH2 RND mutants defined in Chapter II. Surprisingly, PTCH2G465V mutant protein also fails to localize to the primary cilium compared to the other PTCH1 and PTCH2 RND mutant constructs when expressed in NIH/3T3 cells (Fig. 4-3, A-L, arrows). While this construct antagonizes SMO equivalent to PTCH2D469Y (Fig. 2-13 D), it fails to inhibit SHH-mediated pathway activity in NIH/3T3 cells (Fig. 4-3 N). In contrast, the other PTCH1- and PTCH2-RND mutants are indistinguishable from their wildtype counterparts in NIH/3T3 cell assays (Fig. 4-3, M and N). Taken together, these data suggest that Patched ciliary localization may play a role in both LIA and LDA of HH signaling. However, further work is needed to define the mechanisms and functional significance of Patched ciliary targeting.

The analyses described above could be complemented with an unbiased approach using *Drosophila* PTC (*dm*PTC), which does not localize to the primary cilium and is incapable of antagonizing SMO activity when expressed in *Ptch1*$^{-/-}$ MEFs (Fig. 4-2). This provides an opportunity to identify novel PTCH1 functional domains through generating PTCH1/*dm*PTC chimeras to identify regions of PTCH1 that are capable of transforming *dm*PTC into a vertebrate SMO inhibitor. Moreover, candidate CLS motifs can be introduced into *dm*PTC to determine whether they are sufficient for ciliary targeting of heterologous receptors. If ciliary localized *dm*PTC is capable of inhibiting SMO activity, this would suggest that both vertebrate and invertebrate Patched proteins possess fundamentally similar catalytic activities. An additional approach could involve generating PTCH1/DISP1 chimeras, to determine the molecular basis of the divergent activities of these RND permeases in HH signaling.

*Examining the Cell Surface Hedgehog Interactome*

The cell surface HH pathway machinery is thought to function within the context of a complex interaction network. PTCH1 has been shown to form distinct complexes with the HH co-receptors, GAS1, CDON, and BOC (Izzi et al., 2011). Moreover, the co-receptors can also interact with each other and can self-associate (Bae et al., 2011). Similarly, we show that PTCH2 interacts with all three HH co-receptors (Holtz et al., 2013); however, the functional significance of these interactions remains unknown. While the PTCH1-interacting domains have been mapped to the FNIII(1) and FNIII(2) in CDON/BOC, the corresponding regions of PTCH1/2 and GAS1 are unknown (Izzi et al., 2011). Co-immunoprecipitation studies will help to delineate the GAS1/CDON/BOC interacting domains in PTCH1/2. Subsequent cell signaling assays will help to determine the role of these interactions to mediate ligand-dependent HH pathway activation. These receptor complexes should be reconstituted in *Ptch1*$^{-/-}$*;Cdon*$^{-/-}$*;Boc*$^{-/-}$ MEFs to prevent interactions with the endogenous co-receptors. Moreover, further deletion of *Gas1* by CRISPR/CAS9 mediated genome editing may also be necessary to precisely interrogate the functional significance of these interactions (previous attempts to generate *Ptch1;Gas1* double mutants have failed due to their close proximity on chromosome 13).

Moreover, we have no reason to believe that all of the PTCH1-interaction partners have been identified. Proteomics approaches could be used to isolate novel HH pathway components that interact with PTCH1. Towards this end, I have generated *Ptch1*$^{-/-}$ and *Cdon*$^{-/-}$ MEF lines stably expressing HA-tagged PTCH1 and CDON, respectively (Fig. 4-4, A and B). Immunoprecipitation using an HA antibody followed by mass spectrometry could be used to isolate novel HH receptor components, using the parental MEF line as a negative control. Since these MEF lines are HH responsive, it would be interesting to perform these experiments before

and after exposure to HH ligand to determine how the HH receptor complex changes in response to signaling over time. Any novel interacting partners could then be tested in functional assays, with promising candidates followed up through loss-of-function studies in the mouse.

## 4.2 Novel Role for HHIP1 as a Secreted, Heparan Sulfate-Binding Antagonist of Vertebrate HH Signaling that Regulates HH Ligand Distribution

### 4.2.1 Summary of Key Findings

Prior to my studies, HHIP1 was classified as a type-I transmembrane anchored protein that functions at the cell surface to competitively inhibit ligand-dependent HH signaling (Chuang and McMahon, 1999; Jeong and McMahon, 2005). Data presented in Chapter III re-define HHIP1 as a secreted antagonist of HH signaling due to its ability to impact HH signaling over long distances when expressed in the developing chicken neural tube. Strikingly, anchoring HHIP1 to the cell surface using a heterologous transmembrane domain precludes these non-cell autonomous effects, demonstrating that HHIP1 secretion underlies long-range inhibition of HH-dependent patterning and proliferation. Moreover, I provide biochemical evidence that HHIP1 is a secreted protein that associates with the cell surface through cell-type specific interactions with HS. Biochemical studies demonstrate that these interactions are mediated by basic amino acids within the HHIP1 N-terminal CRD. Overall, these data provide the first description of a secreted HH pathway antagonist, which has recently been corroborated through complementary approaches (Kwong et al., 2014).

The novel interaction between HHIP1 and HS is important considering that HS regulates HH signaling during vertebrate and invertebrate embryogenesis (Whalen et al., 2013; Bellaiche et al., 1998; The et al., 1999; Rubin et al., 2002; Chang et al., 2011). Mutagenesis of the HS-

binding site within the HHIP1-CRD (HHIP1$^{\Delta HS1,2}$) leads to enhanced HHIP1 secretion from cells. Paradoxically, HHIP1$^{\Delta HS1,2}$ is significantly compromised in its ability to influence HH signaling over long distances in the developing chick neural tube. This is not due to compromised protein activity, but instead reflects a failure to localize to the basement membrane (BM) of the neuroepithelium. Therefore, HHIP1-HS interactions likely play two key roles: (1) to alter the balance between secretion and cell surface retention of HHIP1 in producing cells and (2) to control the tissue distribution of HHIP1 to epithelial basement membranes to promote effective HH pathway inhibition. These data are consistent with previous studies in *Drosophila* that demonstrate an essential role for HS to control the tissue distribution of HH ligands (Bellaiche et al., 1998; The et al., 1999; Han et al., 2004a; b).

Importantly, I demonstrate that endogenous HHIP1 protein is localized to the basement membrane in the developing neuroepithelium, consistent with our gain-of-function analysis in the chicken neural tube. While I did not detect HHIP1 protein within the developing spinal cord, likely due to low expression levels in this region, *Hhip1* is expressed in the roof plate of the embryonic spinal cord. This dorsal HHIP1 expression in relation to the ventral production of SHH is reminiscent of the expression of secreted BMP inhibitors in the notochord, which counteracts BMP ligands produced dorsally in the roof plate (McMahon et al., 1998; Liem et al., 2000); however, more sensitive tools will be required to determine the localization of HHIP1 protein at this axial level.

*Hhip1* is also expressed in more rostral regions of the neural tube in the developing diencephalon, enabling visualization of endogenous HHIP1 protein distribution. Strikingly, I detected HHIP1 protein localization to the basement membrane over 200μm away from its source of production. This demonstrates that HHIP1 protein is secreted *in vivo* and accumulates

in the neuroepithelial basement membrane. Moreover, I also observed co-localization of endogenous HHIP1 and SHH ligand in discrete puncta within this tissue compartment. Intriguingly, loss of HHIP1 prevents the distal accumulation of SHH in the basement membrane, demonstrating that HHIP1 can directly impact the tissue distribution of SHH. Importantly, these data also implicate the basement membrane as one of the functional routes utilized by SHH to distribute within a tissue. This compartmentalization provides an efficient mechanism to spatially regulate the activity of HH ligands in the developing nervous system, especially when considering that each neural progenitor maintains contact with the basement membrane in this pseudostratified epithelium.

Finally, I also observed endogenous, secreted HHIP1 protein in the developing lung. In this context, HHIP1 is produced by mesenchymal fibroblasts and accumulates within the BM of the developing lung epithelium. This suggests that the localization of HHIP1 to BM may be a generalizable aspect of HHIP1-mediated inhibition of HH signaling. Importantly, HHIP1 plays an essential, non-redundant role to antagonize HH signaling in the developing lung, as *Hhip1*$^{-/-}$ embryos die at birth due to severe defects in lung branching morphogenesis (Chuang, 2003). Despite the presence of PTCH1 feedback up-regulation in the developing lung mesenchyme, PTCH1 fails to compensate for the absence of HHIP1 as occurs during neural patterning (Bellusci et al., 1997; Chuang, 2003; Jeong and McMahon, 2005; Holtz et al., 2013). One intriguing idea is that the secreted activity of HHIP1 underlies its unique requirement in the lung, compared to PTCH1 and PTCH2, which are strictly membrane-bound. This idea can be tested in explant models and using novel genetic tools (described below).

### 4.2.2 Future Directions

*How is HHIP1 Recruited to Basement Membranes In Vivo?*

Several key questions remain concerning the secretion and tissue distribution of HHIP1. While disrupting HS-interactions prevents the BM localization of HHIP1 in the chicken neural tube, it remains to be determined whether this mechanism functions to recruit endogenous HHIP1 to the BM in the neuroepithelium and lung. Strikingly, I demonstrated that HHIP1 co-localizes with the predominant BM HSPG, Perlecan, in the developing neuroepithelium and lung. In fact, I detected HHIP1 accumulation around lung fibroblasts that express Perlecan, suggesting that this may be the relevant core HSPG that controls HHIP1 distribution. It will be critical to determine whether endogenous HHIP1 interacts with endogenous Perlecan through co-immunoprecipitation studies. Moreover, this can be combined with heparanase treatment to determine to what extent this interaction is mediated through HS.

Perlecan mutant mice (*Hspg2*$^{-/-}$) mice display several developmental defects. A subset of these animals exhibits early lethality at E10.5 with severe defects in head development (Arikawa-Hirasawa et al., 1999). The rest die at birth and exhibit exencephaly to varying degrees in addition to skeletal dysplasia (Arikawa-Hirasawa et al., 1999; Costell et al., 1999). It would be interesting to determine whether Perlecan loss alters the tissue distribution of HHIP1 protein in the neural tube and lung of *Hspg2*$^{-/-}$ mice. To date, the glypicans, a family of 6 GPI-anchored HS-decorated proteins, are the only vertebrate HSPGs that have been demonstrated to regulate HH pathway activity (Williams et al., 2010; Capurro et al., 2008; Li et al., 2011a); thus, an analysis of HH-dependent developmental processes in the neural tube, limb, face, and lung of *Hspg2*$^{-/-}$ mice could provide important insights HSPG-regulation of HH signaling during embryogenesis. This type of analysis could be extended to the other glypican family members (GPC1, 2, 4, and 6), which possess the ability to regulate HH signal transduction (Williams et al.,

2010). Moreover, a detailed structure-function analysis of the opposing actions of GPC3 and GPC5 to antagonize and to promote HH signaling, respectively, using cell based assays and chicken in ovo neural tube electroporations would provide valuable insight into HSPG-mediated regulation of HH signaling (Capurro et al., 2008; Li et al., 2011a).

*A Requirement for a Secreted HHIP1 in the Developing Lung?*

I show through gain-of-function approaches that HHIP1 secretion and interactions with HS are required to effectively antagonize HH signaling in the the developing neural tube. However, HHIP1 activity is entirely redundant with PTCH1/2 during neural patterning; thus, it will be important to test these properties in the context of a developing tissue that depends on HHIP1 activity. The lung represents the ideal system to interrogate these questions. One approach involves rescue experiments in *Hhip1*$^{-/-}$ lung explants, which exhibit defects in branching morphogenesis in culture (Chuang, 2003). I have previously attempted to introduce HHIP1 constructs into lung explants by electroporation. While the lung epithelium was amenable to electroporation, I was unable to achieve construct expression in the lung mesenchyme (data not shown), the site of endogenous HHIP1 production (Chuang, 2003). A viral transduction system may prove more useful to introduce HHIP1, HHIP1$^{\Delta HS1,2}$, and HHIP1::CD4 into the lung mesenchyme to determine how these different constructs rescue the lung branching defects. Moreover, driving expression of these constructs with a HH-responsive enhancer could restrict HHIP1 expression to the appropriate regions of the lung mesenchyme, since *Hhip1* is a direct HH target gene (Chuang and McMahon, 1999; Vokes et al., 2008; 2007).

Previous studies have generated transgenes expressing either full-length *Hhip1* or a secreted form of *Hhip1* lacking the C-terminal 22 amino acids to study the role of HHIP1 *in vivo* (Madison et al., 2005; Zacharias et al., 2011; Treier et al., 2001; Chuang, 2003). Another

approach to address the role of secreted HHIP1 would involve engineering novel mouse models to replace the C-terminal 22 amino acids with a CD4 domain at the endogenous *Hhip1* locus. Moreover, point mutations in the HS-binding site within the HHIP1 CRD could be introduced at the endogenous locus to test the role of HHIP1-HS interactions *in vivo*. Generation of these alleles may be facilitated using CRISPR/CAS9 genome engineering (Cong et al., 2013; Yang et al., 2014; 2013). Lung branching defects observed in $Hhip1^{CD4/CD4}$ or $Hhip1^{\Delta HS/\Delta HS}$ mice would directly demonstrate a role for HHIP1 secretion and HS-binding to regulate lung branching morphogenesis. Moreover, an analysis of HHIP1 protein distribution in the diencephalon and lung in these models would help to determine whether HS-interactions recruit HHIP1 to epithelial basement membranes *in vivo*.

*Exploring the Tissue Specific Roles for HHIP1 in Embryonic and Adult Tissues*

In addition, a conditional *Hhip1* allele would prove invaluable to further examine the role of HHIP1 in embryonic and adult tissues. One striking result is that *Hhip1* is highly expressed in the developing roof plate and paraxial mesoderm, but is weakly expressed in ventral neuronal progenitors. Currently, it is assumed that the *Hhip1* produced in ventral progenitors acts to restrict HH signaling during ventral neural patterning; however, it is likely that HHIP1 produced in the roof plate and paraxial mesoderm could also play a role (Jeong and McMahon, 2005). To test this, *Hhip1* could be conditionally ablated in these different tissue compartments to see if they contribute to regulating HH-dependent ventral patterning. Using a GDF7-Cre line, *Hhip1* can be specifically ablated in the developing roof plate (Lee et al., 2000). An expansion of ventral HH-dependent cell fates in *MT-Ptch1;Ptch1*$^{-/-}$*;Hhip1*$^{f/-}$*;Gdf7-Cre* embryos, which lack PTCH1-feedback inhibition combined with specific ablation of *Hhip1* in the roof plate, would

determine whether HHIP1 is produced and secreted from the roof plate to inhibit HH signaling at a distance in the ventral neural tube. Moreover, *Hhip1* can be deleted in the paraxial mesoderm using a *Dll1-Cre* transgene to determine whether HHIP1 produced in the paraxial mesoderm can inhibit HH signaling in ventral progenitors (Wehn et al., 2009). These data would demonstrate novel tissue interactions that regulate HH signaling during embryogenesis.

Throughout the course of my studies, I have also observed that *Hhip1* expression persists into adulthood in several tissues (Fig. 4-5). The most striking examples of this are in the adult lung and intestine. In E18.5 lung tissue, I detect HHIP1 protein expression in PDGFRα-expressing mesenchymal cells in the alveoli (Fig. 4-5, A-D, arrowheads). I also detect HHIP1 expression in myofibroblast-like cells surrounding the larger airways (Fig. 4-5, E-H, arrows). Additionally, HHIP1 is largely excluded from Aquaporin-5+ type I cells and Surfactant Protein C+ type II cells (Fig. 4-5, I-P). This expression pattern is similar in the adult lung (data not shown). Interestingly, I also observe strong *Hhip1* expression in mesenchymal cells within the adult intestine (Fig. 4-5, Q-X); however, the identity of these HHIP1-expressing cells remains unknown. Since *Hhip1*$^{-/-}$ embryos do not survive post-natally, a conditional allele will be essential to determine the role of HHIP1 in the lung, stomach, and in other tissues during adulthood.

*Hhip1 Mice as a Model for Human Lung Diseases*

The persistence of *Hhip1* expression in the adult lung is intriguingly considering that HHIP1 has been implicated in a variety of human lung diseases, including chronic obstructive pulmonary disease (COPD), asthma, and lung cancer (Pillai et al., 2009; Van Durme et al., 2010; Zhou et al., 2012; Young et al., 2010; Li et al., 2011b; Castaldi et al., 2014). One intriguing idea

involves the use of *Hhip1*$^{+/-}$ mice or mice with conditional ablation of *Hhip1* in the adult lung as a model for these various lung diseases. Indeed, my preliminary data demonstrates structural abnormalities in a subset of *Hhip1*$^{+/-}$ lungs, including delayed branching morphogenesis and mesenchymal thickening (data not shown). COPD is characterized by two distinct pathologies. This includes chronic bronchitis, which involves inflammation and remodeling of the larger airways of the lung, and emphysema, or a loss of distal lung tissue resulting in a decreased area for gas exchange (Tuder and Petrache, 2012). Interestingly, my preliminary data suggests that *Hhip1* is expressed in the mature lung in regions affected by COPD (Fig. 4-5).

COPD is primarily a disease related to long term tobacco use (Tuder and Petrache, 2012); thus, the most widely used model to study COPD involves exposing mice to cigarette smoke. This recapitulates many aspects of the disease, including airway remodeling and fibrosis in addition to loss of alveolar structures (Churg et al., 2008; Wright et al., 2008). It would be interesting to monitor the expression of *Hhip1* and other HH pathway components throughout the development of COPD in this model. Moreover, an accelerated development of disease pathology in *Hhip1*$^{+/-}$ mice or in conditional *Hhip1* mutants compared to *wildtype* controls would demonstrate the importance of HHIP1 in COPD progression, which could potentially be mitigated through use of pharmacologic HH pathway inhibitors. A similar approach could be used in other mouse models of lung disease where HH signaling has been implicated, including in bleomyin-induced lung fibrosis (Farrokhi Moshai et al., 2014).

*A Novel Interaction Between HHIP1 and HH Ligands?*

Many questions remain concerning the molecular and biochemical mechanisms underlying HHIP1 function. One key aspect involves the ability of HHIP1 to bind HH ligands.

Two crystallographic studies demonstrated that HHIP1 lacking the N-terminal CRD ($HHIP1^{\Delta N}$) binds to SHH through the β-propeller domain (Bosanac et al., 2009; Bishop et al., 2009). An aspartic acid residue (D383) within this region is essential to coordinate with the zinc ion present within HH ligands (Bishop et al., 2009). Replacing this negative residue with a positively charged arginine (D383N) completely abolishes the physical interaction between $HHIP1^{\Delta N}$ and SHH (Bishop et al., 2009). Based on these data, I generated the analogous mutation in full length HHIP1 ($HHIP1^{D383R}$) to test in chicken electroporation experiments (Fig. 4-6). Strikingly, $HHIP1^{D383R}$ is still capable of inhibiting HH-dependent patterning and growth, albeit in a cell autonomous manner (Fig. 4-6, arrows). These data implicate a novel interaction between the HHIP1 CRD and HH ligands; however, one caveat to these studies is the presence of endogenous HHIP1 in the chicken neural tube, which could interact with $HHIP1^{D383R}$.

Intriguingly, structural studies have demonstrated that the CRDs present in other proteins can directly bind to lipophilic molecules. For example, the CRD in Frizzled receptors bind to the palmitoleyl group of Wnt ligands and the SMO CRD can interact with oxysterols (Janda et al., 2012; Bazan et al., 2012; Myers et al., 2013; Nachtergaele et al., 2013; Nedelcu et al., 2013). One hypothesis involves the HHIP1 CRD interacting with HH ligands either through the cholesterol or palmitate moieties. This should be followed up through biochemical and crystallographic studies combined with cell signaling and chicken electroporation assays. Moreover, recent evidence demonstrates that the secreted GPI-hydrolase and Wnt inhibitor, Notum, can bind to and cleave the palmitoleate residue from Wnt ligands to inhibit signaling (Kakugawa et al., 2015). It will be interesting to determine whether HHIP1 can alter the structural properties of HH ligands in a similar manner.

*HHIP1 as a Multimodal Inhibitor of Morphogen Signaling*

While HHIP1 is primarily thought to act as an inhibitor of HH signaling in mammals, there is evidence that HHIP1 might influence other cell signaling pathways. Interestingly, studies in *Xenopus* demonstrate that WNT, FGF, and BMP signaling can regulate *Hhip1* expression (Cornesse et al., 2005). Subsequent gain- and loss-of-function studies demonstrated that HHIP1 could interfere with FGF8-dependent induction of *Xbra* expression and MAPK-phosphorylation (Cornesse et al., 2005). Moreover, HHIP1 could block the ability of WNT8 ligand to induce secondary axis formation in *Xenopus* embryos (Cornesse et al., 2005). Intriguingly, WNT3A was refractory to HHIP1-inhibition, demonstrating ligand specificity in the ability of HHIP1 to impact WNT signaling (Cornesse et al., 2005). These experiments suggest that HHIP1 might act as a multi-modal inhibitor of morphogen signaling, similar to Cerberus, which antagonizes the activity of BMP, Nodal, and WNT ligand (Piccolo et al., 1999; Bouwmeester et al., 1996).

Several lines of inquiry should be pursued to test whether HHIP1 can antagonize WNT or FGF signaling in mammals. One simple experiment would be to test whether HHIP1 can antagonize these pathways in cell signaling assays. This should be performed using a variety of different WNT and FGF ligands to test the specificity of these interactions. These data could be followed up through biochemical studies to determine whether HHIP1 physically interacts with these signaling ligands or their corresponding receptors. These interaction domains could then be mapped using the HHIP1 domain mutants generated in Chapter III. Finally, a careful examination of WNT- and FGF-dependent developmental processes in *Hhip1*$^{-/-}$ animals may provide *in vivo* evidence that HHIP1 can impact these signaling pathways.

*Exploring Additional HHIP-Related Proteins in Vertebrate HH Signaling*

In addition to HHIP1, vertebrates possess two additional HHIP1-like proteins, HHIP1L1 and HHIP1L2 (Pei and Grishin, 2012). These were identified through sequence homology and share roughly 30% amino acid identity with HHIP1 (data now shown). Both HHIP1L1 and HHIP1L2 possess a conserved N-terminal CRD and a β-propeller domain, but lack the two C-terminal EGF repeats. It would be interesting to determine whether these molecules can influence HH signaling or other signaling pathways. While HHIP1L1/2 lack key residues that are required for HHIP1 interactions with HH ligands, it is possible that these proteins could interact with HH in a mechanism that is distinct from that of HHIP1. Initially, this should be approached through cell signaling assays and chicken electroporation experiments. If overexpression of these molecules does influence HH-dependent ventral neural patterning, it would be important to follow up these studies through targeted mouse mutants to determine their roles *in vivo*. This would demonstrate that HHIP1 proteins comprise a family of HH pathway components that are critical to regulate HH signal transduction during vertebrate embryogenesis.

Overall, data presented in this dissertation demonstrate that the cell surface HH pathway antagonists, PTCH1, PTCH2, and HHIP1, play overlapping and essential roles to restrict HH signaling during vertebrate embryogenesis. In addition, I provide evidence to re-define HHIP1 as a secreted antagonist of HH signaling that controls the localization of HH ligands during development. Moreover, I find that HHIP1 associates with HS to localize to epithelial basement membranes in several tissues during embryogenesis. These results provide novel mechanistic insights into how HH signaling is antagonized during vertebrate embryogenesis and provide a foundation for further investigation into the role of HH pathway inhibitors during development, tissue homeostasis, and disease processes.

## 4.3 Materials and Methods

*Luciferase assays*

*Ptch1*$^{-/-}$ mouse embryonic fibroblasts (MEFs; a gift from Dr. M.P. Scott) were plated at 50,000 cells per well on gelatinized 24-well plates and transfected 16-24 hours later with 150ng of a ptcΔ136-GL3 luciferase reporter (Chen et al., 1999; Nybakken et al., 2005), 100ng of a secreted placental alkaline phosphatase construct, and varying amounts of control (*pCIG*) or experimental constructs using Lipofectamine 2000 (Invitrogen). After 48 hours, cells were changed into low serum media (0.5%) to stimulate ciliogenesis and HH signaling. After another 48 hours, 100µl of medium was removed from each well and transferred to a 96-well clear bottom plate, heat inactivated at 65°C for 1 hour to deactivate the endogenous alkaline phosphatase activity, and then 100µl of alkaline phosphatase substrate was added per well (Alkaline Phosphatase Yellow pNPP Liquid Substrate for ELISA, Sigma-Aldrich). Absorbance at 405nm was read 2 hours later. Cells were also lysed and the luciferase activity was measured using the Luciferase Assay System (Promega). Luciferase values were normalized to alkaline phosphatase activity to control for transfection efficiency. Each condition was performed in triplicate. To measure responsiveness to SHH ligand, varying amounts of either control- or NSHH-conditioned medium were added when cells were switched into low serum medium.

NIH/3T3 cell Luciferase assays were adapted from a previously published protocol (Nybakken et al., 2005; Holtz et al., 2013). Mouse NIH/3T3 fibroblasts were plated at 25,000 cells/well on gelatinized 24-well plates and transfected 16-24 hours later with 150ng of a ptcΔ136-GL3 luciferase reporter (Chen et al., 1999; Nybakken et al., 2005), 50ng of pSV-β-galactosidase (Promega), and 100 ng of control (*pCIG*) or experimental constructs using Lipofectamine 2000 (Invitrogen). After 48 hours, cells were placed in low serum (0.5%) media

with 25µl of conditioned media from control (*pCDNA3*) or NSHH transfected (*NShh-pCDNA3*) COS7 cells. Luciferase (Luciferase Assay System kit, Promega) and β-galactosidase (BetaFluor β-galactosidase Assay Kit, Novagen) activity were measured after 48 hours. Luciferase values were normalized to β-galactosidase activity and expressed as fold induction relative to control treated cells.

*Cellular localization of HH pathway components*

NIH/3T3 fibroblasts were plated at 150,000 cells/well on coverslips and transfected 16-24 hours later. 6 hours post-transfection, cells were placed into low serum (0.5%) media and fixed 48 hours later in 4% PFA for immunofluorescent analysis.

*Chicken in ovo neural tube electroporations*

Electroporations were performed as previously described (Holtz et al., 2013; Tenzen et al., 2006). In brief, DNA (1.0 µg/µl) mixed with Fast Green (50 ng/µl) was injected into Hamburger-Hamilton stage 11-13 embryos and then subjected to electroporation. Embryos were dissected 24 hours post electroporation (hpe), fixed in 4% PFA, and processed for immunofluorescent analysis. Chicken embryos were sectioned at the wing axial level. Electroporated cells were marked by constructs expressing nuclear-localized EGFP (*pCIG*).

*Immunofluorescence*

Immunofluorescence was performed essentially as previously described (Holtz et al., 2013). The following antibodies were used: mouse IgG1 anti-NKX6.1 (1:20, Developmental Studies Hybridoma Bank [DSHB]), mouse IgG1 anti-PAX7 (1:20, DSHB), mouse IgG1 anti-HA

(1:1000, Covance), mouse IgG2b anti-Acetylated Tubulin (1:2500, Sigma-Aldrich), goat IgG anti-HHIP1 (1:200, R&D Systems), rabbit IgG anti-Aquaporin 5 (1:1000, Abcam), rabbit anti-Surfactant Protein C (1:100, Seven Hills Bioreagents), and rabbit IgG anti-β-galactosidase (1:10,000, MP Biomedicals). Nuclei were visualized with DAPI (1:30,000, Molecular Probes). Alexa 488 and 555 secondary antibodies (1:500, Molecular Probes) were visualized on a Leica upright SP5X confocal microscope.

*Western Blot Analysis*

Western blot analysis was performed according to standard methods. Briefly, MEFs were lysed in RIPA buffer (50mM Tris-HCl [pH 7.2], 150mM NaCl, 0.1% TX-100, 1% sodium deoxycholate, 5mM EDTA) containing Complete Mini Protease Inhibitor Cocktail (Roche), centrifuged at 20,000 x g for 30 min at 4°C, and analyzed by SDS-PAGE. Proteins were transferred to PVDF and probed with a mouse IgG1 anti-HA antibody (1:1000, Covance).

*Immunoprecipitation*

1mg of MEF lysates were brought to a concentration of 2mg/ml and pre-cleared with 30µl bead volume of Protein G-Agarose (Roche) for 1 hour at 4°C. Anti-HA antibody (mouse IgG1, Covance) was added to the pre-cleared lysates at 1:200 overnight at 4°C. Immune complexes were pulled down using 30µl bead volume of Protein G-Agarose for 1 hour at 4°C. The beads were washed 5x 10 minutes in wash buffer at 4°C (1% NP-40, 50mM Tris-HCl, 150mM NaCl, 5mM EDTA, pH 7.2) and proteins were eluted from the beads with laemmli buffer for SDS-PAGE analysis.

## 4.4 Figures

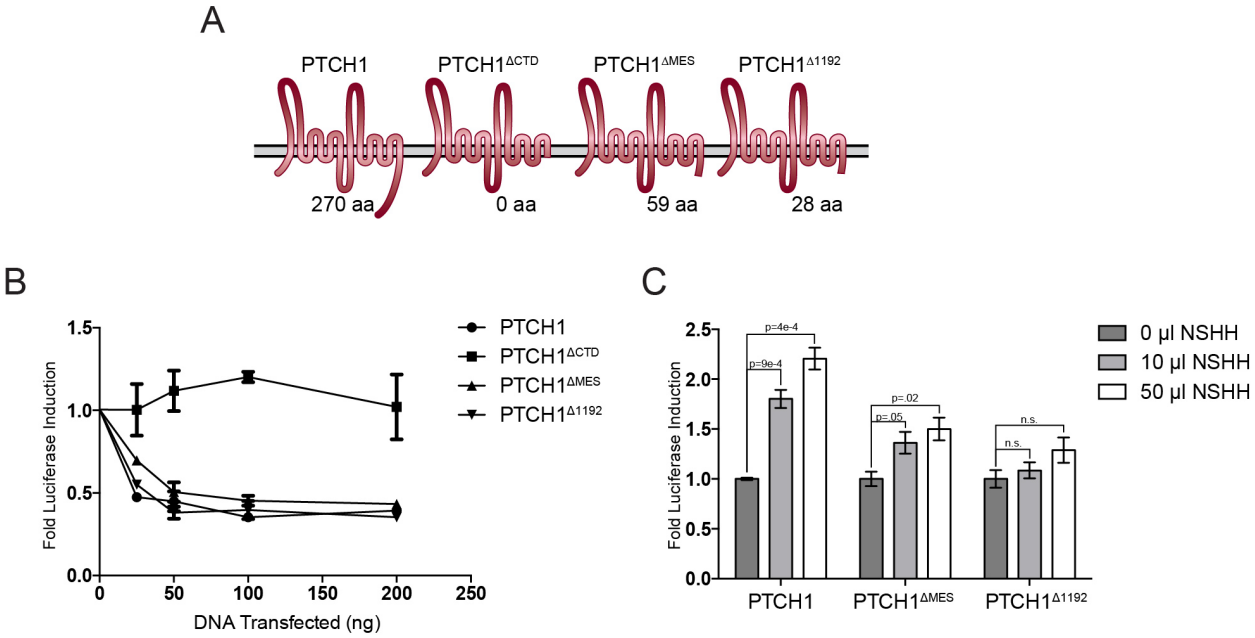


**Figure 4-1. The PTCH1 C-terminal tail is essential for SMO inhibition.** (A) Cartoon schematics of PTCH1 C-terminal tail deletion constructs. The number of amino acids remaining in the C-terminal tail is depicted below each construct. (B) HH-responsive luciferase reporter activity measured from *Ptch1*$^{-/-}$ mouse embryonic fibroblasts (MEFs) transfected with the indicated constructs. Data expressed as luciferase reporter activity normalized to cells transfected with empty vector alone (*pCIG*) and represented as mean +/- SEM. (C) As in B, including treatment with different amounts of NSHH-conditioned media. P-values determined by Student's two-tailed *t*-test (n.s., not significant, p > .05).

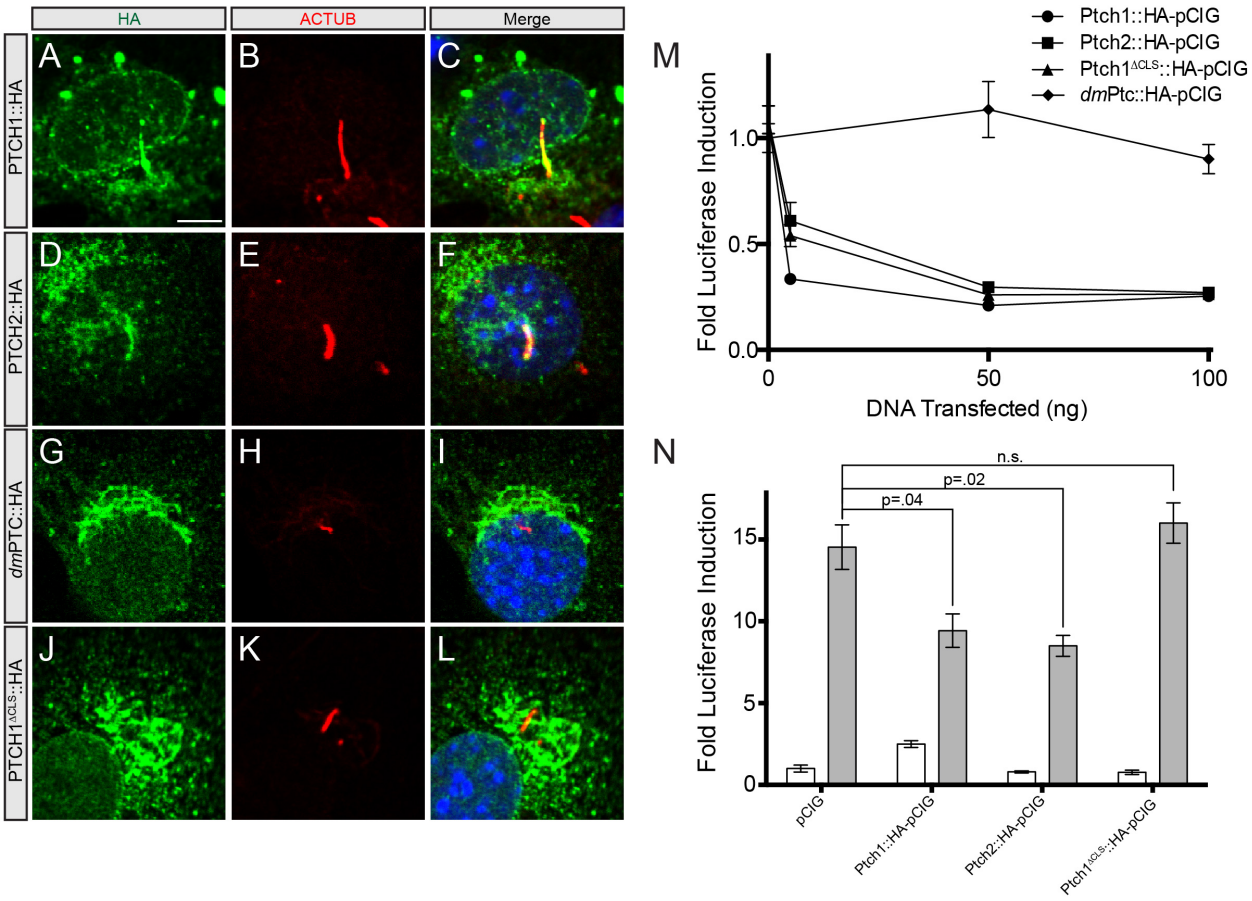


**Figure 4-2. Identification of a cilia localization motif in PTCH1 that is required its full activity.** (A-L) Immunofluorescent detection of HA (green; A, C, D, F, G, I, J, L) and Acetylated Tubulin (ACTUB, red; B, C, E, F, H, I, K, L) in NIH/3T3 cells transfected with *Ptch1::HA* (A-C), *Ptch2::HA* (D-F), *Ptch1*$^{\Delta CLS}$ (G-I), or *dmPtc::HA* (J-L). DAPI labels nuclei (blue; C, F, I, L). (M) *Ptch1*$^{-/-}$ MEFs transfected with a HH-responsive luciferase reporter and co-transfected with the indicated constructs. Luciferase reporter activity is normalized to cells transfected with empy vector alone and presented as mean +/- SEM. (N) HH-responsive luciferase reporter activity measured from NIH/3T3 fibroblasts stimulated with either control- or NSHH-conditioned media and co-transfected with the indicated constructs. Data represented as mean +/- SEM (n.s., not significant, P>.05 two-tailed Student's *t*-test). Scale bar (A): 5µm.

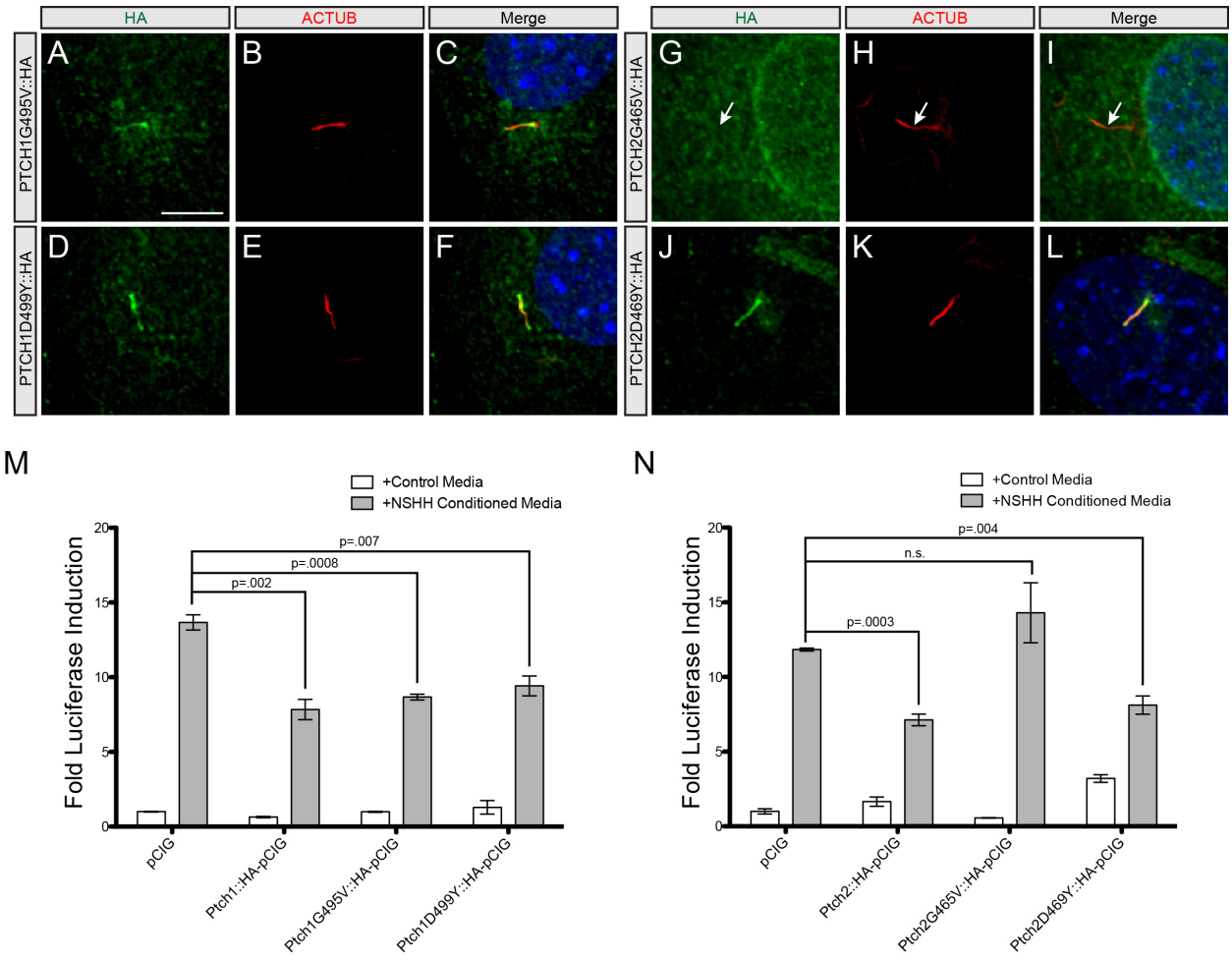


**Figure 4-3. PTCH2G465V fails to localize to the primary cilium to antagonize ligand-dependent HH signaling.** (A-L) NIH/3T3 cells transfected with *Ptch1G495V::HA* (A-B), *Ptch1D499Y::HA* (D-F), *Ptch2G465V::HA* (G-I), *Ptch2D469Y::HA* (J-L) and stained with antibodies to detect the expression of HA (green; A, C, D, F, G, I, J, L) and Acetylated Tubulin (ACTUB, red; B, C, E, F, H, I, K, L). Nuclei are stained with DAPI (blue; C, F, I, L). Arrows (G-I) denote lack of ciliary localization of PTCH2G465V. (M, N) HH-responsive luciferase reporter activity measured from NIH/3T3 fibroblasts transfected with the indicated constructs and treated with with either control- or NSHH-conditioned media. Data presented as mean +/- SEM. P-values determined by Student's two-tailed *t*-test (n.s., not significant, P>.05). Scale bar (A): 5μm.

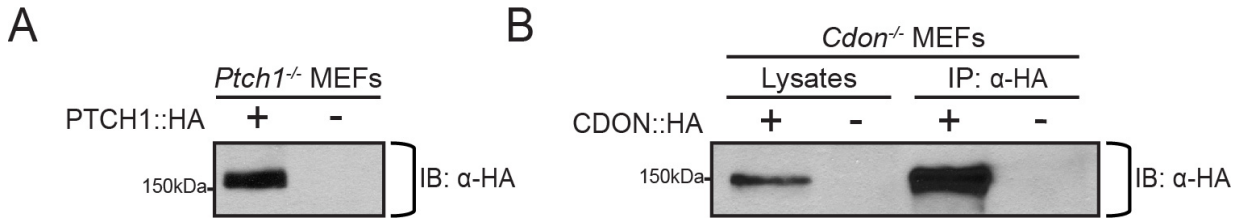


**Figure 4-4. Initial analysis of PTCH1 and CDON stable cell lines.** Western blot analysis of lysates from *Ptch1*$^{-/-}$ (A) and *Cdon*$^{-/-}$ (B) MEF lines stably expressing PTCH1::HA and CDON::HA, respectively, compared to the parental MEF lines. (B) Immunoprecipitation using an HA antibody successfully pulled down CDON::HA in stably transfected *Cdon*$^{-/-}$ MEFs.

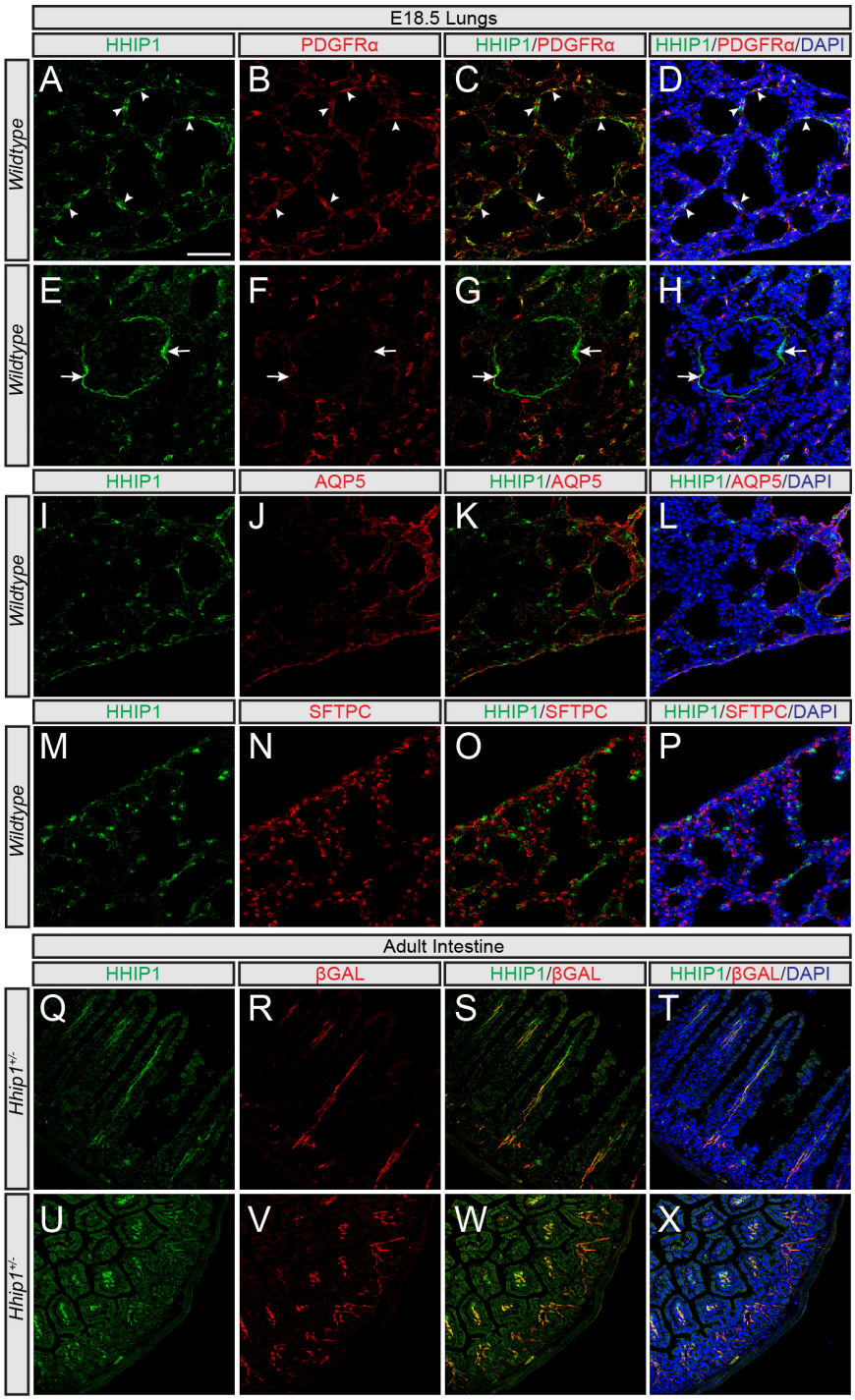


**Figure 4-5. HHIP1 protein detection in mature tissues.** Immunofluorescent detection of HHIP1 (green; A, C, D, E, G, H, I, K, L, M, O, P, Q, S, T, U, W, X), PDGFRα (red; B-D, F-H), Aquaporin 5 (AQP5, red; J-L), Surfactant Protein C (SFTPC, red; N-P), and β-galactosidase (βGAL, red; R-T, V-X) in E18.5 *wildtype* lungs (A-P) and adult *Hhip1*$^{+/-}$ intestines (Q-X). DAPI labels nuclei (blue; D, H, L, P, T, X). Arrowheads (A-D) highlight co-localization between HHIP1 and PDGFRα expression. Arrows (E-H) demonstrate HHIP1 expression in myofibroblast-like cells surrounding the larger airways. Scale bar (A): 50μm.

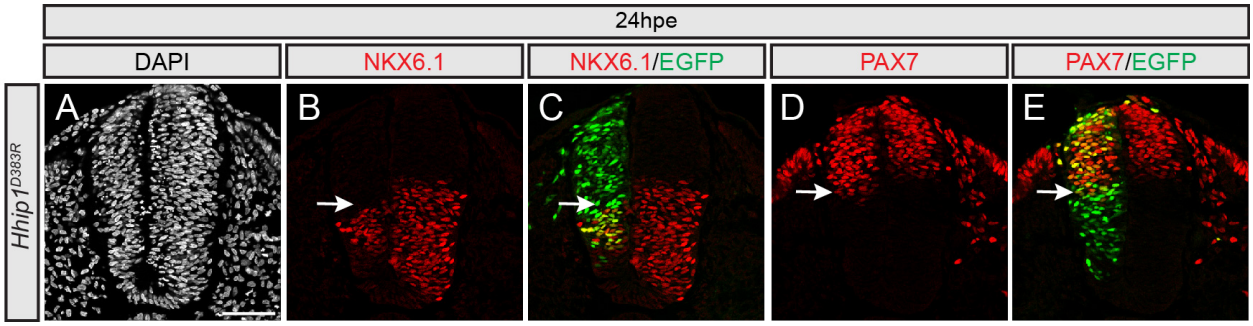


**Figure 4-6. HHIP1$^{D383R}$ antagonizes HH-dependent ventral neural patterning in the chicken neural tube.** Hamburger-Hamilton stage 11-13 embryos were electroporated with *Hhip1$^{D383R}$-pCIG* and isolated 24 hours post-electroporation (24hpe). Embryos were sectioned at the wing axial level and stained with antibodies to detect expression of NKX6.1 (red; B, C) and PAX7 (red; D, E). Nuclear EGFP expression labels electroporated cells (green; C, E). DAPI reveals nuclei (grey; A). Arrows denote repression of NKX6.1 (B, C) or ectopic expression of PAX7 (D, E) resulting from HHIP1$^{D383R}$ expression. Scale bar (A): 50μm.

## 4.5 References


Adolphe, C., E. Nieuwenhuis, R. Villani, Z.J. Li, P. Kaur, C.-C. Hui, and B.J. Wainwright. 2014. Patched 1 and patched 2 redundancy has a key role in regulating epidermal differentiation. *J. Invest. Dermatol.* 134:1981–1990. doi:10.1038/jid.2014.63.

Alfaro, A.C., B. Roberts, L. Kwong, M.F. Bijlsma, and H. Roelink. 2014. Ptch2 mediates the Shh response in Ptch1-/- cells. *Development*. 141:3331–3339. doi:10.1242/dev.110056.

Allen, B.L., J.Y. Song, L. Izzi, I.W. Althaus, J.-S. Kang, F. Charron, R.S. Krauss, and A.P. McMahon. 2011. Overlapping roles and collective requirement for the coreceptors GAS1, CDO, and BOC in SHH pathway function. *Dev. Cell*. 20:775–787. doi:10.1016/j.devcel.2011.04.018.

Arikawa-Hirasawa, E., H. Watanabe, H. Takami, J.R. Hassell, and Y. Yamada. 1999. Perlecan is essential for cartilage and cephalic development. *Nat Genet*. 23:354–358. doi:10.1038/15537.

Bae, G.-U., S. Domené, E. Roessler, K. Schachter, J.-S. Kang, M. Muenke, and R.S. Krauss. 2011. Mutations in CDON, encoding a hedgehog receptor, result in holoprosencephaly and defective interactions with other hedgehog receptors. *Am. J. Hum. Genet.* 89:231–240. doi:10.1016/j.ajhg.2011.07.001.

Bazan, J.F., C.Y. Janda, and K.C. Garcia. 2012. Structural architecture and functional evolution of Wnts. *Dev. Cell*. 23:227–232. doi:10.1016/j.devcel.2012.07.011.

Bellaiche, Y., I. The, and N. Perrimon. 1998. Tout-velu is a Drosophila homologue of the putative tumour suppressor EXT-1 and is needed for Hh diffusion. *Nature*. 394:85–88. doi:10.1038/27932.

Bellusci, S., Y. Furuta, M.G. Rush, R. Henderson, G. Winnier, and B.L. Hogan. 1997. Involvement of Sonic hedgehog (Shh) in mouse embryonic lung growth and morphogenesis. *Development*. 124:53–63.

Berbari, N.F., A.D. Johnson, J.S. Lewis, C.C. Askwith, and K. Mykytyn. 2008. Identification of ciliary localization sequences within the third intracellular loop of G protein-coupled receptors. *Mol. Biol. Cell*. 19:1540–1547. doi:10.1091/mbc.E07-09-0942.

Bishop, B., A.R. Aricescu, K. Harlos, C.A. O'Callaghan, E.Y. Jones, and C. Siebold. 2009. Structural insights into hedgehog ligand sequestration by the human hedgehog-interacting protein HHIP. *Nature Publishing Group*. 16:698–703. doi:10.1038/nsmb.1607.

Bosanac, I., H.R. Maun, S.J. Scales, X. Wen, A. Lingel, J.F. Bazan, F.J. de Sauvage, S.G. Hymowitz, and R.A. Lazarus. 2009. The structure of SHH in complex with HHIP reveals a recognition role for the Shh pseudo active site in signaling. *Nature Publishing Group*. 16:691–697. doi:10.1038/nsmb.1632.

Bouwmeester, T., S. Kim, Y. Sasai, B. Lu, and E.M. De Robertis. 1996. Cerberus is a head-

inducing secreted factor expressed in the anterior endoderm of Spemann's organizer. *Nature*. 382:595–601. doi:10.1038/382595a0.

Capurro, M.I., P. Xu, W. Shi, F. Li, A. Jia, and J. Filmus. 2008. Glypican-3 inhibits Hedgehog signaling during development by competing with patched for Hedgehog binding. *Dev. Cell*. 14:700–711. doi:10.1016/j.devcel.2008.03.006.

Castaldi, P.J., M.H. Cho, R.S.J. Estépar, M.-L.N. McDonald, N. Laird, T.H. Beaty, G. Washko, J.D. Crapo, E.K. Silverman, on behalf of the COPDGene Investigators. 2014. Genome-Wide Association Identifies Regulatory Loci Associated with Distinct Local Histogram Emphysema Patterns. *Am. J. Respir. Crit. Care Med.* doi:10.1164/rccm.201403-0569OC.

Chang, S.-C., B. Mulloy, A.I. Magee, and J.R. Couchman. 2011. Two distinct sites in sonic Hedgehog combine for heparan sulfate interactions and cell signaling functions. *J. Biol. Chem.* 286:44391–44402. doi:10.1074/jbc.M111.285361.

Chen, C.H., D.P. von Kessler, W. Park, B. Wang, Y. Ma, and P.A. Beachy. 1999. Nuclear trafficking of Cubitus interruptus in the transcriptional regulation of Hedgehog target gene expression. *Cell*. 98:305–316.

Chuang, P.T. 2003. Feedback control of mammalian Hedgehog signaling by the Hedgehog-binding protein, Hip1, modulates Fgf signaling during branching morphogenesis of the lung. *Genes & Development*. 17:342–347. doi:10.1101/gad.1026303.

Chuang, P.T., and A.P. McMahon. 1999. Vertebrate Hedgehog signalling modulated by induction of a Hedgehog-binding protein. *Nature*. 397:617–621. doi:10.1038/17611.

Churg, A., M. Cosio, and J.L. Wright. 2008. Mechanisms of cigarette smoke-induced COPD: insights from animal models. *Am. J. Physiol. Lung Cell Mol. Physiol.* 294:L612–31. doi:10.1152/ajplung.00390.2007.

Cong, L., F.A. Ran, D. Cox, S. Lin, R. Barretto, N. Habib, P.D. Hsu, X. Wu, W. Jiang, L.A. Marraffini, and F. Zhang. 2013. Multiplex genome engineering using CRISPR/Cas systems. *Science*. 339:819–823. doi:10.1126/science.1231143.

Cornesse, Y., T. Pieler, and T. Hollemann. 2005. Olfactory and lens placode formation is controlled by the hedgehog-interacting protein (Xhip) in Xenopus. *Developmental Biology*. 277:296–315. doi:10.1016/j.ydbio.2004.09.016.

Costell, M., E. Gustafsson, A. Aszódi, M. Mörgelin, W. Bloch, E. Hunziker, K. Addicks, R. Timpl, and R. Fässler. 1999. Perlecan maintains the integrity of cartilage and some basement membranes. *J. Cell Biol.* 147:1109–1122.

Farrokhi Moshai, E., L. Wémeau-Stervinou, N. Cigna, S. Brayer, J. Marchal Sommé, B. Crestani, and A.A. Mailleux. 2014. Targeting the Hedgehog-Gli Pathway Inhibits Bleomycin-Induced Lung Fibrosis in Mice. *Am. J. Respir. Cell Mol. Biol.* doi:10.1165/rcmb.2013-0154OC.

Goodrich, L.V., L. Milenkovic, K.M. Higgins, and M.P. Scott. 1997. Altered neural cell fates and medulloblastoma in mouse patched mutants. *Science*. 277:1109–1113. doi:10.1126/science.277.5329.1109.

Han, C., T.Y. Belenkaya, B. Wang, and X. Lin. 2004a. Drosophila glypicans control the cell-to-cell movement of Hedgehog by a dynamin-independent process. *Development*. 131:601–611. doi:10.1242/dev.00958.

Han, C., T.Y. Belenkaya, M. Khodoun, M. Tauchi, X. Lin, and X. Lin. 2004b. Distinct and collaborative roles of Drosophila EXT family proteins in morphogen signalling and gradient formation. *Development*. 131:1563–1575. doi:10.1242/dev.01051.

Holtz, A.M., K.A. Peterson, Y. Nishi, S. Morin, J.Y. Song, F. Charron, A.P. McMahon, and B.L. Allen. 2013. Essential role for ligand-dependent feedback antagonism of vertebrate hedgehog signaling by PTCH1, PTCH2 and HHIP1 during neural patterning. *Development*. 140:3423–3434. doi:10.1242/dev.095083.

Izzi, L., M. Lévesque, S. Morin, D. Laniel, B.C. Wilkes, F. Mille, R.S. Krauss, A.P. McMahon, B.L. Allen, and F. Charron. 2011. Boc and Gas1 each form distinct Shh receptor complexes with Ptch1 and are required for Shh-mediated cell proliferation. *Dev. Cell*. 20:788–801. doi:10.1016/j.devcel.2011.04.017.

Janda, C.Y., D. Waghray, A.M. Levin, C. Thomas, and K.C. Garcia. 2012. Structural basis of Wnt recognition by Frizzled. *Science*. 337:59–64. doi:10.1126/science.1222879.

Jeong, J., and A.P. McMahon. 2005. Growth and pattern of the mammalian neural tube are governed by partially overlapping feedback activities of the hedgehog antagonists patched 1 and Hhip1. *Development*. 132:143–154. doi:10.1242/dev.01566.

Kakugawa, S., P.F. Langton, M. Zebisch, S.A. Howell, T.-H. Chang, Y. Liu, T. Feizi, G. Bineva, N. O'Reilly, A.P. Snijders, E.Y. Jones, and J.-P. Vincent. 2015. Notum deacylates Wnt proteins to suppress signalling activity. *Nature*. doi:10.1038/nature14259.

Kawamura, S., K. Hervold, F.-A. Ramirez-Weber, and T.B. Kornberg. 2008. Two patched protein subtypes and a conserved domain of group I proteins that regulates turnover. *J. Biol. Chem.* 283:30964–30969. doi:10.1074/jbc.M806242200.

Kwong, L., M.F. Bijlsma, and H. Roelink. 2014. Shh-mediated degradation of Hhip allows cell autonomous and non-cell autonomous Shh signalling. *Nat Commun*. 5:4849. doi:10.1038/ncomms5849.

Lee, K.J., P. Dietrich, and T.M. Jessell. 2000. Genetic ablation reveals that the roof plate is essential for dorsal interneuron specification. *Nature*. 403:734–740. doi:10.1038/35001507.

Li, F., W. Shi, M. Capurro, and J. Filmus. 2011a. Glypican-5 stimulates rhabdomyosarcoma cell proliferation by activating Hedgehog signaling. *J. Cell Biol.* 192:691–704. doi:10.1083/jcb.201008087.

Li, X., T.D. Howard, W.C. Moore, E.J. Ampleford, H. Li, W.W. Busse, W.J. Calhoun, M. Castro, K.F. Chung, S.C. Erzurum, A.M. Fitzpatrick, B. Gaston, E. Israel, N.N. Jarjour, W.G. Teague, S.E. Wenzel, S.P. Peters, G.A. Hawkins, E.R. Bleecker, and D.A. Meyers. 2011b. Importance of hedgehog interacting protein and other lung function genes in asthma. *J. Allergy Clin. Immunol.* 127:1457–1465. doi:10.1016/j.jaci.2011.01.056.

Liem, K.F., T.M. Jessell, and J. Briscoe. 2000. Regulation of the neural patterning activity of sonic hedgehog by secreted BMP inhibitors expressed by notochord and somites. *Development*. 127:4855–4866.

Madison, B.B., K. Braunstein, E. Kuizon, K. Portman, X.T. Qiao, and D.L. Gumucio. 2005. Epithelial hedgehog signals pattern the intestinal crypt-villus axis. *Development*. 132:279–289. doi:10.1242/dev.01576.

Makino, S. 2001. A Spontaneous Mouse Mutation, mesenchymal dysplasia (mes), Is Caused by a Deletion of the Most C-Terminal Cytoplasmic Domain of patched (ptc). *Developmental Biology*. 239:95–106. doi:10.1006/dbio.2001.0419.

McMahon, J.A., S. Takada, L.B. Zimmerman, C.M. Fan, R.M. Harland, and A.P. McMahon. 1998. Noggin-mediated antagonism of BMP signaling is required for growth and patterning of the neural tube and somite. *Genes & Development*. 12:1438–1452.

Myers, B.R., N. Sever, Y.C. Chong, J. Kim, J.D. Belani, S. Rychnovsky, J.F. Bazan, and P.A. Beachy. 2013. Hedgehog pathway modulation by multiple lipid binding sites on the smoothened effector of signal response. *Dev. Cell*. 26:346–357. doi:10.1016/j.devcel.2013.07.015.

Nachtergaele, S., D.M. Whalen, L.K. Mydock, Z. Zhao, T. Malinauskas, K. Krishnan, P.W. Ingham, D.F. Covey, C. Siebold, and R. Rohatgi. 2013. Structure and function of the Smoothened extracellular domain in vertebrate Hedgehog signaling. *eLife*. 2:e01340. doi:10.7554/eLife.01340.

Nachury, M.V., E.S. Seeley, and H. Jin. 2010. Trafficking to the Ciliary Membrane: How to Get Across the Periciliary Diffusion Barrier? *Annu. Rev. Cell Dev. Biol.* 26:59–87. doi:10.1146/annurev.cellbio.042308.113337.

Nedelcu, D., J. Liu, Y. Xu, C. Jao, and A. Salic. 2013. Oxysterol binding to the extracellular domain of Smoothened in Hedgehog signaling. *Nat Chem Biol*. 9:557–564. doi:10.1038/nchembio.1290.

Nybakken, K., S.A. Vokes, T.-Y. Lin, A.P. McMahon, and N. Perrimon. 2005. A genome-wide RNA interference screen in Drosophila melanogaster cells for new components of the Hh signaling pathway. *Nat Genet*. 37:1323–1332. doi:10.1038/ng1682.

Pei, J., and N.V. Grishin. 2012. Cysteine-rich domains related to Frizzled receptors and Hedgehog-interacting proteins. *Protein Sci.* 21:1172–1184. doi:10.1002/pro.2105.

Piccolo, S., E. Agius, L. Leyns, S. Bhattacharyya, H. Grunz, T. Bouwmeester, and E.M. De

Robertis. 1999. The head inducer Cerberus is a multifunctional antagonist of Nodal, BMP and Wnt signals. *Nature*. 397:707–710. doi:10.1038/17820.

Pillai, S.G., D. Ge, G. Zhu, X. Kong, K.V. Shianna, A.C. Need, S. Feng, C.P. Hersh, P. Bakke, A. Gulsvik, A. Ruppert, K.C. Lødrup Carlsen, A. Roses, W. Anderson, S.I. Rennard, D.A. Lomas, E.K. Silverman, D.B. Goldstein, ICGN Investigators. 2009. A genome-wide association study in chronic obstructive pulmonary disease (COPD): identification of two major susceptibility loci. *PLoS Genet.* 5:e1000421. doi:10.1371/journal.pgen.1000421.

Rohatgi, R., L. Milenkovic, and M.P. Scott. 2007. Patched1 regulates hedgehog signaling at the primary cilium. *Science*. 317:372–376. doi:10.1126/science.1139740.

Rubin, J.B., Y. Choi, and R.A. Segal. 2002. Cerebellar proteoglycans regulate sonic hedgehog responses during development. *Development*. 129:2223–2232.

Taipale, J., M.K. Cooper, T. Maiti, and P.A. Beachy. 2002. Patched acts catalytically to suppress the activity of Smoothened. *Nature*. 418:892–897. doi:10.1038/nature00989.

Tenzen, T., B.L. Allen, F. Cole, J.-S. Kang, R.S. Krauss, and A.P. McMahon. 2006. The cell surface membrane proteins Cdo and Boc are components and targets of the Hedgehog signaling pathway and feedback network in mice. *Dev. Cell*. 10:647–656. doi:10.1016/j.devcel.2006.04.004.

The, I., Y. Bellaiche, and N. Perrimon. 1999. Hedgehog movement is regulated through tout velu-dependent synthesis of a heparan sulfate proteoglycan. *Mol. Cell*. 4:633–639.

Treier, M., S. O'Connell, A. Gleiberman, J. Price, D.P. Szeto, R. Burgess, P.T. Chuang, A.P. McMahon, and M.G. Rosenfeld. 2001. Hedgehog signaling is required for pituitary gland development. *Development*. 128:377–386.

Tuder, R.M., and I. Petrache. 2012. Pathogenesis of chronic obstructive pulmonary disease. *J. Clin. Invest.* 122:2749–2755. doi:10.1172/JCI60324.

Van Durme, Y.M.T.A., M. Eijgelsheim, G.F. Joos, A. Hofman, A.G. Uitterlinden, G.G. Brusselle, and B.H.C. Stricker. 2010. Hedgehog-interacting protein is a COPD susceptibility gene: the Rotterdam Study. *Eur. Respir. J.* 36:89–95. doi:10.1183/09031936.00129509.

Vokes, S.A., H. Ji, S. McCuine, T. Tenzen, S. Giles, S. Zhong, W.J.R. Longabaugh, E.H. Davidson, W.H. Wong, and A.P. McMahon. 2007. Genomic characterization of Gli-activator targets in sonic hedgehog-mediated neural patterning. *Development*. 134:1977–1989. doi:10.1242/dev.001966.

Vokes, S.A., H. Ji, W.H. Wong, and A.P. McMahon. 2008. A genome-scale analysis of the cis-regulatory circuitry underlying sonic hedgehog-mediated patterning of the mammalian limb. *Genes & Development*. 22:2651–2663. doi:10.1101/gad.1693008.

Wehn, A.K., P.H. Gallo, and D.L. Chapman. 2009. Generation of transgenic mice expressing Cre recombinase under the control of the Dll1 mesoderm enhancer element. *Genesis*. 47:309–

313. doi:10.1002/dvg.20503.

Whalen, D.M., T. Malinauskas, R.J.C. Gilbert, and C. Siebold. 2013. Structural insights into proteoglycan-shaped Hedgehog signaling. *Proceedings of the National Academy of Sciences of the United States of America*. doi:10.1073/pnas.1310097110.

Williams, E.H., W.N. Pappano, A.M. Saunders, M.-S. Kim, D.J. Leahy, and P.A. Beachy. 2010. Dally-like core protein and its mammalian homologues mediate stimulatory and inhibitory effects on Hedgehog signal response. *Proceedings of the National Academy of Sciences of the United States of America*. 107:5869–5874. doi:10.1073/pnas.1001777107.

Wright, J.L., M. Cosio, and A. Churg. 2008. Animal models of chronic obstructive pulmonary disease. *AJP: Lung Cellular and Molecular Physiology*. 295:L1–L15. doi:10.1152/ajplung.90200.2008.

Xingwu Lu, S.L.T.B.K. 2006. The C-terminal tail of the Hedgehog receptor Patched regulates both localization and turnover. *Genes & Development*. 20:2539. doi:10.1101/gad.1461306.

Yang, H., H. Wang, and R. Jaenisch. 2014. Generating genetically modified mice using CRISPR/Cas-mediated genome engineering. *Nat Protoc*. 9:1956–1968. doi:10.1038/nprot.2014.134.

Yang, H., H. Wang, C.S. Shivalila, A.W. Cheng, L. Shi, and R. Jaenisch. 2013. One-step generation of mice carrying reporter and conditional alleles by CRISPR/Cas-mediated genome engineering. *Cell*. 154:1370–1379. doi:10.1016/j.cell.2013.08.022.

Young, R.P., C.F. Whittington, R.J. Hopkins, B.A. Hay, M.J. Epton, P.N. Black, and G.D. Gamble. 2010. Chromosome 4q31 locus in COPD is also associated with lung cancer. *Eur. Respir. J.* 36:1375–1382. doi:10.1183/09031936.00033310.

Zacharias, W.J., B.B. Madison, K.E. Kretovich, K.D. Walton, N. Richards, A.M. Udager, X. Li, and D.L. Gumucio. 2011. Hedgehog signaling controls homeostasis of adult intestinal smooth muscle. *Developmental Biology*. 355:152–162. doi:10.1016/j.ydbio.2011.04.025.

Zhou, X., R.M. Baron, M. Hardin, M.H. Cho, J. Zielinski, I. Hawrylkiewicz, P. Sliwinski, C.P. Hersh, J.D. Mancini, K. Lu, D. Thibault, A.L. Donahue, B.J. Klanderman, B. Rosner, B.A. Raby, Q. Lu, A.M. Geldart, M.D. Layne, M.A. Perrella, S.T. Weiss, A.M.K. Choi, and E.K. Silverman. 2012. Identification of a chronic obstructive pulmonary disease genetic determinant that regulates HHIP. *Hum Mol Genet*. 21:1325–1335. doi:10.1093/hmg/ddr569.

Zhulyn, O., E. Nieuwenhuis, Y.C. Liu, S. Angers, and C.-C. Hui. 2015. Ptch2 shares overlapping functions with Ptch1 in Smo regulation and limb development. *Developmental Biology*. 397:191–202. doi:10.1016/j.ydbio.2014.10.023.